FINITE ELEMENT SOLUTIONS OF OPTIMIZATION PROBLEMS WITH STABILITY CONSTRAINTS INVOLVING COLUMNS AND LAMINATED COMPOSITES

İzzet Ufuk ÇAĞDAŞ

Submitted in fulfilment of the academic requirements for the degree of Doctor of Philosophy in the Department of Mechanical Engineering
at University of KwaZulu-Natal

Durban, South Africa
December 2006

Prof. Dr. Sarp ADALI

Acknowledgements

I express my gratitude to my supervisor Prof. Dr. Sarp ADALI for his guidance, encouragement, generous support and kindness; and to my family for their moral support.

Financial assistance from National Research Foundation of South Africa is gratefully acknowledged.

Abstract

The primary aim of this study is to assess the applicability and performance of the finite element method (FEM) in solving structural optimization problems with stability constraints. In order to reach this goal, several optimization problems are solved using FEM which are briefly described as follows:

The strongest column problem is one of the oldest optimization problems for which analytical solutions exist only for some special cases. Here, both unimodal and bimodal optimization of columns under concentrated and/or distributed compressive loads with several different boundary conditions and constraints are performed using an iterative method based on finite elements. The analytical solutions available in the literature for columns under concentrated loads and an analytical solution derived for simply supported columns under distributed loads are used for verification purposes.

Optimization results are presented for fibre-reinforced composite rectangular plates under in-plane loads. The non-uniformity of the in-plane stresses due to stress diffusion and/or in-plane boundary conditions is taken into account, and its influence on optimal buckling load is investigated. It is shown that the exclusion of the in-plane restraints may lead to errors in stability calculations and consequently in optimal design.

The influences of the panel aspect ratio, stacking sequence, panel thickness, and the rotational edge restraints on the optimal axially compressed cylindrical and non-cylindrical curved panels are investigated, where the optimal panel is the one with the highest failure load. The pre-buckling and the first-ply failure loads of the panels are calculated and minimum of these two is selected as the failure load. The results show that there are distinct differences between the behaviour of cylindrical and non-cylindrical panels.

The formulations of the finite elements which are used throughout the study are given and several verification problems are solved to verify the accuracy of the methodology. The computer codes written in Matlab are also given in the appendix sections accompanied with the selected codes used for optimization purposes.

Declaration

I declare that this dissertation is my own unaided work except where due acknowledgement is made to others. This dissertation is being submitted for the Degree of Doctor of Philosophy to the University of Kwa-Zulu Natal, Durban, and has not been submitted previously for any other degree examination.

İzzet Ufuk Çağdaş

December 2006.

Özet

Bu çalismanin ana gayesi sonlu elemanlar yönteminin (SEY) stabilite kisitlari içeren optimizasyon problemlerinin çözümünde kullanimini ve etkinligini degerlendirmektir. Bu hedefe ulasabilmek için asagida kisaca izah edilen optimizasyon problemleri SEY ile çözülmüstür;

En güçlü kolon problemi bazi özel durumlari için analitik çözümler mevcut olan en eski optimizasyon problemlerinden biridir. Burada tekil ve/veya yayili basinç yükleri altindaki kolonlarin çesitli sinir sartlari ve kisitlar için hem tekmodlu hem de çiftmodlu optimizasyonlari yapilmistir. Tekil yükler altindaki kolonlar için mevcut olan çözümler ve yayili yüklü basit mesnetli kolonlar için elde edilmis analitik bir çözüm dogrulama amaciyla kullanilmistir.

Düzlemi içinde yüklü liflerle güçlendirilmis kompozit dikdörtgen plaklarin optimizasyon neticeleri sunulmustur. Gerilme yayilmasi ve/veya düzlem içi sinir sartlari nedeniyle düzlem gerilmelerin düzensizligi göz önünde bulundurulmus ve optimum burkulma yüküne etkisi incelenmistir. Düzlem içi sinir sartlarinin ihmal edilmesinin stabilite hesaplarinda ve bunun neticesinde optimum tasarimda hatalara neden olabilecegi gösterilmistir.

Optimum panel en yüksek göçme yüküne sahip olan panel olmak üzere, panel en/boy orani, katman açisi düzeni, panel kalinligi ve kenarlardaki dönme serbestliklerinin eksenel basinç altindaki optimum silindirik ve silindirik olmayan egri panellere etkisi incelenmistir. Panelin ön-burkulma ve ilk-katman göçmesi yükleri hesaplanmis ve bunlarin en küçügü göçme yükü olarak seçilmistir. Neticeler silindirik ve silindirik olmayan paneller arasinda önemli farklar oldugunu göstermektedir.

Bu çalismada kullanilan sonlu elemanlarin formülasyonlari verilmis ve yöntemin hassasiyetini dogrulayan çok sayida örnek problem çözülmüstür. Matlab kullanilarak yazilan bilgisayar programlari optimizasyon amaciyla kullanilan programlarla beraber ek bölümlerinde verilmistir.

Contents

List of Figures

List of Tables

1. INTRODUCTION

The optimization of structural components has applications in many fields of engineering due to the resulting weight savings which is an important design consideration for weight-sensitive structures. The primary objectives of this study are briefly stated as follows:

i. To assess the applicability and the performance of the finite element method (FEM) in solution of structural optimization problems with stability constraints.
ii. To gather formulations of beam, plate, and shell finite elements which can be used to solve structural stability problems.
iii. To implement FEM in order to model and design structural members such as columns and laminated composite plates, and shells.

Brief information regarding to the sections of this thesis are given below:

In section II, Beam, plate, and shell elements which are used in modeling the optimization problems are defined and formulated. The formulations include the geometric stiffness matrices for linearized stability analysis as this study is mainly focused on stability. Several verification problems are solved which not only verify the computer codes used but also give valuable information on the accuracy of the elements. Some of the details, such as the assembly of global matrices and special equation solution techniques are not given here in order to reduce the volume. Information regarding to the elements, for which the derivations are given here, may be found in several text books, for example in Cook (1973), Hinton and Owen (1977), Allen and Bulson (1980), Kikuchi (1986), Yang (1986), Reddy (1984, 2004), Bathe (1995), Reddy and Miravete (2004) where general information on finite element method and the elements used here are given. However, the information is scattered and the geometric stiffness matrices are not defined clearly in most of the references which include the Hermite beam element given in Cook (1973), iso-parametric plate element given in Hinton and Owen (1977) and the super-parametric shell element formulated by Mallikarjuna and Kant (1992). This is the primary motivation to include a separate chapter on finite element analysis with relevant references mentioned where applicable. Also, necessary information on lamina stress-strain relations, first order shear deformable plate theory (FDST) and first-ply failure analysis are given in order to bridge the gap between theory and analysis.

In Section III, the problem of optimizing the cross-sectional shape of a column to maximize its buckling load is studied, which has been studied in several publications starting with Lagrange (1770-1773). Analytical solutions for statically determinate columns were derived by Keller (1960), and Tadjbakhsh and Keller (1962) considering only the first mode. However, the solution obtained for the clamped-clamped case by Tadjbakhsh and Keller (1962) did not take into account bimodal buckling as pointed out by Olhoff and Rasmussen (1977) who provided the correct solution for the optimal shape. Structural components with non-uniform cross-sections are widely used in many applications and are of specific interest in structural, mechanical and aeronautical engineering due to the resulting weight savings. The logical extension of a non-uniform component is to find the best distribution of the cross-sectional area with a view towards maximizing its load carrying capacity or minimizing its weight subject to certain design requirements which are usually expressed as design constraints. The design problem of particular interest in the present study is the buckling optimization of Euler columns subject to an arbitrary distribution of axially distributed and concentrated loads. The objective is to maximize the buckling load subject to volume and maximum stress constraints.

In Section IV, firstly the influence of the in-plane restraints on the in-plane stresses and the optimization of rectangular composite plates under linearly varying buckling loads are investigated. Such stresses are encountered in practice for example, in the web sections of transversely loaded composite beams and have been studied by various authors with a view towards determining the buckling resistance of plates under in-plane non-uniform loads,

Zureick and Shih (1998), Leissa and Kang (2002), Kang and Leissa (2005), Wang *et al.* (2006), Zhong and Gu (2006), etc. Also, the behavior of rectangular plates that are restrained against in-plane movement is an important research area because in-plane movement is typically restricted in aerospace structures by adjacent panels and stiffeners, as stated by Nemeth (2004).

Next, stacking sequence optimization of axially compressed cylindrical and non-cylindrical curved panels is considered. The influences of the panel aspect ratio, stacking sequence, panel thickness, and the rotational edge restraints on the optimal panels are investigated. The optimization process can briefly be explained as the search for the best lamination angle maximizing the axial load the curved panel can bear without failure. For a given stacking sequence, pre-buckling and first-ply failure loads are calculated and minimum of these two is selected as the failure load. However, the first-ply failure load is not calculated if it is higher than the pre-buckling load as the panel will fail prematurely due to buckling before the first-ply failure load is reached. A maximum strain failure criterion is employed for optimization purposes.

There exist several computer programming languages which could be used to perform the numerical computations. In this study Matlab (stands for Matrix Laboratory) is used in all of the computations due to its ease. The MATLAB codes used here for optimization purposes are listed in appendix sections.

2. THE FINITE ELEMENTS USED IN THIS STUDY

In this section; the beam, plate, and shell elements which are used in modeling the optimization problems are defined and formulated. The formulations include the geometric stiffness matrices for linearized stability analysis as this study is mainly focused on stability. Several verification problems are solved which not only verifies the computer codes used but also gives valuable information on the accuracy of the elements. Some of the details, such as the assembly of global matrices and equation solution techniques are not given here in order to reduce the volume. Information regarding to the elements, for which the derivations are given here, may be found in several text books, for example in Cook (1973), Hinton and Owen (1977), Allen and Bulson (1980), Kikuchi (1986), Yang (1986), Reddy (1984, 2004), Bathe (1995), Reddy and Miravete (2004) where general information on finite element method and the elements used here are given. However, the information is scattered and the geometric stiffness matrices are not defined clearly in most of the references which include the Hermite beam element given in Cook (1973), iso-parametric plate element given in Hinton and Owen (1977) and the super-parametric shell element formulated by Mallikarjuna and Kant (1992). This is the primary motivation to include a separate chapter on finite element analysis with relevant references mentioned where applicable. Also, necessary information on lamina stress-strain relations, first order shear deformable plate theory (FDST) and first-ply failure analysis are given in order to bridge the gap between theory and analysis.

The Hermite beam element used in this study is one of the simplest finite elements complete formulation of which (including the geometric stiffness matrix) is given in Allen and Bulson (1980) or Cook (1973). A modified geometric stiffness matrix for this element which is used for the buckling load calculation of columns under distributed loads is given in Yang (1986).

The parabolic iso-parametric plate bending element based on Mindlin-Reissner plate theory was developed by Hinton et al. (1975) and Rock and Hinton (1974) for homogeneous, cellular and sandwich plates. Hinton (1975) adopted this element for the flexural analysis of laminated composites. Reddy and Chao (1981) studied the effects of reduced integration, mesh size, and element type on the accuracy of a penalty-finite element, based on the theory governing thick, laminated, anisotropic composite plates. Singh and Rao (1988) formulated a similar plate element which has five degrees of freedom per node in order to study the stability aspects of composite plates.

Buckling response is a major design consideration as most of the shell structures are thin and finite element formulations based on classical theory are not widely used in the analysis of composite structures because of the transverse shear effects as stated by Kim and Voyiadjis (1999a, 1999b). Several authors have developed shell elements which give satisfactory results for many situations in practice as reported in Cook (1973) and Ashwell and Gallagher (1976). However, the concept of treating a shell element as a special case of three-dimensional analysis was first used by Ahmad *et al.* (1970) and Pawsey (1970). This concept provides a simple and efficient strategy for development of iso-parametric shell elements as stated by Krishnamoorthy (1987). The Ahmad thick shell element developed by Ahmad *et al.* (1970) was further improved by several researchers such as Pawsey and Clough (1971), Zienkiewicz *et al.* (1971), Talha (1979), and Kanok-Nukulchai (1979). Panda and Natarajan (1981), Figueiras and Owen (1984), Peseux and Dubigeon (1991) presented similar shell finite element formulations to analyze composite shell structures. The degeneration concept has also been applied to the geometrically non-linear analysis of shells. Kim (1996) and Kim *et al.* (1998) formulated a non-linear composite shell finite element based on Mindlin-Reissner theory to study the buckling behavior of laminated plates and panels under axial compression. Several authors presented continuum-based composite shell elements for geometrically non-linear analysis, such as Chang and Sawamiphakdi (1981), Reddy and Liu (1987), Liao and Reddy (1989), and Wung (1997).

2.1 Finite element analysis of beams

The formulation of the beam finite element used in solving the column optimization problems is given in this section. The element is named as the 'Hermite' beam element in the finite element literature due to the shape functions used. The related functions are listed in Appendix A.1. Displacements due to flexure are represented by a third degree polynomial, w, which must satisfy the boundary conditions at the ends of the element. w and its first derivative with respect to x are given by

$$w = ax^3 + bx^2 + cx + d\,, \qquad w' = 3ax^2 + 2bx + c$$

where x is the local coordinate through element length and a, b, c, d are constants, Allen and Bulson (1980). Using the boundary conditions, the expressions for the constants a, b, c and d can be found as,

$$\begin{Bmatrix} a \\ b \\ c \\ d \end{Bmatrix} = \begin{Bmatrix} \left(Lu_4 - 2u_4 + 2u_1 + Lu_2\right)/L^3 \\ \left(-Lu_4 + 3u_3 - 3u_1 - 2Lu_2\right)/L^2 \\ u_2 \\ u_1 \end{Bmatrix}$$

where $u_1 = w(0)$, $u_2 = w'(0)$, $u_3 = w(L)$ and $u_4 = w'(L)$, and L is the element length. Thus,

$$w(x) = \sum_{i=1}^{4} u_i\phi_i = u_1\phi_1(x) + u_2\phi_2(x) + u_3\phi_3(x) + u_4\phi_4(x)$$

where, ϕ_i are shape functions (Hermite polynomials) given by

$$\phi_1 = 2\zeta^3 - 3\zeta^2 + 1, \quad \phi_2 = L\left(\zeta^3 - 2\zeta^2 + \zeta\right), \quad \phi_3 = -2\zeta^3 + 3\zeta^2, \quad \phi_4 = L\left(\zeta^3 - \zeta^2\right)$$

where ζ is equal to x/L.

The total potential energy V of the system is given by

$$V = \int_0^L \frac{EI}{2}\left(\sum u_i\phi_i''\right)^2 dx - \int_0^L \frac{p}{2}\left(\sum u_i\phi_i'\right)^2 dx$$

where p is the axial load, and EI is the bending rigidity. The total potential energy of the system is stationary with respect to variations in w, viz.

$$\frac{\partial V}{\partial u_j} = \int_0^L EI\left(\sum u_i\phi_i''\right)\phi_j''\,dx - \int_0^L p\left(\sum u_i\phi_i'\right)\phi_j'\,dx = 0$$

which results in a set of four equations which is given in a compact form as

$$\left(\mathbf{U}^E - p\,\mathbf{V}^E\right)\mathbf{u} = \mathbf{0}$$

where $\mathbf{u} = \{u_1, u_2, u_3, u_4\}^T$, $U_{ij}^E = \int_0^L EI\phi_i''\phi_j''\,dx$, and $V_{ij}^E = \int_0^L \phi_i'\phi_j'\,dx$. Here, $\mathbf{U}^E$ and $\mathbf{V}^E$ are named as the element stiffness matrix and is the element geometric stiffness matrix respectively

and $\mathbf{V}^E$ represents the reduction of flexural stiffness due to axial force. The symmetry of these matrices can be easily observed. Details of the calculation of some of the elements of $\mathbf{U}^E$ and $\mathbf{V}^E$ are given below;

$$U_{11}^E = \int_0^L EI(\phi_1'')^2\,dx = \frac{36EI}{L^4}\int_0^L (2\zeta - 1)^2\,dx = \frac{12EI}{L^3}$$

$$U_{12}^E = \int_0^L EI(\phi_1'')(\phi_2'')dx = \frac{12EI}{L^3}\int_0^L (2\zeta - 1)(3\zeta - 2)dx = \frac{6EI}{L^2}$$

$$V_{11}^E = \int_0^L (\phi_1')^2\,dx = \frac{36}{L^2}\int_0^L \left(\zeta^2 - 3\zeta\right)^2\,dx = \frac{6}{5L},$$

$$V_{12}^E = \int_0^L (\phi_1')(\phi_2')dx = \frac{6}{L}\int_0^L \left(\zeta^2 - 3\zeta\right)\left(3\zeta^2 - 4\zeta + 1\right)dx = \frac{1}{10}$$

These results are summarized below in matrix form in Eq.(2.1).

$$\mathbf{U}^E = \frac{EI}{L}\begin{bmatrix} \frac{12}{L^2} & \frac{6}{L} & \frac{-12}{L^2} & \frac{6}{L} \\ & 4 & \frac{-6}{L} & 2 \\ & & \frac{12}{L^2} & \frac{-6}{L} \\ sym & & & 4 \end{bmatrix}, \qquad \mathbf{V}^E = \frac{1}{L}\begin{bmatrix} \frac{6}{5} & \frac{L}{10} & \frac{-6}{5} & \frac{L}{10} \\ & \frac{2L^2}{15} & \frac{-L}{10} & \frac{L^2}{30} \\ & & \frac{6}{5} & \frac{-L}{10} \\ sym & & & \frac{2L^2}{15} \end{bmatrix} \tag{2-1}$$

$\mathbf{U}^E$ and $\mathbf{V}^E$ represent the contribution of the elements to the global matrices $\mathbf{U}$ and $\mathbf{V}$ which are the global stiffness and the global geometric stiffness matrices, respectively. Addition of each element's contribution results in a set of equations given by

$$(\mathbf{U} - p\,\mathbf{V})\mathbf{d} = \mathbf{0} \tag{2-2}$$

where $\mathbf{d}$ is the global vector of nodal variables. Equation (2-2) can be recast in the form of an eigenvalue problem by first multiplying both sides by $\mathbf{U}^{-1}$ and then dividing by p, viz.

$$\left(\mathbf{U}^{-1}\mathbf{V} - \frac{1}{p}\mathbf{I}\right)\mathbf{d} = \mathbf{0} \qquad \text{or} \qquad (\mathbf{A} - p^{-1}\,\mathbf{I})\mathbf{d} = \mathbf{0} \tag{2-3}$$

where $\mathbf{A} = \mathbf{U}^{-1}\mathbf{V}$. The highest eigenvalue (p^{-1}) obtained by the solution of this eigenvalue problem corresponds to the lowest value of the buckling load p. However, the second eigenvalue and the corresponding eigenvector are also needed for the solution of the bimodal problem. Considering this, a suitable eigenvalue solution algorithm which gives the first two eigenvalues and the corresponding eigenvectors is used. The buckling loads and the mode shapes can be closely approximated by using a sufficient number of elements.

2.1.1 Consistent geometric stiffness matrix for distributed axial force

The effect of axial force on a beam in bending depends upon the distribution of axial force $p(x)$. Thus, an incremental stiffness matrix, formulation of which is given by Yang (1986), should be used. When the axial load is not constant along the length of the element, in order to reach a closer approximation, the effect of distributed axial load on stiffness should be taken into

account. A beam element is shown below in Figure 2-1, where $p(x)$ is the load distribution function along the element and can be approximated by eq. (2-4).

$$p(x) = p_0\left[1 + r\left(\frac{x}{L}\right)^{\alpha}\right] \tag{2-4}$$

where, p_0, r and α are constants, x is measured from node 1, and $p(x)$ acts in the direction from node 2 to node 1. The axial force at x is,

$$P(x) = P_0 + P_d(x)$$

where, P_0 is the axial force at node 2 and,

$$P_d(x) = \int_x^L p(\xi)\, d\xi = p_0 L\left\{1 - \frac{x}{L} + \frac{r}{1+\alpha}\left[1 - \left(\frac{x}{L}\right)^{1+\alpha}\right]\right\}$$

The element stiffness matrix, $\mathbf{U}^E$, given in eq. (2-1) is used. However, a new geometric element stiffness matrix, $\mathbf{V}^E$, which includes the influence of distributed load, should be used. The elements of $\mathbf{V}^E$ are given below, Yang (1986).

$$V^E_{11} = V^E_{33} = -V^E_{31} = \frac{6P_0}{5L} + p_0\left[\frac{3}{5} + \frac{r}{1+\alpha}\left(\frac{6}{5} - \frac{36}{4+\alpha} + \frac{72}{5+\alpha} - \frac{36}{6+\alpha}\right)\right]$$

$$V^E_{21} = -V^E_{32} = \frac{P_0}{10} + \frac{p_0 rL}{1+\alpha}\left(\frac{1}{10} + \frac{6}{3+\alpha} - \frac{30}{4+\alpha} + \frac{42}{5+\alpha} - \frac{18}{6+\alpha}\right)$$

$$V^E_{41} = -V^E_{43} = \frac{P_0}{10} + p_0 L\left[\frac{1}{10} + \frac{r}{1+\alpha}\left(\frac{1}{10} - \frac{12}{4+\alpha} + \frac{30}{5+\alpha} - \frac{18}{6+\alpha}\right)\right]$$

$$V^E_{22} = \frac{2P_0 L}{15} + p_0 L^2\left[\frac{1}{10} + \frac{r}{1+\alpha}\left(\frac{2}{15} - \frac{1}{2+\alpha} + \frac{8}{3+\alpha} - \frac{22}{4+\alpha} + \frac{24}{5+\alpha} - \frac{9}{6+\alpha}\right)\right]$$

$$V^E_{42} = \frac{-P_0 L}{30} - p_0 L^2\left[\frac{1}{60} + \frac{r}{1+\alpha}\left(\frac{1}{30} - \frac{2}{3+\alpha} + \frac{11}{4+\alpha} - \frac{18}{5+\alpha} + \frac{9}{6+\alpha}\right)\right]$$

$$V^E_{44} = \frac{2P_0 L}{15} + p_0 L^2\left[\frac{1}{30} + \frac{r}{1+\alpha}\left(\frac{21}{15} - \frac{4}{4+\alpha} + \frac{12}{5+\alpha} - \frac{9}{6+\alpha}\right)\right]$$

Similarly, the problem can be recast in the form of an eigenvalue problem, as given in eq. (2-3). Different types of distributed loads can be modelled using this approach by only changing the coefficients in eq. (2-4). For example, for uniformly distributed load α=0, r=0.

2.1.2 Verification problems for the Hermite beam element

The convergence of the fe model for the two different types of loading are investigated. The non-dimensional buckling parameters presented in Tables 2-1 and 2-2 are $\left(\lambda_0 L^2\right)/\left(\pi^2 EI\right)$ values, where λ_0 is the buckling load and the comparisons are based on the results presented in Young (1989). In these tables S-S, C-S, and C-C denote pinned-pinned, clamped-pinned, and clamped-clamped respectively. In the finite element solution, the column is discretized into 50 elements. The buckling parameters of a uniform straight bar under end load P at B, and a uniformly distributed load p are given for several boundary conditions in Table 2-1. The buckling parameters of a uniform straight bar under end load P at B, and a triangularly

distributed load of maximum value p_0 at end B and linearly decreasing to zero at A are given for several boundary conditions in Table 2-2. It is clear that, the accuracy reached is very high and the element can be used confidently to solve column stability problems.

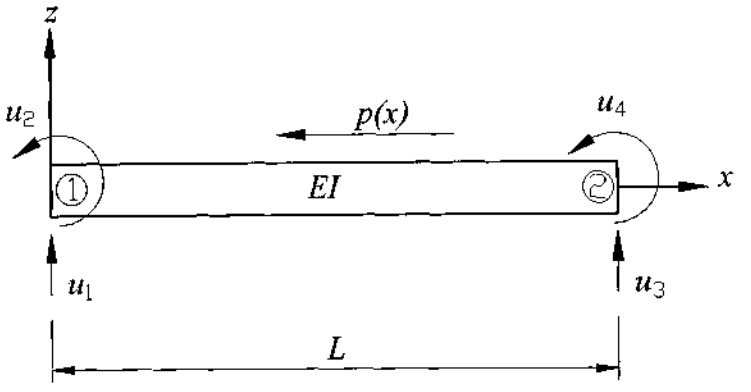

Figure 2-1. Beam finite element with distributed axial load

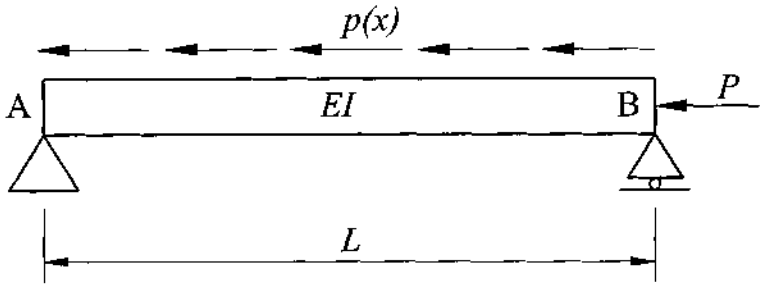

Figure 2-2. Simply supported column under concentrated and distributed axial loads

Table 2-1. Buckling parameters of uniform column under uniformly distributed axial load

$P/(pL)$	S-S[1]	S-S[2]	C-S[1]	C-S[2]	C-C[1]	C-C[2]
-0.25	3.30	3.29	11.30	11.27	13.40	13.35
0.00	1.88	1.88	5.32	5.32	7.56	7.56
0.25	1.30	1.30	3.30	3.30	5.20	5.19
0.50	0.98	0.98	2.37	2.37	3.94	3.94
1.00	0.66	0.66	1.51	1.51	2.65	2.65

[1] Young (1989)
[2] Current work using 50 elements

Table 2-2. Buckling parameters of uniform column under triangularly distributed axial load

$P/(pL)$	S-S[1]	S-S[2]	C-S[1]	C-S[1]	C-C[1]	C-C[2]
-0.25	4.72	4.72	16.10	16.10	21.90	21.92
0.00	3.03	3.04	8.50	8.52	13.40	13.40
0.25	2.22	2.22	5.66	5.66	9.53	9.54
0.50	1.43	1.43	3.36	3.36	6.00	6.01
1.00	0.84	0.84	1.85	1.85	3.44	3.44

[1] Young (1989)
[2] Current work using 50 elements

2.2 Finite element analysis of laminated plates

In this section the plate element used in the calculations is formulated and results of the several verification problems solved are presented. The related functions are listed in Appendix A.2.

Thin plate theory (Kirchoff Theory) does not give accurate results for thick and/or laminated plates where the shear deformations can't be neglected. A better approximation than Kirchoff Theory, Mindlin-Reissner Theory, can be used to include shear deformation. The assumptions of this theory are given below;

* The deflections of the plate (w) are small.
* Normals to the mid-surface before deformation remain straight but not necessarily normal to the mid-surface after deformation.
* Stresses normal to the mid-surface are negligible.

2.2.1 Lamina stress-strain relations

Before proceeding with the formulation of the plate element, the layer stiffnesses should be obtained. The analysis is simplified by assuming that each layer (lamina) is in plane stress state. Most laminates are typically thin and experience a plane-stress state, Reddy (2004). The assumptions for the plane stress condition are given below;

* Thickness is small comparing to side lengths
* There're no surface forces acting on the end faces
* The only nodal displacement components are the mid-surface displacements in the x and y directions, denoted by u and v respectively.

A typical unidirectional lamina is shown below in Fig. 2-3, where 1-2 is the material coordinate system and x-y is the global coordinate system. θ is the angle from the x axis to 1 axis.

For a unidirectionally reinforced lamina in the 1-2 plane, a plane stress state is defined by,

$$\sigma_{11} \neq 0 \qquad \sigma_{22} \neq 0 \qquad \tau_{12} \neq 0$$
$$\sigma_{33} = 0 \qquad \tau_{23} = 0 \qquad \tau_{31} = 0$$

The stress-strain relations in element coordinate system (1-2) are given below in eq. (2-5).

$$\begin{Bmatrix} \sigma_{11} \\ \sigma_{22} \\ \tau_{12} \end{Bmatrix} = \begin{bmatrix} Q_{11} & Q_{12} & 0 \\ Q_{12} & Q_{22} & 0 \\ 0 & 0 & Q_{66} \end{bmatrix} \begin{Bmatrix} \varepsilon_{11} \\ \varepsilon_{22} \\ \gamma_{12} \end{Bmatrix} \tag{2-5}$$

where, for an orthotropic lamina, the reduced stiffness coefficients, Q_{ij}, are;

$$Q_{11} = \frac{E_1}{1-\nu_{12}\nu_{21}} \qquad Q_{12} = \frac{\nu_{12}E_2}{1-\nu_{12}\nu_{21}} = \frac{\nu_{21}E_1}{1-\nu_{12}\nu_{21}} \qquad Q_{22} = \frac{E_2}{1-\nu_{12}\nu_{21}} \qquad Q_{66} = G_{12} \qquad \frac{\nu_{12}}{E_1} = \frac{\nu_{21}}{E_2}$$

When the transverse normal stress is neglected but the transverse shear stresses are included, eq. (2-5) should be appended with the constitutive relations given below;

$$\begin{Bmatrix} \tau_{23} \\ \tau_{13} \end{Bmatrix} = \begin{bmatrix} Q_{44} & 0 \\ 0 & Q_{55} \end{bmatrix} \begin{Bmatrix} \gamma_{23} \\ \gamma_{13} \end{Bmatrix}$$

where $Q_{44} = G_{23}$, and $Q_{55} = G_{13}$.

The (transformed) stress-strain relations in *x-y* coordinate system are given as follows;

$$\begin{Bmatrix} \sigma_x \\ \sigma_y \\ \sigma_{xy} \end{Bmatrix} = \begin{bmatrix} \overline{Q}_{11} & \overline{Q}_{12} & \overline{Q}_{16} \\ \overline{Q}_{21} & \overline{Q}_{22} & \overline{Q}_{26} \\ \overline{Q}_{61} & \overline{Q}_{62} & \overline{Q}_{66} \end{bmatrix} \begin{Bmatrix} \varepsilon_x \\ \varepsilon_y \\ \gamma_{xy} \end{Bmatrix} \quad . \tag{2-6}$$

$$\begin{Bmatrix} \tau_{yz} \\ \tau_{xz} \end{Bmatrix} = \begin{bmatrix} \overline{Q}_{44} & \overline{Q}_{45} \\ \overline{Q}_{45} & \overline{Q}_{55} \end{bmatrix} \begin{Bmatrix} \gamma_{xz} \\ \gamma_{yz} \end{Bmatrix} \tag{2-7}$$

where, the transformed stiffness coefficients, $\overline{Q}_{ij}$, are given below in eq. (2-8);

$$\begin{aligned}
\overline{Q}_{11} &= Q_{11}c^4 + 2(Q_{12} + 2Q_{66})s^2c^2 + Q_{22}s^4 \\
\overline{Q}_{12} &= (Q_{11} + Q_{22} - 4Q_{66})s^2c^2 + Q_{12}(s^4 + c^4) \\
\overline{Q}_{22} &= Q_{11}s^4 + 2(Q_{12} + 2Q_{66})s^2c^2 + Q_{22}c^4 \\
\overline{Q}_{16} &= (Q_{11} - Q_{12} - 2Q_{66})sc^3 + (Q_{12} - Q_{22} + 2Q_{66})s^3c \\
\overline{Q}_{26} &= (Q_{11} - Q_{12} - 2Q_{66})s^3c + (Q_{12} - Q_{22} + 2Q_{66})sc^3 \\
\overline{Q}_{66} &= (Q_{11} + Q_{22} - 2Q_{12} - 2Q_{66})s^2c^2 + Q_{66}(s^4 + c^4) \\
\overline{Q}_{44} &= Q_{44}c^2 + Q_{55}s^2 \\
\overline{Q}_{45} &= (Q_{55} - Q_{44})cs \\
\overline{Q}_{55} &= Q_{44}s^2 + Q_{55}c^2
\end{aligned} \tag{2-8}$$

Here c and s denotes $\cos(\theta)$ and $\sin(\theta)$ respectively. This transformation is explained in detail as follows;

A second order tensor is transformed according to the following rule;

$T'_{ij} = A_{ik}T_{kl}A_{jl}$ or in matrix form $\mathbf{T'} = \mathbf{ATA}^T$

and the transformation matrix, **A**, for the coordinate transformation shown in Fig. 2-3 is;

$$\mathbf{A} = \begin{bmatrix} c & s & 0 \\ -s & c & 0 \\ 0 & 0 & 1 \end{bmatrix}$$

If we re-arrange the transformation equation making use of the relation (for ortho-normal bases) $\mathbf{A}^{-1} = \mathbf{A}^T$, the inverse relation becomes, $\mathbf{T} = \mathbf{A}^T\mathbf{T'}\mathbf{A}$. Stress and strain tensors are second order tensors, thus these transformations apply to both. Let's first calculate the transformed stresses;

$$\begin{bmatrix} \sigma_{11} & \sigma_{12} & \sigma_{13} \\ \sigma_{12} & \sigma_{22} & \sigma_{23} \\ \sigma_{13} & \sigma_{23} & \sigma_{33} \end{bmatrix} = \begin{bmatrix} c & s & 0 \\ -s & c & 0 \\ 0 & 0 & 1 \end{bmatrix} \begin{bmatrix} \sigma_x & \sigma_{xy} & \sigma_{xz} \\ \sigma_{xy} & \sigma_y & \sigma_{yz} \\ \sigma_{xz} & \sigma_{yz} & \sigma_z \end{bmatrix} \begin{bmatrix} c & -s & 0 \\ s & c & 0 \\ 0 & 0 & 1 \end{bmatrix}$$

and re-arrange as given below in eq. (2-9).

$$\boldsymbol{\sigma}' = \mathbf{T}_s\boldsymbol{\sigma} = \begin{Bmatrix}\sigma_{11}\\ \sigma_{22}\\ \sigma_{33}\\ \sigma_{23}\\ \sigma_{13}\\ \sigma_{12}\end{Bmatrix} = \begin{bmatrix} c^2 & s^2 & 0 & 0 & 0 & 2cs \\ s^2 & c^2 & 0 & 0 & 0 & -2cs \\ 0 & 0 & 1 & 0 & 0 & 0 \\ 0 & 0 & 0 & c & -s & 0 \\ 0 & 0 & 0 & s & c & 0 \\ -cs & cs & 0 & 0 & 0 & \left(c^2 - s^2\right) \end{bmatrix} \begin{Bmatrix}\sigma_x\\ \sigma_y\\ \sigma_z\\ \sigma_{yz}\\ \sigma_{xz}\\ \sigma_{xy}\end{Bmatrix} \tag{2-9}$$

In order to apply a failure theory based on stress, the stresses in global coordinate system should be transformed into material coordinates associated with each layer using eq. (2-9). Similar manipulations yield the following results for strains,

$$\begin{bmatrix}\varepsilon_{11} & \varepsilon_{12} & \varepsilon_{13}\\ \varepsilon_{12} & \varepsilon_{22} & \varepsilon_{23}\\ \varepsilon_{13} & \varepsilon_{23} & \varepsilon_{33}\end{bmatrix} = \begin{bmatrix} c & s & 0 \\ -s & c & 0 \\ 0 & 0 & 1 \end{bmatrix} \begin{bmatrix}\varepsilon_x & \varepsilon_{xy} & \varepsilon_{xz}\\ \varepsilon_{xy} & \varepsilon_y & \varepsilon_{yz}\\ \varepsilon_{xz} & \varepsilon_{yz} & \varepsilon_z\end{bmatrix} \begin{bmatrix} c & -s & 0 \\ s & c & 0 \\ 0 & 0 & 1 \end{bmatrix}$$

$$\boldsymbol{\varepsilon}' = \mathbf{T}_\varepsilon\boldsymbol{\varepsilon} = \begin{Bmatrix}\varepsilon_{11}\\ \varepsilon_{22}\\ \varepsilon_{33}\\ 2\varepsilon_{23}\\ 2\varepsilon_{13}\\ 2\varepsilon_{12}\end{Bmatrix} = \begin{bmatrix} c^2 & s^2 & 0 & 0 & 0 & cs \\ s^2 & c^2 & 0 & 0 & 0 & -cs \\ 0 & 0 & 1 & 0 & 0 & 0 \\ 0 & 0 & 0 & c & -s & 0 \\ 0 & 0 & 0 & s & c & 0 \\ -2cs & 2cs & 0 & 0 & 0 & \left(c^2 - s^2\right) \end{bmatrix} \begin{Bmatrix}\varepsilon_x\\ \varepsilon_y\\ \varepsilon_z\\ 2\varepsilon_{yz}\\ 2\varepsilon_{xz}\\ 2\varepsilon_{xy}\end{Bmatrix} \tag{2-10}$$

The following manipulations yield the result given in eq. (2-11), which is the same as eq. (2-8).

$$\begin{aligned}\boldsymbol{\sigma} &= \mathbf{T}_\sigma^{-1}\boldsymbol{\sigma}' = \mathbf{T}_\sigma^{-1}\mathbf{Q}'\boldsymbol{\varepsilon}' = \mathbf{T}_\sigma^{-1}\mathbf{Q}'\mathbf{T}_\varepsilon\boldsymbol{\varepsilon}\\ \mathbf{Q} &= \mathbf{T}_\sigma^{-1}\mathbf{Q}'\mathbf{T}_\varepsilon\end{aligned} \tag{2-11}$$

where, $\mathbf{T}_\sigma^{-1}$ can be calculated simply by interchanging θ by $-\theta$ as shown below;

$$\mathbf{T}_\sigma^{-1} = \begin{bmatrix} c^2 & s^2 & 0 & 0 & 0 & -2cs \\ s^2 & c^2 & 0 & 0 & 0 & 2cs \\ 0 & 0 & 1 & 0 & 0 & 0 \\ 0 & 0 & 0 & c & -s & 0 \\ 0 & 0 & 0 & s & c & 0 \\ cs & -cs & 0 & 0 & 0 & \left(c^2 - s^2\right) \end{bmatrix}$$

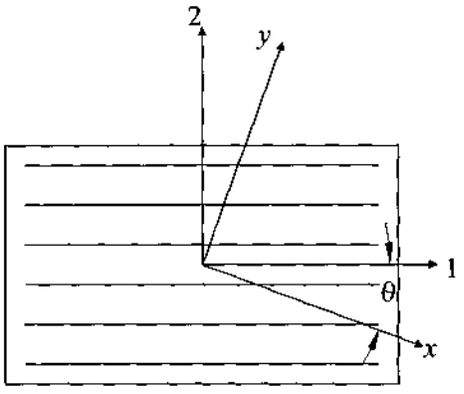

Figure 2-3. A typical unidirectional lamina

2.2.2 First order shear deformable plate theory

The displacement field corresponding to first order shear deformation theory (FSDT) for composite laminated plates is as follows:

$$\begin{aligned} u(x,y,z) &= u_0(x,y) - z\theta_x(x,y) \\ v(x,y,z) &= v_0(x,y) - z\theta_y(x,y) \\ w(x,y,z) &= w_0(x,y) \end{aligned} \tag{2-12}$$

where u_0, v_0, and w_0 are the mid-surface displacement components and θ_x, and θ_y are the rotations of the normal of the mid-surface about x and y axes. The x-y plane coincides with the mid-surface of the plate and the plate thickness is denoted by t.

$$\boldsymbol{\chi} = \begin{Bmatrix} \chi_x \\ \chi_y \\ \chi_{xy} \end{Bmatrix} = -\begin{Bmatrix} \theta_{x,x} \\ \theta_{y,y} \\ (\theta_{x,y} + \theta_{y,x}) \end{Bmatrix} \qquad \boldsymbol{\varepsilon}^0 = \begin{Bmatrix} \varepsilon_x^0 \\ \varepsilon_y^0 \\ \gamma_{xy}^0 \end{Bmatrix} = \begin{Bmatrix} u_{0,x} \\ v_{0,y} \\ (u_{0,y} + v_{0,x}) \end{Bmatrix} \qquad \boldsymbol{\phi} = \begin{Bmatrix} \phi_x \\ \phi_y \end{Bmatrix} = \begin{Bmatrix} \theta_x - w_{,x} \\ \theta_y - w_{,y} \end{Bmatrix}$$

where ϕ_x, ϕ_y are the the rotations due to shear about x and y axes and χ_x, χ_y, χ_{xy} and ε_x^0, ε_y^0, ε_{xy}^0 are the curvatures and mid-surface strains respectively. A comma denotes partial differentiation w.r.t the following variable. These equations are given below in matrix form;

$$\boldsymbol{\chi} = \mathbf{B}_\chi \delta, \qquad \boldsymbol{\varepsilon}^0 = \mathbf{B}_\varepsilon \delta, \qquad \boldsymbol{\phi} = \mathbf{B}_\phi \delta$$

where $\delta = \{u \quad v \quad w \quad \theta_x \quad \theta_y\}^T$ and $\mathbf{B}_\chi$, $\mathbf{B}_\varepsilon$, $\mathbf{B}_\phi$ are given below in equations (2-13), (2-14), and (2-15) in matrix form:

$$\mathbf{B}_\chi = \begin{bmatrix} 0 & 0 & 0 & -\partial/\partial x & 0 \\ 0 & 0 & 0 & 0 & -\partial/\partial y \\ 0 & 0 & 0 & -\partial/\partial y & -\partial/\partial x \end{bmatrix} \tag{2-13}$$

$$\mathbf{B}_c = \begin{bmatrix} \partial/\partial x & 0 & 0 & 0 & 0 \\ 0 & \partial/\partial y & 0 & 0 & 0 \\ \partial/\partial y & \partial/\partial x & 0 & 0 & 0 \end{bmatrix} \tag{2-14}$$

$$\mathbf{B}_\phi = \begin{bmatrix} 0 & 0 & -\partial/\partial x & 1 & 0 \\ 0 & 0 & -\partial/\partial y & 0 & 1 \end{bmatrix} \tag{2-15}$$

Moments, normal forces and shear forces are given below in equations (2-16), (2-17), and (2-18).

$$\mathbf{M} = \begin{Bmatrix} M_x \\ M_y \\ M_{xy} \end{Bmatrix} = \mathbf{D}\boldsymbol{\chi} + \mathbf{B}\boldsymbol{\varepsilon}^0 = \mathbf{D}\begin{Bmatrix} \chi_x \\ \chi_y \\ \chi_{xy} \end{Bmatrix} + \mathbf{B}\begin{Bmatrix} \varepsilon_x^0 \\ \varepsilon_y^0 \\ \gamma_{xy}^0 \end{Bmatrix} \tag{2-16}$$

$$\mathbf{N} = \begin{Bmatrix} N_x \\ N_y \\ N_{xy} \end{Bmatrix} = \mathbf{B}\boldsymbol{\chi} + \mathbf{A}\boldsymbol{\varepsilon}^0 = \mathbf{B}\begin{Bmatrix} \chi_x \\ \chi_y \\ \chi_{xy} \end{Bmatrix} + \mathbf{A}\begin{Bmatrix} \varepsilon_x^0 \\ \varepsilon_y^0 \\ \gamma_{xy}^0 \end{Bmatrix} \tag{2-17}$$

$$\mathbf{Q} = \begin{Bmatrix} Q_x \\ Q_y \end{Bmatrix} = \mathbf{C}_s \begin{Bmatrix} \phi_x \\ \phi_y \end{Bmatrix} \tag{2-18}$$

where, for a laminated composite plate the matrices **A**, **B**, **D**, $\mathbf{C}_s$ are calculated as follows;

$$A_{ij} = \sum_{k=1}^{N} \left(\overline{Q}_{ij}\right)_k (z_k - z_{k-1}) \qquad i,j=1,2,6 \tag{2-19}$$

$$B_{ij} = \frac{1}{2}\sum_{k=1}^{N} \left(\overline{Q}_{ij}\right)_k \left(z_k^2 - z_{k-1}^2\right) \qquad i,j=1,2,6 \tag{2-20}$$

$$D_{ij} = \frac{1}{3}\sum_{k=1}^{N} \left(\overline{Q}_{ij}\right)_k \left(z_k^3 - z_{k-1}^3\right) \qquad i,j=1,2,6 \tag{2-21}$$

$$C_{ij} = \sum_{k=1}^{N} \left(\overline{Q}_{ij}\right)_k (z_k - z_{k-1}) \qquad i,j=4,5 \tag{2-22}$$

$$\mathbf{C}_s = \begin{bmatrix} K_1 C_{55} & \sqrt{K_1 K_2} C_{45} \\ \sqrt{K_1 K_2} C_{45} & K_2 C_{44} \end{bmatrix} \tag{2-23}$$

where K_1 and K_2 are the shear correction factors and z_{k-1}, z_k are the coordinates of the lower and upper surfaces of the k^{th} layer in the z direction. The shear correction factors are taken as equal to 5/6 in this study, unless otherwise stated.

2.2.3 Finite element formulation

2.2.3.1 Linear static analysis using FEM

One of the reasons of selecting the 8 noded elements is to avoid the parasitic shear or shear locking problem which arises when linear iso-parametric elements are used. Using the curved elements and making use of reduced integration shear locking problem can be avoided, Hinton and Owen (1979). The second reason is the ease in modeling complex geometries, Cook (1973). The interpolation function of the displacement field is defined as follows:

$$\begin{Bmatrix} u_0 \\ v_0 \\ w_0 \\ \theta_x \\ \theta_y \end{Bmatrix} = \begin{Bmatrix} u_0 \\ v_0 \\ w_0 \\ w_{,x} + \phi_x \\ w_{,y} + \phi_y \end{Bmatrix} = \sum_{i=1}^{8} S_i \delta_i \,, \tag{2-24}$$

where, S_i is the shape function at node i, and the displacement vector at node i is $\delta_i = \{u_i, v_i, w_i, \theta_{xi}, \theta_{yi}\}^T$. The shape functions, and their first derivatives w.r.t. local coordinates ξ and η are given in equations (2-25a), (2-25b), and (2-25c).

$$\begin{aligned} S_i &= \frac{1}{4}(1+\xi\xi_i)(1+\eta\eta_i)(\xi\xi_i+\eta\eta_i-1) \quad i=1,3,5,7 \\ S_i &= \frac{1}{2}(1-\xi^2)(1+\eta\eta_i) \quad i=2,6 \\ S_i &= \frac{1}{2}(1+\xi\xi_i)(1-\eta^2) \quad i=4,8 \end{aligned} \tag{2-25.a}$$

$$\begin{aligned} S_{i,\xi} &= \frac{1}{4}(2\xi+\eta\xi_i\eta_i+2\xi\eta\eta_i+\eta^2\xi_i) \\ S_{i,\xi} &= -\xi(1+\eta\eta_i) \\ S_{i,\xi} &= \frac{\xi_i}{2}(1-\eta^2) \end{aligned} \tag{2-25.b}$$

$$\begin{aligned} S_{i,\eta} &= \frac{1}{4}(2\eta+\xi\xi_i\eta_i+\xi^2\eta_i+2\xi\eta\xi_i) \\ S_{i,\eta} &= \frac{\eta_i}{2}(1-\xi^2) \\ S_{i,\eta} &= -\eta(1+\xi\xi_i) \end{aligned} \tag{2-25.c}$$

The strain displacement relations for an element are given below,

$$\boldsymbol{\varepsilon}^0 = \left[\mathbf{B}_\varepsilon^{\,1},\ldots,\mathbf{B}_\varepsilon^{\,8}\right]\delta_e \tag{2-26}$$

$$\boldsymbol{\chi} = \left[\mathbf{B}_\chi^{\,1},\ldots,\mathbf{B}_\chi^{\,8}\right]\delta_e \tag{2-27}$$

$$\boldsymbol{\phi} = \left[\mathbf{B}_\phi^{\,1},\ldots,\mathbf{B}_\phi^{\,8}\right]\delta_e \tag{2-28}$$

where, δ_e is the element displacement vector, and the strain-displacement matrices are defined below in equations (2-29) to (2-34).

$$\boldsymbol{\varepsilon}^0 = \begin{Bmatrix} \varepsilon_x^0 \\ \varepsilon_y^0 \\ \gamma_{xy}^0 \end{Bmatrix} = \begin{Bmatrix} u_{0,x} \\ v_{0,y} \\ \left(u_{0,y} + v_{0,x}\right) \end{Bmatrix} = \left[\mathbf{B}_{\varepsilon 1}, \ldots, \mathbf{B}_{\varepsilon 8}\right] \{\delta_1 \ldots \delta_8\}^T \tag{2-29}$$

$$\mathbf{B}_{\varepsilon i} = \begin{bmatrix} \partial N_i/\partial x & 0 & 0 & 0 & 0 \\ 0 & \partial N_i/\partial y & 0 & 0 & 0 \\ \partial N_i/\partial y & \partial N_i/\partial x & 0 & 0 & 0 \end{bmatrix} \tag{2-30}$$

$$\boldsymbol{\chi} = \begin{Bmatrix} \chi_x \\ \chi_y \\ \chi_{xy} \end{Bmatrix} = \begin{Bmatrix} -\theta_{x,x} \\ -\theta_{y,y} \\ -\left(\theta_{x,y} + \theta_{y,x}\right) \end{Bmatrix} = \left[\mathbf{B}_{\chi 1}, \ldots, \mathbf{B}_{\chi 8}\right] \{\delta_1 \ldots \delta_8\}^T \tag{2-31}$$

$$\mathbf{B}_{\chi i} = \begin{bmatrix} 0 & 0 & 0 & -\partial N_i/\partial x & 0 \\ 0 & 0 & 0 & 0 & -\partial N_i/\partial y \\ 0 & 0 & 0 & -\partial N_i/\partial y & -\partial N_i/\partial x \end{bmatrix} \tag{2-32}$$

$$\boldsymbol{\phi} = \begin{Bmatrix} \phi_x \\ \phi_y \end{Bmatrix} = \begin{Bmatrix} \theta_x - w_{,x} \\ \theta_y - w_{,y} \end{Bmatrix} = \left[\mathbf{B}_{\phi 1}, \ldots, \mathbf{B}_{\phi 8}\right] \{\delta_1 \ldots \delta_8\}^T \tag{2-33}$$

$$\mathbf{B}_{\phi i} = \begin{bmatrix} 0 & 0 & -\partial N_i/\partial x & N_i & 0 \\ 0 & 0 & -\partial N_i/\partial y & 0 & N_i \end{bmatrix} \tag{2-34}$$

Using these equations, the total potential energy of element e, π_e, can be written as:

$$\pi_e = \frac{1}{2}\int_A \left(\mathbf{M}^T\boldsymbol{\chi} + \mathbf{Q}^T\boldsymbol{\phi} + \mathbf{N}^T\boldsymbol{\varepsilon}^0\right) dA - \textit{contribution of external loads} \tag{2-35}$$

Rewriting the terms in the integral yields;

$$\mathbf{M}^T\boldsymbol{\chi} = \left(\mathbf{D}\boldsymbol{\chi} + \mathbf{B}\boldsymbol{\varepsilon}^0\right)^T\boldsymbol{\chi} = \boldsymbol{\chi}^T\mathbf{D}\boldsymbol{\chi} + \boldsymbol{\varepsilon}^{0T}\mathbf{B}\boldsymbol{\chi} = \delta_e^T\left(\mathbf{B}_\chi^T\mathbf{D}\mathbf{B}_\chi + \mathbf{B}_c^T\mathbf{B}\mathbf{B}_\chi\right)\delta_e$$

$$\mathbf{Q}^T\boldsymbol{\phi} = \boldsymbol{\phi}^T\mathbf{C}\boldsymbol{\phi} = \delta_e^T\left(\mathbf{B}_\phi^T\mathbf{C}_s\mathbf{B}_\phi\right)\delta_e$$

$$\mathbf{N}^T\boldsymbol{\varepsilon}^0 = \left(\mathbf{A}\boldsymbol{\varepsilon}^0 + \mathbf{B}\boldsymbol{\chi}\right)^T\boldsymbol{\varepsilon}^0 = \boldsymbol{\varepsilon}^{0T}\mathbf{A}\boldsymbol{\varepsilon}^0 + \boldsymbol{\chi}^T\mathbf{B}\boldsymbol{\varepsilon}^0 = \delta_e^T\left(\mathbf{B}_\varepsilon^T\mathbf{A}\mathbf{B}_\varepsilon + \mathbf{B}_\chi^T\mathbf{B}\mathbf{B}_\varepsilon\right)\delta_e$$

The total potential energy can be minimized by differentiating π_e w.r.t. δ_e which results in the element stiffness matrix given below in eq. (2-36).

$$\mathbf{K}_e = \int_{A^e}\left(\mathbf{B}_\chi^T\mathbf{D}\mathbf{B}_\chi + \mathbf{B}_\varepsilon^T\mathbf{B}\mathbf{B}_\chi + \mathbf{B}_\phi^T\mathbf{C}_s\mathbf{B}_\phi + \mathbf{B}_\varepsilon^T\mathbf{A}\mathbf{B}_\varepsilon + \mathbf{B}_\chi^T\mathbf{B}\mathbf{B}_\varepsilon\right)dA \tag{2-36}$$

2.2.3.2 Stability analysis using FEM

The two basic approaches in solution of stability problems of (composite) plates using finite elements are briefly explained as follows:

The first approach is the linearized stability (or eigenvalue) analysis which yields very accurate results for moderately thick symmetrically laminated plate problems. The computational time to obtain the buckling loads is lower comparing to a geometrically non-linear analysis and the computational procedure is simpler if the total d.o.f. is relatively low. Thus, in this study it is concluded to use this approach in solving the stability problems. This approach can only be safely used when certain conditions are satisfied which will be explained in the following section. Linearized stability analysis is also stated to be applicable to developable shell instability problems by Cook (1973). However, nonlinear action is more often found in doubly curved shells than in flat plates, and developable shells. Finally, when dealing with anti-symmetrically laminated plate and doubly curved shell stability problems, a geometrically non-linear analysis, which is computationally expensive, should be performed.

Symmetrically laminated plate stability problems can be approximately and efficiently solved using linearized finite element stability analysis. However, when the mesh is very dense or the structure is large, this simplified analysis necessitates solution of very large eigenvalue problems which introduces a serious computational problem which has to be solved. In this study, the basic eigenvalue solver provided in MATLAB® is used as the number of unknowns is limited. Advanced methods, such as the subspace iteration method, are given in Bathe (1995).

The second approach is performing a geometrically non-linear analysis using shell elements. This can be done either by using a 'Total Lagrangian Formulation' (TLF) or an 'Updated Lagrangian Formulation' (ULF, or moving coordinates), Reddy (2004). Use of the TLF is more complicated comparing to the ULF mainly because of the need to modify the element stiffness matrices. The ULF is the easier, yet very reliable and accurate, Reddy (2004). However, non-linear analysis is beyond the scope of this study as it is computationally more expensive comparing to the linearized stability analysis to be used in solving the optimization problems considered.

2.2.3.2(a) Linearized stability analysis using FEM

The assumptions due to the limitations of the theory are stated below;

Assumptions: Membrane (in-plane) forces can be determined by a linear analysis and they remain constant during the deformation caused by a second set of loads or by buckling. As a consequence of these assumptions, the solution is only valid for symmetric laminates where there is no bending-extension coupling.

The steps of the solution method can be explained as follows, Hinton and Owen (1977);

i) Calculate the membrane forces by using a standard plane-stress analysis, provided that the assumptions are satisfied.
ii) Calculate the initial stress or geometric stiffness matrix using the membrane stresses calculated in step *i*.
iii) Calculate the buckling load parameter λ, which is defined as the ratio of actual buckling load to the applied forces at which the plate buckles, by solving the eigenvalue problem given in eq. (2-37). The element geometric stiffness matrix is derived considering that the plate element is subjected to a prescribed in-plane stress system leading to buckling.

$$\det(\mathbf{K} - \lambda \mathbf{K}_G) = 0 \qquad (2\text{-}37)$$

where $\mathbf{K}$ is the global stiffness matrix and $\mathbf{K}_G$ is the global geometric stiffness matrix. The derivation of the element geometric stiffness matrix, $\mathbf{K}_G^e$, is given next.

2.2.3.2(b) Element geometric stiffness matrix

The non-linear terms of the mid-surface strains associated with the von Karman plate theory are given below in eq. (2-38), Reddy (2004).

$$\boldsymbol{\varepsilon}_{NL}^0 = \begin{Bmatrix} \frac{1}{2} w_{0,x}^2 \\ \frac{1}{2} w_{0,y}^2 \\ w_{0,x} w_{0,y} \end{Bmatrix} \tag{2-38}$$

Here, following Reddy's approach, only some of the non-linear terms of the von Karman strains which are related to bending deformation are kept in formulating the geometric stiffness matrix. It is assumed that the potential energy of the applied stresses arises from the action of these stresses on the corresponding second order strains according to Von Karman plate theory. It should be kept in mind that, this exclusion can cause over-prediction of buckling loads if the plate is too thick. Also, this assumption may lead to erroneous results when in-plane deformations are not negligibly small, because in Von Karman plate theory the second derivatives of the displacements u and v are not taken into account.

The potential energy of the applied stresses, V_e arising from the action of the in-plane stresses on the corresponding second order strains is given below in eq. (2-39)

$$V_e = \frac{1}{2} \int_A \left(\begin{Bmatrix} N_{xx} \\ N_{yy} \\ N_{xy} \end{Bmatrix}^T \cdot \boldsymbol{\varepsilon}_{NL}^0 \right) dA \tag{2-39}$$

where N_{xx}, N_{xy}, N_{yy} are the in-plane forces at the Gauss points which are calculated at the Gauss points by a primer static analysis. Rewriting the terms in the integral yields:

$$V_e = \frac{1}{2} \int_A \boldsymbol{\delta}_e^T \left(\mathbf{G}^T \mathbf{S} \mathbf{G} \right) \boldsymbol{\delta}_e \, dA$$

where,

$$\mathbf{G}\boldsymbol{\delta}^e = \left[\mathbf{G}_1, \ldots, \mathbf{G}_8 \right] \left\{ \boldsymbol{\delta}_1 \ldots \boldsymbol{\delta}_8 \right\}^T = \left\{ w_{0,x} \quad w_{0,y} \right\}^T \tag{2-40}$$

$$\mathbf{G}_i = \begin{bmatrix} 0 & 0 & N_{i,x} & 0 & 0 \\ 0 & 0 & N_{i,y} & 0 & 0 \end{bmatrix} \qquad \text{and } \mathbf{S} = \begin{bmatrix} N_{xx} & N_{xy} \\ N_{xy} & N_{yy} \end{bmatrix} \tag{2-41}$$

The potential energy of the in-plane forces can be minimized by differentiating w.r.t. $\mathbf{d}_e$ which results in the element geometric stiffness matrix given below in eq. (2-42).

$$\mathbf{K}_G^e = \int_{-1}^{1} \int_{-1}^{1} \mathbf{G}^T \mathbf{S} \mathbf{G} |\mathbf{J}| d\xi d\eta \tag{2-42}$$

2.2.3.3 Treatment of inclined boundaries

The finite element code has to be modified to deal with the inclined boundary conditions. The steps to be taken in this modification are given below, Hinton and Owen (1977);

i. For any node to be restrained in local directions, transform the applied nodal forces to coincide with the local axes.
ii. Transform the relevant element stiffness matrices.
iii. Assemble the loads and stiffnesses in the usual way and solve for displacements.
iv. Transform the displacements and reactions in the local directions to the global coordinate system before evaluating the stresses.

Let the coordinate axes related to a node i on the boundary is rotated by θ_i degrees. The global to local transformation matrix for this node of element e becomes:

$$\mathbf{T}_{ie} = \begin{bmatrix} c & s & 0 & 0 & 0 \\ -s & c & 0 & 0 & 0 \\ 0 & 0 & 1 & 0 & 0 \\ 0 & 0 & 0 & c & s \\ 0 & 0 & 0 & -s & c \end{bmatrix} \tag{2-43}$$

where $c = \cos\theta_i$ and $s = \sin\theta_i$. The complete transformation matrix for the element is given below.

$$\mathbf{T}_e = \begin{bmatrix} \mathbf{T}_{1e} & \mathbf{0} & \mathbf{0} \\ \mathbf{0} & \ddots & \mathbf{0} \\ \mathbf{0} & \mathbf{0} & \mathbf{T}_{8e} \end{bmatrix}_{(40\times 40)} \tag{2-44}$$

The displacement vector, load vector, element stiffness matrix, and element geometric stiffness matrix are transformed as shown below;

$$\boldsymbol{\delta}'_e = \mathbf{T}\boldsymbol{\delta}_e,$$
$$\mathbf{f}'_e = \mathbf{T}\mathbf{f}_e,$$
$$\mathbf{K}_e' = \mathbf{T}_e\mathbf{K}_e\mathbf{T}_e^T,$$
$$\mathbf{G}_e' = \mathbf{T}_e\mathbf{G}_e\mathbf{T}_e^T.$$

where the primes denote the transformation.

2.2.3.4 Stress evaluation-smoothing technique

The Gauss points are the best points to calculate stresses, however, especially for comparison reasons, the stresses at the element nodes are also required. To solve this problem the method given in Hinton and Owen, (1977) is used, which is defined as follows. The technique is simply a bilinear extrapolation of the 2×2 Gauss point stress values. The smoothed corner node stresses may be calculated using eq. (2-45) given below;

$$\begin{Bmatrix}\sigma_1\\ \sigma_3\\ \sigma_5\\ \sigma_7\end{Bmatrix}=\begin{bmatrix}1+\frac{\sqrt{3}}{2} & -\frac{1}{2} & 1-\frac{\sqrt{3}}{2} & -\frac{1}{2}\\ & 1+\frac{\sqrt{3}}{2} & -\frac{1}{2} & 1-\frac{\sqrt{3}}{2}\\ & & 1+\frac{\sqrt{3}}{2} & -\frac{1}{2}\\ sym. & & & 1+\frac{\sqrt{3}}{2}\end{bmatrix}\begin{Bmatrix}\sigma_I\\ \sigma_{II}\\ \sigma_{III}\\ \sigma_{IV}\end{Bmatrix} \tag{2-45}$$

where σ_i, $i=1,3,5,7$ and σ_j, $j=I,II,III,IV$ are smoothed stresses at the corner nodes and the stresses at the Gauss points respectively. The stresses at mid-side nodes can be evaluated simply by averaging the values at the associated corner nodes, since the distribution of the smoothed stress is linear along the sides of the element. Smoothed values should subsequently be averaged to obtain unique values at nodes.

2.2.4 First-ply failure analysis using FEM

Several failure criteria have been proposed for application to composites, and the most popular ones are maximum stress, maximum strain, Hoffman's, Tsai-Wu and Tsai-Hill, as stated by Soni (1983). The two additional criteria proposed by Hahn, Erikson and Tsai (1982) and Hashin (1980) are based on separating the stress polynomial into two parts, one related to matrix failure and the other related to fiber failure. A review of several criteria currently in use is given by Rowlands (1985). Generally, it is assumed that the failure occurs at a point in the laminate when stresses or strains satisfy a certain condition at that point.

Here, formulations for Tsai-Hill, Tsai-Wu, and Maximum Strain criteria are given. Several verification problems are solved, however the results given for the first-ply failure analysis of fiber reinforced laminated plates by Reddy and Pandey (1987) could not be obtained. Moreover, their results have been used by Prusty *et al.* (2001) for verification purposes, and it has been claimed that the results were in good agreement. However, numerical and exact results for one of the problems given in Reddy and Pandey (1987) were also given by Cho and Yoon (1998) and the results obtained in this study precisely agree with them. It is evident that the results given by Reddy and Pandey (1987) are in error and therefore their results are not used here for verification purposes. It should be noted that similar problems were solved by Reddy and Reddy (1992), and the results presented are in good agreement with the present results and the results presented by Cho and Yoon (1998).

The maximum stress and maximum strain failure criteria are based on engineering intuition and the maximum strain criterion also provides some interaction between stresses as stated by Groenwold and Haftka (2006). It is stated by Swanson (1997) that, the Tsai-Wu criterion is sensitive to the transverse stresses and overly conservative under condition of multi-axial tensile stress. Also, the Tsai-Wu criterion does not take into account the differences between compressive and tensile strength, which makes the results obtained using this criterion susceptible to error.

As $\sigma_3=0$, only some of the components of the strength tensor need to be cafculated and the failure criteria for FSDT is given below:

$$F_1\sigma_1+F_2\sigma_2+F_{11}\sigma_1^2+F_{22}\sigma_2^2+2F_{12}\sigma_1\sigma_2+F_{44}\sigma_4^2+F_{55}\sigma_5^2+F_{66}\sigma_6^2\geq 1 \tag{2-46}$$

where, the subscripts 1, 2 ,3 ,4 ,5, and 6 denote *x*, *y*, *z*, *yz*, *xz*, and *xy* respectively. The various *F* terms can be related to experimental data on ply failure by evaluating the stress polynomial

given in eq. (2-46) for the various simple material property test conditions, Swanson (1997). Below, the calculation of the F terms for the maximum strain and Tsai-Wu failure criteria and the details of Hill's criterion are given. Here, X_C, Y_C, Z_C are the compressive stress strengths of lamina in the x, y, z directions respectively and X_T, Y_T, Z_T are the tensile stress strengths of lamina in the x, y, z directions respectively. R, S, T are the shear stress strengths of lamina in yz, xz, xy planes respectively.

Maximum Strain Criterion

The F terms are given below, which are obtained using the compliance matrix and the constitutive relation, Reddy and Pandey (1987).

$$F_1^A = \frac{1}{X_T} - \frac{1}{X_C} \qquad F_2^A = \frac{1}{Y_T} - \frac{1}{Y_C} \qquad F_3^A = \frac{1}{Z_T} - \frac{1}{Z_C}$$

$$F_1^{MS} = F_1^A + \frac{S_{12}}{S_{22}} F_2^A + \frac{S_{13}}{S_{33}} F_3^A$$

$$F_2^{MS} = \frac{S_{12}}{S_{11}} F_1^A + F_2^A + \frac{S_{23}}{S_{33}} F_3^A$$

$$F_{11}^{MS} = \frac{1}{X_T X_C} + \left(\frac{S_{12}}{S_{22}}\right)^2 \frac{1}{Y_T T_C} + \left(\frac{S_{13}}{S_{33}}\right)^2 \frac{1}{Z_T Z_C} - \frac{S_{13}}{S_{33}} F_1^A F_2^A - \frac{S_{12}}{S_{22}} F_1^A F_2^A - \frac{S_{12} S_{13}}{S_{22} S_{23}} F_2^A F_3^A$$

$$F_{22}^{MS} = \frac{1}{Y_T Y_C} + \left(\frac{S_{12}}{S_{11}}\right)^2 \frac{1}{X_T X_C} + \left(\frac{S_{23}}{S_{33}}\right)^2 \frac{1}{Z_T Z_C} - \frac{S_{12}}{S_{11}} F_1^A F_2^A - \frac{S_{23}}{S_{33}} F_2^A F_3^A - \frac{S_{12} S_{23}}{S_{11} S_{33}} F_1^A F_3^A$$

$$F_{12}^{MS} = \frac{S_{12}}{S_{11}} \frac{1}{X_T X_C} + \frac{S_{12}}{S_{22}} \frac{1}{Y_T Y_C} + \frac{S_{13} S_{23}}{S_{33}^2} \frac{1}{Z_T Z_C} - \frac{1}{2}\left(\frac{S_{12}^2}{S_{11} S_{22}}\right) F_1^A F_2^A - \frac{1}{2}\left(\frac{S_{12}^2}{S_{11} S_{22}} + 1\right) F_1^A F_2^A \cdots$$
$$- \frac{1}{2}\left(\frac{S_{13} S_{12}}{S_{11} S_{33}} + \frac{S_{23}}{S_{33}}\right) F_1^A F_3^A - \frac{1}{2}\left(\frac{S_{12} S_{23}}{S_{22} S_{33}} + \frac{S_{13}}{S_{33}}\right) F_2^A F_3^A$$

$$F_{44}^{MS} = \frac{1}{R^2} \qquad F_{55}^{MS} = \frac{1}{S^2} \qquad F_{66}^{MS} = \frac{1}{T^2}$$

where S_{ij} are the components of the compliance matrix.

The Tsai-Wu Criterion

The F terms related to the Tsai-Wu criterion are given below, Reddy and Pandey (1987).

$$F_1^{TW} = F_1^A \qquad F_2^{TW} = F_2^A$$

$$F_{11}^{TW} = \frac{1}{X_T X_C}$$

$$F_{22}^{TW} = \frac{1}{Y_T Y_C}$$

$$F_{12}^{TW} = -\frac{1}{\sqrt{X_T X_C Y_T Y_C}}$$

$$F_{44}^{TW} = \frac{1}{R^2}$$

$$F_{55}^{TW} = \frac{1}{S^2}$$

$$F_{66}^{TW} = \frac{1}{T^2}$$

Hill's Criterion

The F terms related to the Hill's criterion are given below, Reddy and Pandey (1987).

$$F_1^H = 0 \qquad F_2^H = 0$$

$$F_{11}^{TW} = \frac{1}{X_T X_C}$$

$$F_{22}^{TW} = \frac{1}{Y_T Y_C}$$

$$F_{12}^{TW} = -\frac{1}{\sqrt{X_T X_C Y_T Y_C}}$$

$$F_{44}^{TW} = \frac{1}{R^2}$$

$$F_{55}^{TW} = \frac{1}{S^2}$$

$$F_{66}^{TW} = \frac{1}{T^2}$$

Alternatively, a stress polynomial can be used, which is given below;

$$\left(\frac{\sigma_1}{X}\right)^2 + \left(\frac{\sigma_2}{Y}\right)^2 - \left(\frac{1}{X^2} + \frac{1}{Y^2} + \frac{1}{Z^2}\right)\sigma_1\sigma_2 + \left(\frac{\sigma_4}{R}\right)^2 + \left(\frac{\sigma_5}{S}\right)^2 + \left(\frac{\sigma_6}{T}\right)^2 \geq 1$$

where, depending upon the sign of the corresponding stress component, the values of X, Y, Z are taken as either X_C, Y_C, Z_C or as X_T, Y_T, Z_T.

2.2.5 Verification problems for the plate element

In this section several plate problems are solved in order to investigate the performance of the iso-parametric plate element. The results are presented in comparison with the results found in the literature. Symmetry is not used in modelling the plates, unless otherwise is stated.

2.2.5.1 Test problems for linear static analysis

2.2.5.1(a) Composite plate made of cross-ply laminates

A simply supported rectangular (0/90/0) laminated plate with side lengths a, and b and thickness h is subject to a uniform load q_0. The lamina thicknesses are equal and the material properties are given as follows,

$E_1/E_2=25$, $\nu_{12}=0.25$, $G_{12}/E_2=G_{13}/E_2=0.5$, $G_{23}/E_2=0.2$,

which corresponds to a high modulus orthotropic graphite/epoxy composite material. The following non-dimensionalizations of the quantities are used;

$$\overline{w} = w_0(0,0)\frac{E_2 h^3}{b^4 q_0},\ \overline{\sigma}_{xx} = \sigma_{xx}\left(0,0,\frac{h}{2}\right)\frac{h^2}{b^2 q_0},\ \overline{\sigma}_{yy} = \sigma_{yy}\left(0,0,\frac{h}{4}\right)\frac{h^2}{b^2 q_0},$$

$$\overline{\sigma}_{xy} = \sigma_{xy}\left(\frac{a}{2},\frac{b}{2},\frac{-h}{2}\right)\frac{h^2}{b^2 q_0},\ \overline{\sigma}_{xz} = \sigma_{xz}\left(\frac{a}{2},0,layer_1\right)\frac{h}{bq_0},\ \overline{\sigma}_{yz} = \sigma_{yz}\left(0,\frac{b}{2},layer_2\right)\frac{h}{bq_0}$$

where, w_0 denotes the mid-point displacement and σ_{xx}, σ_{yy}, σ_{xy}, σ_{xz}, σ_{yz} denote the mid-point stresses. The results obtained are given below in Table 2-3, in comparison with the results given by Reddy (2004) where the abbreviations CFS, 2Q8R, and CLPT stand for closed form solution, 8 node finite elements with reduced integration, and classical plate theory. The plate is modelled using a 4×4 regular mesh.

2.2.5.1(b) Composite plate made of angle-ply laminates

Test problem (a) is solved again for the angle ply laminate case. The displacement and stress values are given below in Tables 2-4 and 2-5 respectively. The stress values presented in Table 2-5 show that for angle ply laminates, the stresses calculated using the 4×4 mesh are not as accurate as the deflections because the stresses are obtained from the second derivatives of the deflections. Taking this into account, it is decided to use a finer mesh to model the composite plates related to the optimization problem.

2.2.5.1(c) Parallelogram isotropic plate under transverse load

Maximum deflections of simply supported and clamped parallelogram isotropic plates under uniformly distributed load are calculated and compared with the results given in Young (1989). The maximum stresses are not compared here, as there's no information on the orientation of the plane of stresses in Young (1989). The value of the displacement at the center of the plate is $\delta_{\max} = \alpha q b^4 / E t^3$, where α is a constant. q, a, b, t, ν, and E denote the intensity of the uniformly distributed load, height, width, thickness, Poisson's ratio, and Young's modulus respectively. The numerical results are tabulated below in Tables 2-6 and 2-7.

For some of the cases, the numerical results presented in Table 2-6 are not very close to the explicit results. However, the results presented in Table 2-7 are in excellent agreement with the explicit results. This discrepancy may be due to an error in results given in Young (1989). Also, as will be observed in the stability analysis of skew plates, the accuracy of the numerical results tends to decrease as the skew angle θ increases. The reason is that, the distortions of finite elements increase with increasing skew angle. This problem can be solved using a finer mesh and/or by a more careful mesh refinement.

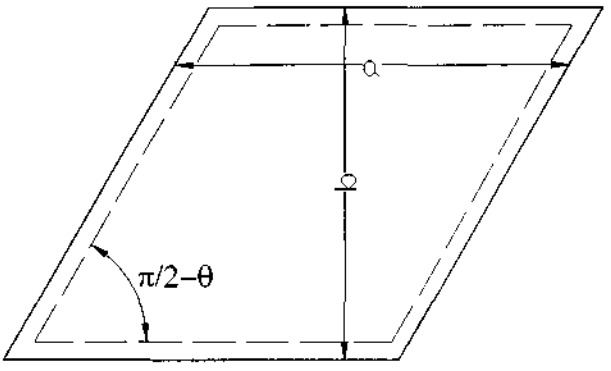

Figure 2-4. Geometry of the parallelogram plate

Table 2-3. Displacements and stresses for composite plates made of cross-ply laminates

a/h	Source	$\overline{w}\times 100$	$\overline{\sigma}_{xx}$	$\overline{\sigma}_{yy}$	$\overline{\sigma}_{xy}$	$\overline{\sigma}_{xz}$	$\overline{\sigma}_{yz}$
10	CFS[1]	0.6627	0.4989	0.3614	0.0241	0.4160	0.1290
	2Q8R[1]	0.6615	0.4842	0.3509	0.0234	0.4040	0.1260
	2Q8R(4×4)[2]	0.6615	0.4844	0.3510	0.0234	0.4048	0.1258
20	CFS[1]	0.4912	0.5273	0.2956	0.0221	0.4370	0.1090
	2Q8R[1]	0.4901	0.5117	0.2870	0.0214	0.4240	0.1060
	2Q8R(4×4)[2]	0.4903	0.5117	0.2871	0.0215	0.4244	0.1060
100	CFS[1]	0.4337	0.5382	0.2704	0.0213	0.4450	0.1010
	2Q8R[1]	0.4319	0.5214	0.2621	0.0206	0.4350	0.1020
	2Q8R(4×4)[2]	0.4321	0.5216	0.2622	0.0207	0.4358	0.1023
8	CLPT[1]	0.4313	0.5387	0.2667	0.0213	(0.3390)[1]	(0.1380)[1]

[1] Reddy (2004)
[2] Current work using a 4×4 mesh

Table 2-4. Displacements ($\overline{w}\times 100$) for composite plates made of cross-ply laminates

a/h	Source	$\theta = 5^\circ$		$\theta = 30^\circ$		$\theta = 45^\circ$	
		$n=2$	$n=10$	$n=2$	$n=10$	$n=2$	$n=10$
2	CFS[1]	3.7849	3.6899	3.3330	2.9934	3.2300	2.9175
	2Q8R[1]	3.7853	3.6903	3.3334	2.9937	3.2303	2.9178
	2Q8R(4×4)[2]	3.7760	3.6812	3.3247	2.9856	3.2218	2.9098
	2Q8R(8×8)[3]	3.7844	3.6894	3.3325	2.9929	3.2295	2.9170
4	CFS[1]	1.3165	1.2611	1.2155	0.8904	1.1576	0.8450
	2Q8R[1]	1.3166	1.2612	1.2156	0.8905	1.1576	0.8451
	2Q8R(4×4)[2]	1.3138	1.2585	1.2128	0.8882	1.1549	0.8429
	2Q8R(8×8)[3]	1.3164	1.2609	1.2153	0.8903	1.1574	0.8449
10	CFS[1]	0.4883	0.4463	0.6099	0.2901	0.5773	0.2647
	2Q8R[1]	0.4883	0.4464	0.6099	0.2901	0.5773	0.2647
	2Q8R(4×4)[2]	0.4874	0.4455	0.6087	0.2895	0.5762	0.2642
	2Q8S(8×8)[3]	0.4883	0.463	0.6098	0.2900	0.5772	0.2647
20	CFS[1]	0.3586	0.3181	0.5224	0.2033	0.4944	0.1818
	2Q8R[1]	0.3586	0.3181	0.5224	0.2033	0.4944	0.1818
	2Q8R(4×4)[2]	0.3579	0.3176	0.5215	0.2029	0.4934	0.1815
	2Q8R(8×8)[3]	0.3586	0.3181	0.5224	0.2033	0.4943	0.1818
50	CFS[1]	0.3216	0.2815	0.4979	0.1789	0.4712	0.1586
	2Q8R[1]	0.3216	0.2815	0.4979	0.1789	0.4712	0.1586
	2Q8R(4×4)[2]	0.3208	0.2809	0.4966	0.1786	0.4700	0.1583
	2Q8R(8×8)[3]	0.3216	0.2815	0.4979	0.1789	0.4711	0.1586
100	CFS[1]	0.3162	0.2763	0.4944	0.1755	0.4678	0.1553
	2Q8R[1]	0.3162	0.2763	0.4944	0.1755	0.4678	0.1553
	2Q8R(4×4)[2]	0.3150	0.2753	0.4919	0.1749	0.4655	0.1549
	2Q8R(8×8)[3]	0.3163	0.2762	0.4944	0.1754	0.4678	0.1553
8	CLPT[1]	0.3145	0.2745	0.4932	0.1745	0.4667	0.1542

[1] Reddy (2004)
[2] Current work using a 4×4 mesh
[3] Current work using an 8×8 mesh

Table 2-5. Stresses for composite plates made of cross-ply laminates

a/h	Source	$\theta = 5^\circ$			$\theta = 30^\circ$			$\theta = 45^\circ$	
		$\overline{\sigma}_{xx}$	$\overline{\sigma}_{yy}$	$\overline{\sigma}_{xy}$	$\overline{\sigma}_{xx}$	$\overline{\sigma}_{yy}$	$\overline{\sigma}_{xy}$	$\overline{\sigma}_{xx}$	$\overline{\sigma}_{xy}$
2	CFS[1]	0.3324	0.0964	0.0850	0.0153	0.0786	0.1688	0.1430	0.1392
	2Q8R[1]	0.3280	0.0957	0.0846	0.1500	0.0774	0.1689	0.1421	0.1401
	2Q8R(4×4)[2]	0.3135	0.0935	0.0834	0.1401	0.0734	0.1667	0.1357	0.1403
	2Q8R(8×8)[3]	0.3279	0.0957	0.0846	0.1500	0.0774	0.1683	0.142	0.1402
4	CFS[1]	0.4423	0.0551	0.0511	0.2011	0.0890	0.1425	0.1430	0.1392
	2Q8R[1]	0.4379	0.0547	0.0510	0.1982	0.0822	0.1423	0.1421	0.1401
	2Q8R(4×4)[2]	0.4239	0.0535	0.0508	0.1882	0.0785	0.1419	0.1357	0.1403
	2Q8R(8×8)[3]	0.4379	0.0547	0.0510	0.1981	0.0822	0.1423	0.1420	0.1402
10	CFS[1]	0.5146	0.0279	0.0289	0.2328	0.0865	0.1252	0.1430	0.1392
	2Q8R[1]	0.5103	0.0277	0.0290	0.2298	0.0854	0.1252	0.1421	0.1401
	2Q8R(4×4)[2]	0.4966	0.0271	0.0294	0.2198	0.0819	0.1255	0.1357	0.1403
	2Q8R(8×8)[3]	0.5103	0.0277	0.029	0.2298	0.0854	0.1252	0.1420	0.1402
20	CFS[1]	0.5286	0.0227	0.0246	0.2389	0.0871	0.1218	0.1430	0.1392
	2Q8R[1]	0.5243	0.0225	0.0247	0.2359	0.0860	0.1219	0.1421	0.1401
	2Q8R(4×4)[2]	0.5106	0.022	0.0252	0.2259	0.0825	0.1224	0.1357	0.1403
	2Q8R(8×8)[3]	0.5243	0.0225	0.0247	0.2359	0.0860	0.1219	0.1420	0.1402
50	CFS[1]	0.5327	0.0211	0.0233	0.2407	0.0873	0.1208	0.1430	0.1392
	2Q8R[1]	0.5284	0.0210	0.0234	0.2377	0.0862	0.1208	0.1421	0.1401
	2Q8R(4×4)[2]	0.5145	0.0205	0.024	0.2276	0.0827	0.1214	0.1356	0.1403
	2Q8R(8×8)[3]	0.5284	0.0210	0.0234	0.2377	0.0862	0.1209	0.1420	0.1402
100	CFS[1]	0.5333	0.0209	0.0231	0.2410	0.0873	0.1207	0.1430	0.1392
	2Q8R[1]	0.5290	0.0207	0.0233	0.2380	0.0862	0.1208	0.1421	0.1401
	2Q8R(4×4)[2]	0.5144	0.0203	0.0237	0.2277	0.0826	0.1211	0.1355	0.1401
	2Q8R(8×8)[3]	0.5290	0.0207	0.0233	0.2379	0.0862	0.1208	0.1420	0.1402
-	CLPT[1]	0.5290	0.0207	0.0233	0.2411	0.0873	0.1206	0.1440	0.1402

[1] Reddy (2004)
[2] Current work using a 4×4 mesh
[3] Current work using an 8×8 mesh

Table 2-6. α values for different θ values (ν=0.2, a/b=2)

θ	0°	30°	45°	60°	75°
$\alpha^{(1)}$	0.1190	0.1180	0.1080	0.0920	0.0110
$\alpha^{(2)}$	0.1167	0.1108	0.0973	0.0614	0.0110

[1] Young (1989)
[2] Current study using a 16×8 mesh

Table 2-7. α values for various θ and a/b values (ν=1/3)

θ	a/b:	1.00	1.25	1.50	1.75	2.00	2.25	2.50
0°	$\alpha^{(1)}$	0.0135	0.0195	0.0235	0.0258	0.0273	-	-
	$\alpha^{(2)}$	0.0135	0.0195	0.0235	0.0258	0.0271	-	-
15°	$\alpha^{(1)}$	0.0127	0.0189	0.0232	0.0257	0.0273	-	-
	$\alpha^{(2)}$	0.0128	0.0189	0.0231	0.0256	0.0269	-	-
30°	$\alpha^{(1)}$	-	0.0168	0.0218	0.0249	0.0268	0.0281	-
	$\alpha^{(2)}$	-	0.0169	0.0217	0.0248	0.0265	0.0274	-
45°	$\alpha^{(1)}$	-	-	0.0165	0.0208	0.0242	0.0265	0.0284
	$\alpha^{(2)}$	-	-	0.0179	0.0223	0.0251	0.0267	0.0275

[1] Young (1989)
[2] Current study using a 16×8 mesh

2.2.5.2 Test problems for linearized stability analysis

2.2.5.2(a) Buckling of a simply supported rectangular plate subject to linearly varying edge loading

The simply supported homogeneous isotropic plate shown below in Figure 2-5 is under the action of a linearly varying edge load. The value of the edge load, N_x, is calculated using eq. (2-47), where α is a constant. $\alpha = 2$, $\alpha < 2$, and $\alpha > 2$ corresponds to pure bending, a combination of bending and compression, and a combination of bending and tension respectively. The critical value of stress, σ_{cr} is calculated using equation (2-48) given below.

$$N_x = N_0\left(1-\alpha\frac{y}{b}\right) \tag{2-47}$$

$$\sigma_{cr} = k\frac{\pi^2 D}{b^2 h} \tag{2-48}$$

where $D = Et^3/12\left(1-\nu^2\right)$ represents the bending rigidity of the plate. The numerical results obtained by an 16×8 finite element mesh are in excellent agreement with the results given by Timoshenko (1936) which are obtained explicitly as shown in Table 2-8.

2.2.5.2(b) Buckling of a rectangular plate with elastic rotational restraints subject to uniform compressive edge loading

The results given in Timoshenko (1936) are compared with the numerical results obtained in Table 2-9. The geometry of the plate is shown in Fig. 2-5. In Table 2-9, A, B, C, D corresponds to the following boundary conditions;

A : S.S. at y=0 (r=0), and free at y=b; S.S. at x=0 and x=a
B : C. at y=0 (r=8), and free at y=b; S.S. at x=0 and x=a
C : E.R. at y=0 (r=2/b), and free at y=b; S.S. at x=0 and x=a
D : E.R. at y=0 (r_b=8/b), and free at y=b; S.S. at x=0 and x=a

where S.S., C., and E.R., represents simply supported, clamped, and elastically restrained boundary conditions and r is the rotational restraint coefficient calculated by $r = C\pi^2/Da^2$, and C is the torsional rigidity of a beam of unit length attached at y=0.

2.2.5.2(c) Buckling of a rectangular plate with nonlinearly distributed compressive loading on two opposite sides

Explicit (approximately taking the stress diffusion or re-distribution into account) and numerical solutions for rectangular plates with different boundary conditions under nonlinearly distributed compressive loading on two opposite sides are given by Devarakonda and Bert (2004). The geometry of the plate and loading is shown in Fig. 2-6. The boundary conditions are given as follows;

$$\sigma_x = \sigma_0\cos\left(\frac{\pi y}{2b}\right) \qquad \tau_{xy} = 0, \qquad \text{at } x = \pm\frac{a}{2}$$

$$\sigma_y = 0 \qquad \tau_{xy} = 0, \qquad \text{at } y = \pm\frac{b}{2}$$

The results obtained by using a 16×8 mesh are given below in Table 2-11 in comparison with the results given by Devarakonda and Bert (2004). The results are in good agreement, and the minor differences are generally due to the differences in the finite element formulations and the mesh densities used. Also, in this study the contribution of the shear deformation is taken into account and the consistent nodal forces are more precisely calculated comparing with the stepwise uniform approximation used by Devarakonda and Bert (2004). The calculation of the consistent nodal forces, F_k, is briefly explained as follows. Let one edge of an 8 noded element is loaded by the distributed load which is a function of y coordinate. The nodes of the edge are numbered as k, k+1, and k+2. 4-point Gauss integration is used to evaluate the related integrals.

$$F_k = \sum_{i=1}^{4} N_k(\xi_i) \times \sigma_0 \cos\left(\frac{\pi}{2b}\sum_{j=1}^{3} N_j(\xi_i) y_j\right)\left(\frac{b}{16}\right), \quad k = 1,2,3$$

$$N_1(\xi) = \frac{1}{2}\xi(\xi - 1), \qquad N_2(\xi) = (1-\xi)(1+\xi), \quad N_3(\xi) = \frac{1}{2}\xi(1+\xi)$$

where N_k are the one dimensional shape functions and ξ is the local coordinate of the sampling point which is equal to -1, 0, 1 at the 1st, 2nd, and 3rd edge nodes respectively. The nodal forces are calculated for each element with loaded edges and summed up to obtain the global force vector. Because of symmetry, only the upper half of the resulting nodal forces applied to the nodes of one of the edges are tabulated below in Table 2-10, (see Figure 2-7).

2.2.5.2(d) Anti-symmetric cross-ply laminated composite rectangular plate

The linearized stability analysis is not applicable to anti-symmetric cross-ply laminated plates. However, results exist in the literature, and considering this a simply supported rectangular anti-symmetric cross-ply laminated plate with side lengths a, and b and thickness h subject to a uniform load q_0 is analyzed here. The lamina thicknesses are equal and the material properties and the non-dimensional buckling load, $\overline{N}$, are given below,

$$G_{12}/E_2 = G_{13}/E_2 = 0.6, \qquad G_{23}/E_2 = 0.25, \qquad \overline{N} = \frac{N_{xx} b^2}{E_2 h^3}.$$

The results obtained are given below in Table 2-12, in comparison with the results given by Miravete and Reddy (2004) where the abbreviations 2Q8R, 2Q9R, and CFS stand for 8 node finite elements with reduced integration, 9 node finite elements with reduced integration, and closed form solution. The plate is modelled using a 16×8 regular mesh and the pre-buckling stress is assumed to be uniform and the pre-buckling deformations are neglected.

2.2.5.2(e) Rhombic plate under uniform compression on all edges

The numerical results obtained for the simply supported rhombic plate under uniform compression on all edges, whose geometry is shown below in Figure 2-8, are given in comparison with the exact results given in Young (1989) in Table 2-13 where the critical value of stress is calculated according to $\sigma_{cr} = K\frac{Et^2}{a^2(1-\nu^2)}$. It is observed that the results are in good agreement except for the case α=45°, where error is equal to 5.4%, which is mainly due to the distorted finite element mesh.

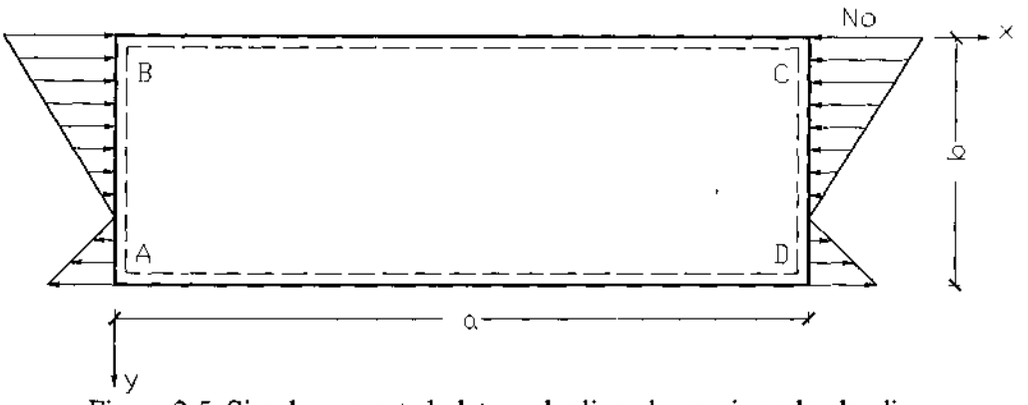

Figure 2-5. Simply supported plate under linearly varying edge loading

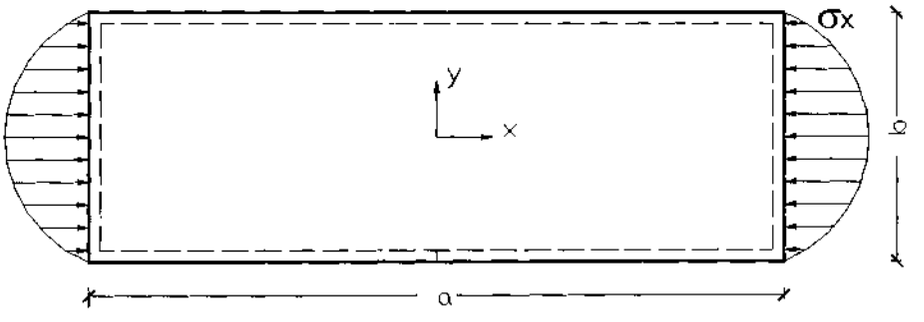

Figure 2-6. Geometry and loading of the plate

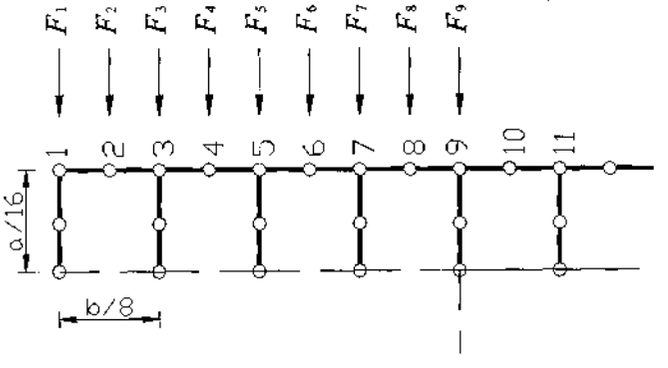

Figure 2-7. Consistent nodal forces acting on the edge nodes

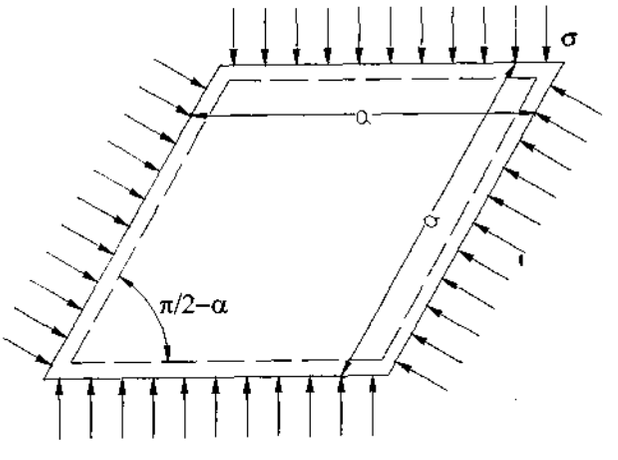

Figure 2-8. Geometry and loading of the rhombic plate

Table 2-8. Numerical values of k in comparison with the explicit results with $t/b = 0.01$.

α	a/b=	0.4	0.5	0.6	2/3	0.75	0.8	0.9	1.0	1.5
2	(1)	29.100	25.600	24.100	23.900	24.100	24.400	25.600	25.600	24.100
	(2)	29.024	25.487	24.096	23.683	24.099	24.459	25.571	25.512	24.112
4/3	(1)	18.700	-	12.900	-	11.500	11.200	-	11.000	11.500
	(2)	18.824	15.012	12.956	12.123	11.467	11.224	10.988	11.004	11.472
1	(1)	15.100	-	9.700	-	8.400	8.100	-	7.800	8.400
	(2)	15.110	11.603	9.729	8.698	8.359	8.123	7.862	7.806	8.361
4/5	(1)	13.300	-	8.300	-	7.100	6.900	-	6.600	7.100
	(2)	13.274	10.043	8.340	7.654	7.105	6.891	6.650	6.590	7.107
2/3	(1)	10.800	-	7.100	-	6.100	6.000	-	5.800	6.100
	(2)	12.205	9.171	7.590	6.950	6.441	6.243	6.018	5.959	6.443
0	(1)	8.410	6.250	5.140	-	-	4.200	4.040	4.000	-
	(2)	8.389	6.238	5.130	4.688	4.335	4.198	4.041	3.997	4.337

(1) Timoshenko (1936)
(2) Current study using a 16×8 mesh

Table 2-9. k values for different boundary conditions with ν=0.25 and $t/b = 0.01$.

a/b	$A^{(1)}$	$A^{(2)}$	$B^{(1)}$	$B^{(2)}$	$C^{(1)}$	$C^{(2)}$	$D^{(1)}$	$D^{(2)}$
0.5	4.400	4.338	-	4.501	-	4.406	-	4.437
1.0	1.440	1.431	1.70	1.693	1.490	1.492	1.580	1.575
1.1	-	1.260	1.56	1.556	-	1.332	-	1.427
1.2	1.135	1.130	1.47	1.462	-	1.214	-	1.321
1.3	-	1.030	1.41	1.398	1.130	1.126	1.250	1.245
1.4	0.952	0.950	1.36	1.358	-	1.059	-	1.192
1.5	-	0.890	1.34	1.335	1.010	1.008	1.160	1.155
1.6	0.835	0.833	1.33	1.325	-	0.970	-	1.131
1.7	-	0.790	1.33	1.327	-	0.942	-	1.117
1.8	0.755	0.753	1.34	1.338	0.920	0.921	1.110	1.113
1.9	-	0.722	1.36	1.356	-	0.907	-	1.115
2.0	0.698	0.696	1.38	1.382	0.900	0.898	1.120	1.123
2.2	-	0.654	1.45	1.450	-	0.892	-	1.154
2.3	-	0.637	-	1.492	0.890	0.895	1.180	1.176
2.4	-	0.622	1.47	1.464	-	0.900	-	1.202
2.5	0.610	0.609	-	1.429	0.900	0.908	1.300	1.230
3	0.564	0.561	-	1.336	0.980	0.979	1.160	1.155
4	0.516	0.515	-	1.383	0.900	0.898	1.120	1.124
5	0.506	0.493	-	1.327	-	0.909	-	1.123

(1) Timoshenko (1936)
(2) Current study using a 16×8 mesh

Table 2-10. Consistent nodal forces acting on the edge nodes

Node	1	2	3	4	5	6	7	8	9
F	0.0021	1.6195	1.6067	4.6120	2.9688	6.9023	3.8789	8.1418	4.1985

Table 2-11. Numerical values of k with $t/b = 0.01$.

k	Source	SSSS	CCCC	SSCC	CCSS
1	[1]	5.410	14.160	10.390	9.460
	[2]	5.414	14.062	9.436	9.373
2	[1]	5.730	11.750	10.340	7.460
	[2]	5.734	11.812	9.444	7.439
3	[1]	5.830	11.540	10.540	6.890
	[2]	5.851	11.623	9.819	6.884

[1] Devarakonda and Bert (2004)
[2] Current study using a 16×8 mesh

Table 2-12. Non-dimensional buckling loads with a/h=10.

Layers	Source	E_1/E_2=	3	10	20	30	40
2	CFS[1]		4.6948	6.1181	7.8196	9.3746	10.8170
	2Q9R[1]		4.7718	6.2465	8.0423	9.7347	11.3553
	2Q8R[2]		4.7437	6.1904	7.9667	9.6444	11.2501
4	CFS[1]		5.7138	9.0164	13.7430	17.7830	21.2800
	2Q9R[1]		5.2543	9.2552	14.3320	18.8150	22.8060
	2Q8R[2]		5.2401	9.2338	14.3025	18.7802	22.7677
6	CFS[1]		5.2670	9.6051	15.0010	19.6394	23.6690
	2Q9R[1]		5.3430	9.7893	15.3940	20.2800	24.5770
	2Q8R[2]		5.3317	9.7773	15.3797	20.2636	24.5598
10	CFS[1]		5.3159	9.9134	15.6690	20.6347	24.9640
	2Q9R[1]		5.3884	10.0600	15.9270	21.0080	25.4500
	2Q8R[2]		5.3786	10.0533	15.9206	21.0010	25.4429

[1] Miravete and Reddy (2004)
[2] Current study using a 16×8 mesh

Table 2-13. K values for different α values with ν=0.3, $t/b = 0.01$.

α	0°	9°	18°	27°	36°	45°
$K^{(1)}$	1.645	1.678	1.783	1.983	2.338	2.898
$K^{(2)}$	1.6435	1.6779	1.7898	2.0097	2.4041	3.1189

[1] Young (1989)
[2] Current study using a 16×8 mesh

2.2.5.3 Test problems for the linearized stability analysis of skew composite plates under uniaxial compression

Several skew plate problems are solved and the results are tabulated in Tables 2-14 to 2-16 in comparison with the results presented in Babu and Kant (1999). The non-dimensional buckling parameter λ_u is defined as, $\lambda_u = \dfrac{N_x b^2}{E_2 h^3}$ where N_x is the buckling load. Only symmetric laminates are considered and anti-symmetric laminates are not considered as true bifurcation buckling can not physically occur for such laminates. The geometry of skew laminate with in-plane loading is shown below in Figure 2-9, where θ is the lamination angle, and ψ is the skew angle. All of the results are given for the a/b=1 case, the outer layers of all of the laminates are of zero degree lamina, and the thickness of the middle layer is taken as twice that of outer layers. The properties of the materials used in computations are given below;

Material I: $E_1/E_2 = 40$, $G_{12}/E_2 = G_{13}/E_2 = 0.5$, $G_{23}/E_2 = 0.2$, $\nu_{12} = \nu_{23} = \nu_{13} = 0.25$

Material II: $E_1/E_2 = 40$, $G_{12}/E_2 = G_{13}/E_2 = 0.6$, $G_{23}/E_2 = 0.5$, $\nu_{12} = \nu_{23} = \nu_{13} = 0.25$

λ_U values for simply supported and clamped skew angle-ply plates are tabulated in Tables 2-14 and 2-15 and it is observed that the effect of boundary conditions on stability of angle-ply laminates reduces as the skew angle increases. Symmetric skew cross-ply laminates (Material II) having a/h=10 and made up of 3,5, and 9 layer lay-ups are analyzed and the results are tabulated below in Table 2-16. According to the results, the error increases as ψ value increases. This is because of the highly distorted finite element mesh. The error can be avoided by using a finer mesh and/or careful mesh generation. Also, a shear correction factor of 5/6 is assumed in this study, which causes extra error.

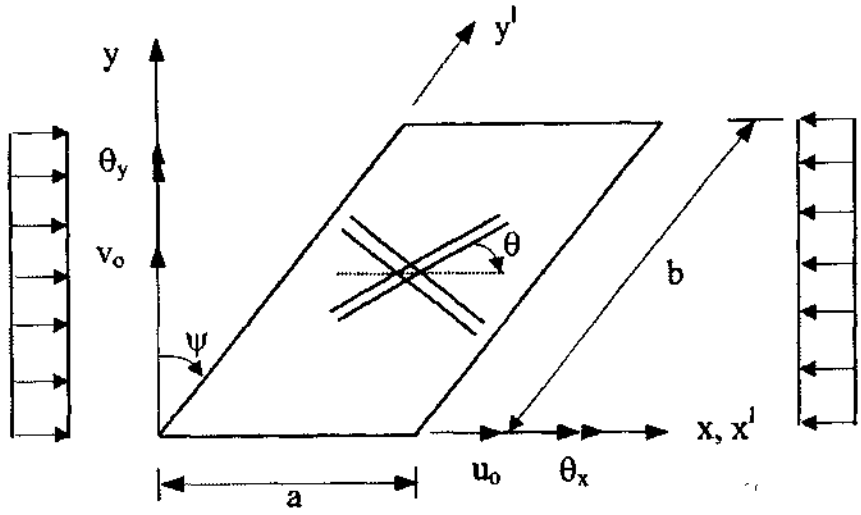

Figure 2-9 The geometry of skew laminate with in-plane loading, Babu and Kant (1999)

Table 2-14. λ_U values for SSSS skew angle-ply plates

Number of layers	θ	Source	ψ			
			0°	15°	30°	45°
3	0°	(1)	20.116	20.569	22.365	27.450
		(2)	20.298	20.7770	22.6464	27.9138
	15°	(1)	19.559	18.882	20.558	27.279
		(2)	19.6154	18.9676	20.6516	27.3222
	30°	(1)	19.278	19.893	22.681	25.748
		(2)	19.0103	19.6958	22.7605	25.8947
	45°	(1)	17.053	17.054	17.755	21.303
		(2)	17.1965	17.1498	17.9169	21.5856
7	0°	(1)	20.116	20.569	22.365	27.450
		(2)	20.2980	20.7770	22.6464	27.9138
	15°	(1)	23.353	23.733	26.316	32.749
		(2)	23.4132	23.8616	26.4867	32.9745
	30°	(1)	27.931	28.838	31.240	34.169
		(2)	27.8166	28.7960	31.3176	34.2648
	45°	(1)	24.168	24.188	25.738	27.985
		(2)	23.9728	24.3116	25.8960	28.0934

(1) Babu and Kant (1999)
(2) Current study using a 16×8 mesh

Table 2-15. λ_U values for CCCC skew angle-ply plates

Number of layers	θ	Source	ψ			
			0°	15°	30°	45°
3	0°	(1)	34.254	34.592	35.757	38.195
		(2)	34.4932	34.8425	36.0494	38.5423
	15°	(1)	29.054	28.968	30.161	33.326
		(2)	29.3473	29.2500	30.4540	33.6770
	30°	(1)	23.800	24.007	25.529	28.463
		(2)	23.9786	24.1683	25.7388	28.6891
	45°	(1)	18.635	18.887	20.330	22.989
		(2)	18.8947	19.143	20.6004	23.2826
7	0°	(1)	34.254	34.592	35.757	38.195
		(2)	34.4932	34.8425	36.0494	38.5423
	15°	(1)	33.813	34.108	35.553	38.185
		(2)	33.9678	34.2713	35.7213	38.3136
	30°	(1)	31.136	31.528	32.844	34.712
		(2)	31.2251	31.6124	32.9221	34.6099
	45°	(1)	25.069	25.426	26.534	28.200
		(2)	25.1930	25.5454	26.6310	28.2490

(1) Babu and Kant (1999)
(2) Current study using a 16×8 mesh

Table 2-16. λ_U values for SSSS and CCCC skew cross-ply plates

Support conditions	ψ	Source	Number of layers		
			3	5	9
SSSS	0°	(1)	23.084	24.821	25.378
		(2)	23.4512	25.0629	25.6063
	15°	(1)	24.505	26.803	27.607
		(2)	24.9185	27.0497	27.8341
	30°	(1)	29.887	33.865	35.195
		(2)	30.4520	34.1322	35.4017
	45°	(1)	40.573	45.754	46.585
		(2)	41.5045	44.1686	43.9225
CCCC	0°	(1)	40.069	41.374	40.689
		(2)	40.4657	41.5806	40.8823
	15°	(1)	40.691	42.073	41.375
		(2)	41.0533	42.1711	41.4941
	30°	(1)	42.454	43.833	43.163
		(2)	42.9092	44.0535	43.3635
	45°	(1)	45.310	46.744	46.097
		(2)	45.6487	46.8506	46.1866

(1) Babu and Kant (1999)
(2) Current study using a 16×8 mesh

2.2.5.4. Test problems for first-ply failure analysis

The geometry of a rectangular laminate with out of plane loading is shown below in Figure 2-10, where a, b, and h denote the length, the width, and the thickness of the plate. The material properties are given below in Table 2-17 and the numerical results are tabulated below in Tables 2-18 and 2-19 for uniformly distributed loading in comparison with the results presented in Cho and Yoon (1998) and Reddy and Reddy (1992), where $\bar{q} = \frac{q_0}{E_2}\left(\frac{a}{h}\right)^4$. The uniformly distributed load can be expressed in double Fourier series form as follows,

$$q(x,y) = \sum_{m=1}^{\infty}\sum_{n=1}^{\infty} q_{mn} \sin\frac{m\pi x}{a}\sin\frac{n\pi y}{b}, \qquad q_{mn} = \frac{16q_0}{\pi^2 mn}, \quad m, n=1, 3$$

The minor differences between the results are due to the differences in mesh density and the coordinates of the sampling points. Note that the failure indices are calculated at the points on the outmost fibers and at the points on the mid-surface of the lamina and the highest are selected as the failure index at the particular sampling point of the lamina.

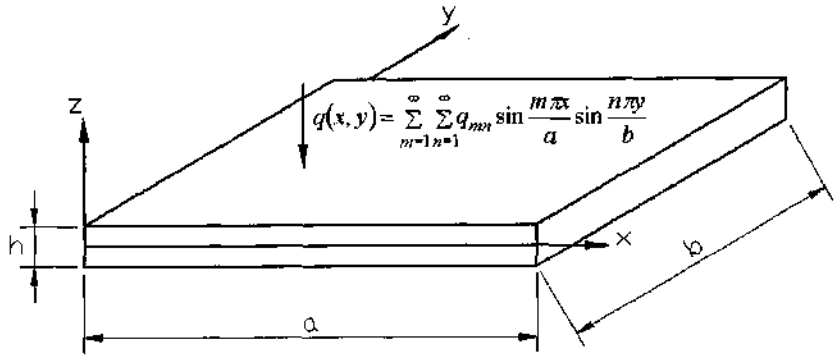

Figure 2-10. Plate geometry and loading

Table 2-17. Material properties of T300/5208 graphite/epoxy pre-preg

Properties	Values	Properties	Values
E_1	19.2×10^6 psi	X_T	219.5×10^3 psi
E_2	1.56×10^6 psi	X_C	246.0×10^3 psi
E_3	1.56×10^6 psi	$Y_T = Z_T$	6.35×10^3 psi
$G_{12} = G_{13}$	0.82×10^6 psi	$Y_C = Z_C$	6.35×10^3 psi
G_{23}	0.49×10^6 psi	R	9.80×10^3 psi
$\nu_{12} = \nu_{13}$	0.24	$S = T$	12.6×10^3 psi
ν_{23}	0.49	h_i (ply thickness)	0.005 in.

Table 2-18. Non-dimensional first-ply failure loads, $\bar{q}$, for a uniformly distributed load for [0/90/0] three layer laminate.

Failure Criterion	Exact[1]	FSDT[1]	FSDT[2]	FSDT[3]
Maximum strain (p)	10435.6	12144.2	12212.6	12184.0
Tsai-Hill	11381.9	11.381.9	11436.8	11409.3
Tsai-Wu	11907.6	11907.6	11646.5	11923.3

[1] Cho and Yoon (1998)
[2] Reddy and Reddy (1992)
[3] Current study using a 16×8 mesh

Table 2-19. Non-dimensional first-ply failure loads, $\bar{q}$, for a uniformly distributed load for [0/90/0] three layer laminates.

Failure Criterion	*a/h*	Exact[1]	FSDT[1]	FSDT[2]
Maximum strain	4	0.4898	0.6208	0.6479
	10	3.7628	4.4872	4.6342
	100	409.62	478.21	489.40
Tsai-Hill	4	0.5379	0.5963	0.6157
	10	4.1090	4.2308	4.3134
	100	446.79	446.79	451.37
Tsai-Wu	4	0.5284	0.6124	0.6388
	10	4.2756	4.3974	4.5430
	100	476.31	467.95	478.56

[1] Cho and Yoon (1998)
[3] Current study using a 16×8 mesh

2.3. Finite element analysis of composite shells

The formulation of the shell element used in computations is given in this section. Several verification problems are solved and the results are presented. The related functions are listed in Appendix A.3.

2.3.1. Element formulation

In this section, the analysis of composite shell structures using an 8 node super-parametric degenerated 3D shell element is defined. The main advantage of this element is that no particular shell theory is used, and the formulation is based on the iso-parametric plate element used in this study. The element's geometry is not completely defined by the shape functions, so the element is of super-parametric kind. The bending-extension coupling is incorporated into the element by taking the contribution of the related terms into account in the energy expression, so that the un-symmetrically laminated shell problems can also be solved.

2.3.1.1. Composite shell element

The shell element defined here is based on the formulation given by Mallikarjuna and Kant (1992) which is a modified form of Ahmad's shell element, Ahmad *et al.* (1970). Here, the higher order terms given in Mallikarjuna and Kant (1992) are omitted in order to simplify the solution, and to be able to use the material matrices derived for the plate element.

2.3.1.2. Geometric definition of the element

The coordinates of a point in the global coordinate system (x,y,z) are calculated as given below in eq. (2-49).

$$\begin{Bmatrix} x \\ y \\ z \end{Bmatrix} = \sum_{i=1}^{nn} \begin{Bmatrix} x \\ y \\ z \end{Bmatrix}_{mid} S_i(\xi,\eta) + \sum_{i=1}^{nn} S_i \zeta \mathbf{V}_{3i} \tag{2-49}$$

where, nn, $S_i(\xi,\eta)$, $\mathbf{V}_{3i}$ denote the total number of nodes, the value of the i^{th} shape function at (ξ,η), and the unit surface normal vector at node i. The ranges of ξ and η are -1 to 1 and the range of ζ is $-t/2$ to $t/2$, where t denotes the thickness of the element.

2.3.1.3. Coordinate systems and coordinate transformations

There are four different coordinate systems used in the formulation which are defined as follows. Also, the transformations between these coordinate systems are explained. The global and nodal coordinate systems are shown below in Figure 2-11, where θ_x, θ_y, α_i, β_i are rotations in the same direction with the unit vectors $\mathbf{e}_2$, $-\mathbf{e}_1$, $\mathbf{V}_{2i}$, $\mathbf{V}_{1i}$ respectively. $\mathbf{V}_{1i}$, $\mathbf{V}_{2i}$, $\mathbf{V}_{3i}$ are the unit vectors related to the nodal coordinate system at node i.

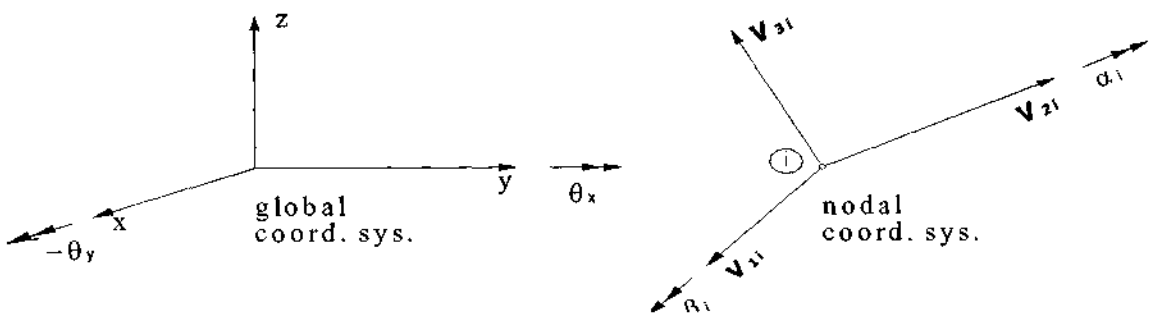

Figure 2-11. Global and nodal coordinate systems

2.3.1.3(a) Global coordinate system

The position of a point on the element is defined by the Cartesian coordinates of the nodes in the global coordinate system, (x,y,z). The unit vectors in x, y, z directions are $\mathbf{e}_1$, $\mathbf{e}_2$, $\mathbf{e}_3$ respectively. The global coordinates of node i are (x_i, y_i, z_i).

2.3.1.3(b) Nodal coordinate system

The coordinates of node i in the nodal coordinate system are given as (V_{1i}, V_{2i}, V_{3i}). The unit vectors in V_{1i}, V_{2i}, V_{3i} directions are $\mathbf{V}_{1i}$, $\mathbf{V}_{2i}$, $\mathbf{V}_{3i}$ respectively. $\mathbf{V}_{1i}$ and $\mathbf{V}_{2i}$ are given below in eq. (2-50) by selecting the direction of the cross product $\mathbf{V}_{3i} \times \mathbf{e}_1$ as the direction of the vector $\mathbf{V}_{1i}$. Another vector can be used instead of $\mathbf{e}_1$, depending on the choice of the user.

$$\mathbf{V}_{1i} = \frac{\mathbf{V}_{3i} \times \mathbf{e}_1}{|\mathbf{V}_{3i} \times \mathbf{e}_1|}, \quad \mathbf{V}_{2i} = \frac{\mathbf{V}_{3i} \times \mathbf{V}_{1i}}{|\mathbf{V}_{3i} \times \mathbf{V}_{1i}|} \tag{2-50}$$

The nodal-global coordinate system transformation matrix, $\boldsymbol{\mu}_i$, is defined below in eq. (2-51).

$$\mu_{irs} = \cos(\mathbf{V}_{ri}, \mathbf{e}_s), \quad r,s = 1,2,3 \text{ or } \quad \boldsymbol{\mu}_i = \begin{bmatrix} l_{1i} & m_{1i} & n_{1i} \\ l_{2i} & m_{2i} & n_{2i} \\ l_{3i} & m_{3i} & n_{3i} \end{bmatrix} \tag{2-51}$$

where, the components of $\boldsymbol{\mu}_i$ are the direction cosines. The transformation and inverse transformation (making use of orthogonality) between the nodal and the global coordinate systems are achieved as follows,

$$\begin{Bmatrix} V_{1i} \\ V_{2i} \\ V_{3i} \end{Bmatrix} = \boldsymbol{\mu}_i \begin{Bmatrix} x \\ y \\ z \end{Bmatrix} \qquad \begin{Bmatrix} x \\ y \\ z \end{Bmatrix} = \boldsymbol{\mu}_i^T \begin{Bmatrix} V_1 \\ V_2 \\ V_3 \end{Bmatrix} \tag{2-52}$$

Using equations (2-51) and (2-52), the global-nodal transformation of the nodal rotations is obtained as given below in equation (2-53).

$$\begin{Bmatrix} \beta_i \\ \alpha_i \end{Bmatrix} = \begin{bmatrix} l_{1i} & m_{1i} \\ l_{2i} & m_{2i} \end{bmatrix} \begin{Bmatrix} -\theta_y \\ \theta_x \end{Bmatrix} \tag{2-53}$$

$\boldsymbol{\mu}_i$ is orthogonal, so the inverse transformation can easily be written as shown below,

$$\begin{Bmatrix} -\theta_y \\ \theta_x \end{Bmatrix} = \begin{bmatrix} l_{1i} & l_{2i} \\ m_{1i} & m_{2i} \end{bmatrix} \begin{Bmatrix} \beta_i \\ \alpha_i \end{Bmatrix} \tag{2-54}$$

The displacement components due to rotations α_i, β_i are denoted by; u_i^{rot}, v_i^{rot}, and w_i^{rot} which are given below,

$$\begin{Bmatrix} u_i^{rot} \\ v_i^{rot} \\ w_i^{rot} \end{Bmatrix} = \boldsymbol{\mu}_i^T \begin{Bmatrix} \alpha_i \varsigma \\ -\beta_i \varsigma \\ 0 \end{Bmatrix} \tag{2-55}$$

Using equations (2-49) and (2-55), the displacements of the same point can be expressed in terms of nodal displacements as shown below in eq. (2-56).

$$\begin{Bmatrix} u \\ v \\ w \end{Bmatrix} = \sum_{i=1}^{nn} \begin{Bmatrix} u_i \\ v_i \\ w_i \end{Bmatrix} S_i + \sum_{i=1}^{nn} S_i \zeta \begin{bmatrix} l_{1i} & -l_{2i} \\ m_{1i} & -m_{2i} \\ n_{1i} & -n_{2i} \end{bmatrix} \begin{Bmatrix} \alpha_i \\ \beta_i \end{Bmatrix} \tag{2-56}$$

where, u, v, w, α_i, β_i, denote the x, y, z components of displacements, and rotations about $\mathbf{V}_{2i}$ and $\mathbf{V}_{1i}$, and the subscript i denotes node i.

2.3.1.3(c) Local coordinate system

At each Gauss point a local coordinate system is defined by shape function interpolation of surface normals and tangents from nodal values. The coordinates of a point in local coordinate system are (x',y',z'). The unit vectors in x', y', z' directions are **x'**, **y'**, **z'** respectively. The interpolation is given below in eq. (2-57).

$$\begin{Bmatrix} \mathbf{x'} \\ \mathbf{y'} \\ \mathbf{z'} \end{Bmatrix} = \sum_{i=1}^{nn} \begin{Bmatrix} \mathbf{V}_{1i} \\ \mathbf{V}_{2i} \\ \mathbf{V}_{3i} \end{Bmatrix} S_i \tag{2-57}$$

The local-global coordinate system transformation matrix is defined below in eq. (2-58).

$$\boldsymbol{\mu}'_{rs} = \cos(\mathbf{x}'_r, \mathbf{e}_s), \quad r,s = 1,2,3 \quad \text{or} \quad \boldsymbol{\mu}' = \begin{bmatrix} l'_1 & m'_1 & n'_1 \\ l'_2 & m'_2 & n'_2 \\ l'_3 & m'_3 & n'_3 \end{bmatrix} \tag{2-58}$$

The transformation and inverse transformation (making use of orthogonality) between the local and the global coordinate systems are achieved as follows,

$$\begin{Bmatrix} x' \\ y' \\ z' \end{Bmatrix} = \boldsymbol{\mu}' \begin{Bmatrix} x \\ y \\ z \end{Bmatrix} = \begin{bmatrix} l'_1 & m'_1 & n'_1 \\ l'_2 & m'_2 & n'_2 \\ l'_3 & m'_3 & n'_3 \end{bmatrix} \begin{Bmatrix} x \\ y \\ z \end{Bmatrix} \qquad \begin{Bmatrix} x \\ y \\ z \end{Bmatrix} = \boldsymbol{\mu}'^{T} \begin{Bmatrix} x' \\ y' \\ z' \end{Bmatrix} \tag{2-59}$$

Using eq. (2-58), the global-local transformations of u, v, and w, and the rotations are,

$$\begin{Bmatrix} u' \\ v' \\ w' \end{Bmatrix} = \boldsymbol{\mu}' \begin{Bmatrix} u \\ v \\ w \end{Bmatrix} = \begin{bmatrix} l'_1 & m'_1 & n'_1 \\ l'_2 & m'_2 & n'_2 \\ l'_3 & m'_3 & n'_3 \end{bmatrix} \begin{Bmatrix} u \\ v \\ w \end{Bmatrix} \quad \text{and} \quad \begin{Bmatrix} -\theta_{y'} \\ \theta_{x'} \end{Bmatrix} = \begin{bmatrix} l'_1 & m'_1 \\ l'_2 & m'_2 \end{bmatrix} \begin{Bmatrix} -\theta_y \\ \theta_x \end{Bmatrix}$$

Thus, the local-nodal coordinate transformation matrix becomes,

$$\mathbf{E} = \boldsymbol{\mu}' \boldsymbol{\mu}_i^{\mathbf{T}} \tag{2-60}$$

The local-nodal transformation of the nodal rotations can be achieved using **E** as shown below;

$$\begin{Bmatrix} -\theta_{y'} \\ \theta_{x'} \\ \theta_{z'} \end{Bmatrix} = \mathbf{E} \begin{Bmatrix} \beta_i \\ \alpha_i \\ \gamma_i \end{Bmatrix} = \begin{bmatrix} E_{11i} & E_{12i} & E_{13i} \\ E_{21i} & E_{22i} & E_{23i} \\ E_{31i} & E_{32i} & E_{33i} \end{bmatrix} \begin{Bmatrix} \beta_i \\ \alpha_i \\ \gamma_i \end{Bmatrix} \tag{2-61}$$

where $\theta_{z'}$ and γ_i are the rotations in z and V_{3i} directions which are not used in the formulation. Finally, the nodal variables in the global and local coordinate systems are transformed into the local coordinate system defined at the Gauss point where $\boldsymbol{\mu}_i$ and $\boldsymbol{\mu}'$ are computed as shown below in eq. (2-62).

$$\begin{Bmatrix} u' \\ v' \\ w' \\ -\theta_{y'} \\ \theta_{x'} \end{Bmatrix} = \begin{bmatrix} l'_1 & m'_1 & n'_1 & 0 & 0 \\ l'_2 & m'_2 & n'_2 & 0 & 0 \\ l'_3 & m'_3 & n'_3 & 0 & 0 \\ 0 & 0 & 0 & E_{11i} & E_{12i} \\ 0 & 0 & 0 & E_{21i} & E_{22i} \end{bmatrix} \begin{Bmatrix} u_i \\ v_i \\ w_i \\ \beta_i \\ \alpha_i \end{Bmatrix} \tag{2-62}$$

2.3.1.3(d) Curvilinear (shape function) coordinate system

The coordinates of any point in the curvilinear element coordinate system are given as (ξ, η). The unit vectors in ξ, η directions are $\boldsymbol{\xi}, \boldsymbol{\eta}$ respectively. $\boldsymbol{\xi}, \boldsymbol{\eta}$ are given below in eq. (2-63).

$$\boldsymbol{\xi} = \frac{\partial x}{\partial \xi}\mathbf{e}_1 + \frac{\partial y}{\partial \xi}\mathbf{e}_2 + \frac{\partial z}{\partial \xi}\mathbf{e}_3, \qquad \boldsymbol{\eta} = \frac{\partial x}{\partial \eta}\mathbf{e}_1 + \frac{\partial y}{\partial \eta}\mathbf{e}_2 + \frac{\partial z}{\partial \eta}\mathbf{e}_3 \tag{2-63}$$

where,

$$\begin{Bmatrix} \frac{\partial x}{\partial \xi} \\ \frac{\partial y}{\partial \xi} \\ \frac{\partial z}{\partial \xi} \end{Bmatrix} = \sum_{i=1}^{8} S_{i,\xi} \begin{Bmatrix} x_i \\ y_i \\ z_i \end{Bmatrix}, \qquad \begin{Bmatrix} \frac{\partial x}{\partial \eta} \\ \frac{\partial y}{\partial \eta} \\ \frac{\partial z}{\partial \eta} \end{Bmatrix} = \sum_{i=1}^{8} S_{i,\eta} \begin{Bmatrix} x_i \\ y_i \\ z_i \end{Bmatrix} \tag{2-64}$$

2.3.1.4. The Jacobian matrix

The Jacobian matrix relates the area integral in the local coordinates to the one in the ξ,η coordinates. The elements of **J** are given below;

$$\begin{Bmatrix} \frac{\partial}{\partial \xi} \\ \frac{\partial}{\partial \eta} \end{Bmatrix} = \mathbf{J} \begin{Bmatrix} \frac{\partial}{\partial x'} \\ \frac{\partial}{\partial y'} \end{Bmatrix} = \begin{bmatrix} \frac{\partial x'}{\partial \xi} & \frac{\partial y'}{\partial \xi} \\ \frac{\partial x'}{\partial \eta} & \frac{\partial y'}{\partial \eta} \end{bmatrix} \begin{Bmatrix} \frac{\partial}{\partial x'} \\ \frac{\partial}{\partial y'} \end{Bmatrix} \quad \text{and} \quad \begin{Bmatrix} \frac{\partial}{\partial x'} \\ \frac{\partial}{\partial y'} \end{Bmatrix} = \mathbf{J}^* \begin{Bmatrix} \frac{\partial}{\partial \xi} \\ \frac{\partial}{\partial \eta} \end{Bmatrix} \tag{2-65}$$

where $\mathbf{J}^*$ is the inverse of **J**. The steps of derivation are explained below. The derivatives of x' and y' w.r.t. ξ and η are calculated using the chain rule of differentiation as follows;

$$J_{11} = \frac{\partial x'}{\partial \xi} = \frac{\partial x'}{\partial x}\frac{\partial x}{\partial \xi} + \frac{\partial x'}{\partial y}\frac{\partial y}{\partial \xi} + \frac{\partial x'}{\partial z}\frac{\partial z}{\partial \xi}$$

$$J_{12} = \frac{\partial y'}{\partial \xi} = \frac{\partial y'}{\partial x}\frac{\partial x}{\partial \xi} + \frac{\partial y'}{\partial y}\frac{\partial y}{\partial \xi} + \frac{\partial y'}{\partial z}\frac{\partial z}{\partial \xi}$$

$$J_{21} = \frac{\partial x'}{\partial \eta} = \frac{\partial x'}{\partial x}\frac{\partial x}{\partial \eta} + \frac{\partial x'}{\partial y}\frac{\partial y}{\partial \eta} + \frac{\partial x'}{\partial z}\frac{\partial z}{\partial \eta}$$

$$J_{22} = \frac{\partial y'}{\partial \eta} = \frac{\partial y'}{\partial x}\frac{\partial x}{\partial \eta} + \frac{\partial y'}{\partial y}\frac{\partial y}{\partial \eta} + \frac{\partial y'}{\partial z}\frac{\partial z}{\partial \eta}$$

The derivatives of x', y', z' w.r.t. x, y, z can be calculated as follows;

$$\begin{bmatrix} \frac{\partial x'}{\partial x} & \frac{\partial y'}{\partial x} & \frac{\partial z'}{\partial x} \\ \frac{\partial x'}{\partial y} & \frac{\partial y'}{\partial y} & \frac{\partial z'}{\partial y} \\ \frac{\partial x'}{\partial z} & \frac{\partial y'}{\partial z} & \frac{\partial z'}{\partial z} \end{bmatrix} = \begin{bmatrix} l'_1 & l'_2 & l'_3 \\ m'_1 & m'_2 & m'_3 \\ n'_1 & n'_2 & n'_3 \end{bmatrix}$$

Jacobian matrix can now be written using the equations above, and eq.(2-64)

$$\mathbf{J} = \begin{bmatrix} \sum_{i=1}^{nn} \left(l'_1 x_i S_{i,\xi} + m'_1 y_i S_{i,\xi} + n'_1 z_i S_{i,\xi} \right) & \sum_{i=1}^{nn} \left(l'_2 x_i S_{i,\xi} + m'_2 y_i S_{i,\xi} + n'_2 z_i S_{i,\xi} \right) \\ \sum_{i=1}^{nn} \left(l'_1 x_i S_{i,\eta} + m'_1 y_i S_{i,\eta} + n'_1 z_i S_{i,\eta} \right) & \sum_{i=1}^{nn} \left(l'_2 x_i S_{i,\eta} + m'_2 y_i S_{i,\eta} + n'_2 z_i S_{i,\eta} \right) \end{bmatrix} \tag{2-66}$$

We are now able to calculate the derivatives of the shape functions w.r.t. x' and y'. These derivatives are needed because the stress resultant/strain matrices are calculated in local coordinate system as given in the next sub-section.

2.3.1.5. Strain-displacement matrices

The strain-displacement matrices are written in the local coordinate system. For ease it is divided into three minor matrices, $\mathbf{B}_{\varepsilon i}$, $\mathbf{B}_{\chi i}$, and $\mathbf{B}_{\phi i}$ which are related to normal, bending, and shear terms respectively.

Mid-surface strains in local coordinates are,

$$\boldsymbol{\varepsilon}'^{0} = \begin{Bmatrix} \varepsilon^0_{x'} \\ \varepsilon^0_{y'} \\ \gamma^0_{x'y'} \end{Bmatrix} = \begin{Bmatrix} u_{0,x'} \\ v_{0,y'} \\ \left(u_{0,y'} + v_{0,x'}\right) \end{Bmatrix} = \left[\mathbf{B}_{\varepsilon 1}, \ldots, \mathbf{B}_{\varepsilon 8}\right]\{\delta_1 \ldots \delta_8\}^T \tag{2-67}$$

where,

$$\mathbf{B}_{\varepsilon i} = \begin{bmatrix} l'_1 S_{i,x'} & m'_1 S_{i,x'} & n'_1 S_{i,x'} & 0 & 0 \\ l'_2 S_{i,y'} & m'_2 S_{i,y'} & n'_2 S_{i,y'} & 0 & 0 \\ l'_2 S_{i,x'} + l'_1 S_{i,y'} & m'_2 S_{i,x'} + m'_1 S_{i,y'} & n'_2 S_{i,x'} + n'_1 S_{i,y'} & 0 & 0 \end{bmatrix} \tag{2-68}$$

Deflections due to bending in local coordinates are,

$$\boldsymbol{\chi}' = \begin{Bmatrix} \chi_{x'} \\ \chi_{y'} \\ \chi_{x'y'} \end{Bmatrix} = \begin{Bmatrix} -\theta_{x',x'} \\ -\theta_{y',y'} \\ -\left(\theta_{x',y'} + \theta_{y',x'}\right) \end{Bmatrix} = \left[\mathbf{B}_{\chi 1}, \ldots, \mathbf{B}_{\chi 8}\right]\{\delta_1 \ldots \delta_8\}^T \tag{2-68}$$

where,

$$\mathbf{B}_{\chi i} = -\begin{bmatrix} 0 & 0 & 0 & E_{22i} S_{i,x'} & E_{21i} S_{i,x'} \\ 0 & 0 & 0 & -E_{12i} S_{i,y'} & -E_{11i} S_{i,y'} \\ 0 & 0 & 0 & E_{22i} S_{i,y'} - E_{12i} S_{i,x'} & E_{21i} S_{i,y'} - E_{11i} S_{i,x'} \end{bmatrix} \tag{2-69}$$

Deflections due to shear in local coordinates are,

$$\boldsymbol{\phi}' = \begin{Bmatrix} \phi_{x'} \\ \phi_{y'} \end{Bmatrix} = \begin{Bmatrix} \theta_{x'} - w_{,x'} \\ \theta_{y'} - w_{,y'} \end{Bmatrix} = \left[\mathbf{B}_{\phi 1}, \ldots, \mathbf{B}_{\phi 8}\right]\{\delta_1 \ldots \delta_8\} \tag{2-70}$$

where,

$$\mathbf{B}_{\phi i} = \begin{bmatrix} l'_3 S_{i,x'} & m'_3 S_{i,x'} & n'_3 S_{i,x'} & E_{22i} S_i & E_{21i} S_i \\ l'_3 S_{i,y'} & m'_3 S_{i,y'} & n'_3 S_{i,y'} & -E_{12i} S_i & -E_{11i} S_i \end{bmatrix} \tag{2-71}$$

2.3.1.6. Material matrices in local coordinates

The material matrices relating bending moments, in-plane forces, and shear forces to the nodal displacements can be easily obtained in local coordinate system where the surface normal coincides with $\mathbf{z}'$. The details are given in the previous section about the composite plates.

2.3.1.7. Element stiffness matrix

The shell element formulated in this section is a direct extension of the plate element formulation of which is given in the previous section. The element stiffness matrix can be formulated by following the same procedure as the plate element stiffness matrix. Thus, this formulation is omitted here.

2.3.1.8. Element load vector

Point loads are simply added to the load vector, but the distributed loads have to be transformed into equivalent nodal loads. For example, equivalent nodal representation of uniform pressure normal to the element surface is explained below. If the shell element is subjected to a uniformly distributed pressure load, p, on the face $\zeta = t/2$ then,

$$\begin{Bmatrix} F_{xi} \\ F_{yi} \\ F_{zi} \end{Bmatrix} = \int_{-1}^{1}\int_{-1}^{1} S_i \boldsymbol{\mu}'^{\mathbf{T}} \begin{Bmatrix} 0 \\ 0 \\ p \end{Bmatrix} |\mathbf{J}| d\xi d\eta \tag{2-72}$$

Different types of distributed load conditions, e.g. self weight, or body forces can be treated in a similar way.

2.3.1.9. Stability analysis of shells using the super-parametric shell element

The theory is an extension of the one used in calculating the buckling loads of laminated plates and the solution presented in this section is valid for only symmetrically laminated and developable shells. The notation used is the same as the one used in deriving plate element matrices. Similarly, the problem reduces to the eigenvalue problem given below in eq. (2-73),

$$\det(\mathbf{K} - \lambda \mathbf{K}_\mathbf{G}) = 0 \tag{2-73}$$

where $\mathbf{K}$ is the global stiffness matrix and $\mathbf{K}_\mathbf{G}$ is the global geometric stiffness matrix. Element geometric stiffness matrix, $\mathbf{K}_\mathbf{G}^e$, is derived below.

According to von Karman approximation, which is suitable for thin plates and shells in which the effects of shear deformation can be ignored, the geometric stiffness is a function of in-plane stress resultants only, Reddy (2004). Thus, the potential energy of the applied stresses, V_e arises from the action of the in-plane stresses on the corresponding second order strains as given below in eq. (2-74)

$$V_e = \frac{1}{2}\int_A \left(\mathbf{N}^T \boldsymbol{\varepsilon}_{NL}^0\right) dA \tag{2-74}$$

where the non-linear parts of the mid-surface strains in local coordinates are,

$$\varepsilon'^{0}_{NL}=\begin{Bmatrix}\frac{1}{2}\left(u'^{2}_{0,x'}+v'^{2}_{0,x'}+w'^{2}_{0,x'}\right)\\ \frac{1}{2}\left(u'^{2}_{0,y'}+v'^{2}_{0,y'}+w'^{2}_{0,y'}\right)\\ u_{0,x'}u_{0,y'}+v_{0,x'}v_{0,y'}+w_{0,x'}w_{0,y'}\end{Bmatrix} \tag{2-75}$$

and, the mid-surface strains including the linear and non-linear terms are given below,

$$\begin{aligned}\varepsilon^{0}_{x}&=u_{0,x}+\frac{1}{2}\left[\left(u_{0,x}\right)^{2}+\left(v_{0,x}\right)^{2}+\left(w_{0,x}\right)^{2}\right]\\ \varepsilon^{0}_{y}&=v_{0,y}+\frac{1}{2}\left[\left(u_{0,y}\right)^{2}+\left(v_{0,y}\right)^{2}+\left(w_{0,y}\right)^{2}\right]\\ \varepsilon^{0}_{xy}&=u_{0,y}+v_{0,x}+\left(u_{0,x}u_{0,y}+v_{0,x}v_{0,y}+w_{0,x}w_{0,y}\right)\end{aligned} \tag{2-76}$$

Let's first calculate the first derivatives of mid-surface displacement components.

$$\mathbf{G}\delta^{e}=\left[\mathbf{G}_{1},\ldots,\mathbf{G}_{8}\right]\left\{\delta_{1}\ldots\delta_{8}\right\}^{T}=\left\{u_{0,x'}\quad v_{0,x'}\quad w_{0,x'}\quad u_{0,y'}\quad v_{0,y'}\quad w_{0,y'}\right\}^{T} \tag{2-77}$$

where,

$$\mathbf{G}_{i}=\begin{bmatrix}l'_{1}S_{i,x'} & m'_{1}S_{i,x'} & n'_{1}S_{i,x'} & 0 & 0\\ l'_{2}S_{i,x'} & m'_{2}S_{i,x'} & n'_{2}S_{i,x'} & 0 & 0\\ l'_{3}S_{i,x'} & m'_{3}S_{i,x'} & n'_{3}S_{i,x'} & 0 & 0\\ l'_{1}S_{i,y'} & m'_{1}S_{i,y'} & n'_{1}S_{i,y'} & 0 & 0\\ l'_{2}S_{i,y'} & m'_{2}S_{i,y'} & n'_{2}S_{i,y'} & 0 & 0\\ l'_{3}S_{i,y'} & m'_{3}S_{i,y'} & n'_{3}S_{i,y'} & 0 & 0\end{bmatrix} \tag{2-78}$$

Rewriting the terms in the integral appearing in eq. (2-74) using equations (27) and (28) yields;

$$\mathbf{N}^{T}\boldsymbol{\varepsilon}^{0}_{NL}=\delta^{T}_{e}\left(\mathbf{G}^{T}\mathbf{S}'\mathbf{G}\right)\delta_{e}$$

where $\mathbf{S}'$ is given below in equation (2-79).

$$\mathbf{S}'=\begin{bmatrix}N_{x'} & 0 & 0 & N_{x'y'} & 0 & 0\\ 0 & N_{x'} & 0 & 0 & N_{x'y'} & 0\\ 0 & 0 & N_{x'} & 0 & 0 & N_{x'y'}\\ N_{x'y'} & 0 & 0 & N_{y'} & 0 & 0\\ 0 & N_{x'y'} & 0 & 0 & N_{y'} & 0\\ 0 & 0 & N_{x'y'} & 0 & 0 & N_{y'}\end{bmatrix} \tag{2-79}$$

where $N_{x'}$, $N_{x'y'}$, $N_{y'}$ are the in-plane forces at the Gauss points in local coordinate system calculated at the Gauss points by a primer static analysis. Reduced (2×2) integration shall be used to avoid the shear locking.

The potential energy of the in-plane forces can be minimized by differentiating eq. (2-74) w.r.t. δ_e which results in the element geometric stiffness matrix given below in eq. (2-80).

$$\mathbf{K}_{\mathbf{G}}^{e} = \int_{-1}^{1}\int_{-1}^{1} \mathbf{G}^{T}\mathbf{S}'\mathbf{G}|\mathbf{J}|d\xi d\eta \tag{2-80}$$

A better approximation than the von Karman approximation can be derived by simplification of the following equation, Moita *et al.* (1996),

$$V_e = \frac{1}{2}\int_{V^e} \sigma_{ij}^{0} u_{s,i} u_{s,j} dV = \frac{1}{2}\int_{A}\left(\int_{-t/2}^{t/2} \sigma_{ij}^{0} u_{s,i} u_{s,j} dz\right) dA \tag{2-81}$$

where u_1, u_2, u_3, and σ_{ij}^{0} denote u, v, and w and initial stress components respectively. The expansion of eq. (2-81), neglecting some of the terms which are of negligible importance, is given below in eq. (2-82).

$$V_e = \frac{1}{2}\int_{A}\begin{bmatrix} N_{x'}\left(u_{0,x'}^2 + v_{0,x'}^2 + w_{0,x'}^2\right) + 2N_{x'y'}\left(u_{0,x'}u_{0,y'} + v_{0,x'}v_{0,y'} + w_{0,x'}w_{0,y'}\right) + \dots \\ N_{y'}\left(u_{0,y'}^2 + v_{0,y'}^2 + w_{0,y'}^2\right) + \dots \\ 2M_{x'}\left(u_{0,x'}\theta_{x',x'} + v_{0,x'}\theta_{y',x'}\right) + 2M_{y'}\left(u_{0,y'}\theta_{x',y'} + v_{0,y'}\theta_{y',y'}\right) + \dots \\ 2M_{x'y'}\left(\theta_{x',x'}u_{0,y'} + \theta_{x',y'}u_{0,x'} + \theta_{y',x'}v_{0,y'} + \theta_{y',y'}v_{0,x'}\right) + \dots \\ 2Q_{x'}\left(\theta_{x'}u_{0,x'} + \theta_{y'}v_{0,x'}\right) + 2Q_{y'}\left(\theta_{x'}u_{0,y'} + \theta_{y'}v_{0,y'}\right) \end{bmatrix} dA \tag{2-82}$$

The terms including the in-plane stresses are the same as the ones in eq. (2-74). The extra terms are the ones including the moment and shear force components. Their contribution to the geometric stiffness is calculated as follows. First define vector $\mathbf{G_2}$ multiplication of which with matrix $\mathbf{S_2}$ below results in the terms between the parentheses in equation (2-82). The modified $\mathbf{K}_{\mathbf{G}}^{e}$ is given in equation (2-83).

$$\mathbf{G_2} = \begin{Bmatrix} u_{0,x'} & v_{0,x'} & \theta_{x',x'} & \theta_{y',x'} & u_{0,y'} & v_{0,y'} & \theta_{x',y'} & \theta_{y',y'} & \theta_{x'} & \theta_{y'} \end{Bmatrix}^{T}$$

$$\mathbf{S_2} = \begin{bmatrix} 0 & 0 & M_{x'} & 0 & 0 & 0 & M_{x'y'} & 0 & Q_{x'} & 0 \\ 0 & 0 & 0 & M_{x'} & 0 & 0 & 0 & M_{x'y'} & 0 & Q_{x'} \\ M_{x'} & 0 & 0 & 0 & M_{x'y'} & 0 & 0 & 0 & 0 & 0 \\ 0 & M_{x'} & 0 & 0 & 0 & M_{x'y'} & 0 & 0 & 0 & 0 \\ 0 & 0 & M_{x'y'} & 0 & 0 & 0 & M_{x'} & 0 & Q_{y'} & 0 \\ 0 & 0 & 0 & M_{x'y'} & 0 & 0 & 0 & M_{x'} & 0 & Q_{y'} \\ M_{x'y'} & 0 & 0 & 0 & M_{x'} & 0 & 0 & 0 & 0 & 0 \\ 0 & M_{x'y'} & 0 & 0 & 0 & M_{x'} & 0 & 0 & 0 & 0 \\ Q_{x'} & 0 & 0 & 0 & Q_{y'} & 0 & 0 & 0 & 0 & 0 \\ 0 & Q_{x'} & 0 & 0 & 0 & Q_{y'} & 0 & 0 & 0 & 0 \end{bmatrix}$$

$$\mathbf{K}_{\mathbf{G}}^{e} = \int_{-1}^{1}\int_{-1}^{1} \mathbf{G}^{T}\mathbf{S}'\mathbf{G}|\mathbf{J}|d\xi d\eta + \int_{-1}^{1}\int_{-1}^{1} \mathbf{G}_{\mathbf{2}}^{T}\mathbf{S}_{\mathbf{2}}\mathbf{G}_{\mathbf{2}}|\mathbf{J}|d\xi d\eta \tag{2-83}$$

2.3.2. Verification problems for the shell element

In this section several sample problems are solved in order to assess the performance of the shell element. Solution of the 2D plate problems solved using 8 node plate elements using the current shell element gives exactly the same results, so they're not repeated here.

2.3.2.1. Verification problems for linear static analysis

2.3.2.1(a) Tip displacement of a homogeneous-isotropic arch

An arch, one edge clamped and the other edges free, is loaded with a horizontal tip load of 1 N as shown in Figure 2-12. The material and geometrical properties are as follows; E=2.07 10^{11} N/m^2, ν=0.0, radius R=1.5 m, width b=0.5 m, thickness h=0.01 m. The results are compared with the analytical solution of a curved beam, obtained using Castigliano Theorem neglecting shear deformation. The maximum value of displacements in y and z directions, δ_y and δ_z are, $\delta_y = \frac{\pi PR^3}{4EI} = 3.0710^{-4}\,\mathrm{m}$, and $\delta_z = \frac{PR^3}{2EI} = 1.95610^{-4}\,\mathrm{m}$ respectively. The same problem is solved when only a uniformly distributed pressure, p, is acting on the arch and the results are given below in Table 2-20 in comparison with the analytical results. The results are in excellent agreement even if the mesh is not dense (2×4 mesh). However, it will be shown that when solving stability problems a coarse mesh does not necessarily yield satisfactory results for most of the cases.

2.3.2.1(b) Clamped Cylindrical Shell

An orthotropic clamped cylindrical shell (R_1=10^{30} in., R_2=20 in., a=20 in., h=1 in.) which is shown in Figure 2-13 is subjected to an internal pressure, $P_0 = 6.41/\pi\ psi$. Only one quarter of the cylinder is modelled due to symmetry. The center deflections are presented in Table 2-21, where 2×2Q8, and 2×2Q9 denote 2×2 meshes composed of 8 and 9 node elements respectively. The material properties are given as follows;

$E_1 = 7.5\times10^6\ psi$, $E_2 = 2\times10^6\ psi$, $G_{12} = 1.25\times10^6\ psi$, $G_{12} = G_{13} = G_{23}$, $\nu_{12} = \nu_{13} = 0.25$.

2.3.2.1(c) Cylindrical shell roof subject to self-weight

An open circular cylindrical shell panel supported at its two ends by rigid diaphragms and its longitudinal edges free is subject to gravitational load due to its own weight. The geometry, loading and finite element meshes used are shown in Fig. 2-14. The properties of the two different materials used are as follows;

Material I: Isotropic shell

$E = 3\times10^6\ psi$, $\nu = 0.0$.

Material II: Laminated composite shell

$E_1 = 25\times10^5\ psi$, $E_2 = E_3 = 1\times10^5\ psi$, $G_{12} = G_{13} = 0.5\times10^5\ psi$, $G_{23} = 0.2\times10^5\ psi$, $\nu_{12} = \nu_{13} = \nu_{23} = 0.25$.

The lamina thickness, gravity load , and stacking sequence are; $t = 0.05\,ft$, $g = 9\,lb/ft^2$, [0/0/0/45/-45/90/90/90/-45/45/0/0/0] respectively. The results are given in Tables 2-22, and 2-23 in comparison with the results given in Wung (1997) where the numerical results presented were obtained using a higher order element.

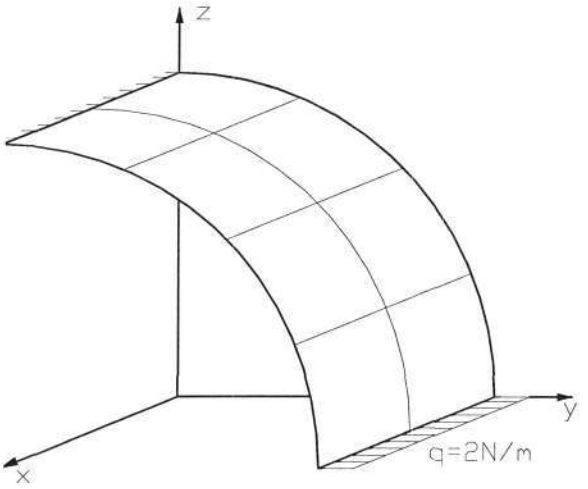

Figure 2-12. Clamped arch geometry and loading

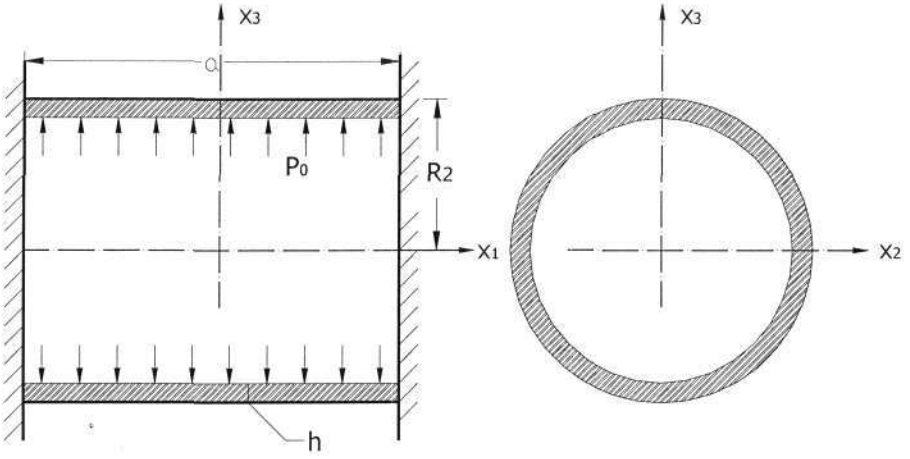

Figure 2-13. Clamped cylinder

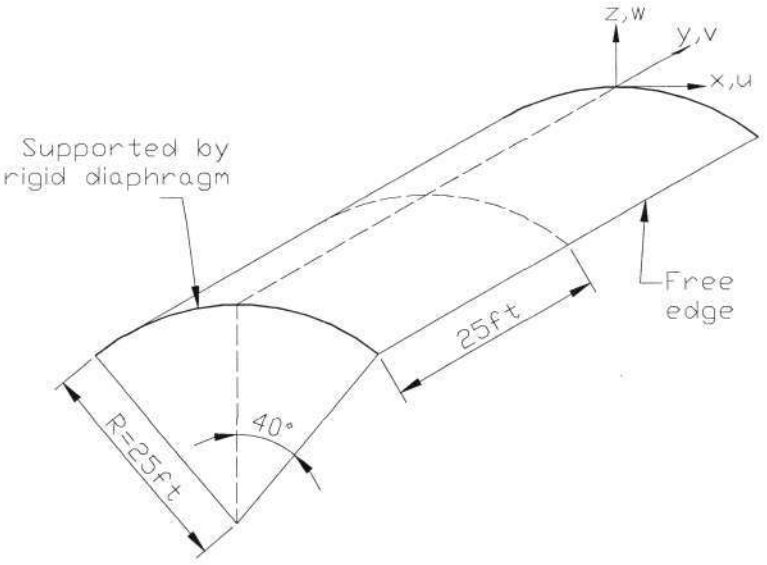

Figure 2-14. A cylindrical shell roof subjected to self weight

Table 2-20. Tip displacements

Displacement component	Line load		Uniform pressure	
	Present	Analytical	Present	Analytical
δ_y	$3.073\ 10^{-4}$	$3.070\ 10^{-4}$	$1.468\ 10^{-4}$	-
δ_z	$1.957\ 10^{-4}$	$1.956\ 10^{-4}$	$1.045\ 10^{-4}$	$1.045\ 10^{-4}$

Table 2-21. Center deflection of a pressurized, clamped cylindrical shell

Stacking sequence	2×2Q8[1]	2×2Q8[2]	2×2Q9[3]	Exact[3]
0°	0.0003733	0.0003706	0.0003727	0.000367
0°/90°	0.0001859	0.0001841	0.0001803	-

[1] Current study
[2] Wung (1997)
[3] Reddy (1984)

Table 2-22. Deflections of the isotropic shell roof

Angle	W (ft.) at mid-span			
	Exact	Fem[1]	Fem[2]	Fem[3]
0°	0.043745	0.045912	0.043912	0.0456217
20°	-0.077860	-0.078810	-0.077793	-0.0785754
40°	-0.308609	-0.307203	-0.300641	-0.306307
	V (ft.) at mid-span			
	Exact	Fem[1]	Fem[2]	Fem[3]
0°	0.000248	0.000174	0.000417	0.0001577
20°	0.002719	0.002744	0.002728	0.0027332
40°	-0.012611	-0.012654	-0.012474	-0.0125639

[1] Results obtained by 6×6 mesh, Wung (1997).
[2,3] Current work solutions by using a 4×4 mesh and a 16×8 mesh respectively

Table 2-23. Deflections of the composite shell roof

	W (ft.) at mid-span		
Angle	Fem[1]	Fem[2]	Fem[3]
0°	-0.0364529	-0.0362692	-0.0362185
10°	-0.0435197	-0.0434629	-0.0434504
20°	-0.0623128	-0.0630153	-0.06240149
30°	-0.0865092	-0.0875434	-0.0866377
40°	-0.1100042	-0.1110222	-0.1100824
	V (ft.) at mid-span		
Angle	Fem[1]	Fem[2]	Fem[3]
0°	0.0036092	0.0036500	0.00361035
10°	0.0032598	0.0032138	0.00325179
20°	0.0017436	0.0016402	0.00173062
30°	-0.0024160	-0.0022981	-0.0023987
40°	-0.0121372	-0.0119913	-0.012004

[1] Results obtained by 6×6 mesh, Wung (1997).
[2,3] Current work solutions by using a 4×4 mesh and a 16×8 mesh respectively

2.3.2.2. Verification problems for stability analysis

In this section problems related to buckling of cylindrical panels and tubes are presented. The solution of plate problems using the shell element defined in this section yields exactly the same results, so they are not repeated.
In the finite element analysis the pre-buckling stress states are prescribed as a uniform in-plane pre-stress state to be able to compare the results with the analytical results unless otherwise is stated.

2.3.2.2(a) Cylindrical tubes under compression and/or pressure

Problem I: Thin walled circular tube under uniform longitudinal compression

The geometry of the circular tube is shown below in Figure 2-15. The directions of the global and nodal directions are also shown. The tube is under the axial compression and the ends are simply supported. The x, y, z components of displacement at the upper boundary nodes the x, y components of displacement at the lower boundary nodes are restrained against translation in the fem model. An approximate analytical formula for the buckling load calculation of axially compressed simply supported cylindrical tubes is given below in eq. (2-84), Young (1989). The formula is most accurate for very long tubes, but applicable if length is several times as great as $1.72\sqrt{Rt}$, which is the length of a half-wave of buckling.

$$\sigma' = \frac{Et}{R\sqrt{3\left(1-\nu^2\right)}} \qquad \left(R/t > 10\right) \tag{2-84}$$

where σ', E, t, R, and ν denote critical value of compressive stress, Young's modulus, thickness, radius, and Poisson's ratio respectively. The ratios of analytical results to numerical results obtained using a total of 64 elements are given below in Table 2-24 where L denotes the length of the tube. Although the mesh is severely distorted for some of the cases, the results are still very accurate. This is one of the advantages of the curved element used over the flat shell elements. Examining the results presented in Table 2-24, it can be observed that the numerical results are very close to the results obtained by the approximate analytical formula It is also observed that the numerical results obtained are highly dependent on mesh density, and the influence of the boundary restraints is higher for lower L/R ratios. The differences between the analytical and numerical results are higher for higher thicknesses due to the influence of shear deformation.

Problem II: Thin walled circular tube under uniform external lateral pressure

An analytical formula is given in Allen and Bulson (1980) for the critical value of pressure as shown below in eq. (2-85). For particular values of L/R and R/t, the n yielding the smallest eigenvalue is determined by trial.

$$\frac{p_{cr}R}{Et} = \frac{\left[(\pi R/L)^2 + n^2\right]^2}{n^2} \frac{(t/R)^2}{12\left(1-\nu^2\right)} + \frac{(\pi R/L)^4}{n^2\left[(\pi R/L)^2 + n^2\right]^2} \tag{2-85}$$

The numerical results are presented below in Table 2-25. The x, y components of displacement at the upper and lower boundary nodes are restrained against translation in the fem model. Error is mainly due to low mesh density, and element distortion, and the influence of boundary conditions on the distribution of membrane forces. The same conclusions can be drawn as for the axially loaded case. It is also observed that, the accuracy is lower comparing to the axially loaded cylinder. This is due to the fact that the pre-buckling deformations are higher for this

case. The buckling mode shapes substantially differ for axial compression and external pressure cases. It is observed that the buckling mode shapes of the externally pressurized cylinders are more complicated than the axially compressed cylinders. This is one of the reasons of the higher accuracy reached when solving axially compressed cylinders as the formulation is displacement based. This means that the results can only be reliable if the displaced geometry can be accurately defined by the finite element mesh used to model the structure. While modelling a structure, it should be kept in mind that the optimal mesh density differs for different load conditions.

Problem III: Laminated circular tube under compression, uniform pressure or a combination of compression and pressure

The results given by Anastasiadis *et al.* (1994) which are based on first order shear deformable shell theory are given in Table 2-26 below in comparison with the numerical results obtained using a total of 128 elements for both L/R= 2 ,5. Here, L, R, h denote length, radius and total thickness respectively. The tube is simply supported, and R=190.5 mm. The material properties are given as follows;

$$G_1 = 206.844\times10^9\,\text{Pa},\ E_2 = 18.6159\times10^9\,\text{Pa},\ G_{12} = G_{13} = 4.48162\times10^9\,\text{Pa},$$
$$G_{23} = 2.55107\times10^9\,\text{Pa},\ \nu_{12} = \nu_{13} = 0.21,\ \nu_{23} = 0.25.$$

The numerical results given in Table 2-26 are not in excellent agreement with the analytical results. However, it is observed that the difference between the numerical and analytical results decrease with increasing length. This is because the stress distribution is more uniform in longer tubes, and the influence of the boundary conditions is lower. However, comparing to the other verification problems solved, the difference between the results are high especially for the external pressure loading case. It is observed that the differences between the analytical and numerical results are lower for higher L/R ratios and thicknesses. Examining the results it is concluded that the linearized stability analysis of tubes under external pressure is prone to errors. Note that, it is stated by Ram and Babu (2002) that a geometrically non-linear analysis is required for this case.

2.3.2.2(b) Cylindrical panels under compression or pressure

Problem I: Homogeneous-isotropic panel under uniform compression

An analytical formula is given in Wang and Reddy (2005) for simply supported, homogeneous-isotropic panels under the action of uniform compression in y direction whose geometry is shown above in Figure 2-16. The ratios of the numerical results to the analytical ones are tabulated below in Table 2-27, where t, β, a, b, $N_{cr,num}$, $N_{cr,ref}$ denote thickness, central angle, length, width, numerical buckling load, and analytical buckling load respectively. The results are in good agreement.

Problem II: Cylindrical composite panel under uniform external lateral pressure

The cylindrical panel shown in Figure 2-16 is subjected to uniform radial pressure. The material properties are given below (in GPa where applicable);

$$E_1 = 413.7,\ \frac{E_2}{E_1} = 0.025,\ \frac{G_{12}}{E_1} = 0.015,\ \nu_{12} = 0.25.$$

The numerical results obtained for a cross-ply laminated clamped cylindrical panel using a 16×8 mesh are given below in Table 2-28 in comparison with the results given in Mateus *et al.*

(1997). The non-dimensional buckling parameter $\overline{\lambda}$ is defined as, $\overline{\lambda} = \frac{p_{crit} RL^2}{\pi^2 \sqrt{D_{11} D_{22}}}$. The variables related to the geometry of the panel are as follows; R = 2540mm., $R/L = 5$, $\beta = 0.2\text{rad}$. For $[0°/90°]_s$ the results obtained in this study using FSDT are between CPT (Kirchoff-Lowe classical laminate theory) and HSDT, which is the expected case. However, for $[90°/0°]_s$ the FSDT results are found out to be closer to the CPT.

Problem III: Cylindrical composite panel under uniform axial compression

The boundary conditions of the simply supported panel shown in Figure 2-16 are taken as follows. $u = v = w = 0$ at curved edge AB, $u = v = 0$ at curved edge CD, and $v = w = 0$ at straight edges AC and BD. No bending rotations are constrained on the edges. The material properties are given as follows;

Material I: $E_1 = 13.75\,\text{Msi}$, $E_2 = 1.03\,\text{Msi}$, $G_{12} = G_{13} = G_{23} = 0.42\,\text{Msi}$, $\nu_{12} = 0.25$.

Material II: $E_1 = 10.0\,\text{Msi}$, $\nu_{12} = 0.30$.

The buckling loads (in lbs/in) are given in Table 2-29 in comparison with the results given in Jaunky and Knight (1999). Note that, different shell theories give different buckling loads, as shown in Table 2-29, where λ_{s-k}, λ_{Donnel} denote critical loads based on Sanders-Koiter, and Donnel shell theories respectively. The numerical results obtained here, $\lambda_{present}$, are very close to the numerical results given in Jun and Hong (1988), λ_{Stags}, calculated using Stags finite element software by assuming a uniform distribution of pre-buckling stress and using a 30×30 mesh. The results are in good agreement and it is evident that the numerical results are more accurate for lower R/t ratios.

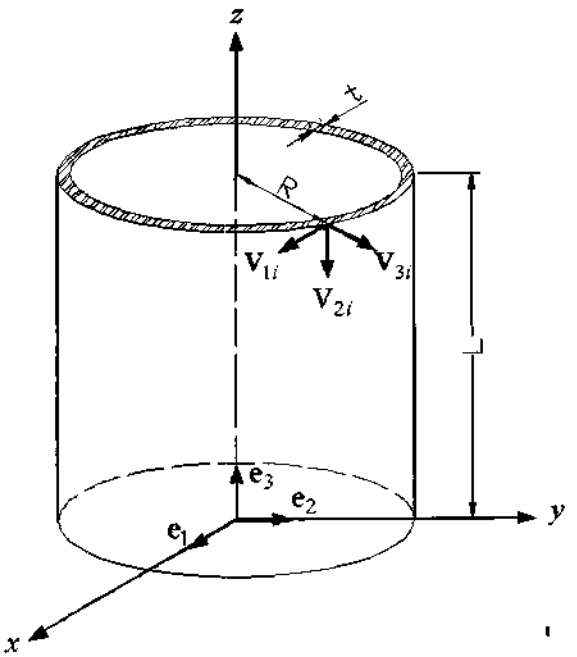

Figure 2-15. Geometry of the cylinder problem

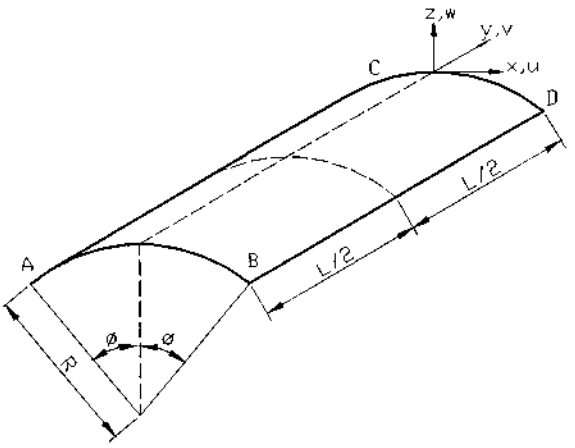

Figure 2-16. Geometry of the panel

Table 2-24. Ratio of analytical to numerical critical load

L/R	$t = R/10$	$t = R/20$	$t = R/50$
1	1.0542	1.0068	0.9975
2	1.0619	1.0349	0.9660

Table 2-25. Ratio of analytical to numerical critical load

L/R	$t = R/10$	$t = R/20$	$t = R/50$
1	1.0967	0.9849	0.8912
2	0.9628	0.9798	0.9411

Table 2-26. Critical values of axial compression (N/m$\times 10^{-6}$) and pressure (Pa$\times 10^{-6}$). Stacking sequence $(45°/45°/-45°)_s$

L/R	Loading	$t = 3.175$mm		$t = 6.35$mm		$t = 12.7$mm	
		(1)	(2)	(1)	(2)	(1)	(2)
2	Compression	0.869	0.9497	3.48	3.5709	13.90	13.1890
	Pressure	1.310	1.6587	7.72	7.7143	42.05	40.0470
5	Compression	0.837	0.9892	3.27	3.6719	12.73	13.4840
	Pressure	0.483	0.5207	2.96	2.6254	16.00	15.2958

(1) Anastasiadis *et al.* (1994)
(2) Current study using a 16×8 mesh

Table 2-27.Ratio of analytical to numerical results

t(mm.)	β(rad)	a(mm.)	b(mm.)	$N_{cr,num}/N_{cr,ref}$
1	0.5	250	250	1.0340
2	0.5	250	250	1.0172
3	0.5	250	250	1.0556
4	0.5	250	250	1.0502
1	$\pi/4$	100	200	1.0670
2	$\pi/4$	100	200	1.0298
3	$\pi/4$	100	200	1.0690
4	$\pi/4$	100	200	1.0349

Table 2-28. $\bar{\lambda}$ for a cross-ply laminated clamped cylindrical panel

R/t	L/t	Laminate	$\bar{\lambda}$ (SLR)[1]	$\bar{\lambda}$ (HSDT)[2]	$\bar{\lambda}$ (CPT)[2]	$\bar{\lambda}$ [3]
800	160	$[0°/90°]_s$	23.39	23.00	21.52	22.724
		$[90°/0°]_s$	7.402	6.925	6.865	6.8399

[1] Palazatto and Dennis (1992)
[2] Mateus *et al.* (1997)
[3] Current study using a 16×8 mesh

Table 2-29. Buckling loads for curved panels for different R/t ratios with L=60 in., t=0.24

Material	R/t	L/R	λ_{s-k} [1]	λ_{Donnel} [1]	λ_{Stags} [1]	$\lambda_{present}$ [2]
I	100	2.5	4685.8	4810.2	4585.2	4677.0
	200	1.25	2475.8	2475.9	2349.7	2387.6
	600	0.417	774.2	774.2	757.4	770.14
II	100	2.5	14336.0	14378.4	14204.4	14922.3
	200	1.25	7243.3	7243.3	7222.13	7397.25
	600	0.417	2421.1	2421.1	2424.2	2154.15

[1] Jaunky and Knight (1999)
[2] Current study using a 16×8 mesh

3. OPTIMIZATION OF COLUMNS UNDER CONCENTRATED AND DISTRIBUTED AXIAL LOADS

3.1 Introduction

Structural components with non-uniform cross-sections are widely used in many applications and are of specific interest in structural, mechanical and aeronautical engineering due to the resulting weight savings. The logical extension of a non-uniform component is to find the best distribution of the cross-sectional area with a view towards maximizing its load carrying capacity or minimizing its weight subject to certain design requirements which are usually expressed as design constraints. The design problem of particular interest in the present study is the buckling optimization of Euler columns subject to an arbitrary distribution of axially distributed and concentrated loads. The objective is to maximize the buckling load subject to volume and maximum stress constraints. The minimum cross-section under a stress constraint is not known a priori as it depends on the maximum buckling load which in turn depends on the optimum shape. The optimization is carried out over the cross-sectional area A which is related to the moment of inertia I by the relations $I=\alpha_n A^n$ where n=1, 2 or 3 and subject to a minimum area or maximum stress constraint as well as a volume constraint. Here, α_n is a dimensional constant depending on the cross section. For a rectangular cross-section, the cases n=1, 2, and 3 correspond to constant depth-variable width, constant height to width ratio, and constant width-variable depth, respectively. The corresponding α_n values for these cases are $\alpha_1 = h^2/12$, $\alpha_2 = h/12b$ and $\alpha_3 = 1/12b^2$ where h denotes the depth and b width of the cross-section. For an equilateral triangle cross-section n=2, $\alpha_2 = \sqrt{3}/18$ and for a solid circle n=2, $\alpha_2 = 1/4\pi$. For sandwich columns of rectangular cross section with fixed width and variable face-sheet thickness, n=1 and $\alpha_1 = H^2$, where $2H$ is the fixed core thickness. In the case of thin walled circular columns of similar cross sections, n=1, $\alpha_1 = D^2/8$ if the design variable is the wall thickness, and n=3, $\alpha_3 = 1/8\pi^2 t^2$ if the design variable is the diameter where D is the cross-sectional diameter and t the wall thickness, Adali (1979). Also, a general formula for regular polygonal cross-sections with m integer sides and with a cross-sectional depth of h with n=2 is given by Arbabi and Li (1991).

The problem of optimizing the cross-sectional shape of a column to maximize its buckling load has been studied in several publications starting with Lagrange (1770-1773). Analytical solutions for statically determinate columns were derived by Keller (1960), and Tadjbakhsh and Keller (1962) considering only the first mode. However, the solution obtained for the clamped-clamped case by Tadjbakhsh and Keller (1962) did not take into account bimodal buckling as pointed out by Olhoff and Rasmussen (1977) who provided the correct solution for the optimal shape.

Three aspects of this optimization problem received relatively little attention in the literature, namely, axially distribute loads, elastically clamped boundary conditions and stress constraints. Buckling of non-uniform columns subject to axially distributed loads was studied by Vaziri and Xie (1992), Panayatounakos (1994) and Li (2000, 2001a, 2001b, 2003) who obtained closed-form solutions for several cases which also included the elastically restrained boundary conditions and multi-step non-uniformity. Results involving the design optimization of columns involving these three complicating factors have been few as most of the work focused on concentrated axial loads, non-compliant boundary conditions and minimum area constraints as opposed to maximum stress constraints. The recent examples of this work include Tada and Wang (1995), Egorov and Kodratiev (1995), Coello Coello *et al.* (1996), Manickarajah *et al.* (2000), Maalawi (2002), Olhoff and Seyranian (2002), Cagdas and Adali (2007), and Adali and Cagdas (2007), where several issues concerning the optimization of columns have been studied

with the bimodal buckling behaviour receiving special attention. Maalawi (2002) considered only stepped columns for the optimization under clamped-free and clamped-clamped boundary conditions.

Optimization of columns under axially distributed loads was obtained for elastically clamped-free boundary conditions by Adali (1979) subject to a minimum area constraint with the buckling mode of the optimal column being a unimodal one. Elastic support conditions were studied by Seyranian (1995), Privalova and Seyranian (1999), and Seyranian and Privalova (1999) in the course of studying the post-buckling behaviour of optimal columns. The most recent study of this problem involving the optimization of an elastically restrained column under a concentrated axial load was given by Seyranian (2003) who obtained the analytical solutions for geometrically similar cross-sections and without a minimum area constraint. In this study it was shown that elastically clamped boundary conditions lead to bimodal solutions and failing to take this into account results in a non-optimal design.

The present study includes the three complicating factors mentioned above, namely, axially distributed buckling load, elastically restrained boundaries and a stress constraint in the optimization of the column and gives results for n=1, 2 and 3. The main tools of the solution are the optimality criteria derived by a variational analysis, slack variable technique for constrained design problems (Haftka et. al, 1990) and the finite element method for the numerical solution of the coupled equations involving the governing differential equation and the bimodal optimality criteria. An optimization algorithm is developed in terms of an iterative method of solution and is applied to the optimal design problem subject to a maximum stress constraint. The designs subject to a minimum area constraint are also studied and comparative results are given.

Even though the stress and the minimum area constraints can be considered equivalent for columns under a concentrated load, this consideration does not apply to axially distributed buckling loads as the stress level changes from point to point. This results in optimal designs with minimum cross-sections which are smaller when the total distributed load is low and larger when the total distributed load builds up. In other words the areas at the minimum cross-sections depend on the location along the column and the direction of the load. Another difference is that an area constraint specifies the minimum area *a priori* and can be included in the solution as an input parameter. However, the minimum area required to satisfy a stress constraint cannot be not known *a priori* as it depends on the buckling load which in turn depends on the optimal cross-sectional shape which depends on the minimum area. This situation necessitates an iterative method of solution with the column shape and the buckling load converging to an optimal distribution and the maximum load, respectively. This difference in the solutions of the problems involving the area and stress constraints applies to distributed as well as concentrated buckling loads.

The present study first derives the unimodal optimality conditions which are used to start the iterative solution procedure which switches to the use of bimodal optimality conditions when the second eigenvalue becomes less than or equal to the first eigenvalue. Both unimodal and bimodal optimality conditions are derived for minimum area and maximum stress constraints. The finite element solution is formulated for a column under concentrated and distributed buckling loads. Numerical results are given to show the accuracy and the convergence of the proposed method. Optimal shapes of columns are obtained for several cases and the effects of various problem parameters on the maximum buckling load and the design efficiency are investigated.

Two iterative techniques based on successive integrations and finite differences are formulated to solve the non-linear optimization problems iteratively, which give satisfactory results. The details of these two techniques are explained by Adali and Cagdas (2006), which is given in the appendix section. The numerical results obtained by these two iterative methods are in excellent

agreement wih the results obtained by the finite element iterative technique However, the ease of implementation of the finite element technique is a great advantage over these methods and considering this, the iterative method is selected to be based on finite elements.. One other reason of using FEM is that, it is straightforward to extend the technique to solve similar problems due to the versatility of the finite element method.

The derivations of the one dimensional beam finite elements used in this section are given in Section 5 accompanied with the verification problems solved. The elements for which the derivations are given are the Hermite beam element, and the special Hermite beam element under distributed loads. A sample program showing the basic steps of the numerical iterative technique for a selected problem is given in the appendix section.

3.2 Problem formulation

The differential equation governing the buckling of a variable cross-section column which is under a constant axial load P and a distributed compressive load $Q(X)$, as shown in Fig. 3-1, is given by

$$\frac{d^2}{dX^2}\left(EI(X)\frac{d^2W}{dX^2}\right)+\lambda_0\frac{d}{dX}\left[\left(\int_X^L Q(t)dt+P\right)\frac{dW}{dX}\right]=0 \tag{3-1}$$

where E, $I(X)$, λ_0, L and W represent the modulus of elasticity, moment of inertia, load factor, length of the column and deflection function, respectively. $\lambda_0 Q(X)$ is the non-uniformly distributed axial load per unit length.

The column is elastically supported at the end points X=0 and X=l with the elastic restraints having rotational spring constants of β_A and β_B as shown in Fig. 3-1. The boundary conditions are given by

$$W=EI(X)\frac{d^2W}{dX^2}-\beta_A\frac{dW}{dX}=0 \quad \text{at} \quad X=0 \tag{3-2}$$

$$W=EI(X)\frac{d^2W}{dX^2}+\beta_B\frac{dW}{dX}=0 \quad \text{at} \quad X=L \tag{3-3}$$

The moment of inertia $I(X)$ can be expressed in terms of the area distribution $A(X)$ as

$$I(X)=\alpha_n\left[A(X)\right]^n \tag{3-4}$$

where α_n is a dimensional constant depending on the cross section and n can be 1, 2, or 3 depending on the relation between $I(X)$ and $A(X)$. The following non-dimensional variables are introduced

$$\begin{aligned} &x=X/L \qquad w=W/L \qquad t=T/L \qquad a(x)=A(X)L/V \\ &S=\int_0^L Q(t)dt \qquad p=P/S \qquad \gamma=\frac{\lambda_0 L^{n+2}S}{E\alpha_n V^n} \qquad q(x)=LQ(X)/S \end{aligned} \tag{3-5}$$

The non-dimensional form of the differential equation can be expressed as

$$(a^n w'')''+\gamma\left[\left(\int_x^1 q(t)dt+p\right)w'\right]'=0 \tag{3-6}$$

using the variables defined in eq.(3-5). The dimensionless boundary conditions are given as

$$w(0) = \left(a^n w'' - k_A w'\right)_{x=0} = 0 \tag{3-7}$$

$$w(1) = \left(a^n w'' + k_B w'\right)_{x=1} = 0 \tag{3-8}$$

where

$$k_A = \frac{\beta_A L^{n+1}}{E\alpha_n V^n}, \qquad k_B = \frac{\beta_B L^{n+1}}{E\alpha_n V^n} \tag{3-9}$$

are dimensionless spring constants. Integrating the differential equation (3-6) twice and using the boundary condition (3-7), one obtains

$$a^n w'' + \gamma\, pw + \gamma\left[w \int_x^1 q(t)dt + \int_0^x w(t)q(t)dt \right] = c_1 x + c_2 \tag{3-10}$$

from which the bending moment $m(x)$ can be computed as

$$m(x) = c_1 x + c_2 - \gamma\left(pw + w\int_x^1 q(t)\,dt + \int_0^x w(t)q(t)\,dt \right) \tag{3-11}$$

where c_1 and c_2 are integration constants which can be determined using boundary conditions (3-7) and (3-8), viz.

$$c_1 = \gamma \int_0^1 w(t)q(t)\,dt - k_B \left.\frac{dw}{dx}\right|_{x=1} - k_A \left.\frac{dw}{dx}\right|_{x=0} \tag{3-12}$$

$$c_2 = k_A \left.\frac{dw}{dx}\right|_{x=0} \tag{3-13}$$

An expression for the buckling load can be obtained by multiplying the governing equation (3-6) by $w(x)$ and integrating the resulting expression taking into account the boundary conditions (3-7) and (3-8). This procedure gives the Rayleigh quotient the minimization of which over all kinematically admissible displacement fields gives the non-dimensional buckling load,

$$\gamma = \min_{w(x)} \frac{\int_0^1 a^n (w'')^2 dx + k_A \left(w'|_{x=0}\right)^2 + k_B \left(w'|_{x=1}\right)^2}{\int_0^1 (w')^2 \left(p + \int_x^1 q(t)\,dt \right) dx} \tag{3-14}$$

Optimal design problems. The constraints of the optimal design problems involve volume, minimum cross-sectional area, maximum stress and the first and second buckling loads. These constraints are formulated next.

i) Volume is constant, i.e., $\int_0^L A\,dX = V$, which is given in a non-dimensional form as

$$\int_0^1 a\,dx = 1 \tag{3-15}$$

ii) Cross-sectional area satisfies the inequality $A \geq A_0$, where A_0 is the minimum allowable area. In non-dimensional form this is expressed as

$$a \geq A_0 L/V = a_0 \tag{3-16}$$

iii) The stress, which is not constant along the length of the column due to distributed axial load, must not exceed the yield stress of the material, i.e., $G(X)/A(X) \leq \sigma_{ys}$, where σ_{ys} represents the yield stress, and $G(X)$ is the total axial load at X. The constraint can be expressed as

$$\frac{\lambda_0}{A(X)}\left(P + \int_X^L Q(T)\,dT\right) \leq \sigma_{ys} \tag{3-17}$$

and in non-dimensional form as

$$\frac{\gamma}{a}\left(p + \int_x^1 q(t)\,d(t)\right) \leq s_{ys} \tag{3-18}$$

using the non-dimensional quantities defined in (3-5) and the non-dimensional stress parameter

$$s_{ys} = \frac{\sigma_{ys} L^{n+1}}{E\ \alpha_n\ V^{n-1}} \tag{3-19}$$

iv) The first buckling load should be less than or equal to the second one, i.e.,

$$\gamma_1 \leq \gamma_2 \tag{3-20}$$

where γ_1 and γ_2 represent the buckling loads corresponding to first and second buckling modes, respectively.

The minimum area and the maximum stress constraints are to be studied in separate problems which are named as Problem I and Problem II. The statements of these design problems are given next.

Problem I. Find the cross-sectional area $a(x)$ of the optimal column for given values of n, k_A, k_B, p, $q(x)$ and a_0 such that the buckling load γ is the maximum subject to the volume constraint $\int_0^1 a\,dx = 1$, and minimum area constraint $a \geq a_0$.

Problem II. Find the cross-sectional area $a(x)$ of the optimal column for given values of n, k_A, k_B, p, $q(x)$ and s_{ys} such that the buckling load γ is the maximum subject to the volume constraint $\int_0^1 a\,dx = 1$, and the maximum stress constraint $\frac{\gamma}{a}\left(p + \int_x^1 q(t)\,d(t)\right) \leq s_{ys}$.

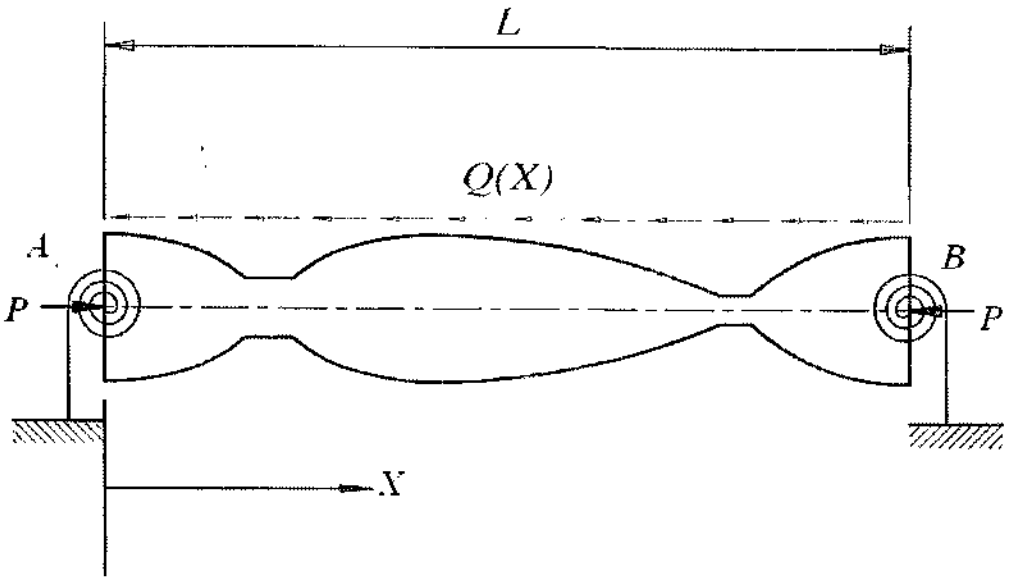

Figure 3-1. Elastically clamped column with distributed and constant axial loads

3.3 Optimality conditions

For statically determinate columns, the optimal shape can be found using a unimodal formulation which is also applicable to clamped-clamped columns when the constraint on minimum cross-sectional area is above a certain value as shown by Olhoff and Rasmussen (1977) in their ground breaking work. For the elastically clamped columns, a unimodal optimality condition without a constraint on minimum area leads to zero cross sectional areas and to a buckling load which is less than that of a uniform column (Olhoff and Rasmussen, 1977). In the present formulation, the unimodal solutions are applicable to the limiting cases of $k_A = k_B = 0$ and $k_A = 8$, $k_B = 0$ which correspond to simply supported and clamped-simply supported columns, respectively. In the general case of k_A, $k_B = 0$, the bimodal formulation involving the first and second buckling modes has to be used unless the minimum area is above a certain value.

The objective of the design problems is the maximization of the buckling load γ corresponding to the first mode. However, maximization of the first eigenvalue using a unimodal optimality condition can lead to a non-optimal design, where the second eigenvalue becomes smaller than the first one. Incorporation of the inequality constraint $\gamma_1 \leq \gamma_2$ into the optimization formulation ensures that the first buckling load γ_1 is smaller than or equal to the second one γ_2. Next the derivations of the optimality conditions are given for Problems I and II.

Unimodal optimality condition for Problem I. The optimization problem can be solved using the Lagrange multiplier technique. We introduce the Lagrangian given by

$$L_{U1} = \frac{\int_0^1 a^n (w'')^2 dx + k_A \left(w'|_{x=0}\right)^2 + k_B \left(w'|_{x=1}\right)^2}{\int_0^1 (w')^2 \left(p + \int_x^1 q(t)\,dt\right) dx} - \lambda_1 \left(\int_0^1 a\,dx - 1\right) + \int_0^1 \lambda_2(x)\left[-h^2(x) - a_0 + a\right] dx \tag{3-21}$$

where, λ_1 and $\lambda_2(x)$ are Lagrange multipliers and $h(x)$ is a slack variable. The variation of L_{U1} with respect to w gives the differential equation and the boundary conditions. The variation of L_{U1} with respect to $a(x)$ yields

$$\int_0^1 \frac{n a^{n-1} (w'')^2}{\int_0^1 (w')^2 \left(p + \int_x^1 q(t)\,dt\right) dx} \delta a\,dx - \lambda_1 \int_0^1 \delta a\,dx + \int_0^1 \lambda_2(x)\,\delta a\,dx = 0 \tag{3-22}$$

where δa is arbitrary. Thus,

$$\frac{n a^{n-1} (w'')^2}{\int_0^1 (w')^2 \left(p + \int_x^1 q(t)\,dt\right) dx} - \lambda_1 + \lambda_2(x) = 0 \tag{3-23}$$

The variation of L_{U1} with respect to $h(x)$ yields

$$\lambda_2(x) h(x) = 0 \tag{3-24}$$

This equation implies that $h(x)$ must be equal to zero when $\lambda_2(x) \neq 0$, and $\lambda_2(x)$ must be zero when $h(x) \neq 0$. As a result, $\lambda_2(x)$ in eq. (3-23) can be discarded since it is equal to zero when the minimum area constraint is not active. Using equations (3-23) and (3-24) results in the following optimality condition

$$n a^{n-1} (w'')^2 = C \int_0^1 (w')^2 \left(p + \int_x^1 q(t)\,dt\right) dx \tag{3-25}$$

where C is an arbitrary constant. Multiplying both sides of (3-25) by a^{n+1}, replacing $a^{2n}(w'')^2$ by $m(x)^2$, and re-arranging yields,

$$a = \begin{cases} C \left[\dfrac{m(x)^2}{\int_0^1 (w')^2 \left(p + \int_x^1 q(t)\,dt\right) dx} \right]^{1/(n+1)} & \text{for} \quad x \in x_a \\ a_0 & \text{for} \quad x \in x_b \end{cases} \tag{3-26}$$

where x_a and x_b represent the regions where minimum area constraint is active and inactive, respectively. Substituting the expression (3-26) into the volume constraint, one finds

$$\int_0^1 a\,dx = \int_{x_a} C\left[\frac{m^2}{\left(p+\int_x^1 q(t)d(t)\right)}\right]^{1/n+1} dx + \int_{x_b} a_0 = 1 \tag{3-27}$$

Unimodal optimality condition for Problem II. In the above procedure, the minimum area constraint is replaced by the maximum stress constraint using the Valentine's technique and the parenthesis in the last term of the Lagrangian given by (3-21) becomes

$$s_{ys} - \frac{\gamma}{a}\left(p+\int_x^1 q(t)d(t)\right) + h^2(x) = 0 \tag{3-28}$$

where the constraint is active only when $h(x)$ is equal to zero. The variation of the Lagrangian with respect to $a(x)$ and $h(x)$ yields,

$$\int_0^1 \frac{na^{n-1}(w')^2}{\int_0^1\left(\frac{dw}{dx}\right)^2\left(p+\int_x^1 q(t)dt\right)dx}\delta a\,dx - \lambda_1\int_0^1 \delta a\,dx - \int_0^1 \lambda_2(x)\frac{\gamma}{a^2}\left(p+\int_x^1 q(t)d(t)\right)\delta a\,dx = 0 \tag{3-29}$$

and

$$\lambda_2(x)h(x) = 0 \tag{2-30}$$

respectively. Removing $\lambda_2(x)$ and $h(x)$ from (3-29), and rearranging the equations, the area distribution can be obtained as

$$a(x) = \begin{cases} C\left[\dfrac{m^2}{\int_0^1 (w')^2\left(p+\int_x^1 q(t)dt\right)dx}\right]^{1/n+1} & \text{for} \quad x \in x_a \\ \dfrac{\gamma}{s_{ys}}\left(p+\int_x^1 q(t)d(t)\right) & \text{for} \quad x \in x_b \end{cases} \tag{3-31}$$

which is similar to the area distribution given by (3-26) with the exception that in the constrained region, i.e., $x \in x_b$, the expression for $a(x)$ is a function of x which is the major difference between the area constrained and stress constrained optimal design problems. Thus, for this problem, the constraint on the maximum allowable stress is not equivalent to a minimum area constraint, because the minimum area required is a function of x and varies along the length of the column. The volume constraint for this case is given by

$$\int_0^1 a\,dx = \int_{x_a} C\left[\frac{m^2}{\int_0^1 (w')^2\left(p+\int_x^1 q(t)dt\right)dx}\right]^{1/n+1} dx + \int_{x_b} \frac{\gamma}{s_{ys}}\left(p+\int_x^1 q(t)d(t)\right) = 1 \tag{3-32}$$

The maximization of the first buckling load by optimizing the area distribution using the unimodal optimality condition may lead to a non-optimal design where the second buckling load can become smaller than the first one. This problem can be solved by incorporating an inequality constraint into the formulation which specifies that γ_1 is smaller than or equal to γ_2 as stated by the constraint (3-20). Using Valentine's technique this constraint can be written as

$$\gamma_2 - \gamma_1 - z^2 = 0 \qquad \text{where} \quad z \in \Re \tag{3-33}$$

and $\Re$ is the set of real numbers. The corresponding Lagrangian is given below where λ is a Lagrangian multiplier

$$L_B = \gamma_1 + \lambda\left(\gamma_2 - \gamma_1 - z^2\right) + (\text{relevant constraints}) \tag{3-34}$$

Variation of L_B with respect to z yields $\lambda z = 0$. Thus, the constraint is active when $z = 0$ and $\lambda \neq 0$, and inactive when $\lambda = 0$ and $z \neq 0$. When $\gamma_2 \geq \gamma_1$, there will not be a contribution coming from the second mode since $\lambda = 0$, and conversely when $\gamma_2 \leq \gamma_1$, the constraint will be active, i.e., $\lambda \neq 0$. In the solution procedure, the iterations start using the unimodal optimality condition and the bimodal optimality condition is employed only when the constraint becomes active during the iterative process.

Bimodal optimality condition for Problem I. The functional for Problem I is taken as

$$L_{B1} = \gamma_1 + \lambda_1\left(\gamma_2 - \gamma_1 - z^2\right) - \lambda_2\left(\int_0^1 a\,dx - 1\right) + \int_0^1 \lambda_3(x)\left[-h^2(x) - a_0 + a\right]dx \tag{3-35}$$

where z, λ_1, λ_2 and $\lambda_3(x)$ are undetermined Lagrange multipliers. The bimodal optimality condition can be derived by calculating the variation of L_{B1} with respect to $a(x)$ and $h(x)$ which yields

$$\begin{aligned}(1-\lambda_1)\int \frac{n a^{n-1}\left(w_1''\right)^2}{\left[\int_0^1 \left(w_1'\right)^2\left(p + \int_x^1 q(t)\,dt\right)dx\right]}\,\delta a\,dx + \lambda_1 \int \frac{n a^{n-1}\left(w_2''\right)^2}{\left[\int_0^1 \left(w_2'\right)^2\left(p + \int_x^1 q(t)\,dt\right)dx\right]}\,\delta a\,dx = \\ = \lambda_2 \int_0^1 \delta a\,dx - \int_0^1 \lambda_3(x)\,\delta a\,dx\end{aligned} \tag{3-36}$$

$$\lambda_2(x)\,h(x) = 0 \tag{3-37}$$

where w_1 and w_2 are the first and the second buckling modes. By removing $\lambda_2(x)$ and $h(x)$ from the optimality condition, and rearranging the equations, one obtains

$$(1-\gamma)a^{n-1}\left(w_1''\right)^2\left[\int_0^1 \left(w_2'\right)^2\left(p + \int_x^1 q(t)\,dt\right)dx\right] + \gamma\, a^{n-1}\left(w_2''\right)^2\left[\int_0^1 \left(w_1'\right)^2\left(p + \int_x^1 q(t)\,dt\right)dx\right] = c \tag{2-38}$$

where c is an unknown constant. By replacing the definite integrals appearing on the left hand side of (3-38) by K_1 and K_2, one can write down the optimality condition in a more compact form as

$$(1-\gamma)a^{n-1}\left(w_1''\right)^2 K_1 + \gamma\, a^{n-1}\left(w_2''\right)^2 K_2 = c \tag{3-39}$$

Multiplication of both sides of (3-39) by a^{n+1}, and rearranging yields

$$(1-\gamma)m_1^2K_1+\gamma\ m_2^2K_2=c\,a^{n+1} \tag{3-40}$$

where $m_1=a^n w_1$ and $m_2=a^n w_2$. Now area can be calculated using the optimality condition as

$$a=\begin{cases}\left[\dfrac{(1-\gamma)m_1^2K_1+\gamma\ m_2^2K_2}{c}\right]^{1/n+1} & \text{for} \quad x\in x_a\\ a_0 & \text{for} \quad x\in x_b\end{cases} \tag{3-41}$$

The constant c can be calculated using the volume constraint, viz.

$$\int_0^1 a\,dx=\int_{x_a}\left[\frac{(1-\gamma)m_1^2K_1+\gamma m_2^2K_2}{c}\right]^{1/n+1}dx+\int_{x_b}a_0dx=1 \tag{3-42}$$

The variation of L_{B1} with respect to z gives

Bimodal optimality condition for Problem II. The Lagrangian for this case is given as

$$L_{B2}=\gamma_1+\lambda_1\left(\gamma_2-\gamma_1-z^2\right)-\lambda_2\left(\int_0^1 a dx-1\right)+\int_0^1\lambda_3(x)\left[s_{ys}-\frac{\gamma_1}{a}\left(p+\int_x^1 q(t)d(t)\right)+h^2(x)\right]dx \tag{3-43}$$

where $\lambda_1, z,\ \lambda_2$ and $\lambda_3(x)$ are undetermined Lagrange multipliers. The variation of L_{B2} with respect to $a(x)$ yields

$$\begin{aligned}(1-\gamma)\int\frac{na^{n-1}\left(w_1''\right)^2}{\left[\int_0^1\left(w_1'\right)^2\left(p+\int_x^1 q(t)dt\right)dx\right]}\delta a\,dx+\gamma\int\frac{na^{n-1}\left(w_2''\right)^2}{\left[\int_0^1\left(w_2'\right)^2\left(p+\int_x^1 q(t)dt\right)dx\right]}\delta a\,dx=\\ =\lambda\int_0^1\delta a\,dx-\int_0^1\lambda_2(x)\frac{\gamma}{a^2}\left(p+\int_x^1 q(t)d(t)\right)\delta a\,dx\end{aligned} \tag{3-44}$$

Removing $\lambda_2(x)$ and $h(x)$ from the optimality conditions (3-37) and (3-44), and rearranging the equations, a relation between the area and moment functions can be obtained which is the same as (3-41). Thus the optimal area function is given by

$$a(x)=\begin{cases}\left[\dfrac{(1-\gamma)m_1^2K_1+\gamma\ m_2^2K_2}{c}\right]^{1/n+1} & \text{for} \quad x\in x_a\\ \dfrac{\gamma}{s_{ys}}\left(p+\int_x^1 q(t)d(t)\right) & \text{for} \quad x\in x_b\end{cases} \tag{3-45}$$

For a given value of γ, the constant c can be calculated using the volume constraint (3-15) which gives

$$\int_0^1 a\,dx=\int_{x_a}\left[\frac{(1-\gamma)m_1^2K_1+\gamma m_2^2K_2}{c}\right]^{1/n+1}dx+\int_{x_b}\frac{\gamma}{s_{ys}}\left(p+\int_x^1 q(t)dt\right)dx=1 \tag{3-46}$$

3.4 Numerical solution procedure

The one dimensional eigenvalue problem is solved using the finite element technique which is summarized in Chapter I.

Iterative Solution. Iterations start using the unimodal optimality condition and switch to the bimodal optimality condition only when the constraint (2-20) on the first and second buckling loads become active during the iterative process. The iterative scheme is given next.

i) i=1, assume a uniform area distribution.
ii) Compute $p_{1(i)}$, $p_{2(i)}$, $w_{1(i)}$, $w_{2(i)}$, $w'_{1(i)}$, $w'_{2(i)}$
iii) Calculate $m_{1(i)}$, $m_{2(i)}$ using (3-11).
iv) If i>3
Terminate if
$\left|p_{1(i)} - p_{2(i)}\right| < 10^{-5}$, or $\left|p_{1(i)} - p_{1(i-1)}\right| < 10^{-5}$.
v) If $p_{1(i)} < p_{2(i)}$, use unimodal optimality condition.
vi) Assume a value for C.
vii) Calculate $a_{(i)}$, x_a and x_b according to (3-26) or (3-31).
viii) Calculate C using (3-27) or (3-32)
ix) Go to Step (vii) until C value converges.
x) Elseif $p_1 \geq p_2$, use bimodal optimality condition.
xi) Calculate γ by using a one-dimensional optimization algorithm
a. Assume a value for C.
b. Calculate $a_{(i)}$, x_a and x_b according to equation (3-41) or (3-45)
c. Calculate C using equation (3-42) or (3-46).
d. Go to step b until C value converges.
xii) Replace a_i according to (3-47) below.
xiii) $i = i + 1$
xiv) Go to Step (ii).

To increase numerical stability of the iterations, a_i is taken as the weighted average of the area calculated in the current iteration step, and the one computed in the preceding one, a_{i-1}, that is,

$$a_i = \frac{\theta a_i + (1-\theta) a_{i-1}}{100} \tag{3-47}$$

where $\theta \in [0,1]$, and its value is taken as 0.98 in the present study.

The scheme defined in this section can be used to solve problems which are unimodal by setting γ=0 and bypassing step (x).

3.5 Numerical results

Results are given for n=1, 2 and 3 for minimum area (Problem I) and maximum stress (Problem II) constrained problems. The effect of two different distributed axial loads on the optimal shape is investigated, namely, the uniformly distributed load $q(x)$=1 and the triangular load $q(x)$=2(1-x) with the total distributed load being equal to unity. The direction of the distributed load is from x=0 (end B in Fig. 3-1) towards the end x=0 (end A in Fig. 3-1).

The efficiency of an optimal design, η_{eff}, is computed from

$$\eta_{\text{eff}} = \frac{\gamma_{\max} - \gamma_{un}}{\gamma_{un}} \times 100 \tag{3-48}$$

which indicates the percent increase in the buckling parameter as compared to a uniform column. In equation (3-48), $\gamma_{\max}$ and γ_{un} are the buckling parameters for the optimal and the uniform columns, respectively.

3.5.1 Elastically restrained columns

The optimal area functions of clamped-elastically restrained columns under distributed and triangular loads are given in Fig. 3-2 with n=1, p=0, a_0=0.0 and s_{ys}=8 where the rotational spring constants at x=0 and x=1 are k_A=8 and k_B=4, respectively. The corresponding graphs for n=2 and 3 are given in Figs. 3-3 and 3-4. It is observed that the optimal areas become larger towards the clamped end due to the axial load increasing towards this end. Also the cross-sectional areas do not become zero even though there are no thickness constraints. This is due to buckling mode being bimodal, which is the case up to a certain minimum area after which the solutions become unimodal. It is observed that uniformly and triangularly distributed loads have distinct effects on the optimal shape as comparisons of Figs. 3-2a, 3-3a and 3-4a with Figs. 3-2b, 3-3b, and 3-4b indicate. The differences in the optimal shapes for different values of n are observed from a comparison of Figs. 3-2, 3-3 and 3-4 with the increasing n leading to optimal shape becoming more uniform. It is noted that the unsymmetry in the optimal shapes is due to both total axial load increasing towards x=0 which is zero at x=1 and unity at x=0 as well as due to the unsymmetry in the boundary conditions.

Fig. 3-5 shows the corresponding graphs for n=1, 2 and 3 under the uniformly distributed load q=1 and the axial load p=0.5, i.e., a concentrated axial load is also acting on the column in addition to the distribute load. Comparisons of the graphs in Fig.3-5a, b and c with those in Figs. 3-2a, 3-3a and 3-4a, respectively, corresponding to n=1, 2 and 3 show that the main change brought about by the addition of the concentrated load is that the section at x=0 becomes smaller. This is due to the fact that the axial load distribution on the column becomes more uniform when p>0 as compared to the case when p=0. However, the change is minimal in the absence of a stress constraint.

Next the effect of stress and area constraints on the optimal shape is studied. Fig. 3-6 shows the optimal cross-sectional areas of elastically restrained columns for n=1 subject to the minimum area constraint a_0=0.7 and the maximum stress constraint s_{ys}=90 with $q(x)$=1. It is observed from Fig. 3-6a that minimum areas are different at both locations where the column narrows for the stress constrained design since the axial load, hence the stress, increases towards the end x=0 under the action of distributed axial load. This point illustrates the main difference between area and stress constrained column designs when the compressive load is distributed. In the area constrained design, minimum areas are the same at both locations while in the stress constrained design they are different with the minimum area increasing as the load increases. Comparison of Figs. 3-6a (p=0) and 3-6b (p=0.5) indicates that the minimum area around x=0.9 is larger when p=0.5. This is due to increased stress as a result of the addition of the concentrated load. However, the minimum area around x=0.3 is smaller when p=0.5 (Fig. 3-6b). This is due to the fact that the buckling parameter γ is smaller when p=0.5 and consequently the stress is less at x=0.3 as compared to the stress when only the distributed load acts. This example clearly shows the substantial differences between area and stress constrained designs when a distributed axial load is acting on the column.

The corresponding results for n=2 and n=3 are given in Figs. 3-7 and 3-8 where similar characteristics can be observed. Comparison of Figs. 3-6, 3-7 and 3-8 indicates that the relative sizes of the areas for the minimum area and stress constrained designs at x=0 change as n increases.

The curves of the buckling parameter γ are plotted against the stress constraint s_{ys} in Fig. 3-9 for the clamped-elastically restrained columns under the axial load $q(x)$=1 with k_B=4 and k_B=10. It is observed that γ shows a large increase initially with the increase tapering off quickly when s_{ys} is above a certain value. If s_{ys} is too small, an optimal design does not exist for the specified volume constraint and yield failure occurs. It is noted that higher values of n and k_B (increased rotational stiffness) lead to higher γ.

Fig. 3-10 shows the curves of η_{eff} plotted against s_{ys} for the same problem parameters as the ones employed in Fig. 3-10. It is observed that increase in the rotational stiffness leads to lower buckling load efficiency. However, higher n values provide more efficient designs with the efficiency of the design with n=3 being almost twice the efficiency of the design with n=1.

3.5.2 Simply supported columns

The optimal area functions of simply supported columns under the distributed load $q(x) = 1$ are given in Fig. 3-11 for n=1, 2 and 3 with p=0, a_0=0.0 and s_{ys}=8 . It is observed that the optimal shapes are unsymmetrical with respect to the mid-point x=0.5 with the area functions becoming larger towards the end x=0 due to the axial load increasing towards this end. The unsymmetry in the optimal shapes is due to the total axial load increasing towards x=0 which is zero at $x = 1$ and unity at $x = 0$. It is noted that the areas of the optimal shapes at the end points $x = 0$ and $x = 1$ are theoretically equal to zero. The non-zero values which appear at the end points are due to the finite element solution with the finite elements having a finite thickness. The corresponding figures for a combination of the distributed axial load $q(x)$=1 and the concentrated axial load $p = 0$ acting on the column are given in Fig. 3-11. It is observed that the effect of the concentrated load $p = 0.5$ on the optimal shape is to make shapes more symmetrical as a comparison of Figs. 3-11 and 3-12 indicates. It is noted that as p goes to infinity, the optimal shapes of simply supported columns become completely symmetrical with respect to the mid-point $x = 0.5$. The differences in the optimal shapes for different values of n are observed from a comparison of Figs. 3-11a to 3-11c, and 3-12a to 3-12c with the increasing n leading to optimal shapes becoming more uniform.

Next the effect of stress and area constraints on the optimal shape is studied. Figs. 3-13, 3-14 and 3-15 show the corresponding graphs for n = 1, 2 and 3, respectively, with the optimal columns subject to the minimum thickness constraint $a(x)=a_0$=0.5 and the maximum stress constraint $s(x)=s_{ys}$=90. The loadings are taken as the distributed load $q(x)$=1 only (p = 0), and a combination of the distributed load $q(x)$=1 and the concentrated load p = 0.5. It is observed from Figs. 3-13, 3-14 and 3-15 that, in the case of stress constrained designs with s_{ys}=90, minimum areas at x = 0 are larger than the ones at x = 0 and x = 1. This is due to the fact that the axial load, hence the stress, increases towards the end x=0 under the action of distributed axial load necessitating a larger area to satisfy the stress constraint. This point illustrates the main difference between area and stress constrained column designs when the compressive load is distributed. In the area constrained design, minimum areas remain the same at both locations while in the stress constrained design they are different with the minimum area becoming larger as the load increases. Comparison of Figs. 3-13a, 3-14a and 3-15a (p=0) with Figs. 3-13b (p=0.5) indicates that the minimum area around x=1.0 is larger when p=0.5. This is due to increased stress as a result of the addition of the concentrated load. However, the minimum area around x=0.0 is smaller when p=0.5 (Figs. 3-13b, 3-14b, 3-15b). This is due to the fact that the buckling parameter γ is smaller when p=0.5 and consequently the stress becomes less at x=0.0 as compared to the stress when only the distributed load acts. Figs 3-13, 3-14 and 3-15 clearly show the substantial differences between area and stress constrained designs when a distributed axial load is acting on the column. Comparison of Figs. 3-13, 3-14 and 3-15 indicates that the relative sizes of the minimum areas for the constrained designs change as n increases.

The curves of the buckling parameter γ are plotted against the stress constraint s_{ys} in Fig. 3-16 for the simply supported columns with n = 1, 2, 3 under the axial loads $q(x)$ = 1, p = 0.0 and $q(x)$ = 1, p = 0.5. It is observed that γ shows a large increase initially with the increase tapering off quickly when s_{ys} is above a certain value. In the initial parts of the curves (the steep parts), the failure occurs by yield and the equation of the curve in this region is given by

$$\gamma = \left(p + \int_0^1 q(t)\,d(t) \right)^{-1} a_{const}\, s_{ys} \tag{3-49}$$

where a_{const} is the constant area needed to satisfy the stress constraint. If s_{ys} is too small, an optimal design does not exist for the specified column volume as the column fails to satisfy the stress constraint. It is noted that higher values of n and lower values of p lead to higher γ. As the buckling parameter for a uniform column is γ_{un}=18.57, the efficiencies are 29.0% for $n=1$, 46.9% for $n=2$, and 59.4% for $n=3$ as $s_{ys} \to \infty$ when $q(x)=1$ and $p=0$. The corresponding values for $q(x)=1$ and $p=0.5$ are (γ_{un}=9.71) 23.4% ($n=1$), 36.6% ($n=2$), and 45.4% ($n=3$).

3.5.3 Unconstrained analytical solution of the optimal design problem for n=1

Closed form solution of the design problem can be obtained for the case of a column subject to $q(x)$, $p>0$ with $a_0=0.0$, $s_{ys}=\infty$, and $n=1$. This result can be used to validate the results obtained by the iterative algorithm. The results are given for only simply supported columns but the method is valid for different support conditions leading to unimodal behavior. From eq. (3-26) it follows that w'' =constant for the optimal beam with $n=1$.

The optimal area distribution maximizing the load factor of a simply supported column of constant volume without a constraint on minimum area or maximum stress is given below in eq. (3-50)

$$a = Cm^{2/n+1} \tag{3-50}$$

where m denotes moment distribution and C is a constant which can be determined using the constraint on volume as follows,

$$C = \frac{1}{\int_0^1 m^{2/n+1} dx} \tag{3-51}$$

Examining eq.(3-50), it can be seen that when n=1 a becomes equal to Cm, which means that for this case w'' is constant. w' and w can be obtained by integration as follows,

$$w'' = \text{constant} = c, \qquad w' = cx + b, \qquad w = cx^2/2 + bx + d.$$

The integration constants b and d can be found by using the boundary conditions. Thus, for a simply supported column,

$$w' = c(x - 1/2), \qquad w = c\left(x^2 - x\right)/2.$$

An equation giving the nondimensional bending moment at an interior point, $m(x)$,can be obtained by integrating the governing d.e. twice, which is given in eq.(3-11). The integration constants c_1 and c_2 can be determined using equations (3-12) and (3-13) as shown below,

$$c_1 = \gamma \int_0^1 w(t)q(t)\,dt\,, \qquad c_2 = 0\,.$$

Letting c=1 and re-arranging eq.(3-11) yields,

$$a = \frac{f(x)}{\int_0^1 f(x)dx} \tag{3-52}$$

where,

$$f(x) = x\int_0^1 w(t)q(t)dt - pw - w\int_x^1 q(t)dt - \int_0^x w(t)q(t)dt \tag{3-53}$$

Inserting w, w' into eq.(3-53) and the carrying out the integrations $f(x)$, and $a(x)$ can easily be calculated. The buckling parameter γ is given below,

$$\gamma = \frac{1}{\int_0^1 f(x)dx} \tag{3-54}$$

γ can also be calculated using eq. (3-55) which is given below.

$$\gamma = \frac{\int_0^1 a(w'')^2\,dx}{\int_0^1 (w')^2\left(p + \int_x^1 q(t)\,dt\right)dx} = \frac{c^2}{\int_0^1 (w')^2\left(p + \int_x^1 q(t)\,dt\right)dx} = \frac{1}{\int_0^1 (x-1/2)^2\left(p + \int_x^1 q(t)\,dt\right)dx} \tag{3-55}$$

The optimality condition given in eq. (3-50) is valid only for a distributed load which is continuous over the entire column length. In this study, to be able to use the same optimality condition, the partially distributed load is expanded over the entire length using the Fourier series expansion. Let the Fourier expansion corresponding to a given distributed load be in the form given below in eq. (3-56),

$$q(x) = a + b\sum_{n=1}^{\infty}\left[A\cos(2n\pi x) + B\sin(2n\pi x)\right] \tag{3-56}$$

$f(x)$ can be calculated using eq. (3-53) as given below in eq. (3-57),

$$f(x) = p\frac{(x - x^2)}{2} + \frac{a}{12}(4x^3 - 9x^2 + 5x) + \sum_{n=1}^{\infty}\left[f_1(x,n) + f_2(x,n)\right] \tag{3-57}$$

$$f_1(x,n) = \frac{1}{24n^3\pi^4}\left[\cos(2n\pi x)(3An\pi b - 6An\pi bx - 3Bb) + \sin(2n\pi x)(3Bn\pi b - 6Bn\pi bx - 3Ab)\right]$$

$$f_2(x,n)=\frac{1}{8n^3\pi^3}\left(2Bn^2\pi^2x^2+3An\pi x-2Bn^2\pi^2x+B-An\pi\right)$$

and γ is given below in eq. (3-58)

$$\gamma=\frac{24}{2p+a+\sum_{n=1}^{\infty}\frac{Bb\left(6-n^2\pi^2\right)}{n^3\pi^3}} \tag{3-58}$$

In eq.(3-56) a and b are constants and A and B are functions of n. Thus, the integrations will yield the same results for different loads which can be expressed in the form of eq.(3-56). By changing the constants a, b, and the variables A, B, which are functions of n, different load cases can be modelled. $a(x)$ and γ can be obtained by substituting for a, b, A and B in equations (3-52)-(3-58). Here, 6 different load cases are considered and the variables related to the load cases considered are given below in Table 3-1.

Numerical solution of this problem using 50 elements with $q_0=1$, $p=0.5$ gives the buckling load as $\gamma=11.98$. This value is very close to 12, which is the exact value calculated from equation (2-55). Also, for $q_0=1$, $p=0.3$ exact result is 15 where numerical result is $\gamma=14.97$. The comparisons of the analytical results with the numerical results are given below in figures 3-17 to 3-22. This comparison shows that the numerical technique is also very accurate for non-continuously distributed loads.

3.5.4 Clamped columns

Optimal shapes of columns are given for $n=1,2$ and 3 for unconstrained designs (Figs. 3-23 to 3-27) and the constrained designs for the minimum area (Problem I) and the maximum stress (Problem II) problems (Figs. 3-28 to 3-30). The maximum values of the buckling load parameter γ corresponding to optimal columns are plotted in Fig. 3-31 against the maximum stress s_{ys}. In the numerical results, the effect of axial load distribution, i.e., the degree of non-uniformity of the axial load, on the optimal shape is investigated. This is done by considering the uniformly distributed axial load $q(x)=1$ and the triangular load $q(x)=2(1-x)$ with the total distributed load being equal to unity. The direction of the distributed load is taken from $x=1$ (end B in Fig. 1) towards the end $x=0$ (end A in Fig. 1).

The optimal area functions of clamped-clamped columns under distributed and triangular loads are given in Fig. 3-23 with $n=1$, $p=0$, $a_0=0.0$ and $s_{ys}=\infty$. The corresponding graphs for $n=2$ and 3 are given in Figs. 3-24 and 3-25. It is observed that the optimal areas become larger towards the end A ($x=0$) due to the axial load increasing towards this end. It is noted that the cross-sectional areas do not become zero even though there are no thickness constraints due to bimodal optimality which can be seen more clearly for $n=2$ and 3 (Figs. 3-24 and 3-25). It is also observed that the narrow sections located close to ends A and B have different thicknesses due to the axial load increasing towards the end A. Comparisons of Figs. 3-23a, 3-24a and 3-25a with Figs. 3-23b, 3-24b, and 3-25b indicate the effect of the uniformly and triangularly distributed axial loads on the optimal shape. Thicknesses of the narrow sections and the cross-sectional areas of the end points at A and B differ for different loadings. The differences in the optimal shapes for different values of n are observed from a comparison of Figs. 3-23, 3-24 and 3-25 with the increasing n leading to optimal shape becoming more uniform. It is noted that the unsymmetry in the optimal shapes with respect to mid-point $x=0.5$ is due to the total axial load increasing towards $x=0$ which is zero at $x=1$ and unity at $x=0$. This contrasts with the

optimal columns under concentrated loads, i.e., $q(x)=0$ and $p>0$, for which optimal shapes are symmetrical with respect to mid-point due to the symmetry in the loading.

Fig. 3-26 shows the corresponding graphs for optimal columns with $n=1,2$ and 3 under a uniformly distributed load $q(x)=1$ and an axial load $p=0.5$, i.e., under both concentrated and distributed axial loads. Comparisons of the graphs in Figs. 3-26a, b and c with those in Figs. 3-23a, 3-24a and 3-25a, respectively, show that the main change brought about by the action of the concentrated load is that the sections at $x=0$ become smaller and the sections at $x=1$ larger. This is due to the fact that the axial load distribution on the column becomes more uniform when $p>0$ as compared to the case when $p=0$. However, the change is small in the absence of a stress constraint.

Next the effects of stress and area constraints on the optimal shape are studied. Fig. 3-27 shows the optimal clamped columns for $n=1$ subject to the minimum area constraint $a_0=0.7$ (Problem I) and the maximum stress constraint $s_{ys}=90$ (Problem II) with $q(x)=1$. It is observed from Figs. 3-27a and 3-27b that minimum areas differ at locations where the stress constraint is active. This is due to the fact that the axial load, hence the stress, increases towards the end $x=0$ leading to a thicker section towards the end A. This point illustrates the main difference between the area and stress constrained optimal designs when the compressive load is distributed. In the area constrained design, minimum areas are the same at both locations while in the stress constrained design they are different with the minimum area increasing as the load increases. Comparison of Figs. 3-27a ($p=0$) and 2-27b ($p=0.5$) indicates that the minimum area around $x=0.72$ is smaller when $p=0.5$. Similarly, the minimum area around $x=0.23$ is smaller when $p=0.5$ (Fig. 3-27b). This is due to the fact that the buckling parameter γ is smaller when $p=0.5$ and consequently the stress is less as compared to the stress when only the distributed load acts. This example clearly shows the substantial differences between area and stress constrained designs when a distributed axial load acts on the column.

Corresponding graphs for $n=2$ and 3 are given in Figs. 3-28 and 3-29, respectively, where similar characteristics can be observed. Comparison of Figs. 3-27, 3-28 and 3-29 indicates that the relative sizes of the areas at $x=0$ for the minimum area and stress constrained designs decrease as n increases.

The curves of the buckling parameter γ are plotted against the stress constraint s_{ys} in Fig. 3-30 for optimal columns under the axial loads $q(x)=1$, $p=0$ (Fig. 3-30a) and $q(x)=1$, $p=0.5$ (Fig. 3-30b). It is observed that γ shows a large increase initially with the increase tapering off quickly when s_{ys} reaches a certain value. If s_{ys} is too small, an optimal design does not exist for the specified volume constraint and yield failure occurs. It is noted that higher values of n and lower values of p lead to higher γ.

For high values of s_{ys}, the efficiencies are $\eta_{\text{eff}}=27.9$ for $n=1$, $\eta_{\text{eff}}=46.7$ for $n=2$, and $\eta_{\text{eff}}=58.2$ for $n=3$ for the loading case $q(x)=1$, $p=0$ indicating that higher n values provide more efficient designs. The efficiency curves for the loading $q(x)=1$, $p=0$ are shown in Fig. 3-31.

Table 3-1. A, B, and b for different load cases (a=1 for all load cases)

Load Case	$q(x)$	A	B	b
1	1	0	0	0
2	$\begin{cases} 0 & 0 \le x < 1/2 \\ 2 & 1/2 \le x \le 1 \end{cases}$	$\dfrac{\sin(2n\pi)-\sin(n\pi)}{n}$	$\dfrac{\cos(n\pi)-\cos(2n\pi)}{n}$	$\dfrac{2}{\pi}$
3	$\begin{cases} 2 & 0 \le x < 1/2 \\ 0 & 1/2 \le x \le 1 \end{cases}$	$\dfrac{\sin(n\pi)}{n}$	$\dfrac{1-\cos(n\pi)}{n}$	$\dfrac{2}{\pi}$
4	$\begin{cases} 0 & 0 \le x < 1/4 \\ 2 & 1/4 \le x \le 3/4 \\ 0 & 3/4 \le x < 1 \end{cases}$	$\dfrac{\sin(3n\pi/2)-\sin(n\pi/2)}{n}$	$\dfrac{\cos(n\pi/2)-\cos(3n\pi/2)}{n}$	$\dfrac{2}{\pi}$
5	$\lim\limits_{\delta\to 0}\begin{cases} 0 & 0 \le x < 1/2-\delta \\ 1/\delta & 1/2-\delta \le x \le 1/2 \\ 0 & 1/2 \le x < 1 \end{cases}$	$2\cos(n\pi)$	0	1
6	$\lim\limits_{\delta\to 0}\begin{cases} 0 & 0 \le x < 1/4-\delta \\ 1/\delta & 1/4-\delta \le x \le 1/4 \\ 0 & 1/4 \le x < 1 \end{cases}$	$2\cos(n\pi/2)$	$2\sin(n\pi/2)$	1

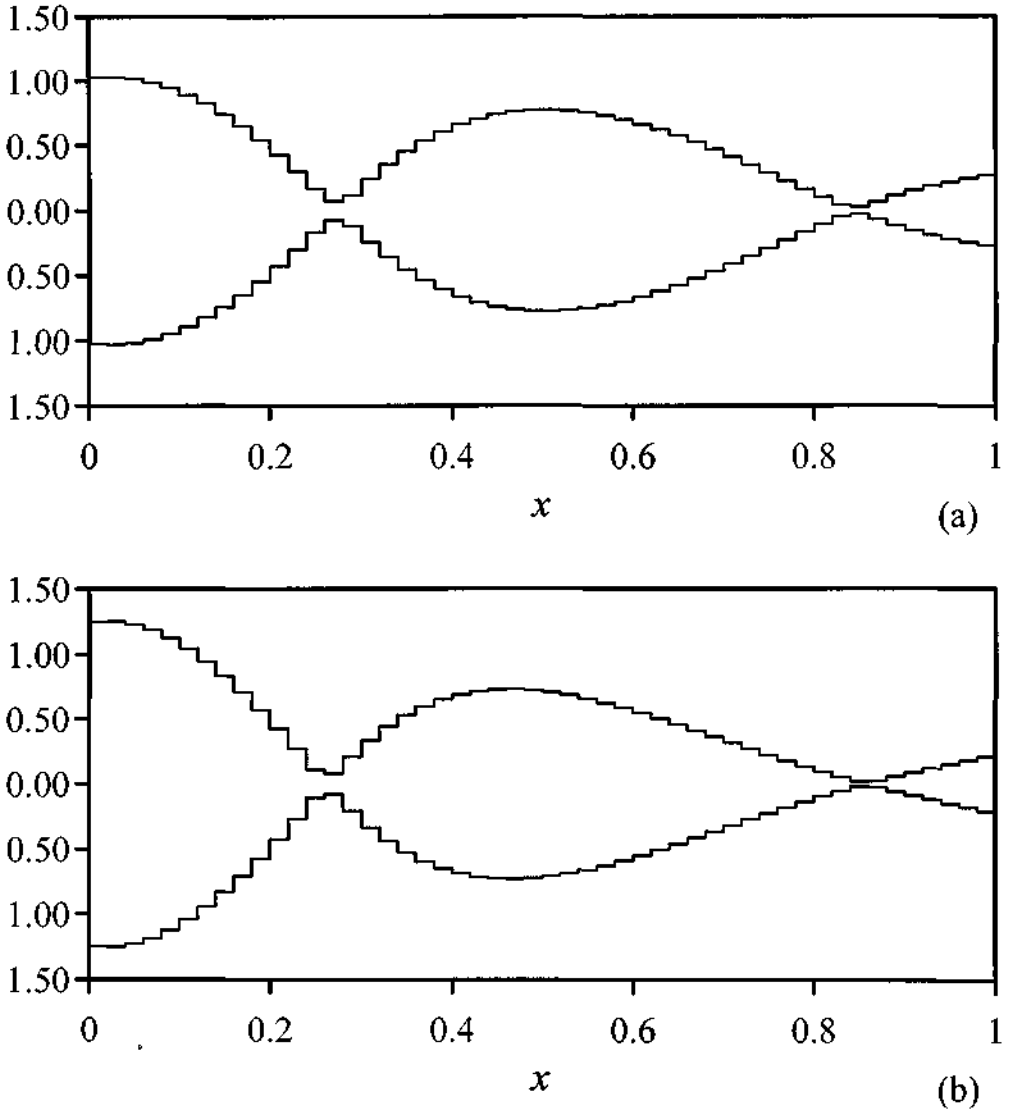

Figure 3-2. Optimal areas of clamped-elastically restrained columns under axial loads (a) $q(x)=1$ and (b) $q(x)=2(1-x)$ with $n=1$, $p=0$, $a_0=0.0$, $s_{ys}=8$ and $k_B=4$.

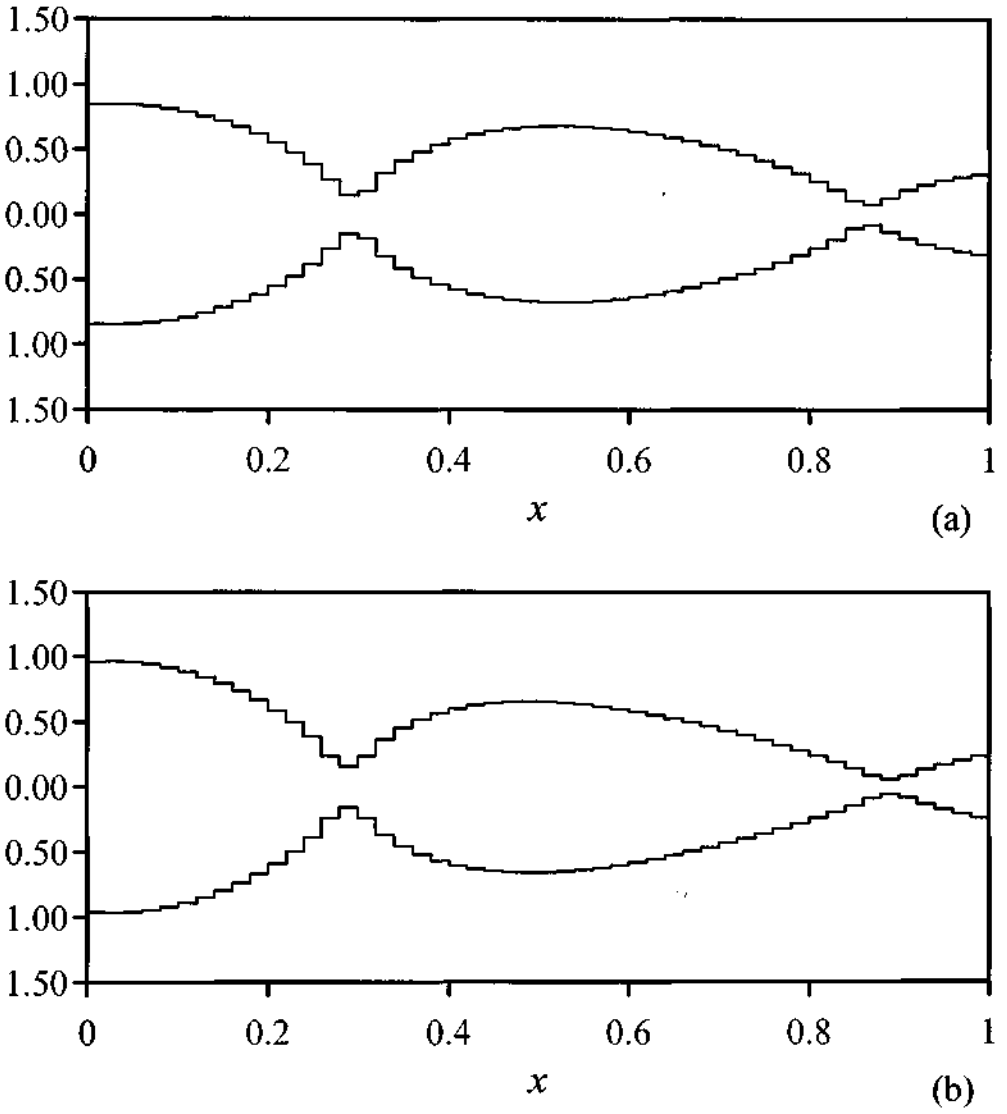

Figure 3-3. Optimal areas of clamped-elastically restrained columns under axial loads (a) $q(x)=1$ and (b) $q(x)=2(1-x)$ with $n=2$, $p=0$, $a_0=0.0$, $s_{vs}=8$ and $k_B=4$.

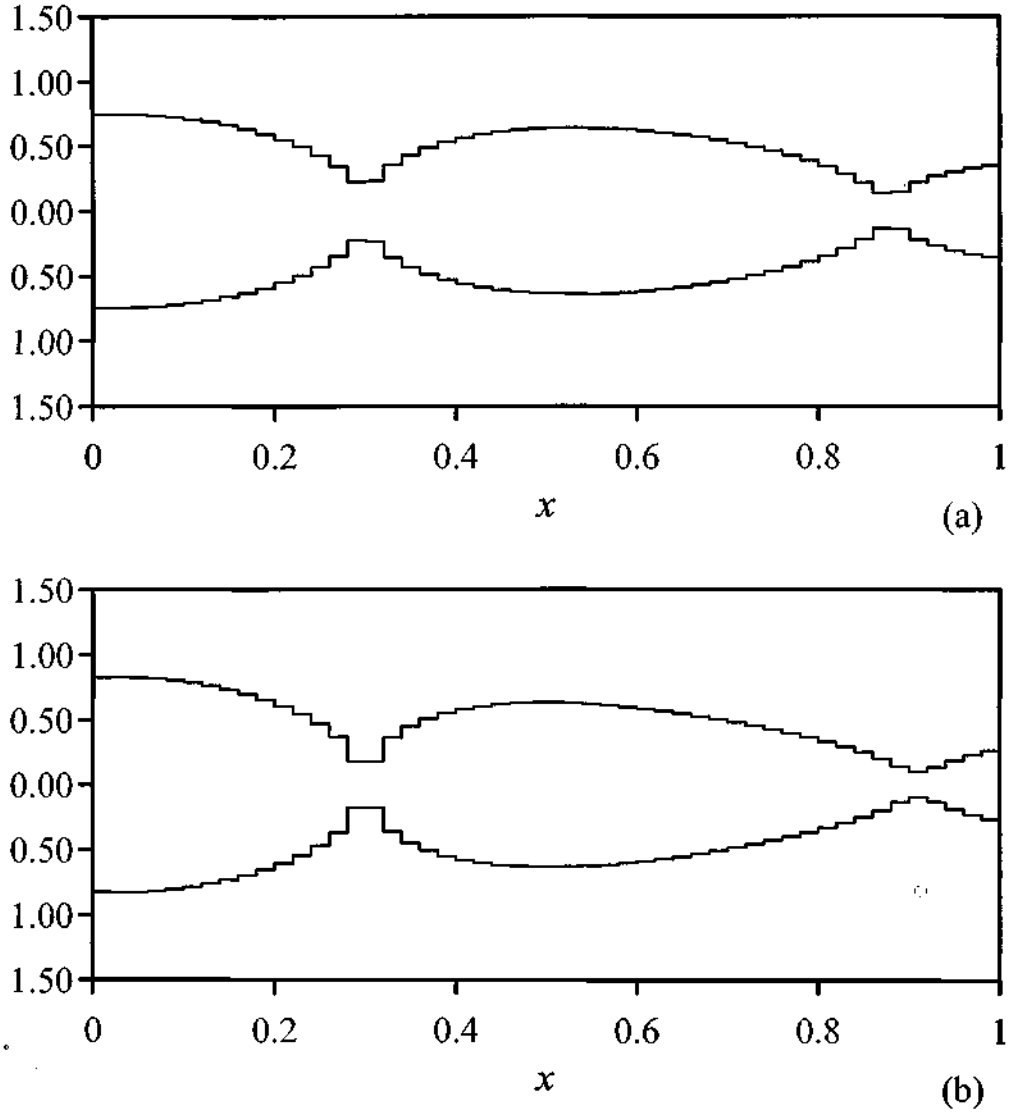

Figure 3-4. Optimal areas of clamped-elastically restrained columns under axial loads (a) $q(x)=1$ and (b) $q(x)=2(1-x)$ with $n=3$, $p=0$, $a_0=0.0$, $s_{ys}=8$ and $k_B=4$.

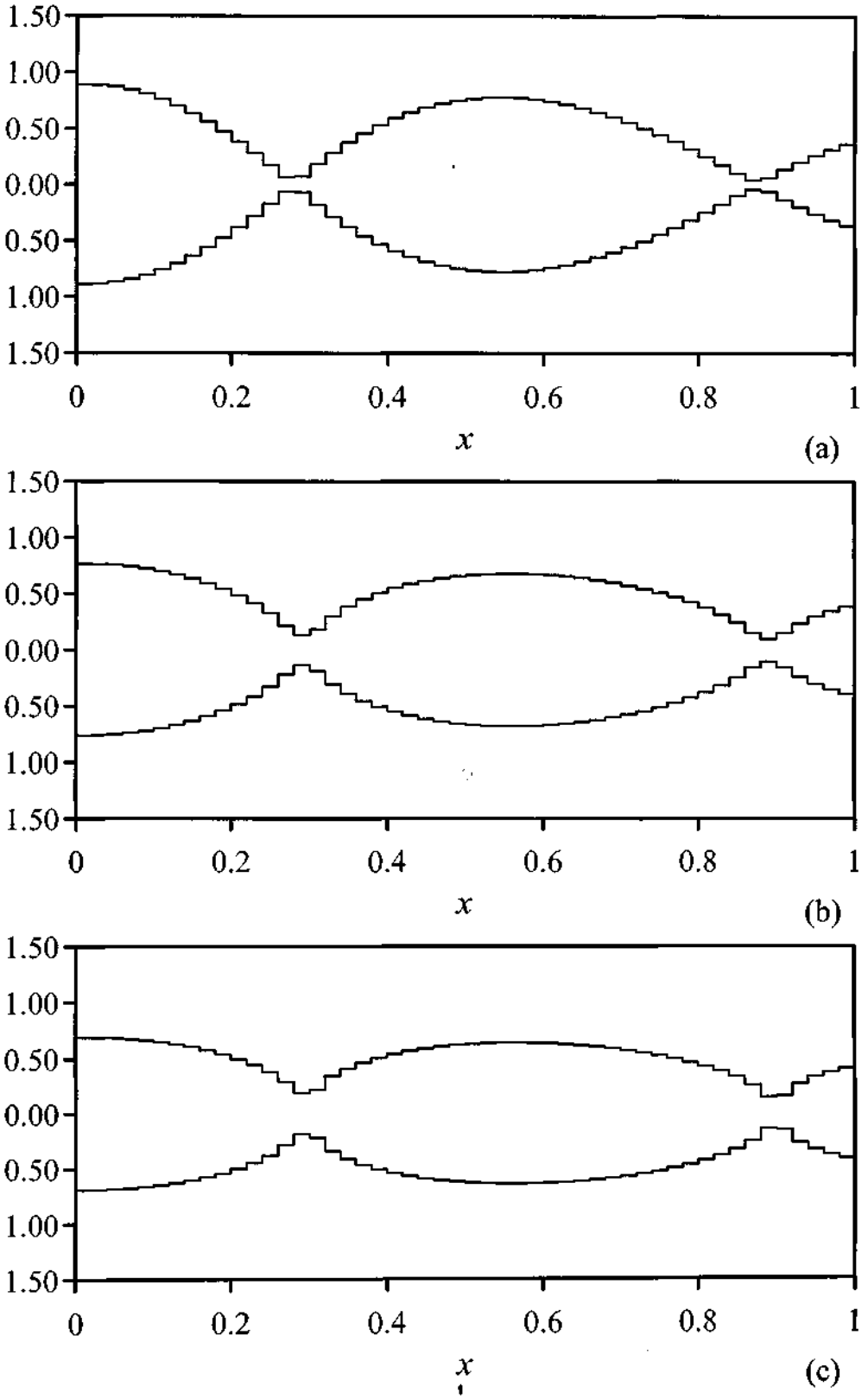

Figure 3-5. Optimal areas of clamped-elastically restrained columns under axial loads $q(x)=1$ and $p=0.5$ with $a_0=0.0$, $s_{ys}=8$, $k_B=4$, (a) $n=1$, (b) $n=2$, (c) $n=3$.

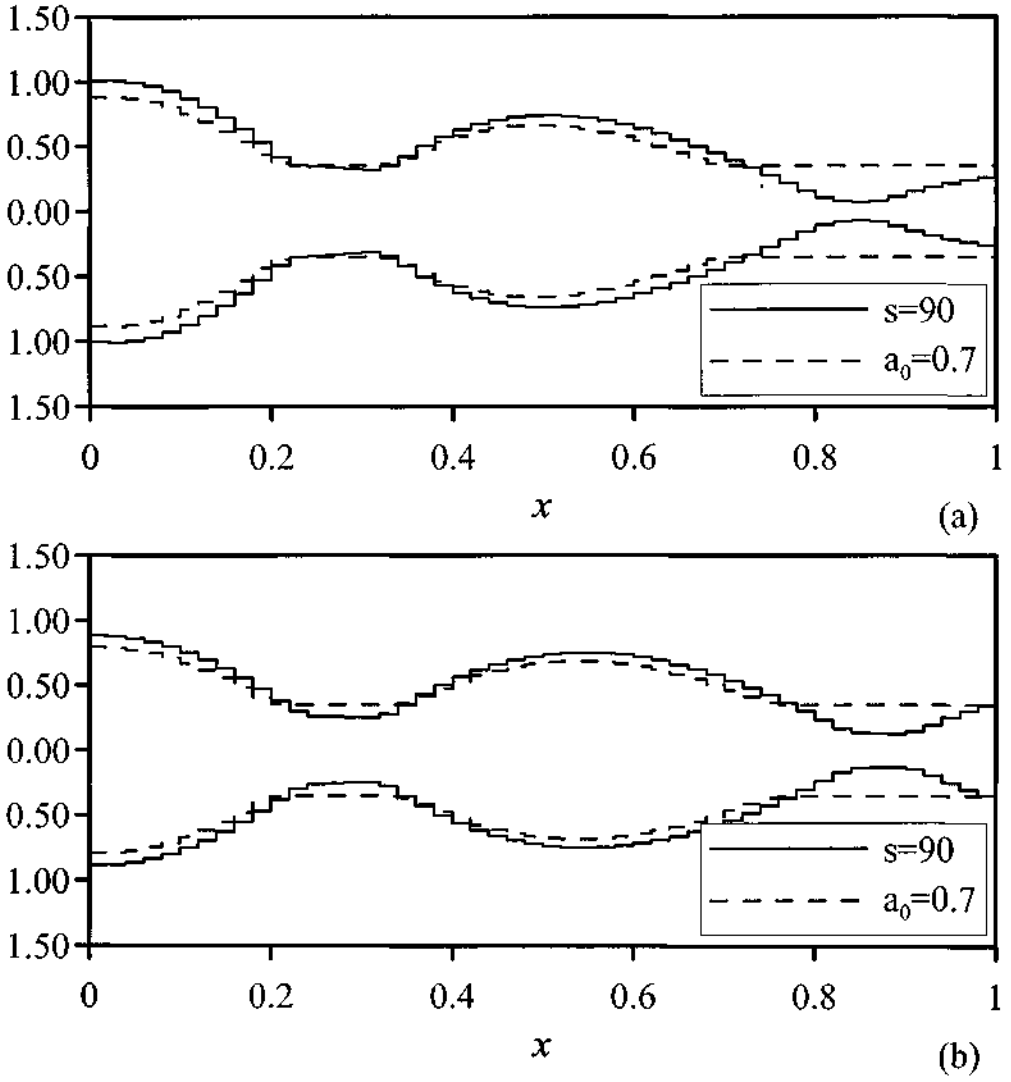

Figure 3-6. Optimal areas of clamped-elastically restrained columns under axial load $q(x)=1$ with $n=1$, $p=0$, $a_0=0.7$, $s_{ys}=90$ and $k_B=4$, (a) $p=0$, (b) $p=0.5$.

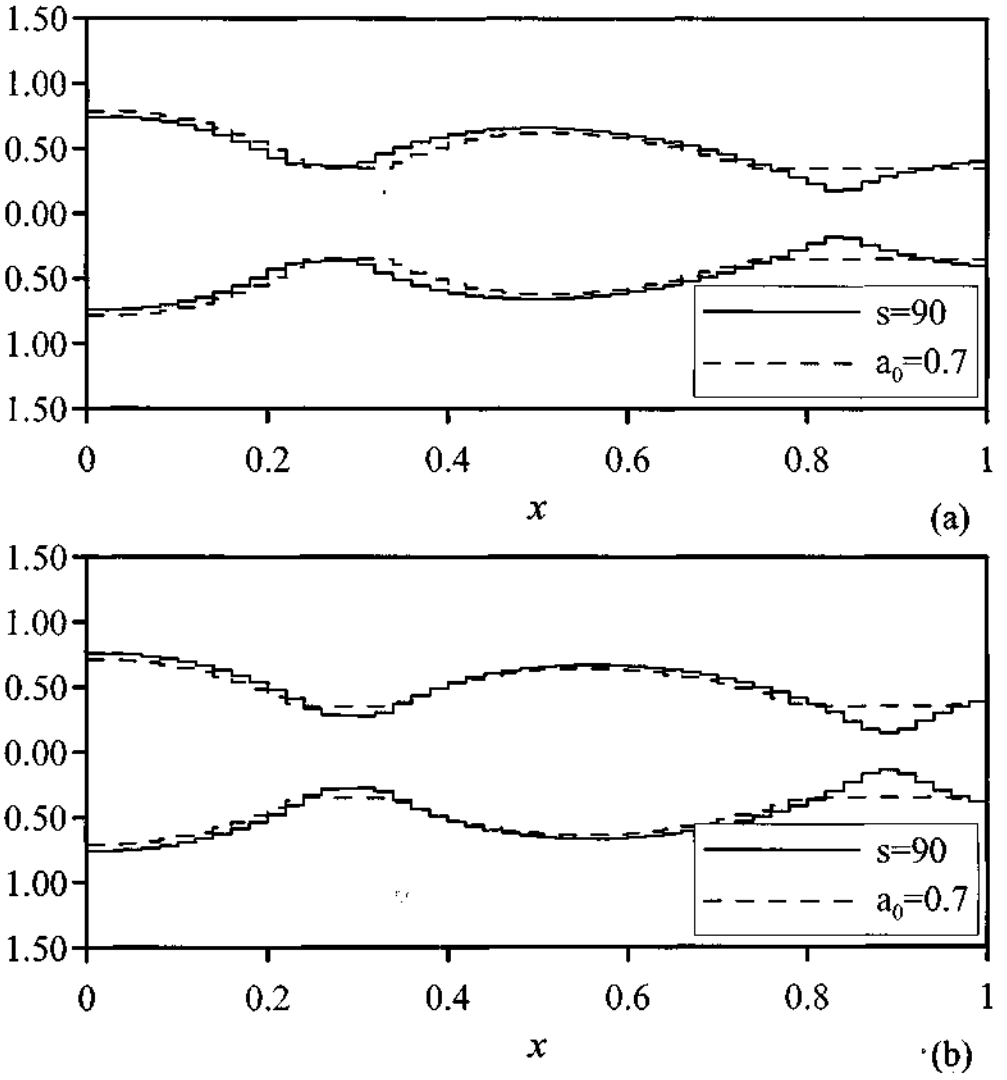

Figure 3-7. Optimal areas of clamped-elastically restrained columns under axial load $q(x)=1$ with $n=2$, $p=0$, $a_0=0.7$, $s_{vs}=90$ and $k_B=4$, (a) $p=0$, (b) $p=0.5$.

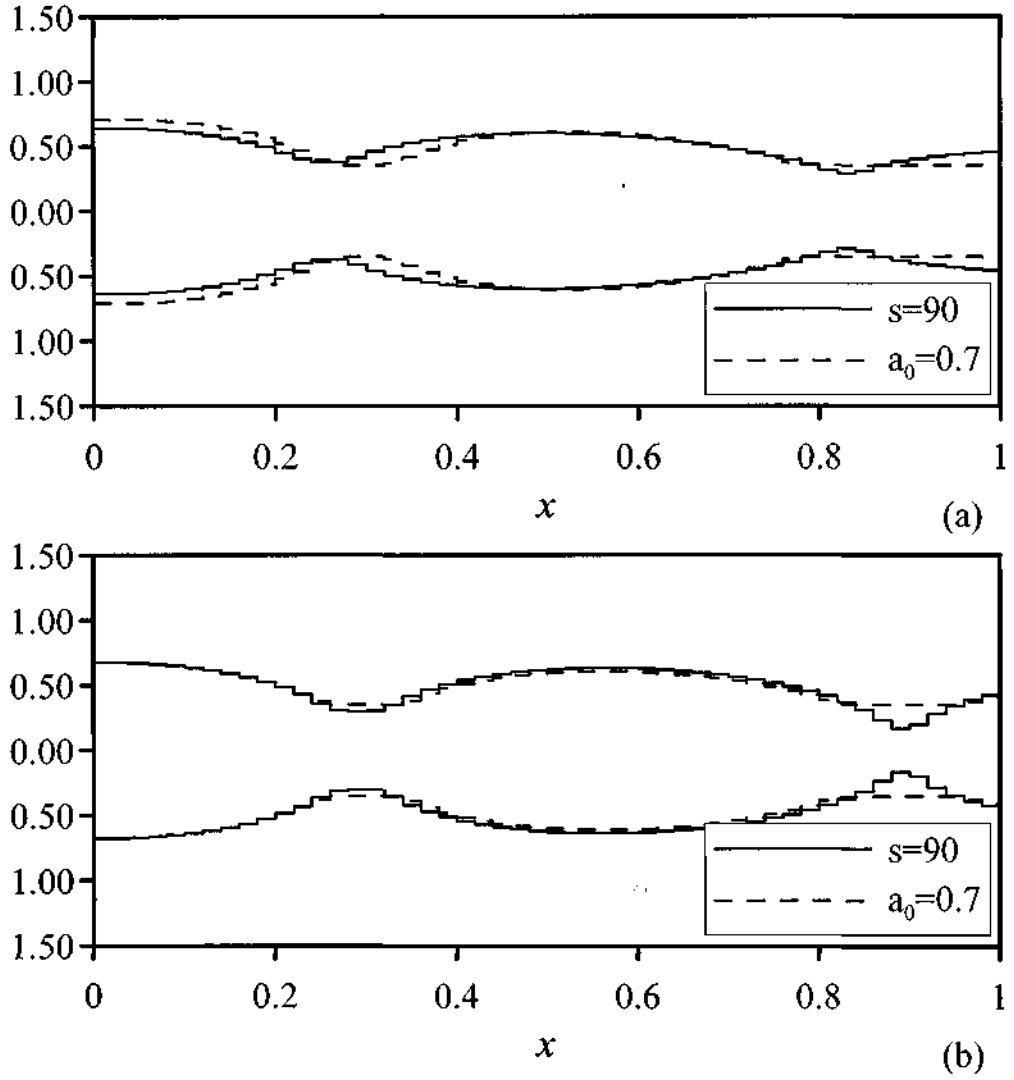

Figure 3-8. Optimal areas of clamped-elastically restrained columns under axial load $q(x)=1$ with $n=3$, $p=0$, $a_0=0.7$, $s_{ys}=90$ and $k_B=4$, (a) $p=0$, (b) $p=0.5$.

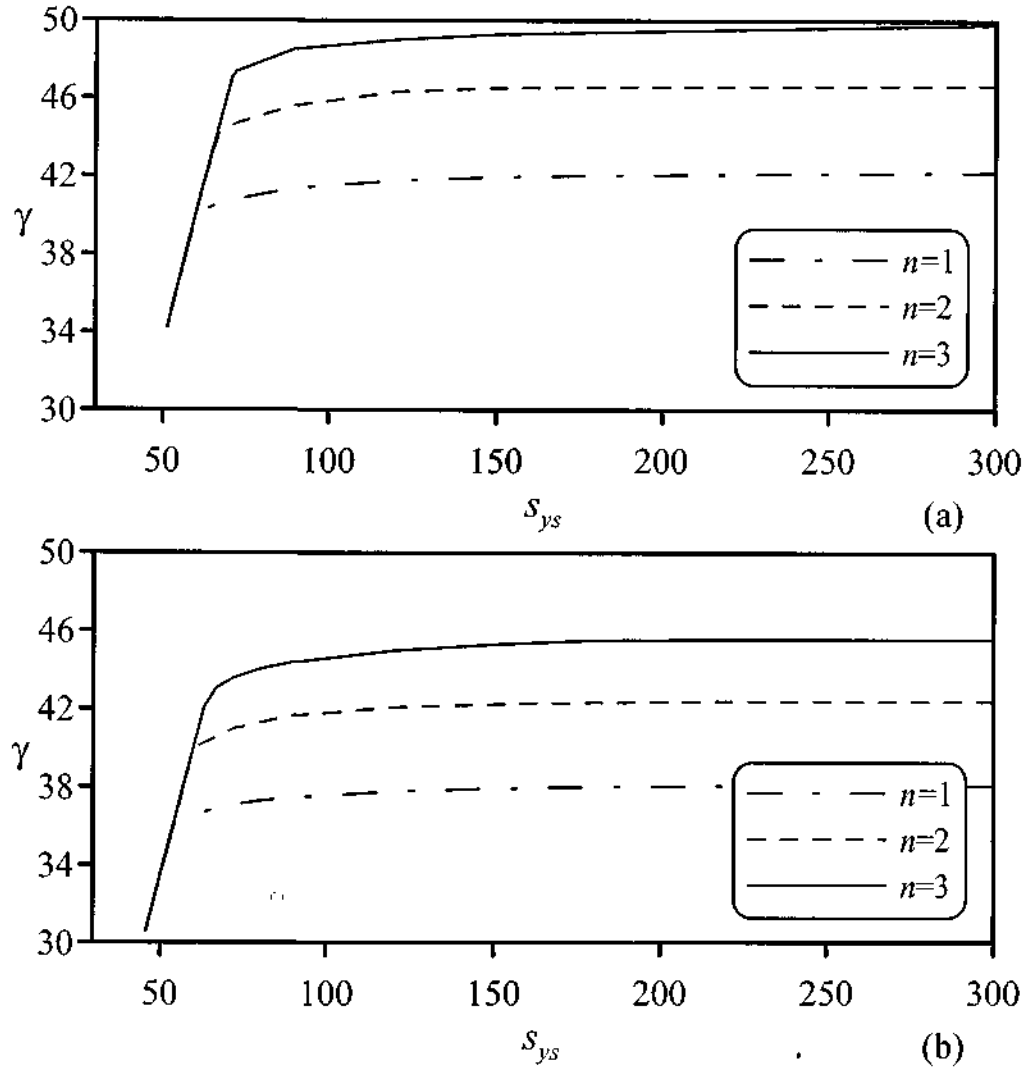

Figure 3-9. Buckling parameters of optimal clamped-elastically restrained columns plotted against s_{ys} subject to the axial load $q(x)=1$, $p=0$, (a) $k_B=4$, (b) $k_B=10$.

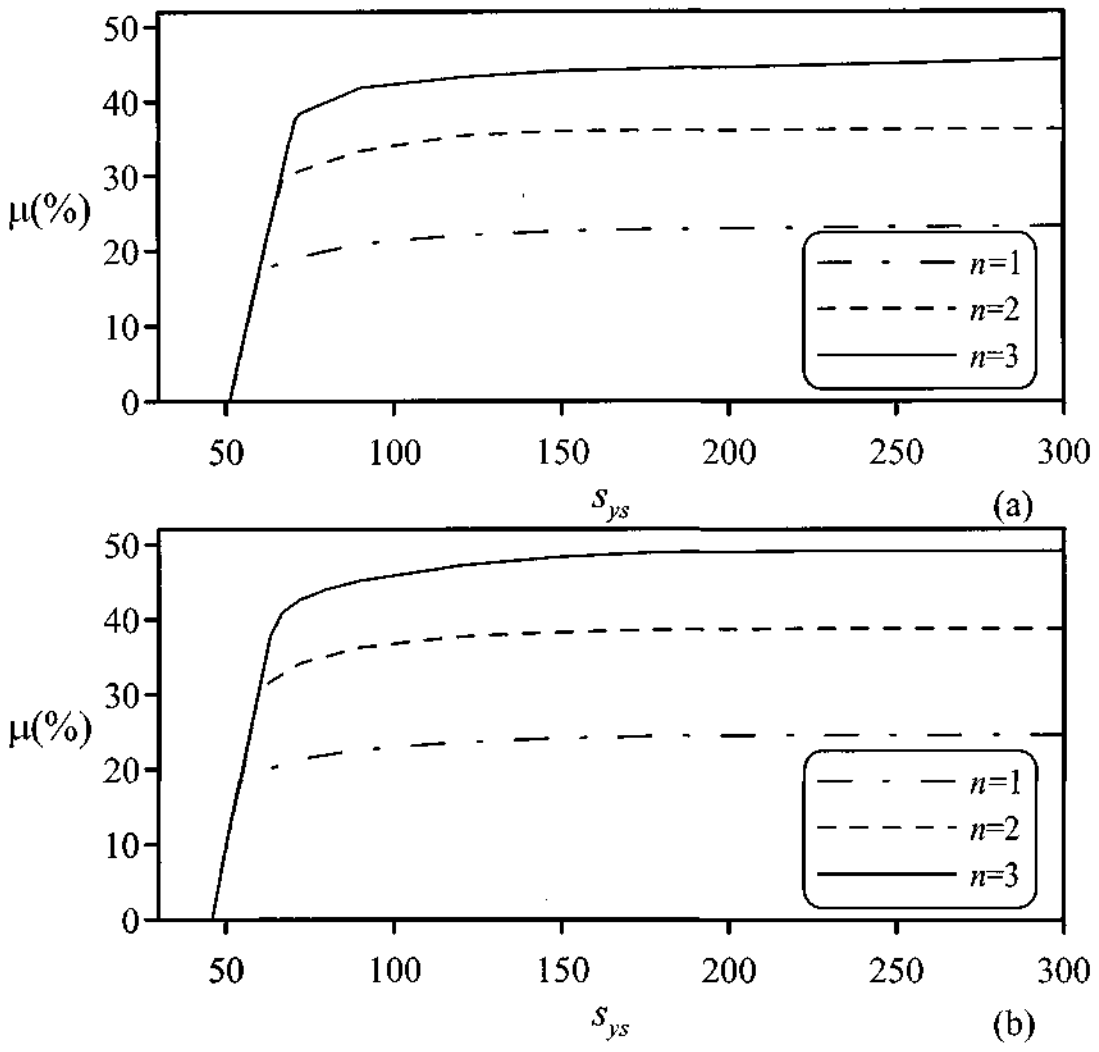

Figure 3-10. Efficiencies of optimal clamped-elastically restrained columns plotted against s_{ys} subject to the axial load $q(x)=1$, $p=0$, (a) $k_B=4$, (b) $k_B=10$.

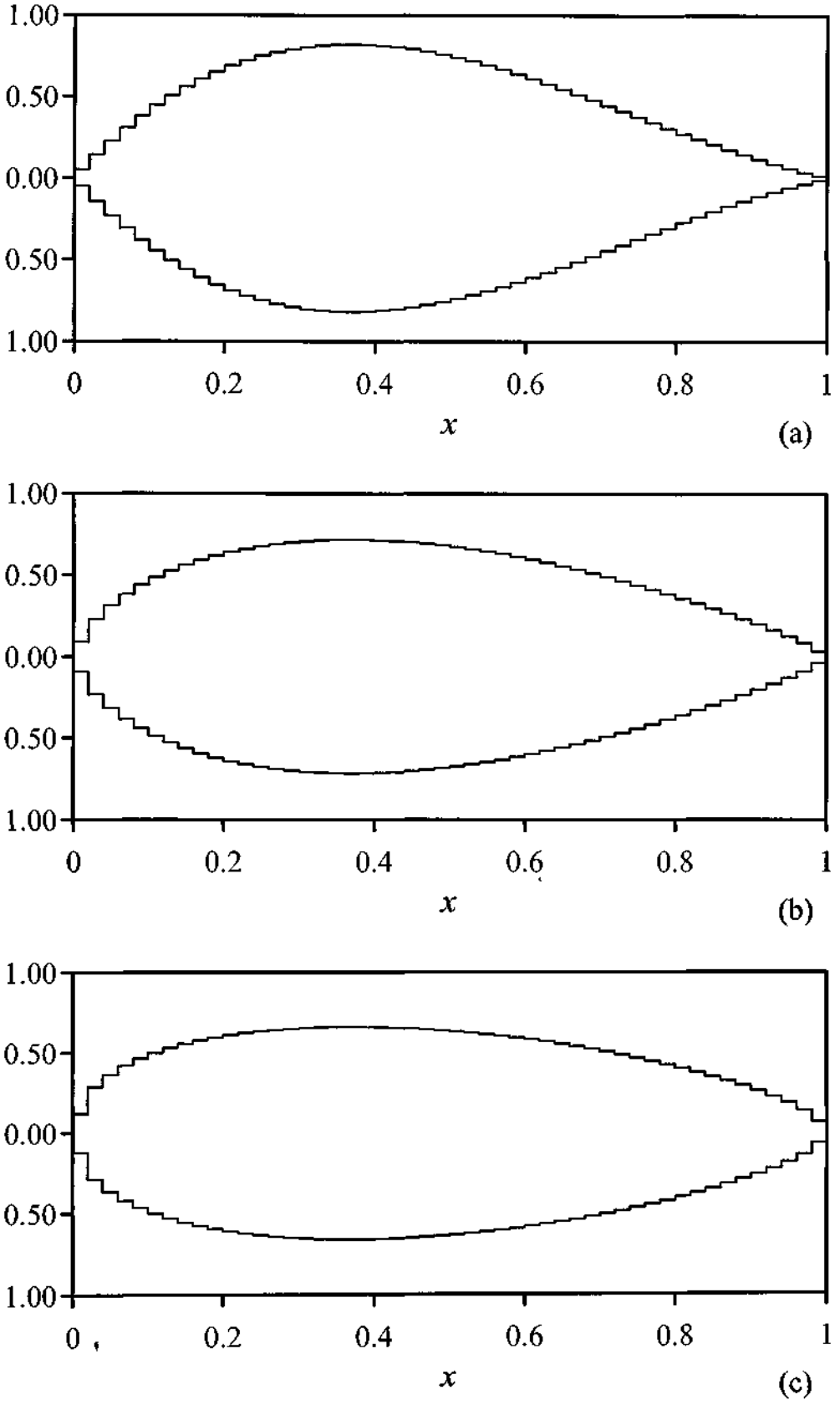

Figure 3-11. Optimal cross-sectional areas under axial loads, $q(x)=1$ with $p=0$, $a_0=0.0$, $s_{ys}=\infty$, (a) $n=1$, (b) $n=2$, (c) $n=3$.

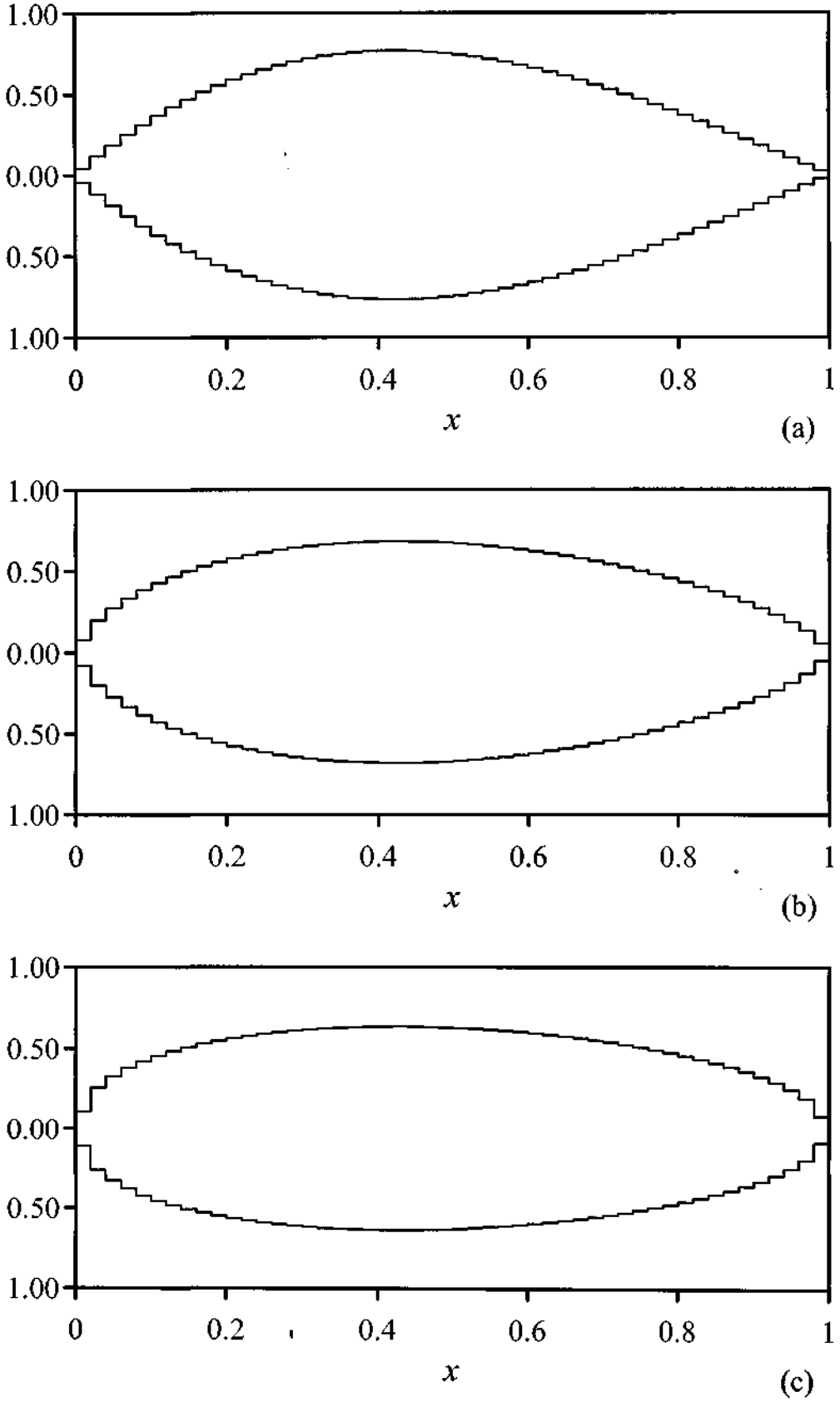

Figure 3-12. Optimal cross-sectional areas under axial loads, $q(x)=1$ with $p=0.5$, $a_0=0.0$, $s_{ys}=\infty$, (a) $n=1$, (b) $n=2$, (c) $n=3$.

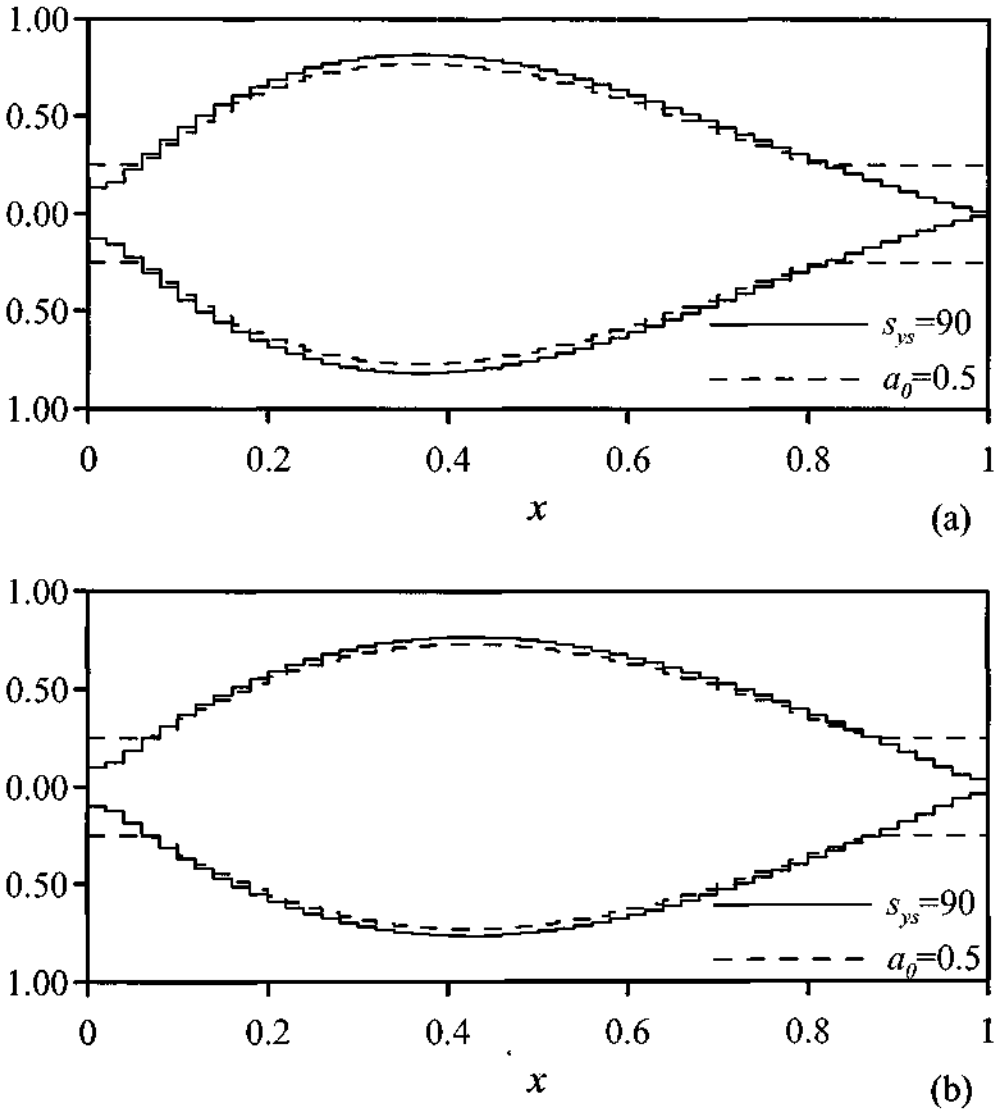

Figure 3-13. Optimal cross-sectional areas under axial loads $q(x)=1$ with $n=1$, $a_0=0.5$ or $s_{ys}=90$, (a) $p=0$, (b) $p=0.5$.

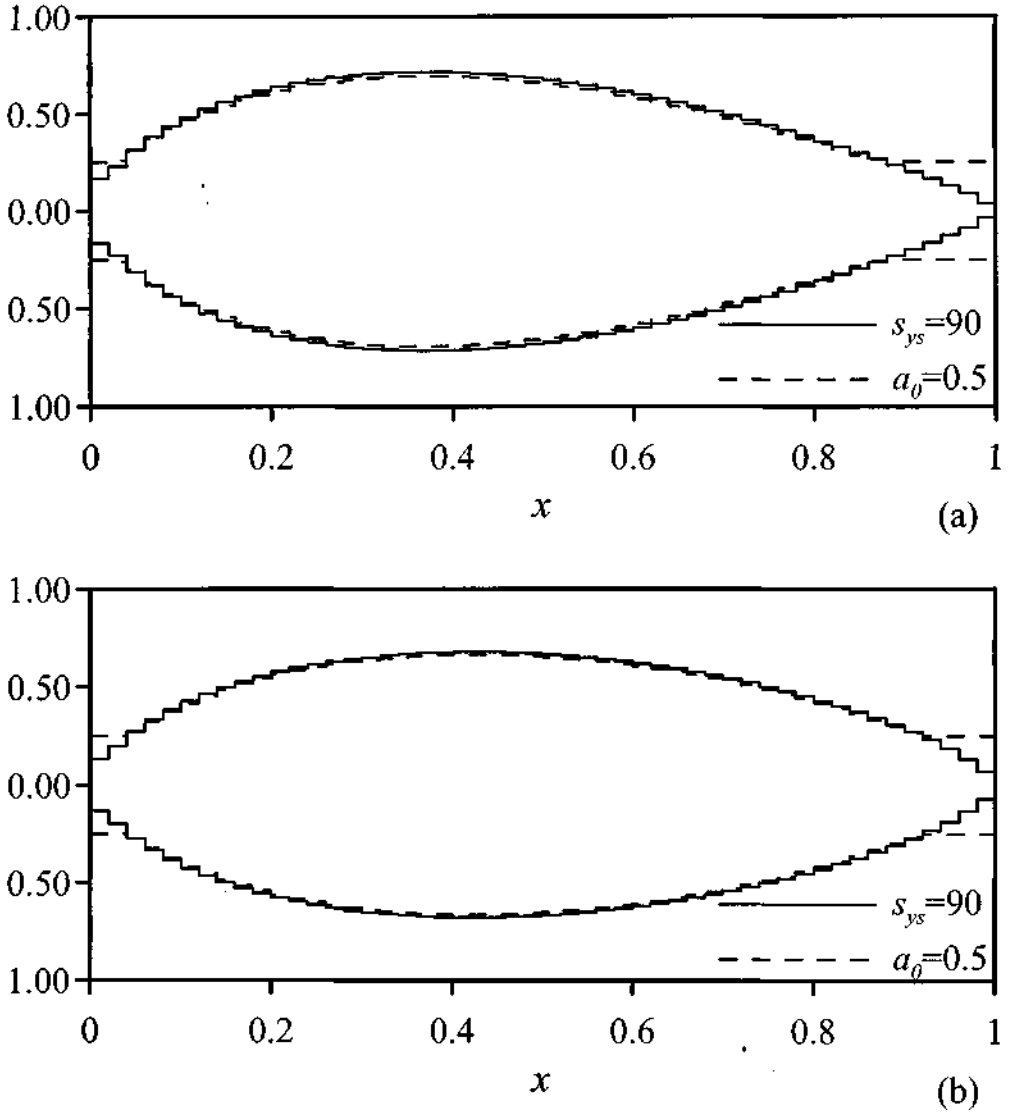

Figure 3-14. Optimal cross-sectional areas under axial loads $q(x)=1$ with $n=2$, $a_0=0.5$ or $s_{ys}=90$, (a) $p=0$, (b) $p=0.5$.

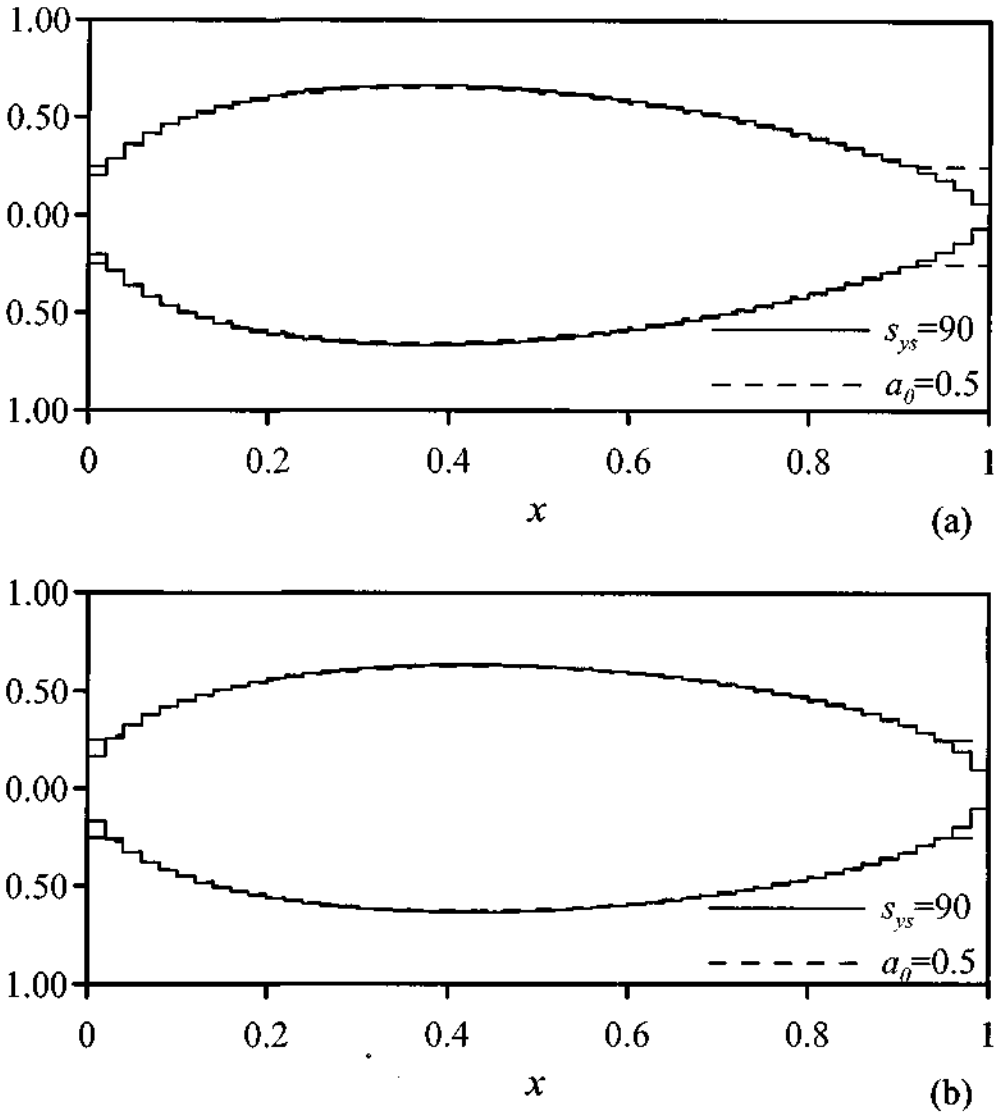

Figure 3-15. Optimal cross-sectional areas under axial loads $q(x)=1$ and $p=0$ with $n=3$, $a_0=0.5$ or $s_{ys}=90$, (a) $p=0$, (b) $p=0.5$.

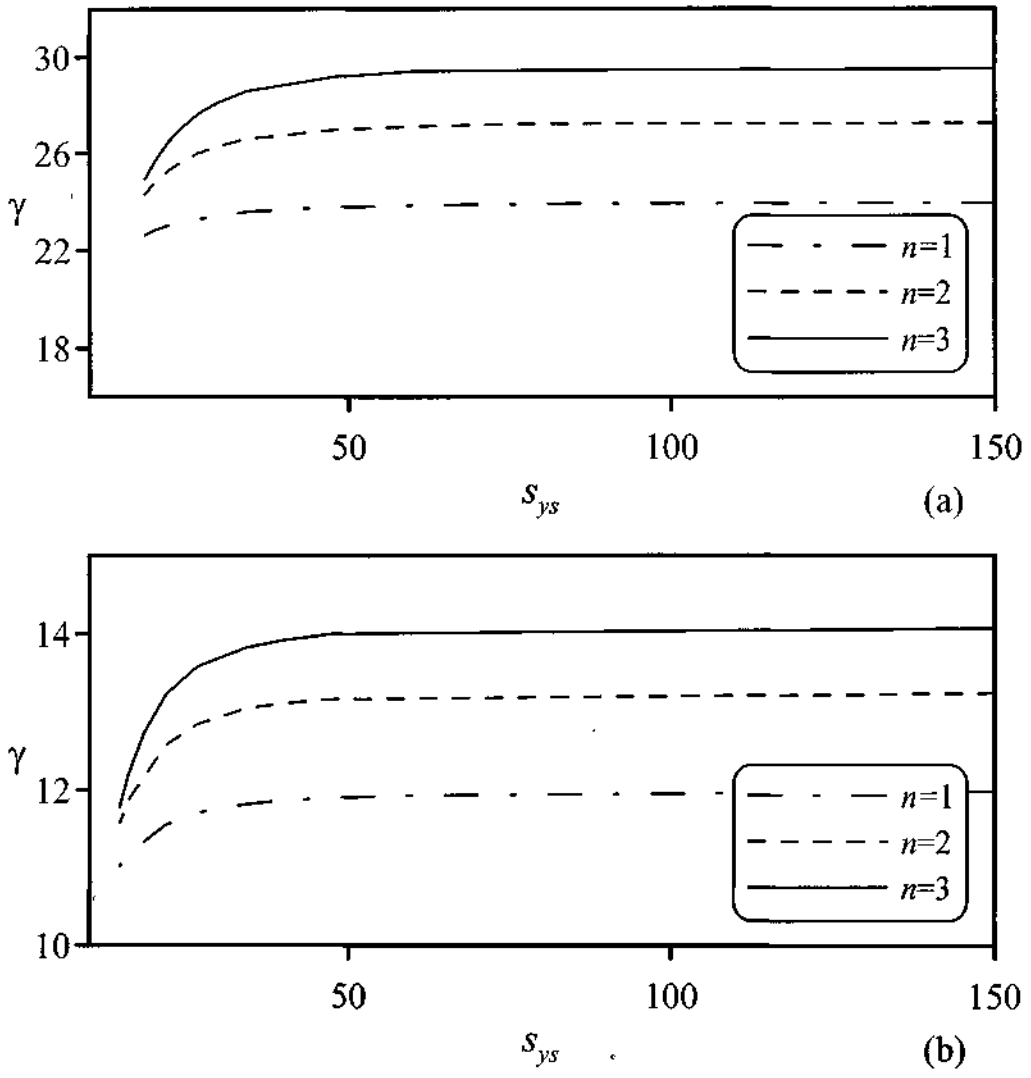

Figure 3-16. Buckling parameters γ of optimal columns plotted against s_{ys} subject to the axial load $q(x)=1$ with $a_0=0.0$, $s_{ys}=\infty$, (a) $p=0$, (b) $p=0.5$.

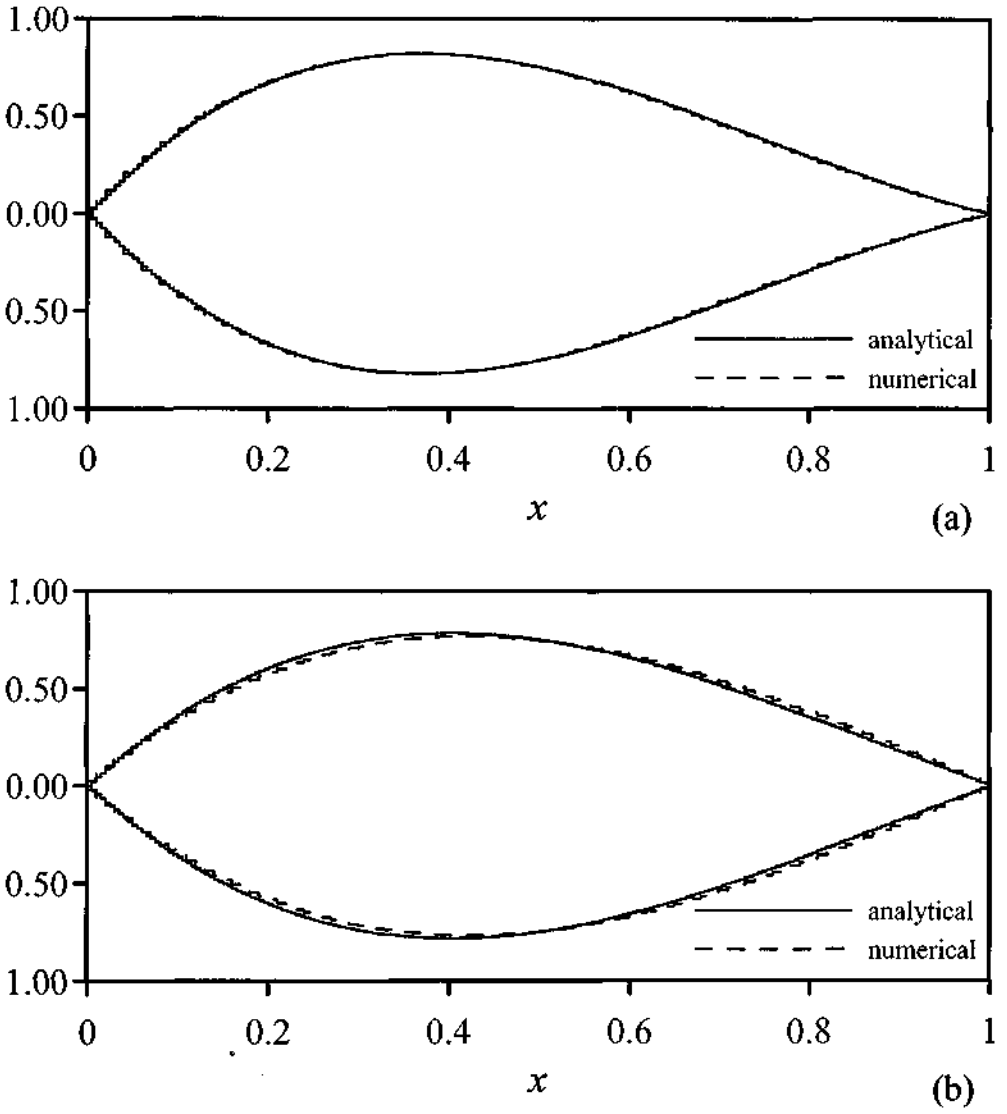

Figure 3-17. Case 1, Problem I, s_{ys}=8 , a_o=0,
a) p=0, $\gamma_{opt,exact}$=24, $\gamma_{opt,num.}$=23.9861, b) p=0.5, $\gamma_{opt,exact}$=12, $\gamma_{opt,num.}$=11.9931

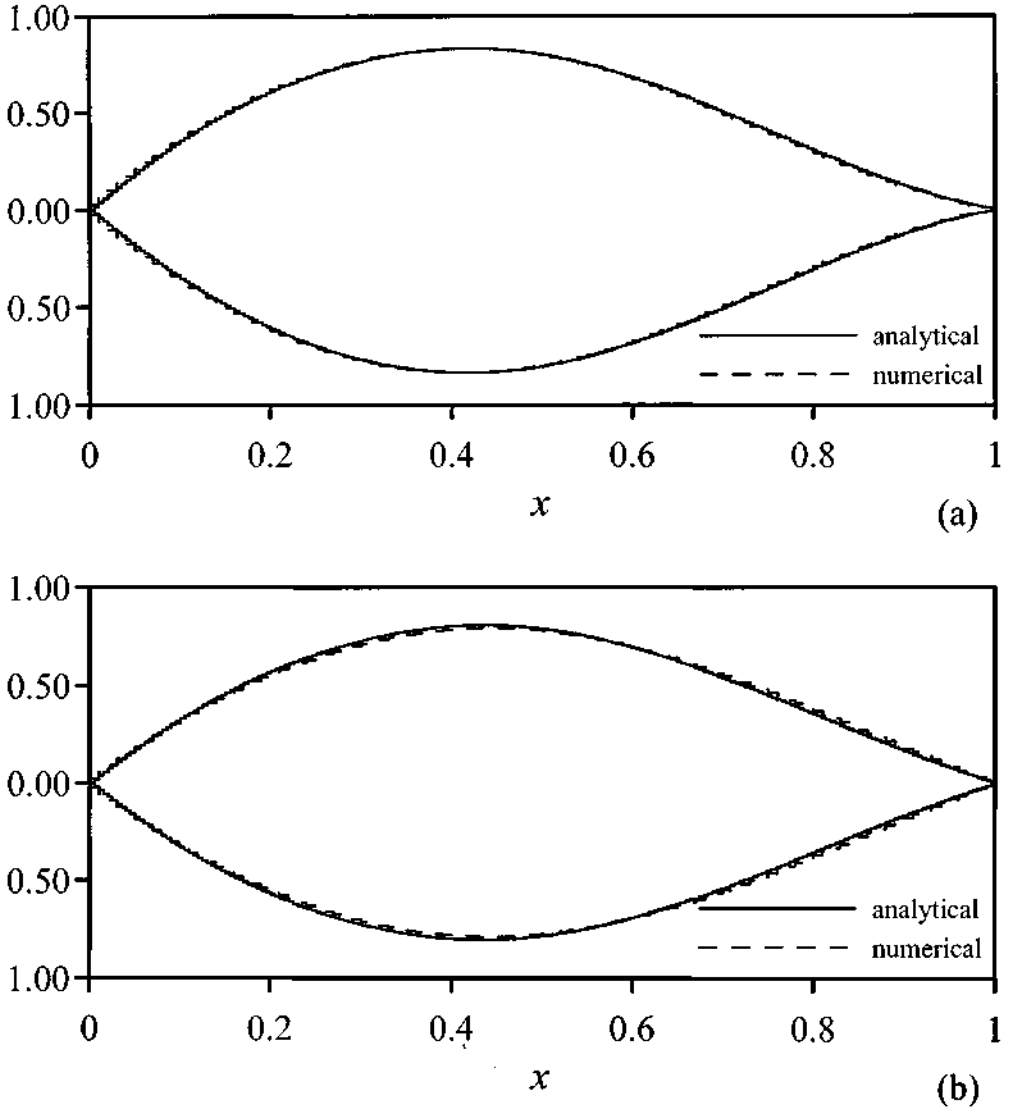

Figure 3-18. Case 2, Problem I, s_{ys}=8 , a_o=0,
a) p=0, $\gamma_{opt.exact}$=19.2001, $\gamma_{opt.num.}$=19.1892, b) p=0.5, $\gamma_{opt.exact}$=10.6669, $\gamma_{opt.num.}$=10.6611

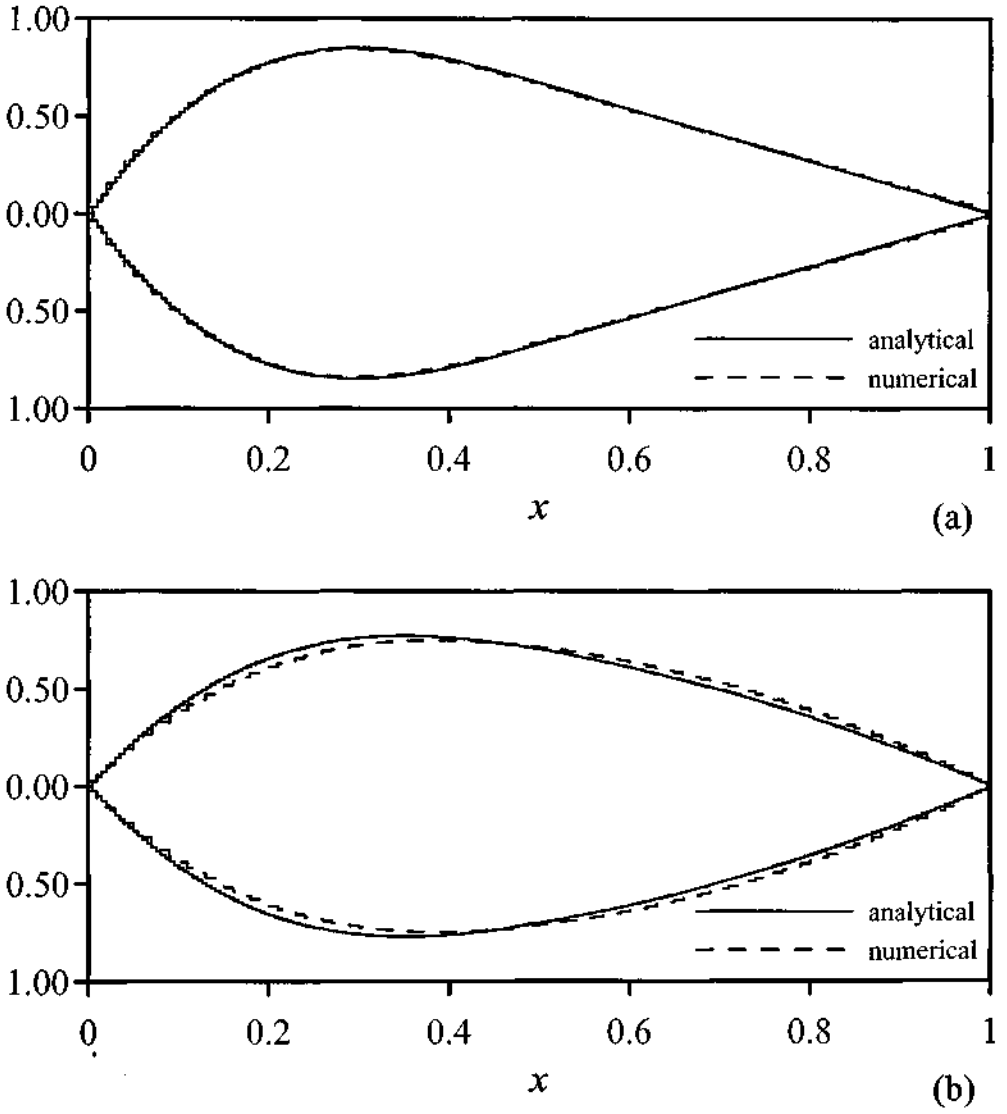

Figure 3-19. Case 3, Problem I, s_{ys}=8 , a_o=0,
a) p=0, $\gamma_{opt,exact}$=32, $\gamma_{opt,num.}$=31.9570, b) p=0.5, $\gamma_{opt,exact}$=13.7139, $\gamma_{opt,num.}$=13.7045

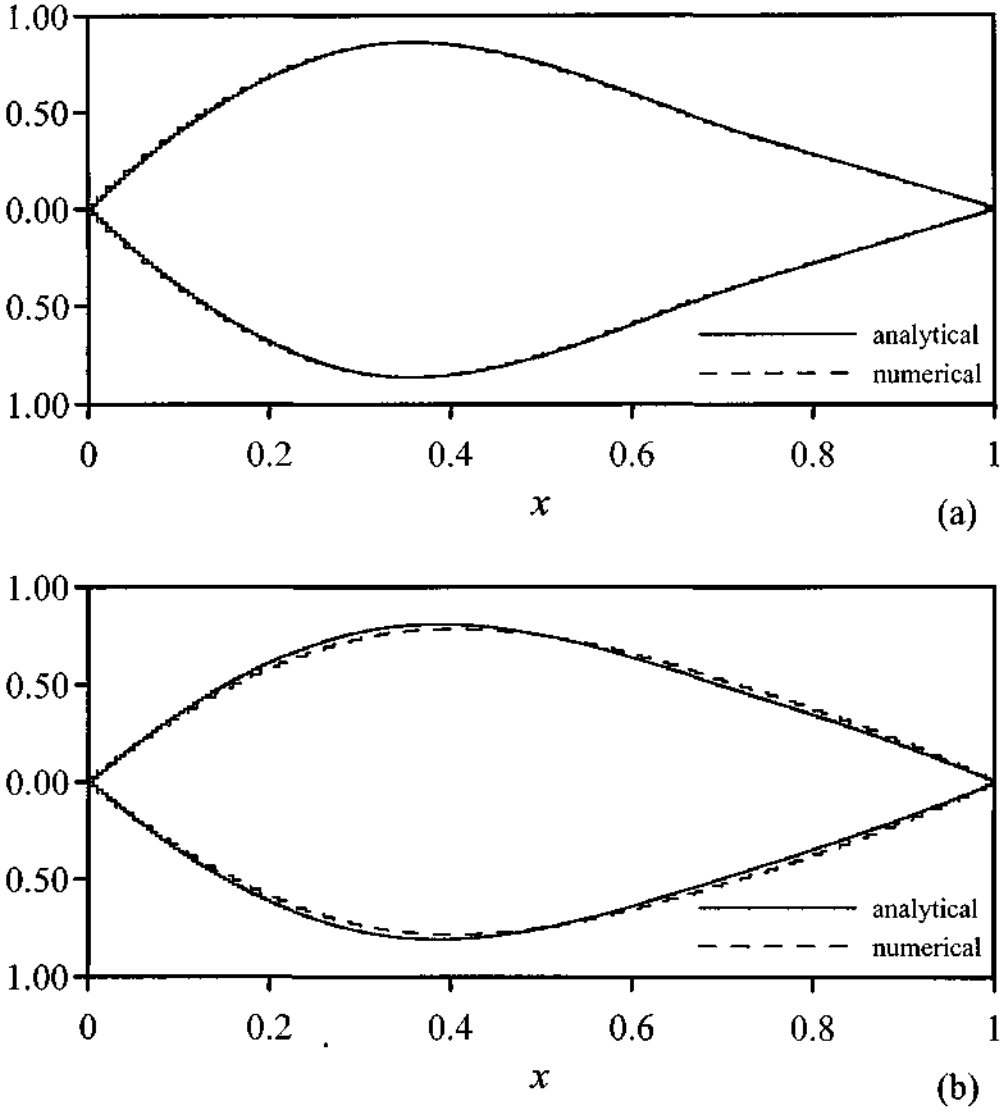

Figure 3-20. Case 4, Problem I, s_{ys}=8 , a_o=0,
a) p=0, $\gamma_{opt,exact}$=24, $\gamma_{opt,num.}$=23.9823, b) p=0.5, $\gamma_{opt,exact}$=12, $\gamma_{opt,num.}$=11.9922

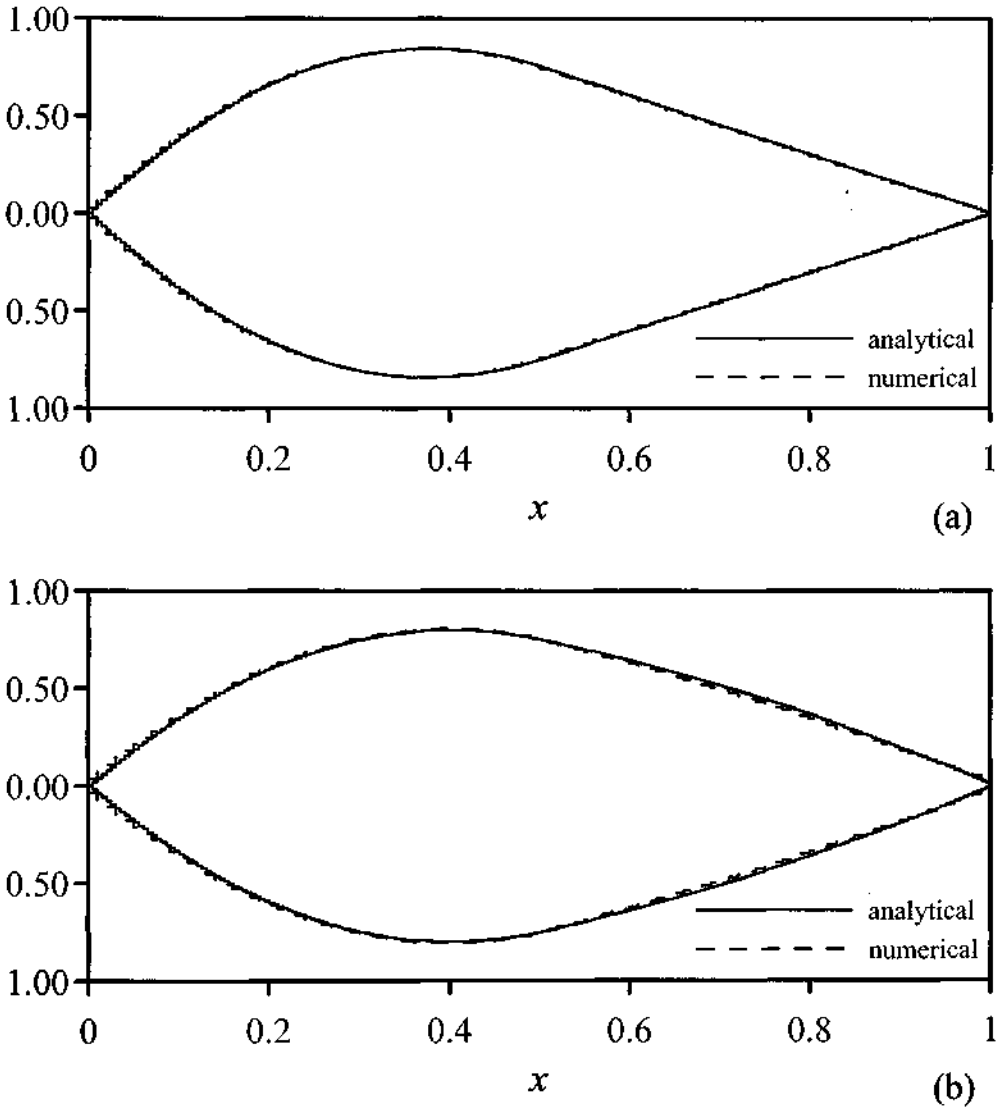

Figure 3-21. Case 5, Problem I, s_{ys}=8 , a_o=0,
a) p=0, $\gamma_{opt,exact}$=24, $\gamma_{opt,num.}$=23.9859, b) p=0.5, $\gamma_{opt,exact}$=12, $\gamma_{opt,num.}$=11.9182

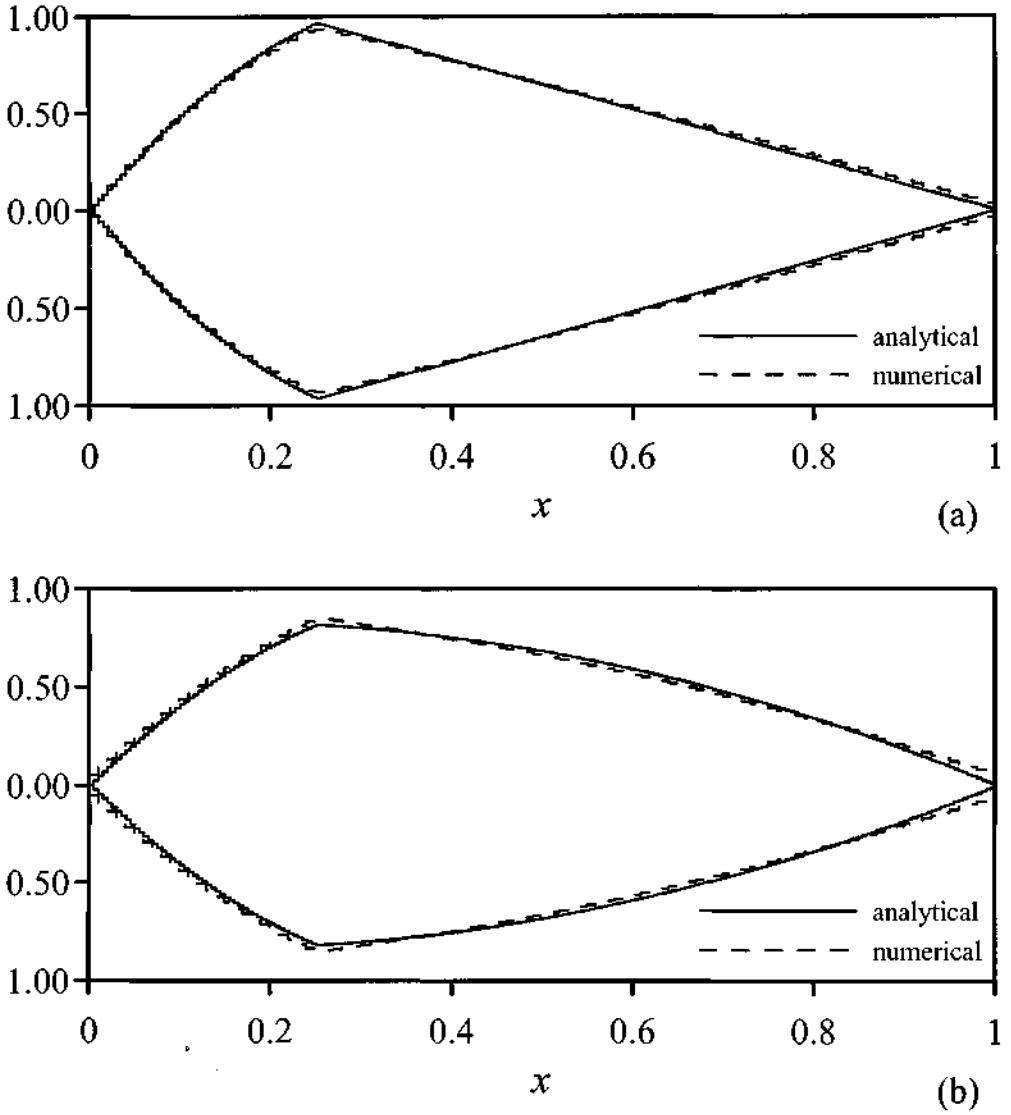

Figure 3-22. Case 6, Problem I, s_{ys}=8 , a_o=0,
a) p=0, $\gamma_{opt.exact}$=27.4261, $\gamma_{opt.num.}$=27.4964, b) p=0.5, $\gamma_{opt.exact}$=12.7995, $\gamma_{opt.num.}$=12.6443

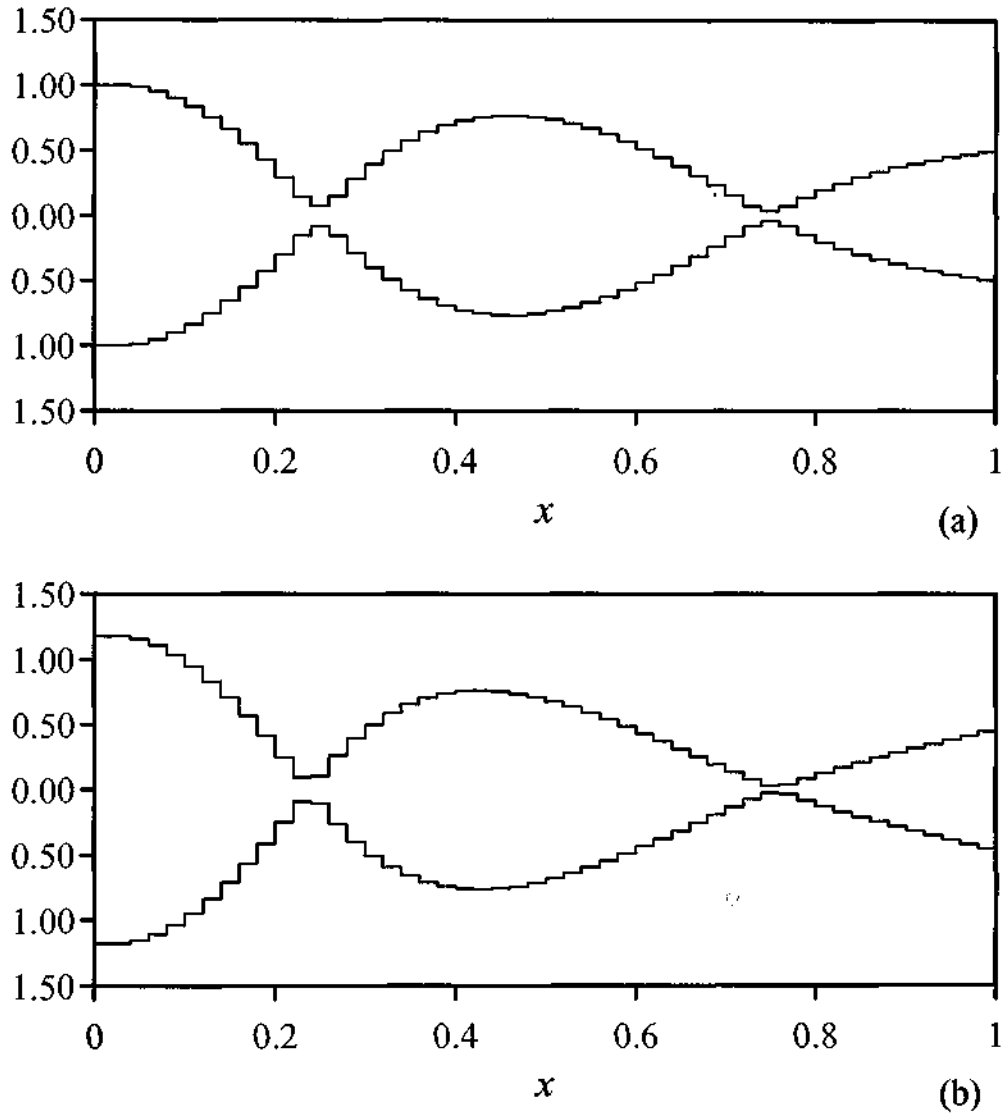

Figure 3-23. Optimal columns under axial loads (a) $q(x)=1$ and (b) $q(x)=2(1-x)$ with $n=1$, $p=0$, $a_0=0.0$ and $s_{ys}=\infty$.

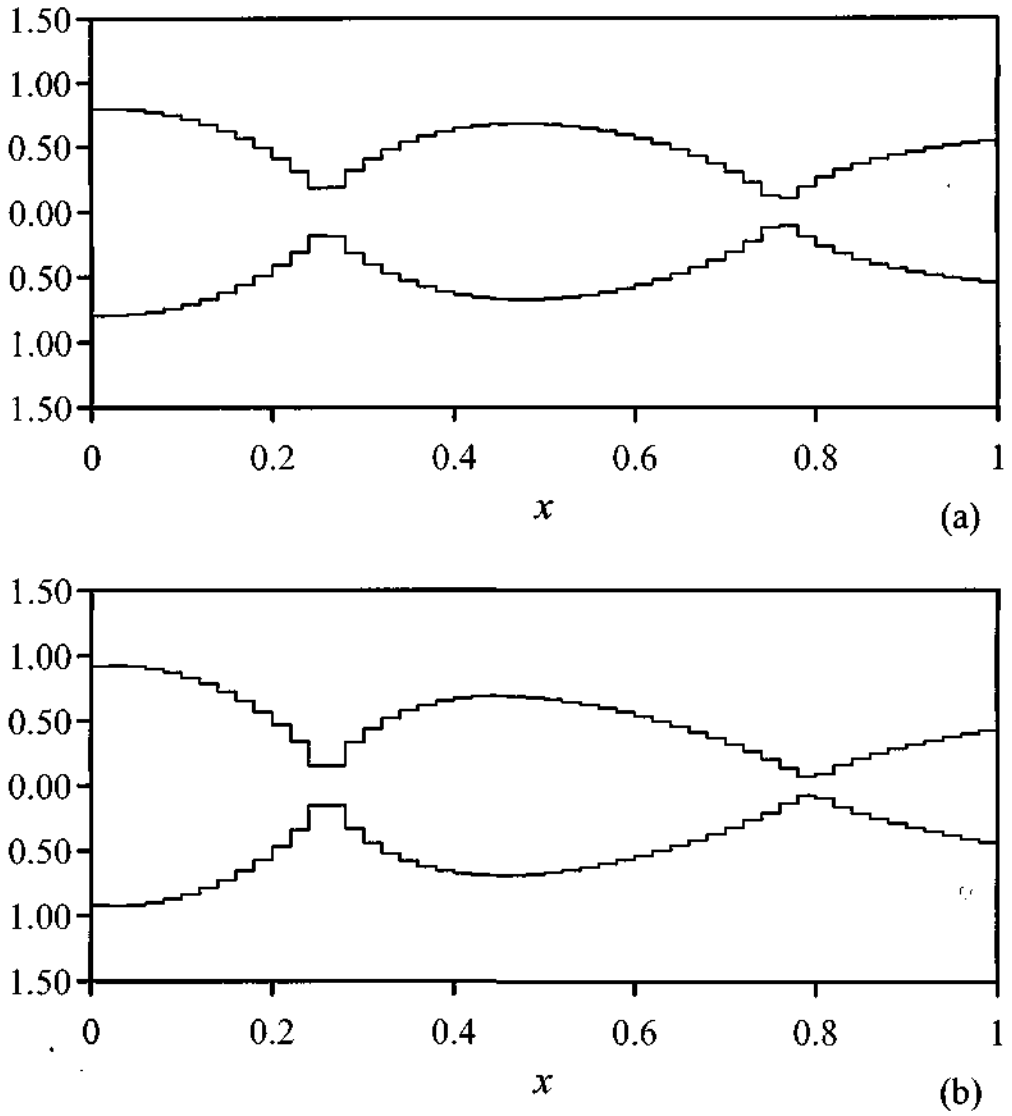

Figure 3-24. Optimal columns under axial loads (a) $q(x)=1$ and (b) $q(x)=2(1-x)$ with $n=2$, $p=0$, $a_0=0.0$ and $s_{ys}=\infty$.

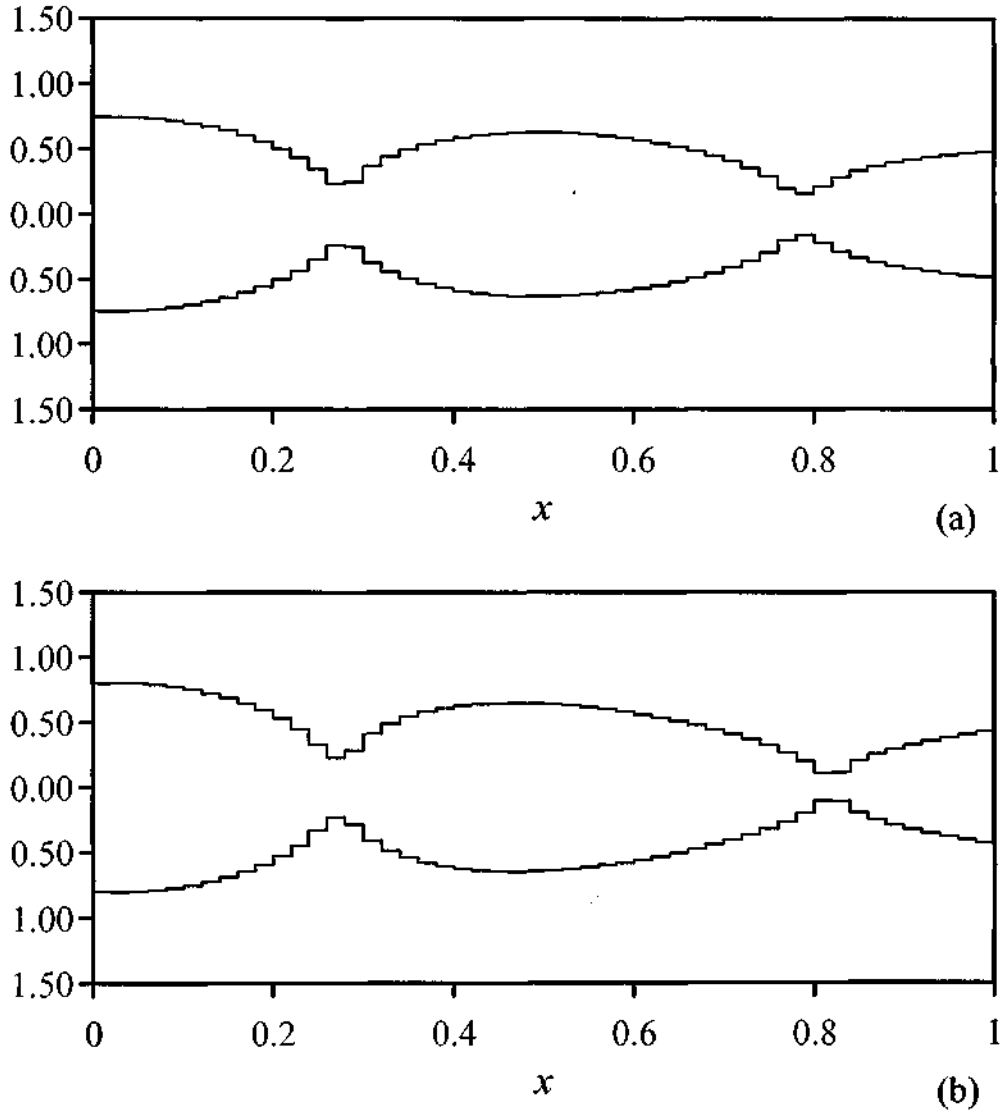

Figure 3-25. Optimal columns under axial loads (a) $q(x)=1$ and (b) $q(x)=2(1-x)$ with $n=3$, $p=0$, $a_0=0.0$ and $s_{ys}=\infty$.

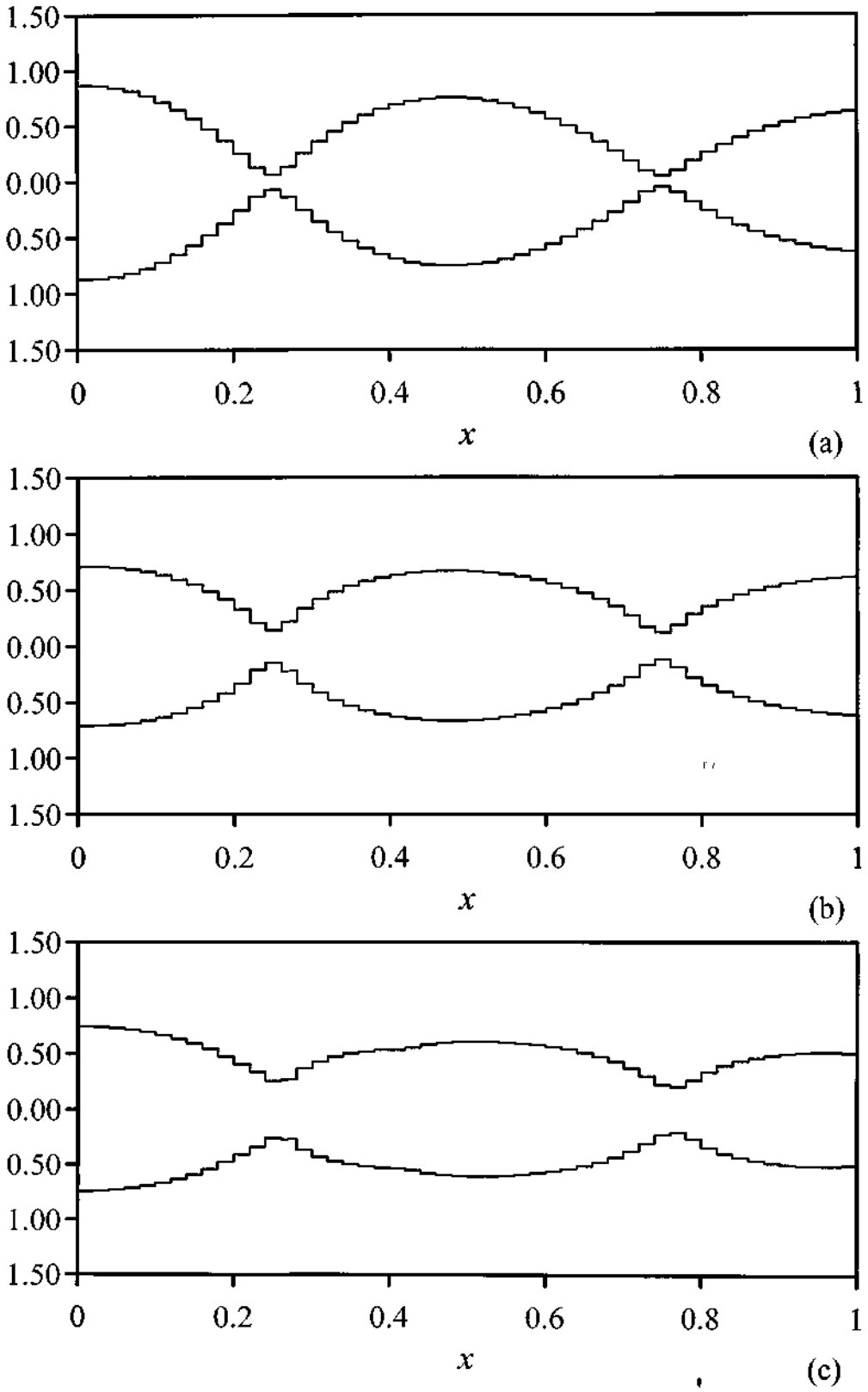

Figure 3-26. Optimal columns under axial loads $q(x)=1$ and $p=0.5$ with $a_0=0.0$ and $s_{ys}=\infty$, (a) $n=1$, (b) $n=2$, (c) $n=3$.

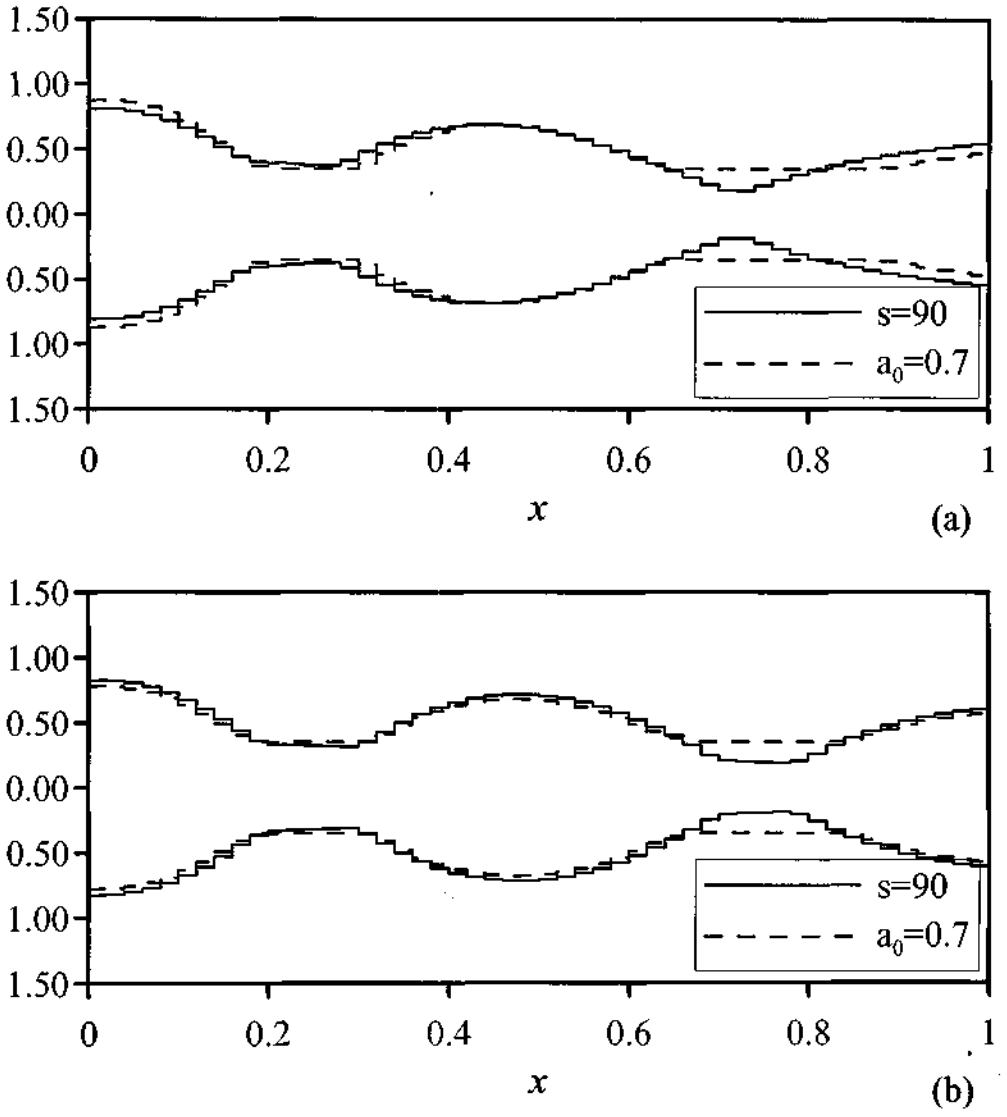

Figure 3-27. Thickness and stress constrained optimal columns under axial load $q(x)=1$ with $n=1$, (a) $p=0$, (b) $p=0.5$.

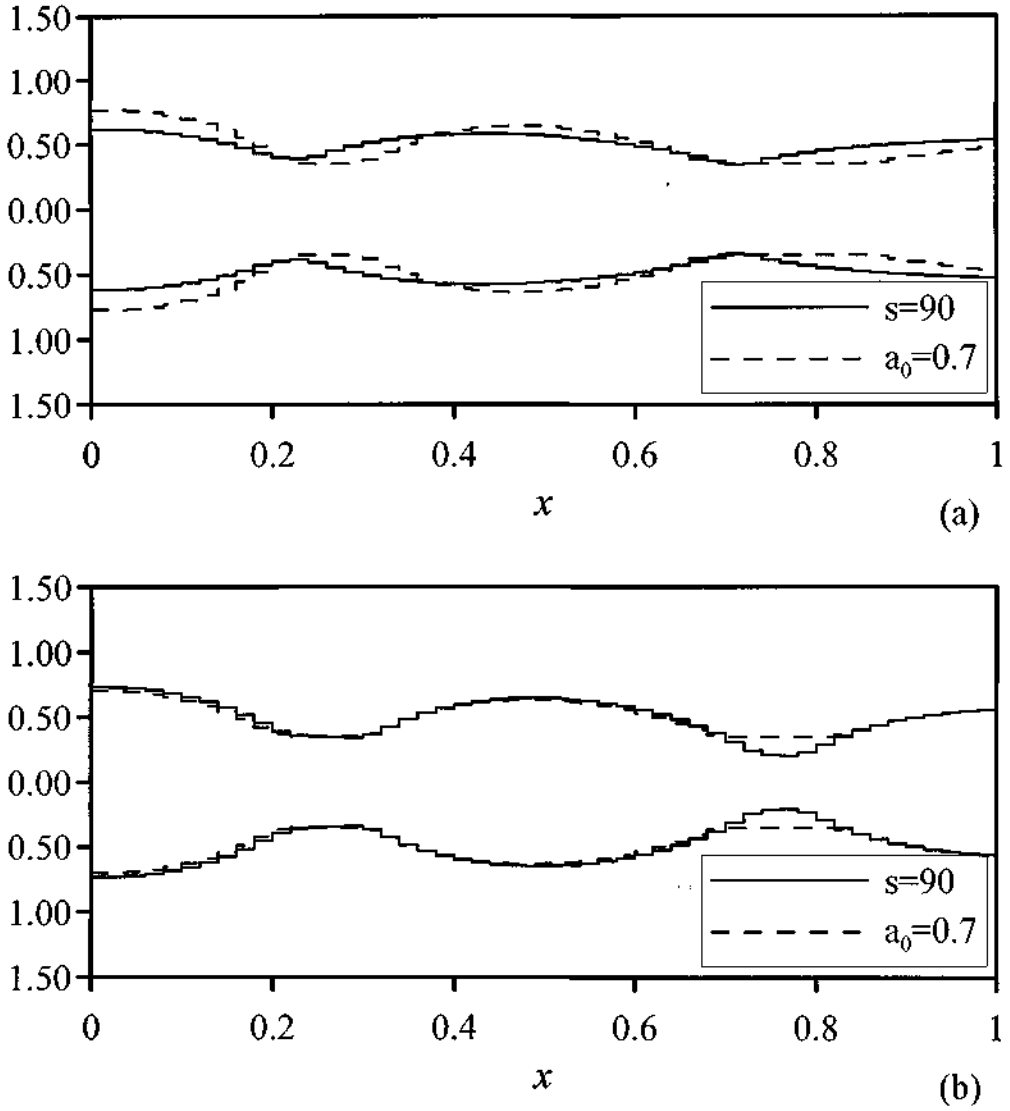

Figure 3-28. Thickness and stress constrained optimal columns under axial load $q(x)=1$ with $n=2$, (a) $p=0$, (b) $p=0.5$.

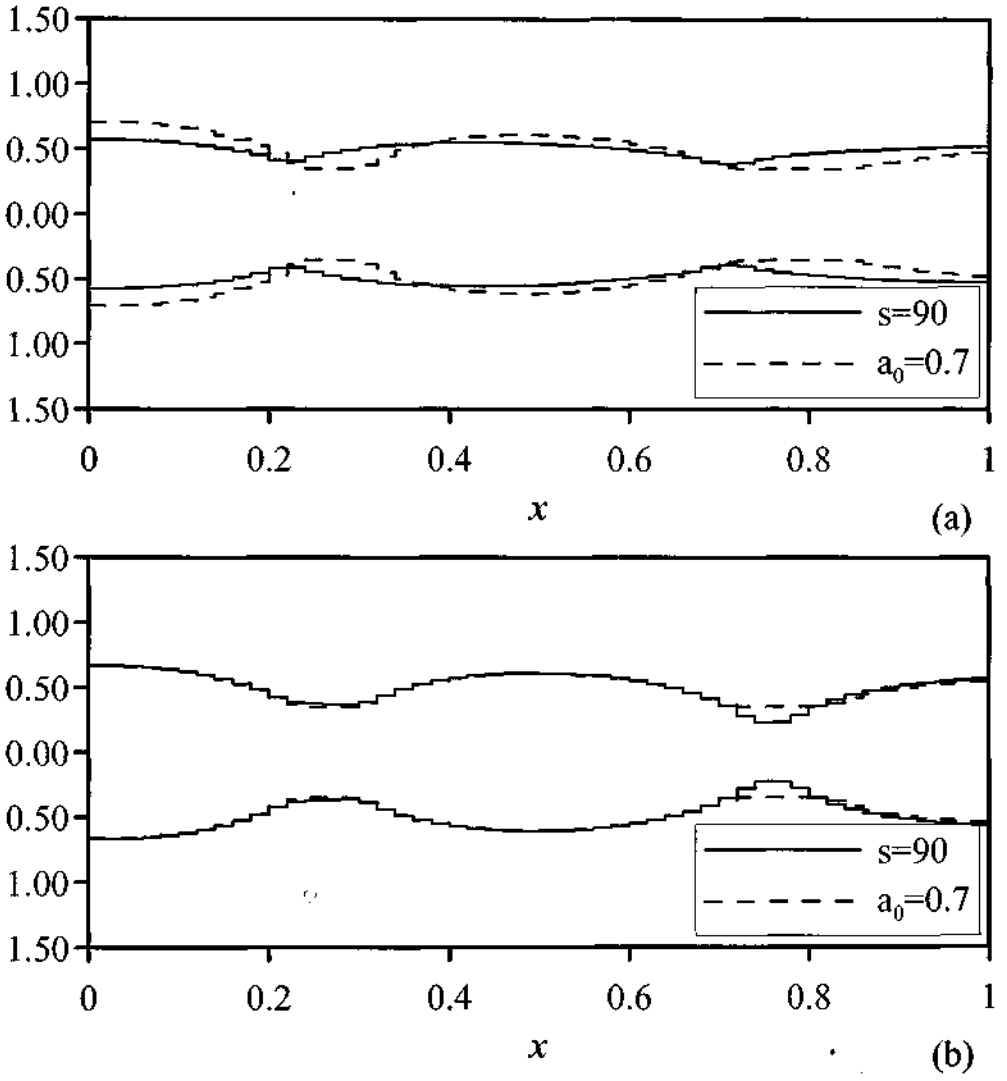

Figure 3-29. Thickness and stress constrained optimal columns under axial load $q(x)=1$ with $n=3$, (a) $p=0$, (b) $p=0.5$.

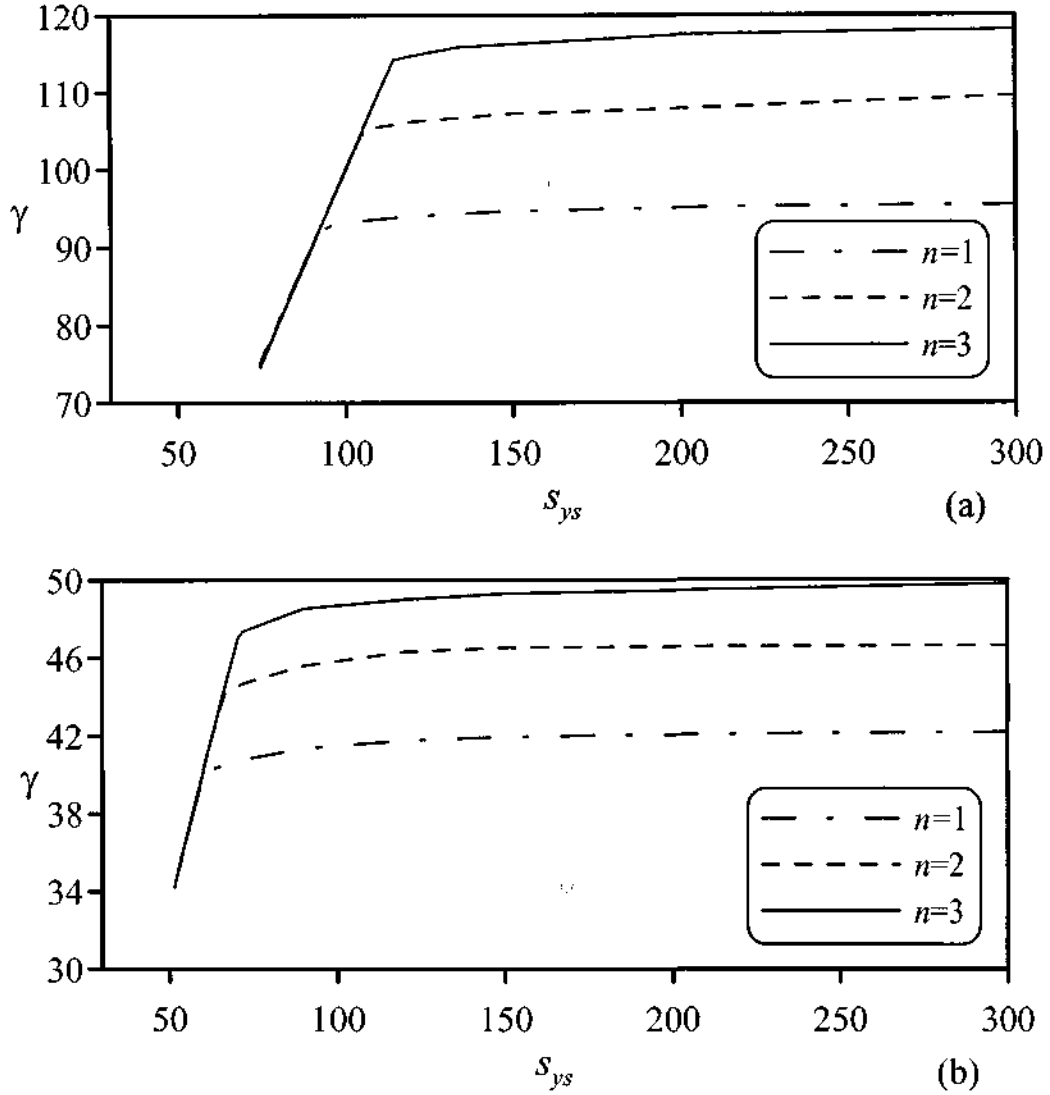

Figure 3-30. Buckling parameter γ of optimal columns plotted against s_{ys} subject to the axial load $q(x)=1$, (a) $p=0$, (b) $p=0.5$.

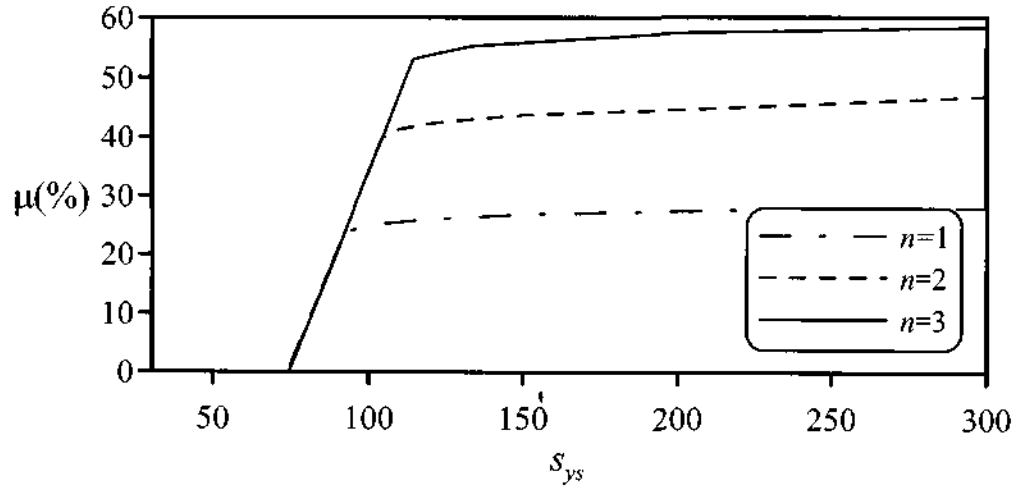

Figure 3-31. Efficiencies of optimal clamped-clamped columns plotted against s_{ys} subject to the axial load $q(x)=1$, $p=0$.

3.6 Conclusion

Optimal cross-sectional shapes of elastically restrained columns under distributed and concentrated axial loads were given for n=1, 2 and 3 where n indicates the relation between the moment of inertia and the area as given by eq. 2-4. The constant volume optimal designs were subjected to minimum area (Problem I) and maximum stress (Problem II) constraints. Unimodal and bimodal optimality conditions were derived by means of a Lagrangian formulation and a computational solution by finite element method has been formulated. An iterative solution method has been developed which starts with a unimodal solution, but uses the bimodal optimality condition if the buckling load of the second buckling mode drops below that of the first mode. The accuracy and convergence of the iterational procedure have been studied with the area distribution taken as the average of the last two distributions to increase the numerical stability. The results were compared with the results available in the literature and a high level of accuracy of the present method has been observed for all values of n.

Numerical results were given for various values of n and the rotational spring constants. The optimal cross-sectional shapes indicate that the value of n and the stiffness of the boundary spring have a distinct influence on the area function as well as on the minimum thickness of the cross-sectional area. It was found that the minimum area at which the solution transforms from a bimodal to a unimodal buckling mode increases with increasing n, but decreases with decreasing spring constant. It was also observed that the same maximum stress constraint leads to different minimum areas for different boundary conditions highlighting the major difference between a minimum thickness and a maximum stress constraint. Minimum thickness constraint will lead to the same minimum area regardless of the boundary condition while the maximum stress constraint will lead to different minimum areas depending on the boundary condition due to differences in the maximum buckling loads. Since the maximum buckling load is not known *a priori* and only determined once the optimal shape of the column is obtained, the maximum stress constraint is of more practical value in a structural optimization problem. The stress constraint leads to the correct minimum thickness to carry the maximum load while a solution with a minimum thickness constraint may or may not provide enough thickness to carry the stress.

The maximum buckling loads and efficiencies of optimal columns were given as a function of the minimum thickness and maximum stress constraints for various n values and spring constants. These graphs indicate that the higher values of n and the spring constants lead to higher buckling loads and higher efficiencies. The maximum buckling load was also studied as a function of the spring constants which quantitatively showed the relations between the stiffness of the rotational springs and the buckling load. It was observed that the buckling load increases sharply as the spring constants increase, but this increase tapers off at the higher values of these constants.

Use of a material with a high yield strength, i.e., a high strength material, leads to bimodal behaviour making the bimodal optimization necessary. It was stated by Manickarajah *et al.* (2000) that the difference between unimodal and bimodal solutions is very small. Even though this is true, the resulting column shape from a unimodal formulation will not be correct and the column will buckle before reaching the computed buckling load.

4. OPTIMIZATION OF LAMINATED COMPOSITES

Multilayered, angle-ply composite plates and shells are important structural elements which are extensively used in a number of areas of engineering. Examples include lightweight aircraft frames and panels, composite shafts, sports equipment, and pressure vessels. These lightweight structures, most of which are generally thin-walled, are subjected to different types of loading and their resistance to buckling is an important area of research as they are prone to buckling failure under compression loads. It is possible to increase their buckling resistances, by tailoring lamination angles and/or layer thicknesses. Here, optimization of rectangular plates and laminated shells under buckling loads are examined.

4.1 Optimization of rectangular plates

In this section, the influence of the in-plane restraints on the in-plane stresses and the optimization of rectangular composite plates under linearly varying buckling loads is investigated. Such stresses are encountered in practice for example, in the web sections of transversely loaded composite beams and have been studied by various authors with a view towards determining the buckling resistance of plates under in-plane non-uniform loads, Zureick and Shih (1998), Leissa and Kang (2002), Kang and Leissa (2005), Wang *et al.* (2006), Zhong and Gu (2006), etc. Also, the behavior of rectangular plates that are restrained against in-plane movement is an important research area because in-plane movement is typically restricted in aerospace structures by adjacent panels and stiffeners, as stated by Nemeth (2004).

Papazoglou *et al.* (1992) investigated the buckling of symmetric laminates under linearly varying biaxial in-plane loads combined with shear, using the Rayleigh Ritz method based on classical lamination theory. Leissa and Kang (2002) obtained exact solutions for the free vibration and buckling of rectangular plates having two opposite edges simply supported and the other two clamped, with the simply supported edges subjected to a linearly varying normal stress. Some research efforts have been made in the buckling analysis of laminated composite plates using the first-order shear deformation theory, but this work was restricted to uniform load, Khdeir (1988); Khdeir and Librescu (1988). As a preliminary attempt H. Zhong, C. Gu (2006) developed an analytical solution for the buckling of simply supported rectangular Reissner–Mindlin plates subjected to linearly varying in-plane loading. Noor (1975) and Khdeir and Librescu (1988) showed that the buckling load obtained by the classical laminated plate theory can have significant errors increasing with an increase in the degree of orthotropy of the individual layers and thickness of the plate. Thus, finite element formulations based on classical theory are of limited use in the analysis of composite structures due to the relatively high importance of transverse shear effects in comparison with isotropic structures, Kim (1996). Considering this, the plate finite element is selected to be based on first order shear deformable theory. Wang *et al.* (2006) employed a differential quadrature analysis of vibration and buckling of an SS-C-SS-C rectangular thin plate loaded by linearly varying in-plane stresses. Cagdas and Adali (2007) studied the effect of in-plane boundary conditions on the non-uniform buckling loads of rectangular composite plates.

Optimization of composite plates under buckling loads has been studied with a view towards tailoring the fiber orientations so that the buckling resistance of the plate is maximized. Hirano (1973, 1979) investigated the optimum stacking sequence to maximize the uni-axial buckling load of a thin angle-ply laminate. Wang (1982) showed that a thin angle-ply laminate with orientation $[\theta\text{-}\theta]_s$ is superior to a thin cross-ply with $[0°/90°]_s$ when subjected to axial loads, Singh and Rao (1987). Lin and Yu (1991) investigated optimal designs for the minimum weight of composite laminated plates subjected to size, displacement, buckling, and natural frequency constraints by using a technique combining finite element method and mathematical programming. Chai and Khong (1993a, 1993b) studied the optimization of laminated composite rectangular plates under a linearly varying in-plane load using the finite strip method.

The influence of non-linear buckling loads and in-plane restraints on the optimal design of laminated plates has been investigated by Walker *et al.* (1997). Optimal fiber angles to maximize the buckling loads were determined for symmetrically laminated plates taking the presence of in-plane restraints and bending-twisting coupling into account. It was shown that the reduction in the buckling load depends on the aspect ratio. Bedair (1997a, 1997b) have also presented results that include the effects of restrained in-plane movement, along with the presence of non-uniform compresive loads. Nemeth (2004) investigated the behavior of thin rectangular laminates that are subject to uniform axial compression loads and elastically restrained against in-plane expansion, contraction and shear deformation. The same effects have also been examined in similar studies by Harris (1975), Obraztsov and Vasil'ev (1989) and Sherbourne and Pandey (1992).

In most of the previous optimization studies stated above, the stress distribution inside the boundaries of the plate was assumed to be constant in buckling load calculations and also the boundary conditions are not fully described, i.e. the in-plane boundaries at the supports. One of the reasons is the use of finite elements which do not include the in-plane deformations as nodal degrees of freedom. The boundaries are generally defined as either simply supported or clamped which causes a discrepancy because the in-plane boundary conditions should also be described in order to model a structure more precisely. Considering this problem, the in-plane stress distribution can be taken as constant to be able to compare the results with the results found in the literature. However, due to in-plane restraints and/or discontinuities such as holes or cracks, stress re-distribution occurs as stated by Akbulut and Sayman (2001), which significantly influences the buckling load. Devarakonda and Bert (2004) explained the stress diffusion phenomena and showed that the membrane force distribution is not constant inside the plate, and presented explicit results for buckling loads in comparison with numerical results obtained using finite element method. Stiffeners also considerably change the stress distribution in the plates as stated by El-Ghazaly *et al.* (1984). However, in this study only the effect of in-plane/membrane boundary conditions is investigated and the real in-plane stress distributions under external loads are calculated before performing the linearized stability analysis by FEM. It is shown that the exclusion of the in-plane restraints may lead to errors in stability calculations, and consequently in optimal design. The MATLAB codes used here for optimization purposes are listed in Appendix V.

4.1.1 Problem definition

The rectangular plate of lateral dimensions $a \times b$, and thickness H is subjected to linearly varying compressive edge loading as shown in Figure 4-1. N_{xx}, N_{yy}, N_{xy} are normal forces per unit length of plate in the x and y directions, and shearing force per unit length in the xy-plane, respectively. The normal forces per unit length at the edges x=0 and x=a are given below in eq. (4-1). (The other edges are stress free).

$$N_{xx} = -N_0\left(1-\alpha\frac{y}{b}\right), \quad N_{yy}=0, \qquad N_{xy}=0 \tag{4-1}$$

where, N_0 is the intensity of N_{xx} at the edge y=0 and α is a constant. By changing α we can obtain different load cases, i.e. $\alpha=2$, $\alpha<2$, and $\alpha>2$ corresponds to pure bending, a combination of bending and compression, and a combination of bending and tension respectively. For all values of α, $N_{xx}=N_0$ at $y=0$. $N_{xx}=0$ at $y=b$ for $\alpha=1$, $N_{xx}=0$ at $y=b/2$ and $N_{xx}=-N_0$ at $y=b$ for $\alpha=2$. The non-dimensional buckling load parameter, λ_{cr}, is calculated using eq. (4-2) given below.

$$\lambda_{cr} = \frac{N_{xx} b^2}{\pi^2 D} \tag{4-2}$$

where D denotes the flexural rigidity of the plate defined by $D = \frac{E_1 H^3}{12\left(1 - \nu_{12}^2\right)}$.

The Gauss point stresses are used during numerical integration to calculate the element geometric stiffness matrix, $\mathbf{K}_{\mathbf{G}}^{e}$, which is repeated here for clarity as given below;

$$\mathbf{K}_{\mathbf{G}}^{e} = \int_{-1}^{1}\int_{-1}^{1} \mathbf{G}^T \mathbf{S} \mathbf{G} |\mathbf{J}| d\xi d\eta$$

The entries of the **S** matrix given in eq. (2.41) of Section 2 are the in-plane forces at the Gauss points which are calculated at the Gauss points by a primer static analysis. For this purpose, a linear static analysis should be performed prior to linearized stability analysis. Thus, the calculation of the buckling load parameter involves two stages, the first stage being the linear static analysis and the second stage being the linearized stability analysis.

The details of the lamina stress-strain relations, the first order shear deformation theory (FSDT), and the finite element formulation are given in Sections 2.2.1, 2.2.2, and 2.2.3 respectively. The buckling load parameter λ, which is defined as the ratio of actual buckling load to the applied forces at which the plate buckles is calculated by linearized stability analysis using FEM as defined in Section 2.2.2.2.

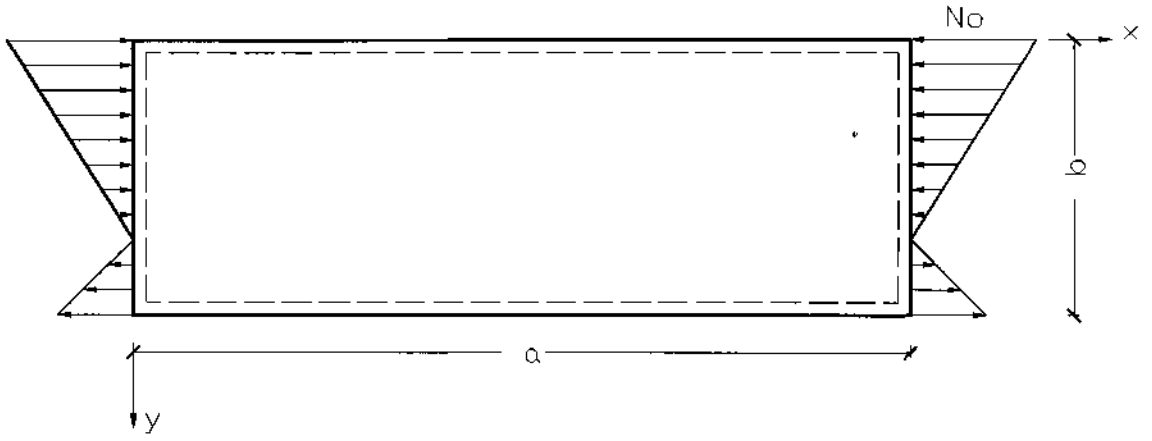

Figure 4-1. Plate geometry and linearly varying edge loading

4.1.2 Boundary conditions

The 6 different sets of boundary conditions are tabulated in Table 4-1 given below. The boundary sets BC V and BC VI, which are used for comparison purposes, result in uniform membrane force distributions under the applied edge loads and they correspond to the cases when all of the edges are free and restrained against rotation, respectively. Rotational restraints are the same for BC II and BC V and BC IV and BC VI and the only differences are the in-plane boundary conditions. In both of the boundary sets BC V and BC VI, the nodes at x=0, y=0 and x=a, y=b are restrained against translation in y direction and the node at the position x=a/2, y=b/2 is restrained against translation in x direction. The boundary sets BC I, BC II, and BC V are grouped as the simply supported plates (SS) and the boundary sets BC III, BC IV, and BC VI are grouped as the clamped plates (C). The comparisons are made using boundary sets BC V

and BC VI which yield uniform in-plane stress distributions. For the SS plates, BC I and BC II are compared with each other and with BC V. For the C plates, BC III and BC IV are compared with each other and with BC VI.

Table 4-1. Boundary conditions; 1: free, 0: restrained

Edge	Boundary set	u	v	w	θ_x	θ_y
AC	I	0	0	0	1	0
	II	0	0	0	1	0
	III	0	0	0	0	0
	IV	0	0	0	0	0
	V*	1	1	1	1	1
	VI*	1	1	1	0	0
BD	I	1	1	0	1	0
	II	1	1	0	1	0
	III	1	1	0	0	0
	IV	1	1	0	0	0
	V*	1	1	1	1	1
	VI*	1	1	1	0	0
AB	I	1	1	0	0	1
	II	0	0	0	0	1
	III	1	1	0	0	0
	IV	0	0	0	0	0
	V*	1	1	1	1	1
	VI*	1	1	1	0	0
CD	I	1	1	0	0	1
	II	0	0	0	0	1
	III	1	1	0	0	0
	IV	0	0	0	0	0
	V*	1	1	1	1	1
	VI*	1	1	1	0	0

* u and v are restrained at the nodes at $x=a/2$ and $y=b/2$.

4.1.3 Optimal design problems

The objective is to maximize the non-dimensional buckling load parameter, of the symmetrically laminated rectangular plate of total thickness H, total layer number n by optimizing ply thicknesses, H_i, or by optimizing the ply lamination angles, θ_i where $i=1,2,...,n$ and the lamination angle is the angle between x axis and fibre direction. The related problems, Problem I and Problem II, are defined below in equations (4-3) and (4-4) respectively.

Problem I. Determine the ply thicknesses $H_i, i=1,2,...,n$ of a symmetric cross-ply laminate of total thickness H such that the buckling load parameter, λ_{cr}, will be maximized, viz.

$$\max_{H_i} \lambda_{cr} \qquad \text{such that} \qquad \sum_{i=1}^{n} H_i = H \qquad i=1,2,...,n \tag{4-3}$$

Problem II. Determine the ply angles $\theta_i, i=1,2,...,n$ of a symmetric angle-ply laminate of total thickness H such that the buckling load parameter, λ_{cr}, will be maximized, viz.

$$\max_{\theta_i} \lambda_{cr} \qquad \text{such that} \qquad 0 \le \theta_i \le 90 \qquad i=1,2,...,n \tag{4-4}$$

In Problem II, the ply thicknesses of the layers are kept constant. In order to distinguish between the optimization problems the non-dimensional buckling load is denoted by λ_1 and λ_2 for Problem I and Problem II respectively. The *Golden Section* method is employed in the optimization stage, Haftka *et al.* (1990).

4.1.4 Numerical results

The numerical results are obtained using a 16x8 mesh, which consists of eight-noded iso-parametric plate finite elements. It is decided that this mesh is capable of accurately modeling the laminated plates considered, depending on the experience obtained while solving the verification problems related to plate stability. The computer codes used here are listed in the Appendix section.

The side to thickness ratio a/H was taken as $a/H=100$ in the numerical examples. The reason of selecting a relatively high a/H ratio is to minimize the contribution of shear deformation on the results. Lower a/H ratios may give different results due to the contribution of shear. Also, the plate is assumed to be thin enough to make sure that failure due to buckling is dominant over failure due to first-ply failure.

The material properties are given as follows;

$$E_1/E_2=25,\ G_{12}/E_2=G_{13}/E_2=0.5,\ G_{23}/E_2=0.3,\ \nu_{12}=\nu_{23}=\nu_{13}=0.25$$

4.1.4.1 Analysis of in-plane stresses

The applied edge loads are converted into nodal loads by integration and a primer linear static analysis is performed in order to obtain the normal force distribution inside the plate. The normal forces at the Gauss points are extrapolated to the element corner nodes to be able to plot the normal force distributions. The stress evaluation-smoothing technique described in Section 2.2.2.4 of this thesis is used for this purpose.

We first consider a cross-ply laminate with four layers of equal thickness under axial compression N_{xx} given by eq. (4-1) having a stacking sequence $(0^\circ/90^\circ/90^\circ/0^\circ)$. The effect of boundary conditions on the in-plane stress distribution is to be observed in comparison to the cases of BC V and BC VI which produce a distribution of N_{xx} identical to the applied stress as shown in Fig. 4-2 for $\alpha=0,1,2$ (N_0=1). Fig. 4-2 shows that the in-plane stress distribution matches the applied stress for simply supported and clamped boundary conditions when there are no constraints in the x and y directions, i.e., when $u(x,y)$ and $v(x,y)$ are free. Fig. 4-3 shows the in-plane stress distribution for the boundary conditions BC II for $\alpha=0,1,2$. In this case $u(x,0)$=u(x,b)=0 and $v(x,0)$=$v(x,b)$=0, i.e., in-plane deflections of the horizontal sides of the plate (Fig. 4-1) are restrained, but all the edges are free to rotate, i.e., moments are zero. Moreover $u(0,y)$=$v(0,y)$=0, but $u(a,y)$ and $v(a,y)$ are free, i.e., in-plane deflections are restrained only on the left side of the plate. The resulting distribution of N_{xx} is shown in Fig. 4-3 which shows the Poisson effect due to restrained horizontal edges as well as the non-symmetric stress distribution due to the non-symmetry of boundary conditions. Fig. 4-3a corresponding to a uniformly distributed axial load (α=0) shows that even under this loading boundary conditions lead to a non-uniform stress distribution. Next the stress distribution for BC IV is studied which is similar to BC II except the rotations of the edges are restrained making the edges clamped. Fig. 4-4 shows the in-plane stress distributions for this case with $\alpha=0,1,2$. A comparison of Figs. 4-3 and 4-4 shows that the stress distribution patterns are similar for boundaries with or without rotational restraints. However the magnitudes of the stresses differ with smaller N_x values in the case of BC IV.

Next the corresponding results for an angle-ply laminate are given taking the stacking sequence as $(45^\circ/-45^\circ/-45^\circ/45^\circ)$. Fig. 4-5 shows the stress distribution for the boundary condition BC II with $\alpha = 0,1,2$. It is observed that the stress distribution patterns differ substantially as compared to the cross-ply case (Fig. 4-3). Moreover the patterns for $\alpha = 0,1,2$ are also dissimilar. The stress distributions for BC IV are shown in Fig. 4-6. It is observed that except for the case $\alpha = 1$, the stress distributions for BC II and IV are considerably different. Figs. 4-3 to 4-6 demonstrate the fact that in-plane stress distributions which arise due to constrained in-plane deflections u and v depend not only on the boundary conditions, but also on the stacking sequence and the distribution of the axial load, i.e., on α.

4.1.4.2 Optimal design for maximum buckling load

Next we investigate the effect of various problem parameters on the optimal values of the design variables and the buckling load. For the 4 layered symmetric cross-ply laminate, the non-dimensional thicknesses of the 0° and 90° layers are denoted by h_0 and h_{90}, respectively. As H is constant, h_{90} can be written in terms of h_0 as $h_{90} = \frac{1}{2} - h_0$. Fig. -7 shows the curves of λ_1 plotted against h_0 for boundary conditions BC II and V (Fig. 4-7a) and for BC IV and VI (Fig. 4-7b) with $\alpha = 0,1,2$. It is observed that pure bending, i.e., $\alpha = 2$ yields the highest and the lowest values of λ_{cr} for all boundary conditions. However, these cases are also the most sensitive to the value of h_0. The least sensitive to h_0 are the cases for $\alpha = 0,1$ for the boundary conditions V and VI. Thus an optimal design based on classical boundary conditions of simply supported or clamped laminates will show little improvement over the laminate with equal-thickness layers ($h_0 = h_{90} = 0.25$). However, the real danger lies in the fact that in all cases of $\alpha = 0,1,2$, the buckling loads of equal-thickness laminates are smaller for the BC II and BC IV as compared to BC V and BC VI, respectively. This implies that equal-thickness laminates will fail at a load below the design buckling load if plate is not free to move in its plane, i.e., if the in-plane deformations are restrained as often the case in practice. A further implication of Fig. 4-7 is that the buckling load of cross-ply laminates can be increased considerably by optimal thickness design if the boundaries are restrained against in-plane movement, i.e., for BC II and BC IV, since at the optimal points these boundary conditions yield the higher buckling loads as compared to BC V and BC VI, respectively. This increase is observed to be higher for the case $\alpha = 2$. However the sensitivity of buckling load to the optimal thickness needs to be taken into account in a design situation. The optimization results for the symmetric cross-ply laminates (Problem I) with different aspect ratios a/b are given in Tables 4-2, 4-3, and 4-4 for $\alpha = 0,1,2$, respectively.

The corresponding results for an angle-ply laminate $(\theta/-\theta/-\theta/\theta)$ are given in Fig. 4-8 as λ_2 vs θ curves. It is observed that for the BC II and BC V, the optimal θ value lies around 40° for $\alpha = 0,1,2$. For BC IV and BC VI, the optimal θ is 0° with the exception of pure bending case $\alpha = 2$. For this case the dependence of the buckling load on θ also differs considerably with the BC II having two maxima as opposed to a single maximum for BC VI. As expected constraining the plate against in-plane movement improves the buckling load for all values of θ. The optimization results for the symmetric angle-ply laminates (Problem II) with different aspect ratios a/b are given in Tables 4-5, 4-6, and 4-7 for $\alpha = 0,1,2$, respectively.

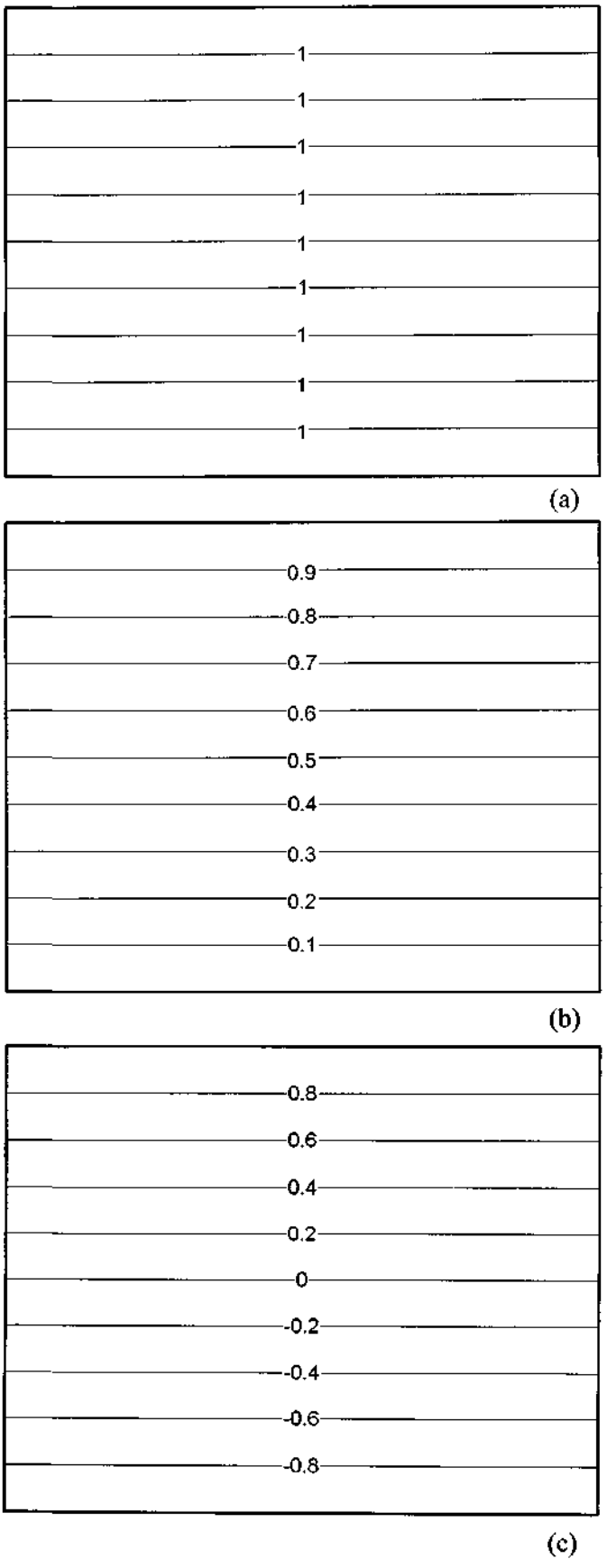

Figure 4-2. Distribution of normal force N_{xx} for Problem I, BC V-VI

a) α=0 b) α=1 c) α=2

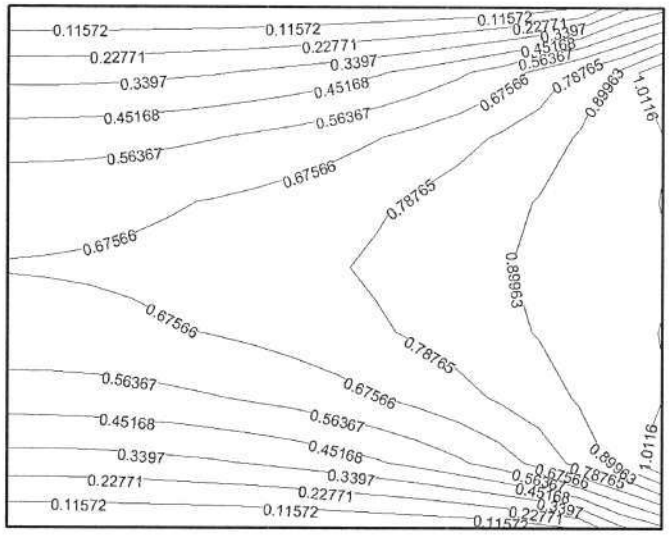

(a)

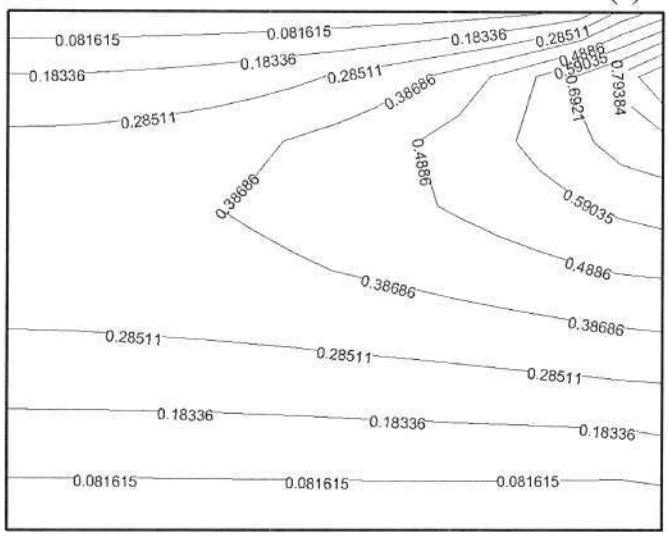

(b)

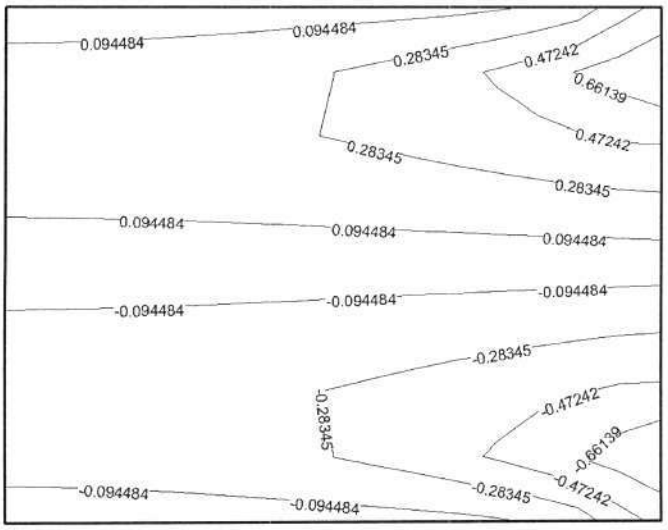

(c)

Figure 4-3. Distribution of normal force N_{xx} for Problem I, BC II

a) α=0 b) α=1 c) α=2

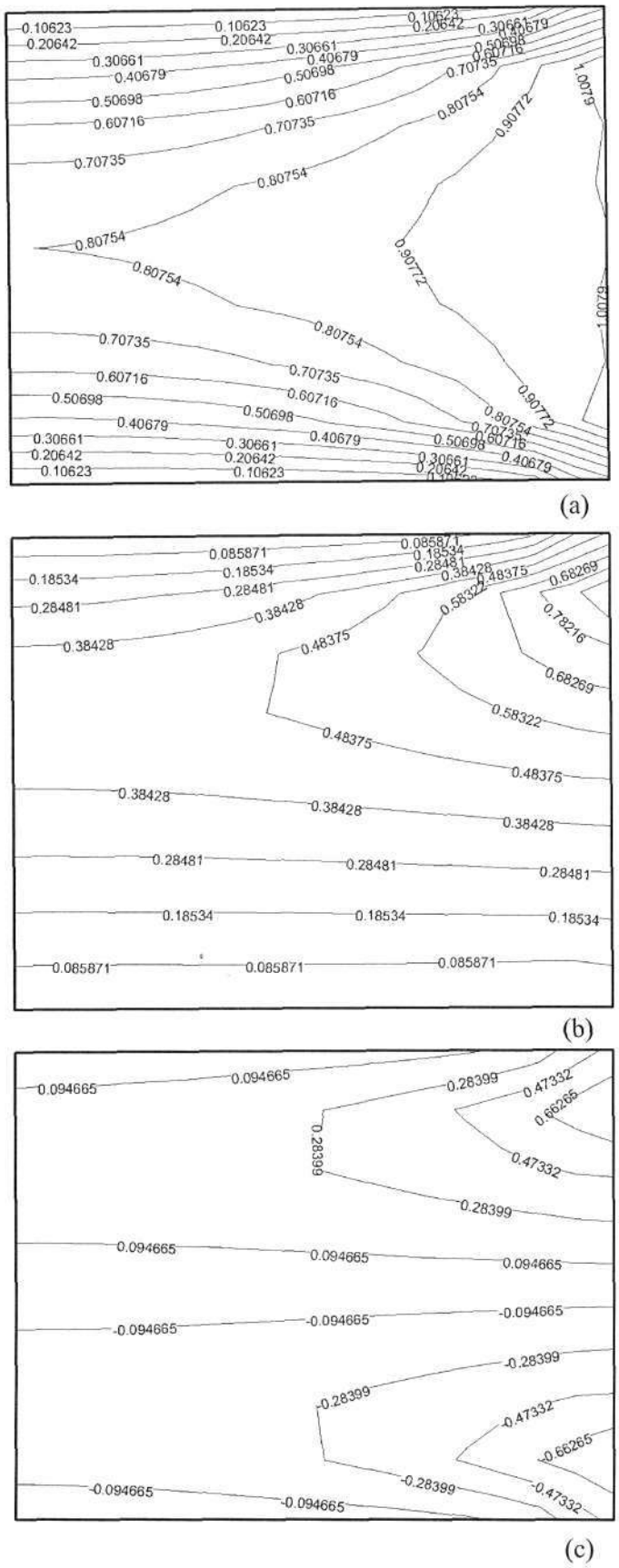

Figure 4-4. Distribution of normal force N_{xx} for Problem I, BC IV

a) α=0 b) α=1 c) α=2

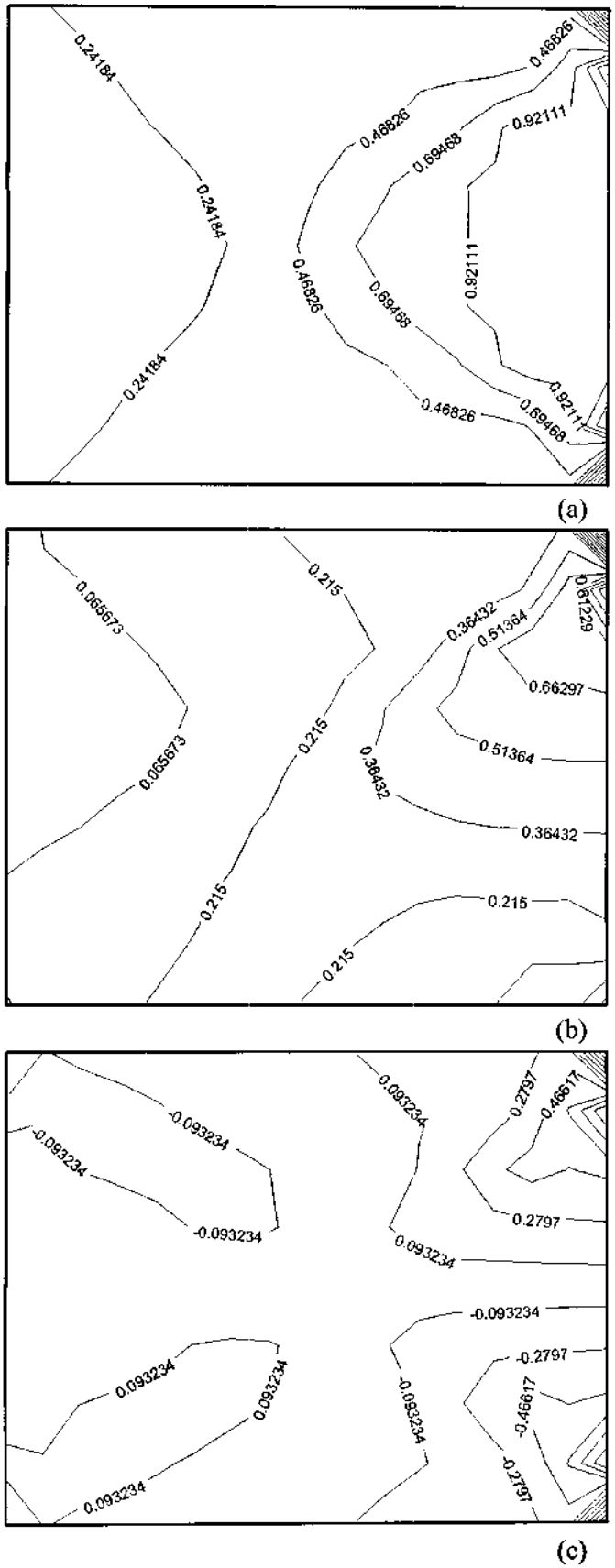

Figure 4-5. Distribution of normal force N_{xx} for Problem II, BC II

a) α=0 b) α=1 c) α=2

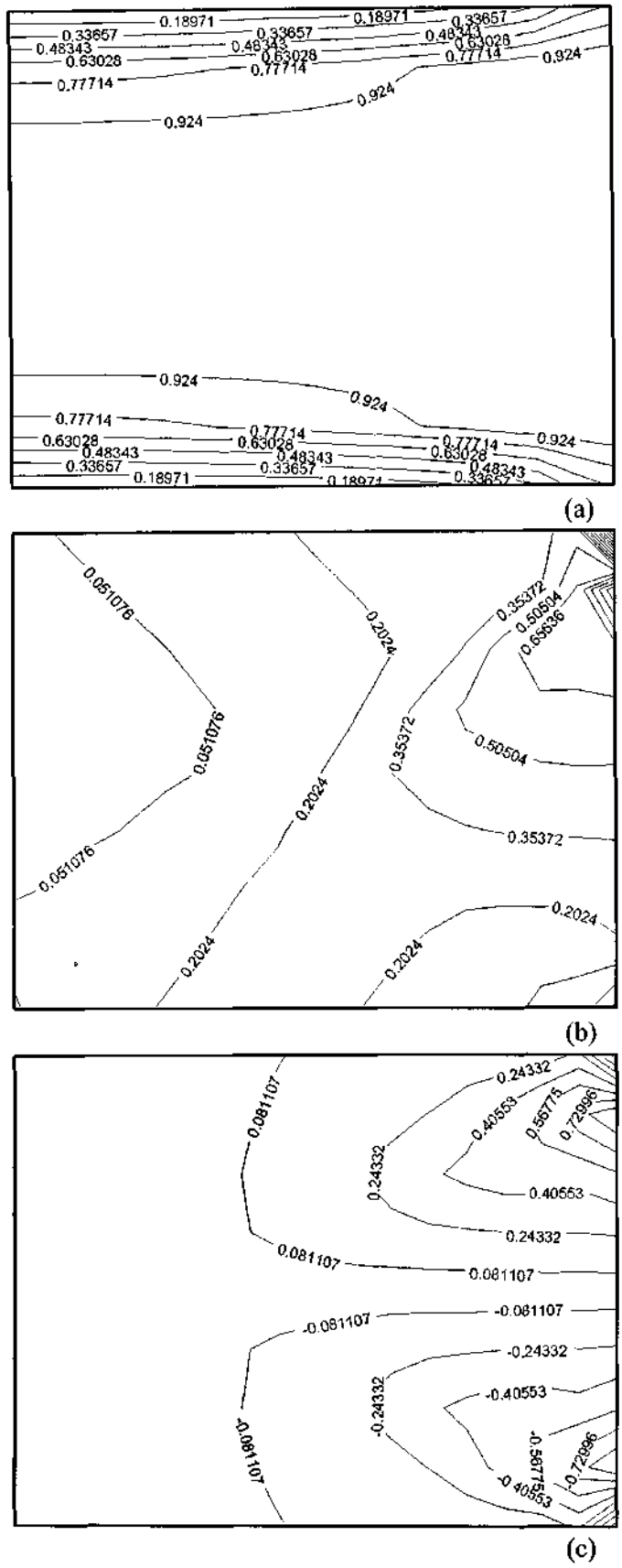

Figure 4-6. Distribution of normal force N_{xx} for Problem II, BC IV

a) α=0 b) α=1 c) α=2

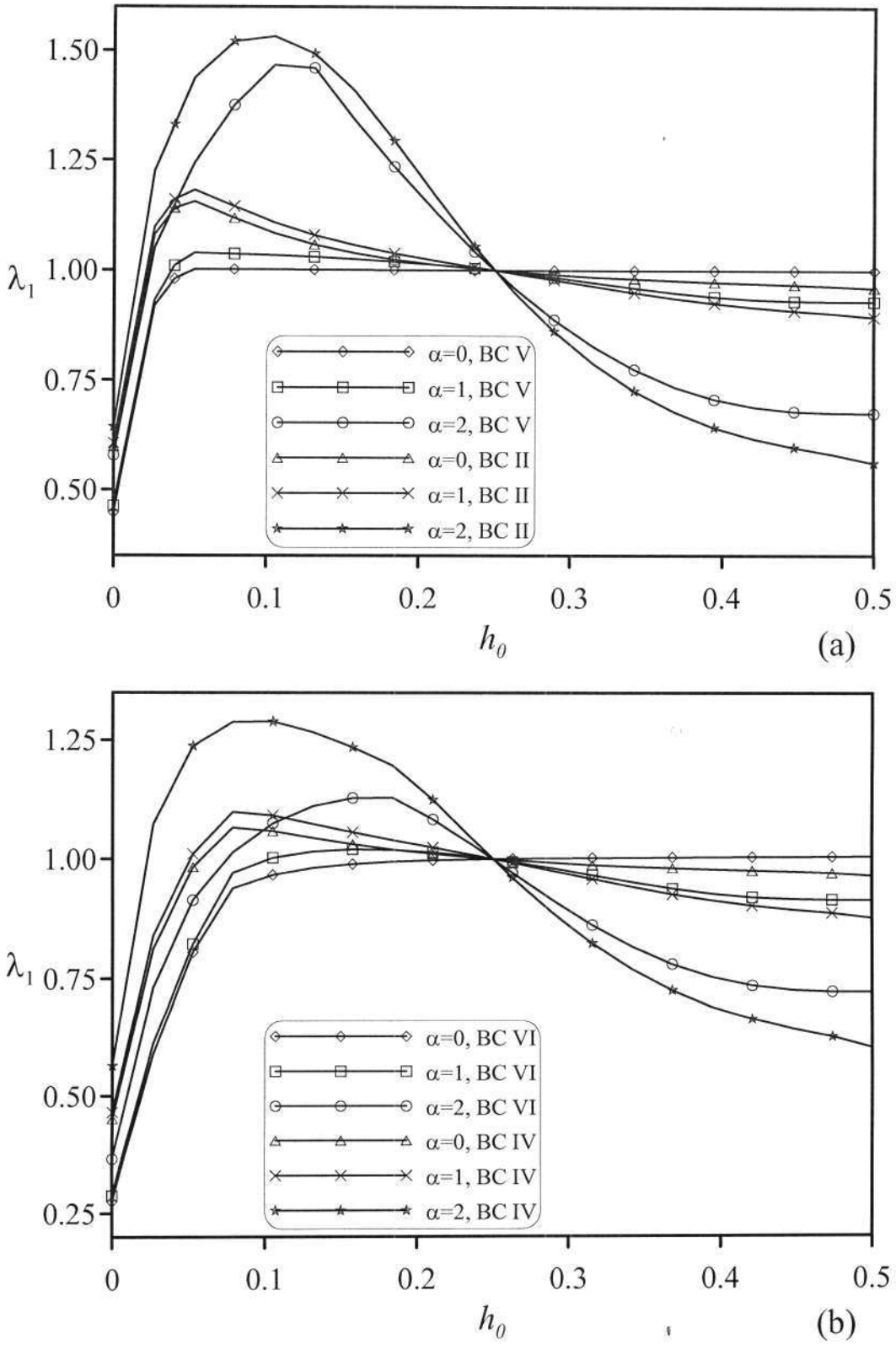

Figure 4-7. λ_1 vs. h_0

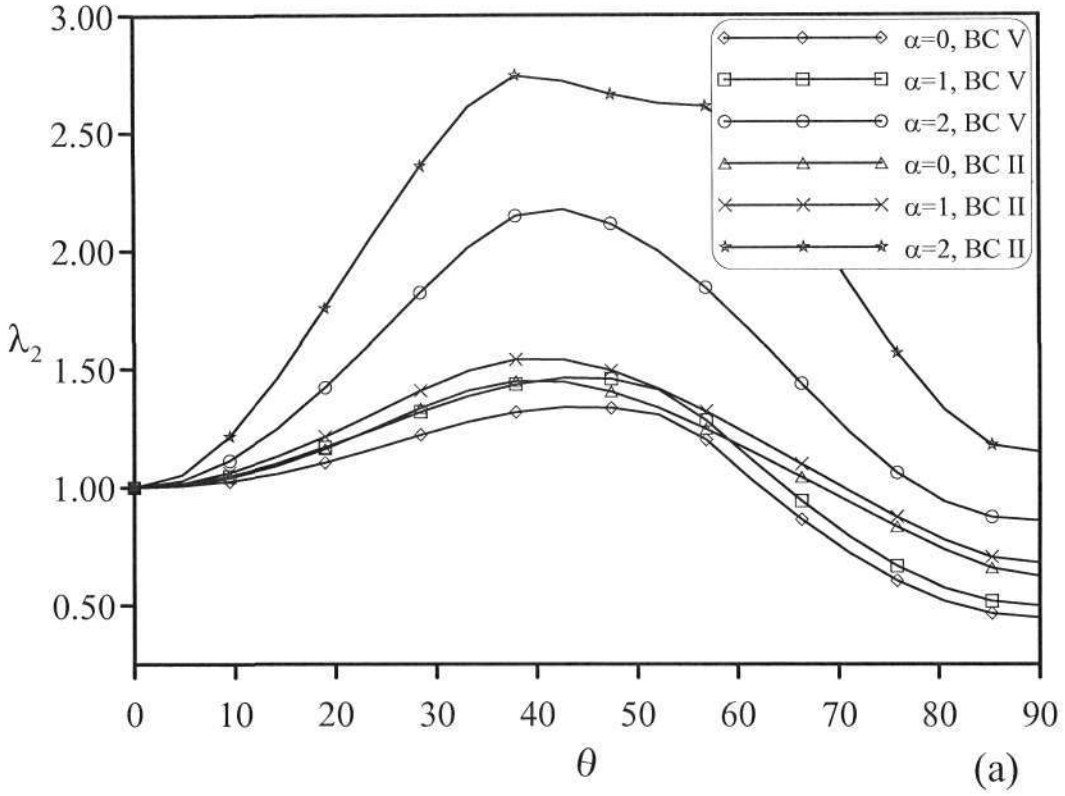

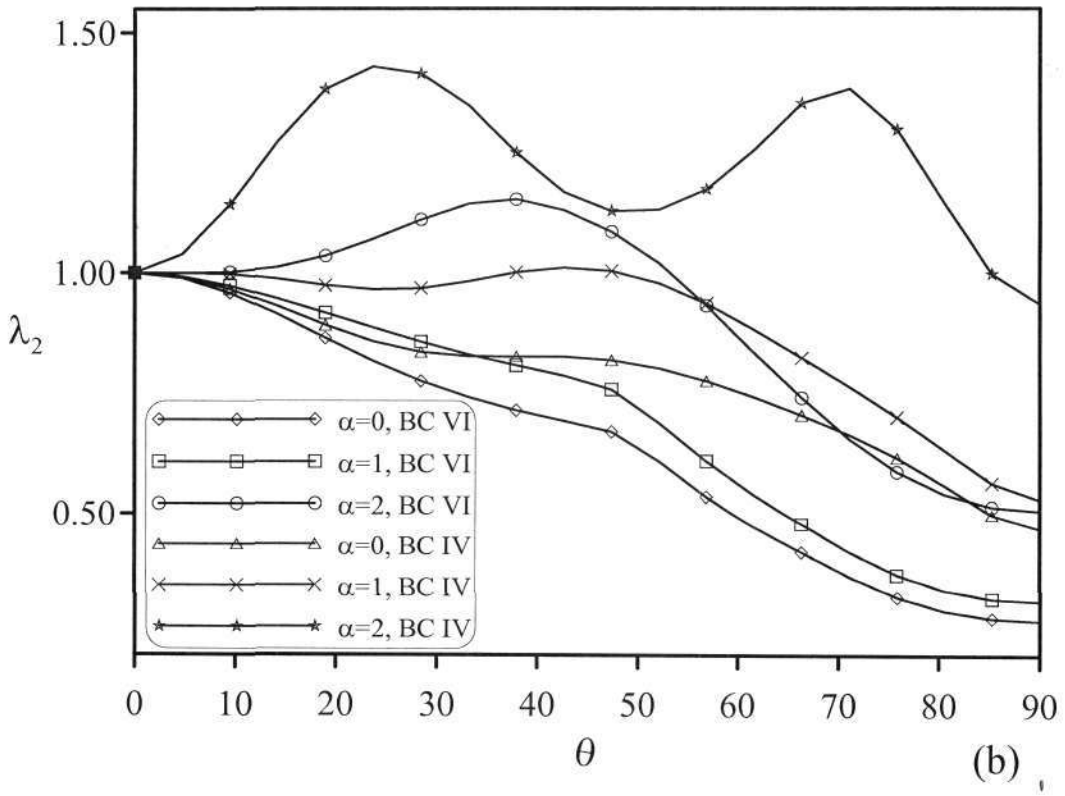

Figure 4-8. λ_2 vs. θ

4.1.4.3 Numerical results for problem I

Maximize the buckling load of a rectangular 4 layer symmetric cross-ply laminated plate under axial compression as shown in Figure 1, with 0° plies stacked at the outer, and 90° plies stacked at the inner layers. The thickness of the plate is denoted by H, and the non-dimensional thicknesses of the 0° and 90° plies are denoted by h_0 and h_{90} respectively. As the plate thickness is constant, h_{90} can be written in terms of h_0, so that the only unknown is h_0 as follows; $1 = 2h_0 + 2h_{90}$, $h_{90} = \frac{1}{2} - h_0$. The optimization results for different values of a/b are given in Tables 4-2, 4-3, and 4-4 for α=1,2,3 respectively, where $\lambda_{1,initial}$ corresponds to the case h_0=0.25. $\lambda_{1,opt}$ and $h_{0,opt}$ denote the optimal values of non-dimensional buckling load λ_1 and h_0. Efficiency (η) for Problem I is defined as follows; $\eta = \frac{\lambda_{1,opt} - \lambda_{1,initial}}{\lambda_{1,initial}} \times 100$.

4.1.4.4 Numerical results for problem II

Maximize the buckling load of a rectangular 4 layer symmetric cross-ply laminated plate under axial compression as shown in Figure 1, assuming that the thicknesses of the plies are equal, i.e. $h_0 = 0.25$, and the stacking sequence is $[\theta,-\theta]_s$. The optimal θ values for different values of a/b are given in Tables 4-5, 4-6, and 4-7 for α=1,2,3 respectively, where $\lambda_{2,0^\circ}$ corresponds to the case $\theta = 0^\circ$ and $\lambda_{2,opt}$ denotes the optimal values of non-dimensional buckling load λ_2. Efficiency (η) for Problem II is defined as follows; $\eta = \frac{\lambda_{2,opt} - \lambda_{2,0^\circ}}{\lambda_{2,0^\circ}} \times 100$.

4.1.4.5 Discussion of optimization results for rectangular plates

Problem I:

Results related to design problem I are given in Tables 4-2, 4-3, and 4-4 for α=0,1,2 respectively. It is observed from these tables that, the differences between the results obtained for BC I and BC V for simply supported plates and BC III and BC VI for clamped plates are negligible. This means that restraining the in-plane deformations of the edge x=0, which is perpendicular to the direction of loading, does not considerably influence the results related to Problem I (However, this is not the case for Problem II). Therefore, the results pertaining to boundary conditions BC I and BC III will not be considered here. The results also show that a/b ratio has pronounced effects on both $\lambda_{1,opt}$ and $h_{0,opt}$.

The behaviour of the clamped plates is similar to that of the simply supported ones from this point of view. For both simply supported and clamped plates, the influence of in-plane restraints on the optimization results is negligible at a/b=0.5. The efficiencies corresponding to the cases α=0,1,2 at a/b=0.5 are around 12%, 3%, 1% respectively. Also, the initial buckling loads do not differ considerably in the presence of in-plane restraints.

The influence of the in-plane restraints can only be observed at a/b ratios 1.0 and 2.0. Comparisons of the $\lambda_{1,opt}$ values corresponding to the SS and C plates with and without in-plane restraints show that, for both α=0 and α=1 and at a/b=2.0 the inclusion of in-plane restraints cause an increase of around 50% in $\lambda_{1,opt}$. The gain in $\lambda_{1,opt}$ for the case α=0 at a/b=1.0 is around 30% for the SS plates and around 10% for the C plates. Similar observations may be made for most the other load cases and geometries, which lead to the conclusion that,

optimization of simply supported plates (Problem I) result in higher gains comparing to clamped plates when α=0 or α=1.0. However, it is observed for the case α=2 and a/b=2.0 that, $\lambda_{1,opt}$ value corresponding to BC IV is nearly 100% higher than the one for BC VI and $\lambda_{1,opt}$ value corresponding to BC II is around 60% higher than the one for BC V. Thus, the last conclusion deduced can not be generalized, and it is only valid for uniaxial and triangularly distributed loads.

For both SS and C plates and for the case α=0, $h_{0,opt}=0.5$ at a/b=0.5 which means that, the uniaxial load in x-direction is carried mainly by the plies in y-direction for this case, however, $h_{0,opt}$ value gradually decreases with increasing α. At a/b=1.0, $h_{0,opt}$ takes a value between 0 and 0.1 for both SS and C plates except for the case a=0, where $h_{0,opt}$ values corresponding to the cases BC III and BC VI are both found out to be equal to 0.5. It may be concluded that, the load is mainly carried by the 90° plies for this case; i.e. at a/b=1.0. Finally, at a/b=2.0, $h_{0,opt}$ values for both SS and C plates with α=0,1,2 are around 0.1, which implies a/b ratio is the main parameter determining $h_{0,opt}$.

It is also observed that, the buckling load of the optimized plates are very sensitive to changes in h_0 for a/b=0.5. However, this sensitivity rapidly vanishes with increasing a/b.

Problem II:

Results related to design problem II are given in Tables 4-5, 4-6, and 4-7 for α=0,1,2 respectively. It is observed that, efficiencies related to SS and C plates with different in-plane boundary conditions do not considerably differ for the cases α=0 and α=1.0. However, in case of pure bending, i.e. α=2, the efficiencies are found out to be considerably different. For α=0, and α=1 and at a/b=0.5, and a/b=1.0 the initial buckling loads are slightly affected by the presence of in-plane restraints.

First, the results for the case α=0 are examined. The plate becomes stiffer with decreasing a/b, so the buckling load increases, while the clamped plates have greater buckling loads than those of simply supported plates. For simply supported plates, the optimal θ increases initially as a/b increases, from a minimum value of 0° at a/b=0.5 to 29.5°, 40°, and 44.4° at a/b=1.0 for BC I, BC II and BC V respectively. However, for these boundary conditions, θ_{opt} values at a/b=2.0 are around 45°, which implies that θ_{opt} does not considerably change at a/b ratios greater than 1.0. Similarly, η increases as a/b increases, from a minimum value of 0% at a/b=0.5 to 15.7%, 45.1%, 33.7% at a/b=1.0 for BC I, BC II and BC V respectively. The efficiencies for these cases at a/b=2.0 are 139.8%, 170.9%,182.3%. For clamped plates; at aspect ratios a/b=0.5 and a/b=1.0, optimization results in no gain, i.e. θ_{opt}=0 for these cases. However, at a/b=2.0, θ_{opt} values are around 45° and the efficiencies are 16.1%, 83.4%, 38.9% for boundary conditions III, IV, and VI respectively. The η values corresponding to the simply supported cases at a/b=2.0 are much higher than those of the clamped cases. This signifies that, the influence of in-plane restraints is higher for simply supported plates, comparing to the clamped plates.

For all α and at a/b=2.0, θ_{opt} values corresponding to all boundary conditions tend to 45° while for the clamped plates with a/b=0.5 the optimal fiber angles are found out to be around 0°.

The results obtained for Problem II are in accordance with the results obtained for Problem I. Similarly, for α=0 the uniaxial load in x-direction is carried mainly by the plies in y-direction at a/b=0.5. Thus, $\lambda_{1,opt}=\lambda_{2,opt}$ for the case α=0. Also, at a/b=0.5, the differences between $\lambda_{1,opt}$

and $\lambda_{2,opt}$ values of both SS and Cd plates are negligibly small for the cases α=0 and α=1 and the differences are less than 10% for the case α=2. For nearly all of the SS plates with α=0 and α=1; $\lambda_{2,opt} > \lambda_{1,opt}$, but $\lambda_{2,opt} < \lambda_{1,opt}$ for α=2. For nearly all of the C plates at a/b=1.0 and a/b=2.0, $\lambda_{2,opt} < \lambda_{1,opt}$. This means that, thickness optimization yields better results for both SS and C plates under pure bending and for C plates under uniaxial and triangularly distributed loads. Results obtained by optimizing the lamination angles are superior to corresponding results obtained by thickness optimization for SS plates under uniaxial and triangularly distributed loads.

Table 4-2. Optimization results, problem I, (α=0)

a/b	Boundary set	$\lambda_{1,initial}$	$h_{0,opt}$	$\lambda_{1,opt}$	η (%)
0.5	I	3.3666	0.4998	3.7892	12.6
	II	3.3889	0.4792	3.7889	11.8
	III	12.4220	0.4997	14.0780	13.3
	IV	12.4405	0.5000	14.0473	12.9
	V	3.3668	0.5000	3.7875	12.5
	VI	12.4234	0	14.0750	13.3
1	I	1.0659	0.0789	1.0674	0.1
	II	1.1291	0.0465	1.3081	15.9
	III	3.9225	0.5000	3.9417	0.5
	IV	4.1148	0.0834	4.3912	6.7
	V	1.0659	0.0757	1.0675	0.2
	VI	3.9227	0.5000	3.9439	0.5
2	I	0.9010	0.0693	1.0675	18.5
	II	1.0991	0.0918	1.5397	40.1
	III	2.047	0.1225	2.8271	38.1
	IV	3.1750	0.0878	4.3898	38.3
	V	0.9010	0.0775	1.0675	18.5
	VI	2.4048	0.1224	2.8272	38.1

Table 4-3. Optimization results, problem I, (α=1)

a/b	Boundary set	$\lambda_{1,initial}$	$h_{0,opt}$	$\lambda_{1,opt}$	η (%)
0.5	I	5.3154	0.3880	5.4852	3.2
	II	5.4855	0.3516	5.6297	2.6
	III	18.7565	0.5000	19.3363	3.1
	IV	19.3240	0.3491	19.8259	2.6
	V	5.3161	0.3902	5.4862	3.2
	VI	18.7605	0.5000	19.3651	3.2
1	I	2.0279	0.0366	2.1089	4.0
	II	2.1915	0.0455	2.5933	18.3
	III	7.2541	0.1640	7.4022	2.0
	IV	7.8373	0.0841	8.6236	10.0
	V	2.0280	0.0331	2.1096	4.0
	VI	7.2545	0.1640	7.4025	2.0
2	I	1.7798	0.0573	2.1063	18.3
	II	2.1788	0.0923	3.0387	39.5
	III	4.5785	0.1266	5.4383	18.8
	IV	6.2342	0.0880	8.6365	38.5
	V	1.7799	0.0567	2.1066	18.4
	VI	4.5787	0.1266	5.4384	18.8

Table 4-4. Optimization results, problem I, (α=2)

a/b	Boundary set	$\lambda_{1,initial}$	$h_{0,opt}$	$\lambda_{1,opt}$	η (%)
0.5	I	8.1516	0.2032	8.2347	1.0
	II	8.9873	0.1585	9.3017	3.5
	III	27.3696	0.2209	27.4825	0.4
	IV	30.2182	0.1879	30.7423	1.7
	V	8.1510	0.2031	8.2343	1.0
	VI	27.3710	0.2209	27.4838	0.4
1	I	5.2006	0.1214	7.8349	50.7
	II	7.1878	0.0971	11.0265	53.4
	III	15.6502	0.1784	17.7172	13.2
	IV	21.4938	0.0916	27.7771	29.2
	V	5.2005	0.1214	7.8351	50.7
	VI	15.6504	0.1784	17.7176	13.2
2	I	5.2011	0.1082	6.9772	34.1
	II	8.5450	0.1026	11.2631	31.8
	III	11.5696	0.1220	14.2395	23.1
	IV	22.0330	0.0956	29.5556	34.1
	V	5.2011	0.1081	6.9772	34.1
	VI	11.5697	0.1222	14.2397	23.1

Table 4-5. Optimization results, problem II, (α=0)

a/b	Boundary set	θ_{opt} (°)	$\lambda_{2,0^\circ}$	$\lambda_{2,opt.}$	η (%)
0.5	I	0	3.7892	3.7892	0.0
	II	0	3.7879	3.7879	0.0
	III	0	14.0784	14.0784	0.0
	IV	0	14.0473	14.0473	0.0
	V	0	3.7875	3.7875	0.0
	VI	0	14.0750	14.0750	0.0
1	I	29.5	1.0658	1.2335	15.7
	II	40	1.0842	1.5728	45.1
	III	0	3.9417	3.9417	0.0
	IV	0	3.9721	3.9721	0.0
	V	44.4	1.0660	1.4248	33.7
	VI	0	3.9439	3.9439	0.0
2	I	43.3	0.4783	1.1469	139.8
	II	44.9	0.5399	1.4628	170.9
	III	43.3	1.6091	1.8681	16.1
	IV	46.6	1.8152	3.3292	83.4
	V	43.8	0.4786	1.3509	182.3
	VI	41.2	1.6104	2.2351	38.8

Table 4-6. Optimization results, problem II, (α=1)

a/b	Boundary set	θ_{opt} (°)	$\lambda_{2,0^\circ}$	$\lambda_{2,opt.}$	η (%)
0.5	I	9.8	5.4862	5.5100	0.4
	II	9.6	5.5535	5.5873	0.6
	III	0	19.3363	19.3363	0.0
	IV	0	19.5599	19.5599	0.0
	V	11	5.4891	5.5292	0.7
	VI	0	19.3651	19.3651	0.0
1	I	32.2	1.8837	2.3454	24.5
	II	40.1	1.9595	3.0253	54.4
	III	0	6.6277	6.6277	0.0
	IV	43.1	6.8767	6.9258	0.7
	V	44.5	1.8847	2.7561	46.2
	VI	0	6.6351	6.6351	0.0
2	I	43.8	0.9343	2.2858	144.7
	II	44.9	1.0679	2.8110	163.2
	III	43.3	3.0858	3.6516	18.3
	IV	46.4	3.5615	7.0826	98.9
	V	44.1	0.9350	2.6121	179.4
	VI	40.7	3.0883	4.2862	38.8

Table 4-7. Optimization results, problem II, (α=2)

a/b	Boundary set	θ_{opt} (°)	$\lambda_{2,0^\circ}$	$\lambda_{2,opt.}$	η (%)
0.5	I	26.2	7.4761	8.6210	15.3
	II	44.1	7.7149	11.3481	47.1
	III	0	25.3193	25.3193	0.0
	IV	8.6	26.0966	26.1980	0.4
	V	31.3	7.4776	8.9011	19.0
	VI	0	25.3495	25.3495	0.0
1	I	41.3	3.5103	6.1546	75.3
	II	38.5	4.0332	11.0587	174.2
	III	0	11.2871	11.2871	0.0
	IV	24.7	12.9595	18.5344	43.0
	V	41.4	3.5116	7.6476	117.8
	VI	36.9	11.2946	13.0302	15.4
2	I	44.6	3.26560	6.1038	86.9
	II	33	4.5455	10.5626	132.4
	III	42.3	7.5380	9.8904	31.2
	IV	71.6	11.8675	20.8635	75.8
	V	43.8	3.2666	7.3904	126.2
	VI	42.4	7.5406	11.5614	53.3

4.2 Optimization of curved panels

In this section, stacking sequence optimization of axially compressed cylindrical and non-cylindrical curved panels is considered. The influences of the panel aspect ratio, stacking sequence, panel thickness, and the rotational edge restraints on the optimal panels are investigated.

The previous works on shell stability were mainly on the performance of the special shell elements formulated and the problems related to design optimization were generally not considered. Kim *et al.* (1998) have investigated the performance of a special degenerated shell element with special emphasis on curved panels under axial compression. Moita *et al.* (1996) have formulated a higher order displacement model and have presented results for the stability analysis of clamped-curved panels. Due to the existence of several shell theories, different results were given in different references for the same problems about shell stability as stated by Jaunky and Knight (1999), who assessed the accuracy of several theories for buckling of cylindrical panels. For comparison purposes, Jaunky and Knight (1999) used the nine-node quadrilateral continuum based shell element, formulated by Park and Stanley (1986), which is independent of any shell theory. Ram and Babu (2002) examined buckling of composite shells under transverse loads using geometrically non-linear finite elements, and concluded that the linear buckling analysis technique is not applicable to shell problems at all in case of transverse loading. Muc (1992) investigated the buckling of axisymmetric clamped composite shells and observed that the buckling pressures calculated by linearized buckling analysis are in error. This is due to the fact that, linearized stability analysis is valid only when the membrane forces remain constant during buckling. Considering this, in this study, optimization of curved panels under transverse loads is not considered. However, the geometrically non-linear analysis using the degenerated shell element used here is an easy and straight-forward process comparing to the other available shell elements, which is a great advantage of the element used here, Bathe (1995). Thus, the extension of the current work to include load conditions other than axial compression is possible but beyond the scope of this study at this stage. The geometrically non-linear analysis brings an extra difficulty but its use to solve the problem is tempting because of some numerical advantages. Firstly, the solution of a large eigenvalue problem is not as easy as equation solution using special numerical methods as the so called 'frontal method' which uses the hard drive. The advantages and disadvantages of several complicated numerical techniques which can be used in solving large eigenvalue problems are discussed in detail in Cook (1973). As a second advantage of the geometrically non-linear analysis is that, material non-linearity can be easily included in a geometrically non-linear analysis which is not possible in a linearized stability analysis.

The optimal design for buckling loads of composite shell structures has been studied by several authors. Mota Soares *et al.* (1995) presented a discrete model for the sensitivity analysis and optimization of thin laminated plate-shell structures and the optimal lamination angles maximizing the buckling load parameter of a two layered conical panel under uniform pressure were given. Mateus *et al.* (1997) investigated optimal designs maximizing the buckling load parameters of cylindrical and conical shells in a similar study. Hirano (1982) investigated the optimal design of cylindrical composite shells under axial compression. Nshanian (1983), Onoda (1985), Sun (1989), Zimmermann (1995), Cohen and Haftka (1989), Weaver (2000) studied the optimization of cylindrical composite shells for maximum buckling load. Messager (2002), Smerdov (2000 b), Liang *et al.* (2003), Ostwald (1990) studied optimization of composite cylindrical shells under combined loads including external pressure. Computer codes related to optimization of shells have been used by Bushnell (1986), Anderson and Strout (1979), Strout and Anderson (1981), Stein and Williams (1978), etc.

Smerdov (2000 a) studied optimal design of laminated cylindrical shells under axial compression and stated that increasing the number of layers does not result in an increase in the optimal buckling load after a certain layer number, but has the advantage of reducing the

sensitivity of design to the variations in lamination angles. Jun and Hong (1988) investigated the effects of the variations of panel width and fiber angles on buckling behavior of laminated cylindrical panels under axial compression, and observed that buckling deformations and buckling modes are greatly influenced by the change of fiber angles and buckling stress shows great variation as a result of the change in panel widths. Rao and Tripathy (1991) studied the optimization of simply supported composite cylindrical panels under axial compression and observed that use of ±45° plies significantly increases the critical buckling load comparing with the use of 0° and 90° plies. Sambandam (2003) studied the elastic buckling characteristics of laminated cross-ply elliptical cylindrical shells under axial compression. Abouhamze and Shakeri (2006) and Hu and Yang (2006) studied buckling optimization of cylindrical panels.

The optimization process can briefly be explained as the search for the best lamination angle maximizing the axial load the curved panel can bear without failure. For a given stacking sequence, pre-buckling and first-ply failure loads are calculated and minimum of these two is selected as the failure load. However, the first-ply failure load is not calculated if it is higher than the pre-buckling load as the panel will fail prematurely due to buckling before the first-ply failure load is reached. A maximum strain failure criterion is employed for optimization purposes. The panels are modelled using the eight-noded super-parametric shell element formulation of which is given in Section 2.3 and brief information on first-ply failure analysis is given in Section 2.2.4. The MATLAB code used here for optimization purposes is listed in Appendix B.

4.2.1 Problem definition

The symmetrically laminated curved panels considered in this study, a cylindrical and a non-cylindrical panel are shown in Figure 4-9, which are of length a, width b and thickness H. These two sample panel geometries are selected in order to study the effect of panel geometry. The origin of the coordinate system xyz is located at the mid-point of edge CD. The panels are constructed of eight orthotropic layers of equal thickness $H_k=H/8$ and fiber orientation θ_k where $k=1,\ldots,4$. The panels are under uniaxial compressive loading N_{yy} in the y direction. Here N_{yy} denotes the normal forces per unit length at the edge $y=-a$, and no other loads are applied to the other edges. The panel thickness to width ratio $h=H/b$ varies from 0.005 to 0.020. The results presented are obtained for panels with aspect ratios $a/b=0.5$ and $a/b=1$.

The non-dimensionalized failure load parameter N_f is defined as given below in eq. (4-5),

$$N_f = \frac{N_{\min} b^2}{H^3 E_0} \tag{4-5}$$

where, $N_{\min}$ is the dimensional failure load, and E_0 is a reference value having the dimension of Young's modulus and is taken as $E_0=1$ MPa. The failure load is defined as follows;

$$N_{\min} = \min\left(N_{cr}, N_{MS}\right) \tag{4-6}$$

where N_{cr} is the dimensional critical buckling load and N_{MS} is the dimensional first-ply failure load calculated according to the maximum strain theory defined in Section 2.2.4.

Solution of this problem analytically is not possible due to the following difficulties: The geometry of the curved panel is not always simple and the normal force distribution is not uniform because of the in-plane restraints. Considering these difficulties, FEM is selected as the computational tool for structural analysis in this study. The details of the formulation of the composite shell element used here are given in Section 2.3.1 and the linearized stability analysis of composite shells using FEM is defined in Section 2.3.1.9.

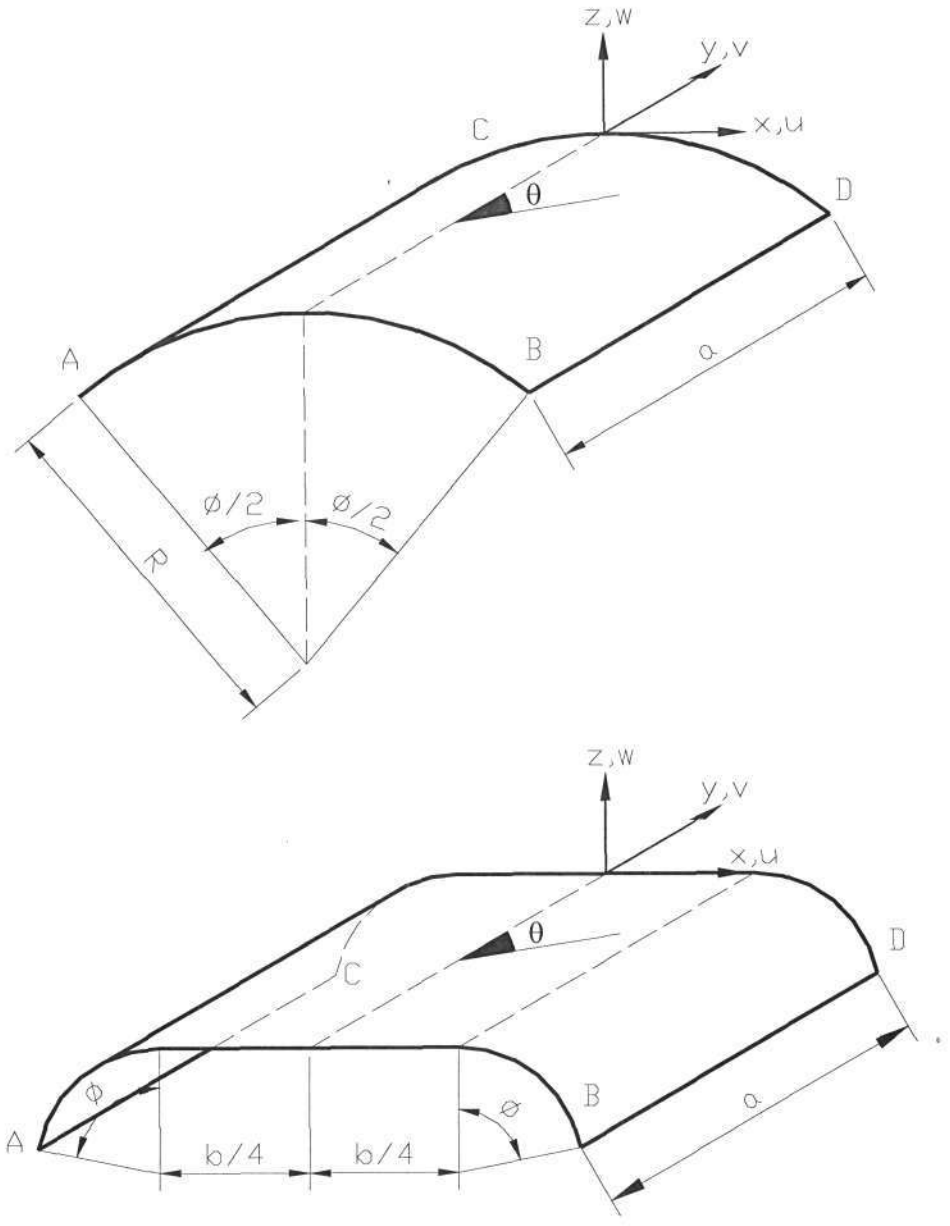

Figure 4-9 Panel geometry
a) Cylindrical panel b) Non-cylindrical panel

4.2.2 Boundary conditions

The effect of rotational boundary conditions is studied by considering three combinations of simply supported (S) and clamped (C) boundary conditions, which are tabulated in Table 4-8 given below. In particular, the following cases are studied: CCCC, SSSS, SCSC where the first, second, third, and fourth letter refers to the edges AB, BD, CD, and AC respectively. In other words, CCCC, SSSS, SCSC corresponds to all edges clamped, all edges simply supported, and straight edged clamped - curved edges simply supported cases respectively.

The curved edges are not parallel to the *xyz* coordinate system, which necessitates the use of a nodal coordinate system in order to be able to define the rotational boundary conditions. The details of the coordinate systems and transformation relations between them are given in Section 2.3.1.3. Here, $\mathbf{V}_3$ is defined as the outward unit normal to the panel mid-plane, i.e. it is in z

direction for x=0. $\mathbf{V}_2$ is selected to be in y direction. Thus, the unit vector $\mathbf{V}_1$ inside the panel boundaries can easily be obtained by vector multiplication; $\mathbf{V}_1 = \frac{\mathbf{V}_3 \times \mathbf{e}_2}{|\mathbf{V}_3 \times \mathbf{e}_2|}$. In Table 4-1, u, v, w, denote the x, y, z components of displacement on the panel mid-surface and α, and β denote the rotations about unit vectors $\mathbf{V}_2$ and $\mathbf{V}_1$, respectively. At the clamped edges α=β=0, at the simply supported curved edges α=0 and $\beta\neq$0, at the simply supported straight edges $\alpha\neq$0 and β=0. The x and z components of displacement, namely u and w, are restrained at all of the four edges. The y component of displacement, v, is restrained only at the edge CD. The in-plane boundary conditions are taken as the same for all cases.

Table 4-8. Boundary conditions for the curved panels (1: free, 0:restrained)

	(SSSS)/(CCCC)/(CSCS)			(SSSS)		(CCCC)		(CSCS)	
Edge	u	v	w	α	β	α	β	α	β
AB	0	1	0	0	1	0	0	0	1
CD	0	0	0	0	1	0	0	0	1
AC	0	1	0	1	0	0	0	0	0
BD	0	1	0	1	0	0	0	0	0

4.2.3 Optimal design problem

The objective is to maximize the non-dimensional failure load parameter N_b of the symmetrically laminated rectangular panel of total thickness H, total layer number n by optimizing the ply lamination angles, θ_i. The related problem is defined below.

Problem. Determine the ply angles $\theta_i, i = 1,2,...,n$ of a symmetric angle-ply laminate of total thickness H such that N_f will be maximized, viz.

$$\max_{\theta_i} N_f \qquad \text{such that} \qquad 0 \le \theta_i \le 90 \qquad \text{and} \qquad FI < 1 \tag{4-7}$$

where i=1,...,n, θ_i is the lamination angle of the i^{th} ply and FI denotes the failure index calculated according to the 'maximum strain' theory.

4.2.4 Numerical results

The numerical results are obtained using a 16x8 mesh, which consists of eight-noded super-parametric shell finite elements. 16 elements are used along a curved edge, an 8 along a straight edge. Depending on the experience obtained while solving the verification problems given in Section 2 of this thesis, it is decided that the mesh used is capable of appropriately modeling the structure. Note that, more elements should be used if a/b ratio is higher than 1, as the elements will be highly distorted.

Cylindrical and non-cylindrical panels with various h and stacking sequences and boundary conditions are analyzed and the failure load vs. lamination angle, θ, graphs are plotted where θ takes values between 0° and 90°. The first-ply failure loads are not calculated if they are greater than the buckling load, as the failure will be due to buckling before the first-ply failure load is reached, i.e. the strength constraint is not active. The optimization results are tabulated in Tables 4-9 to 4-20, where θ_{opt}, $N_{f,opt}$, and the corresponding failure mode are given for the pre-selected stacking sequence, h, and a/b ratio, where the best optimal results are written in bold.

The properties of the material used in calculations and the stacking sequence details are given below;

Material: $E_1 = 181\,\text{GPa}$, $E_2 = 10.3\,\text{GPa}$, $G_{12} = 7.17\,\text{GPa}$, $\nu_{12} = 0.28$.
X_T=1500 MPa, X_C=1500 MPa, Y_T=40 MPa, Y_C=246 MPa, T=68 MPa.

Stacking sequences: SS_A: $[\theta/-\theta/90°/0°]_s$ SS_B: $[\theta/-\theta/\theta/-\theta]_s$. SS_C: $[90°/0°/\theta/-\theta]_s$
SS_D: $[0°/90°/\theta/-\theta]_s$ SS_E: $[\theta/-\theta/0°/90°]_s$

The use of pre-designated stacking sequences with only one unknown (θ) gives the designer the ability to select the stacking sequence which maximizes N_f and which is the least sensitive to variations in θ. N_f vs. θ graphs for cylindrical and non-cylindrical panels are shown in Figures 4-10 to 4-21. These graphs show that some of the pre-designated stacking sequences are more sensitive to differences in θ. It is also observed that the possibility to get stuck into local optima is very high especially for cylindrical panels. Therefore, it is decided to obtain the optimal values graphically. In order to reach this goal, N_f values for all θ values are calculated, where the increment for θ is taken as 5° and $\theta \in [0°, 90°]$. This approach may increase the computational time, however, the results are reliable and it is possible to observe the state of constraints for all θ values, i.e. active or not. It is expected that, for very low h values buckling constraint will be active only, and for moderate h values buckling and strength constraints will both be active, and for very high h values strength constraint will be active only. It is also possible to calculate the real optimal values after graphically obtaining the approximate values. However, in this study, no further optimization work to calculate θ_{opt} more precisely is done as the results show the general behavior clearly. Furthermore, due to construction difficulties, it may not be feasible to make more precise calculations.

For a given θ value, first the buckling load, N_{cr}, is calculated and it is checked whether if this load causes first-ply failure according to maximum strain theory. If first-ply failure occurs, the first-ply failure load, N_{MS}, is calculated using a one dimensional optimization algorithm. The *Golden Section* method is employed here in first-ply failure load calculations, Haftka *et al.* (1990). Else, there's no need to calculate N_{MS} as the panel will fail prematurely due to buckling before the first-ply failure load is reached.

4.2.4.1 Cylindrical panels

A cylindrical panel which is under uniaxial compressive loading N_{yy} in the y direction is shown in Figure 4-9a. ϕ is taken as $\phi = \pi/4$. The failure load vs. θ graphs of cylindrical SSSS, CCCC, and CSCS panels with h=0.005, 0.010, 0.015, 0.020 and a/b=0.5 and a/b=1.0 are shown in Figures 4-10 to 4-15, where □ denotes 1st ply failure. The best stacking sequence for each h value is selected and written next to the corresponding h value.

It is observed from Figures 4-10 and 4-11 that, the trends are very similar in general for the cases a/b=0.5 and a/b=1.0 even though the N_f values are different. For all h, and at both a/b=0.5 and a/b=1.0; N_f increases with increasing θ and attains a maximum when θ=30°. There is a sharp decline in N_f for θ>30° followed by a mild increase but N_f gradually decreases for θ>60°. The buckling constraint is active for nearly all of the θ values for h=0.005 but strength constraint becomes more and more active with increasing h and finally dominates the design. At a/b=0.5, the strength constraint is active for $40° \le \theta \le 50°$, $30° \le \theta \le 60°$,

$\theta \geq 20^\circ$, and $0^\circ \leq \theta \leq 90^\circ$ and the best stacking sequences are E, E, D, C for h=0.005, 0.010, 0.015, and 0.020 respectively. At a/b=1.0, the strength constraint is active for $40^\circ \leq \theta \leq 45^\circ$, $35^\circ \leq \theta \leq 55^\circ$, $30^\circ \leq \theta \leq 55^\circ$ and $\theta \geq 5^\circ$ and the best stacking sequences are E, E, A, D for h=0.005, 0.010, 0.015, and 0.020 respectively.

It is observed from Figures 4-12 and 4-13 that, the behavior differs considerably for the cases a/b=0.5 and a/b=1.0. At a/b=0.5, the strength constraint is active for $35^\circ \leq \theta \leq 50^\circ$ and $65^\circ \leq \theta \leq 70^\circ$, $0^\circ \leq \theta \leq 90^\circ$, and $0^\circ \leq \theta \leq 90^\circ$ for h=0.010, 0.015, and 0.020 respectively and never active for h=0.005. The best stacking sequences are E, E, B, B for h=0.005, 0.010, 0.015, and 0.020 respectively. At a/b=1.0, the strength constraint is never active for h=0.005 and 0.010 and active for $\theta \geq 35^\circ$ and $0^\circ \leq \theta \leq 90^\circ$ for h=0.015 and 0.020. The best stacking sequences are E, E, E, D for h=0.005, 0.010, 0.015, and 0.020 respectively. Note that, in Figure 4-4, as the stacking sequences are different, the N_f values calculated for the case h=0.010 corresponding to θ values (approximately) higher than 30° are higher than those of h=0.015, and 0.020.

It is observed from Figures 4-14 and 4-15 that, the trends are very similar in general for the cases a/b=0.5 and a/b=1.0. At a/b=0.5, the strength constraint is active for $35^\circ \leq \theta \leq 50^\circ$, and $\theta \geq 15^\circ$, $0^\circ \leq \theta \leq 90^\circ$ for h=0.010, 0.015, and 0.020 respectively and never active for h=0.005. The best stacking sequences are E, E, D, C for h=0.005, 0.010, 0.015, and 0.020 respectively. At a/b=1.0, the strength constraint is never active for h=0.005 and active for $\theta \geq 35^\circ$ and $0^\circ \leq \theta \leq 90^\circ$ for h=0.015 and 0.020. The best stacking sequences are E, E, E, D for h=0.005, 0.010, 0.015, and 0.020 respectively.

4.2.4.2 Non-cylindrical panels

A non-cylindrical panel which is under uniaxial compressive loading N_{yy} in the y direction is shown in Figure 4-9b. ϕ is taken as $\phi = \pi/4$.

The failure load vs. θ graphs of non-cylindrical SSSS, CCCC, and CSCS panels with h=0.005, 0.010, 0.015, 0.020 and a/b=0.5 and a/b=1.0 are shown in Figures 4-8 to 4-13, where □ denotes 1st ply failure. The best stacking sequence for each h value is selected and written next to the corresponding h value.

It is observed from Figures 4-16 and 4-17 that, the behavior is similar for the cases a/b=0.5 and a/b=1.0, except for the case a/b=0.5 and h=0.020 where a significant reduction in N_f occurs for lamination angles between 30° and 55° due to the strength constraint. At a/b=0.5, the strength constraint is active for $30^\circ \leq \theta \leq 55^\circ$ for h= 0.020 and never active for the other h values. The best stacking sequences are E, E, E, A for h=0.005, 0.010, 0.015, and 0.020 respectively. At a/b=1.0, the strength constraint is active only for h=0.020 and $\theta = 45^\circ$. The best stacking sequence is E for all of the h values.

It is observed from Figures 4-18 and 4-19 that, the variations of N_f with θ are different for the cases a/b=0.5 and a/b=1.0. At a/b=0.5, the strength constraint active for $25^\circ \leq \theta \leq 65^\circ$, $0^\circ \leq \theta \leq 75^\circ$, and $0^\circ \leq \theta \leq 90^\circ$ for h=0.010, 0.015, and 0.020 respectively and never active for h=0.005. The best stacking sequences are B, B, B, D for h=0.005, 0.010, 0.015, and 0.020 respectively. At a/b=1.0, the strength constraint is active only for h=0.020 and $45^\circ \leq \theta \leq 90^\circ$. The best stacking sequences are E, D, D, D for h=0.005, 0.010, 0.015, and 0.020 respectively.

It is observed from Figures 4-20 and 4-21 that, like the SSSS panels, the behavior is similar for the cases a/b=0.5 and a/b=1.0, except for the case a/b=0.5 and h=0.020. At a/b=0.5, the strength constraint is active for $30^\circ \le \theta \le 75^\circ$ for h= 0.020 and never active for the other h values. At a/b=1.0, the strength constraint is active only for h=0.020 and $45^\circ \le \theta \le 50^\circ$. The best stacking sequence is E for all a/b ratios and h values.

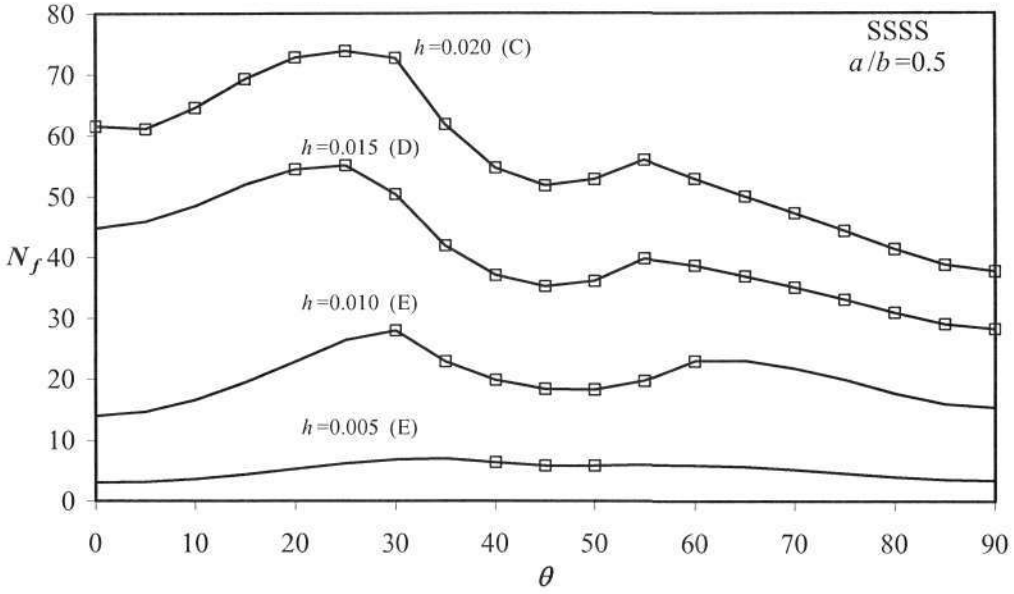

Figure 4-10. Failure load vs. θ for cylindrical panel, SSSS, and a/b=0.5

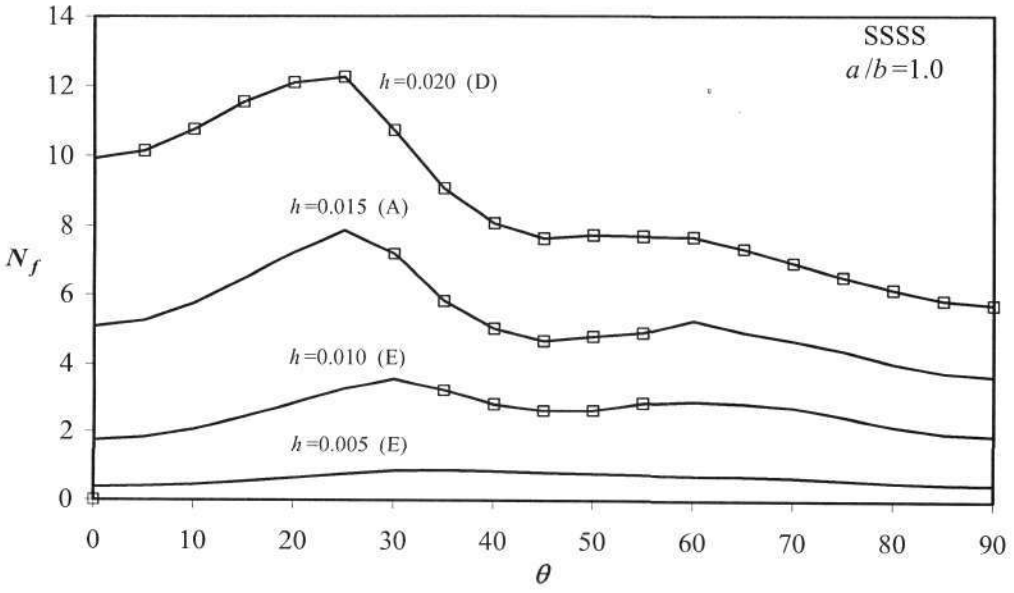

Figure 4-11. Failure load vs. θ for cylindrical panel, SSSS, and a/b=1.0

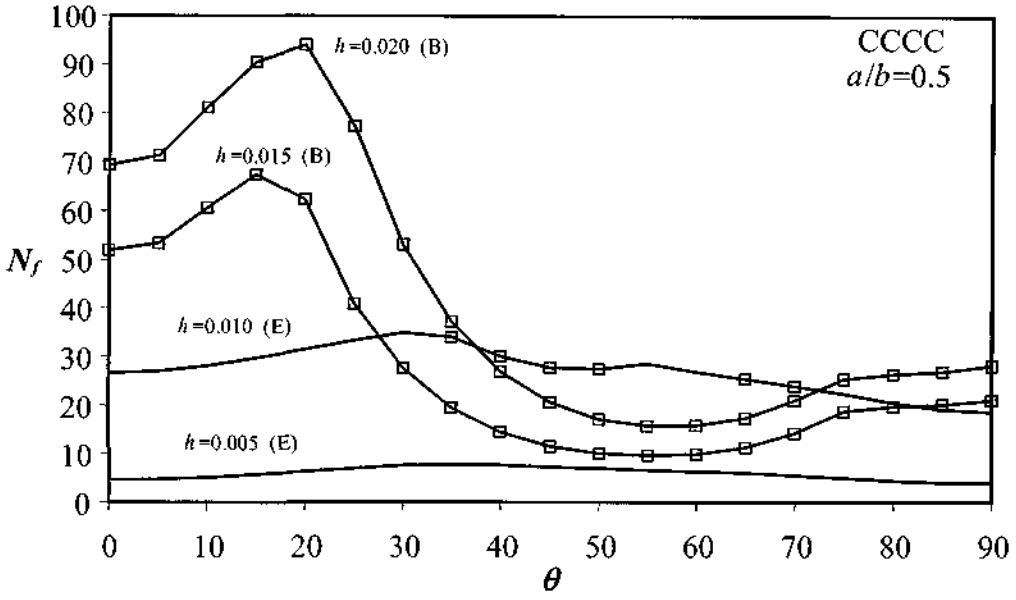

Figure 4-12. Failure load vs. θ for cylindrical panel, CCCC, and a/b=0.5

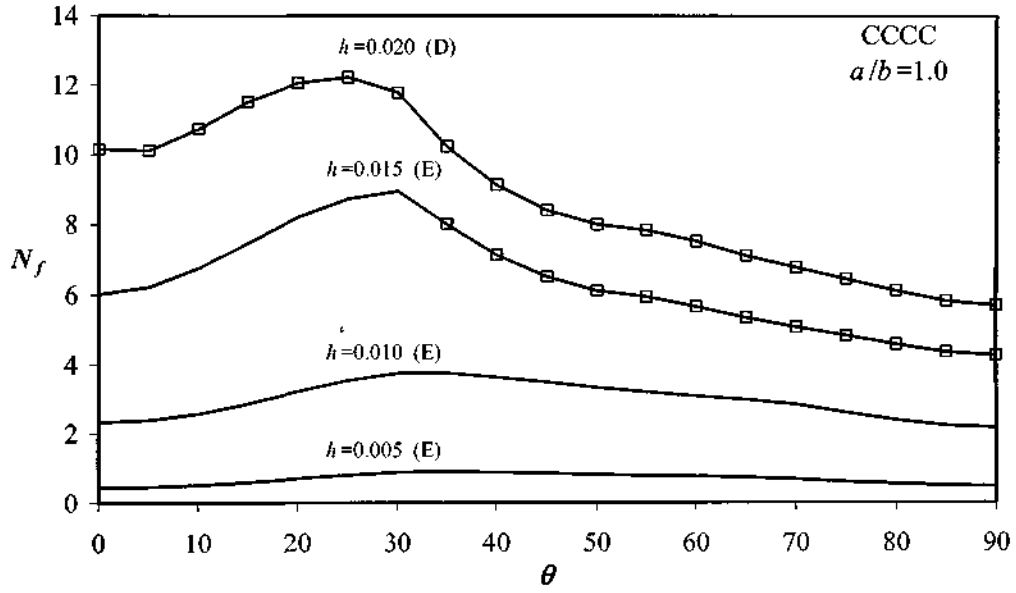

Figure 4-13. Failure load vs. θ for cylindrical panel, CCCC, and a/b=1.0

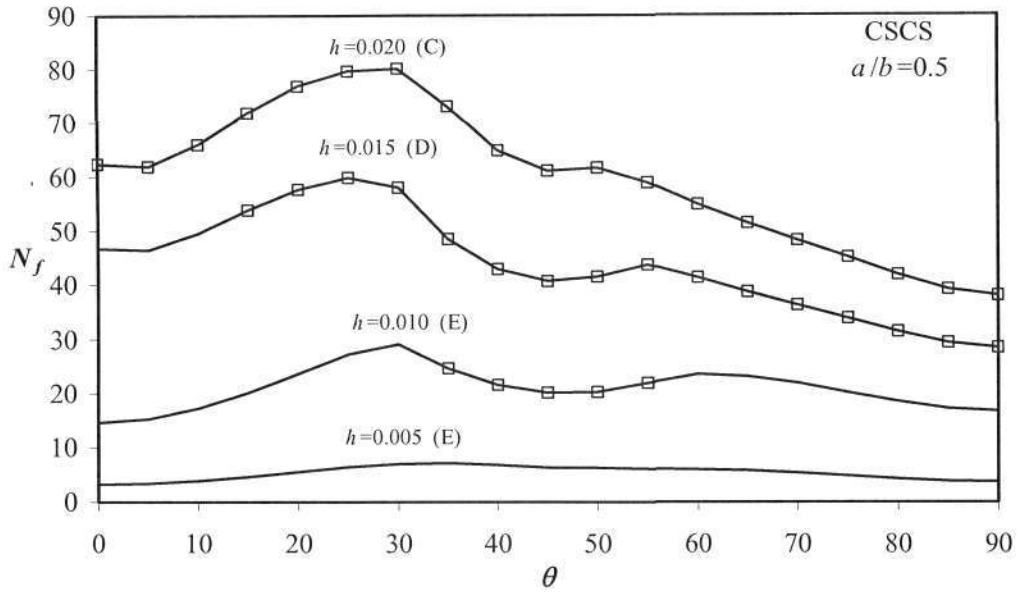

Figure 4-14. Failure load vs. θ for cylindrical panel, CSCS, and a/b=0.5

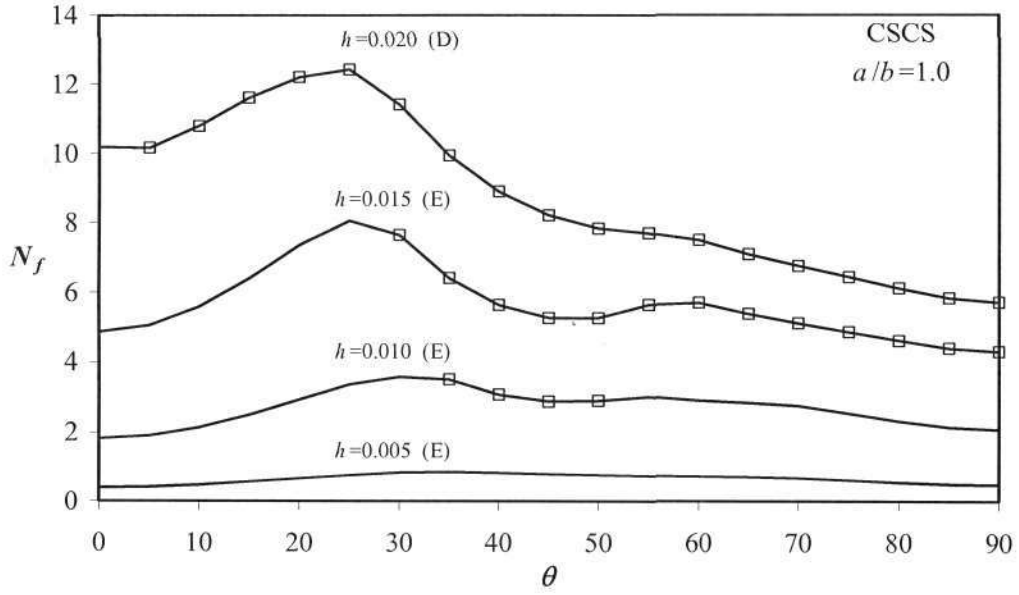

Figure 4-15. Failure load vs. θ for cylindrical panel, CSCS, and a/b=1.0

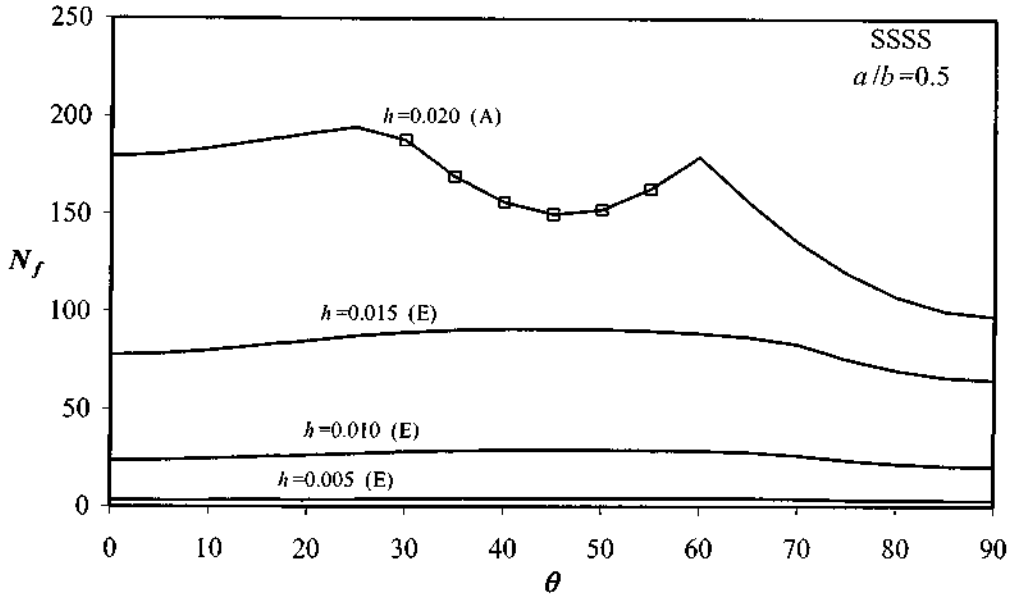

Figure 4-16. Failure load vs. θ for non-cylindrical panel, SSSS, and a/b=0.5

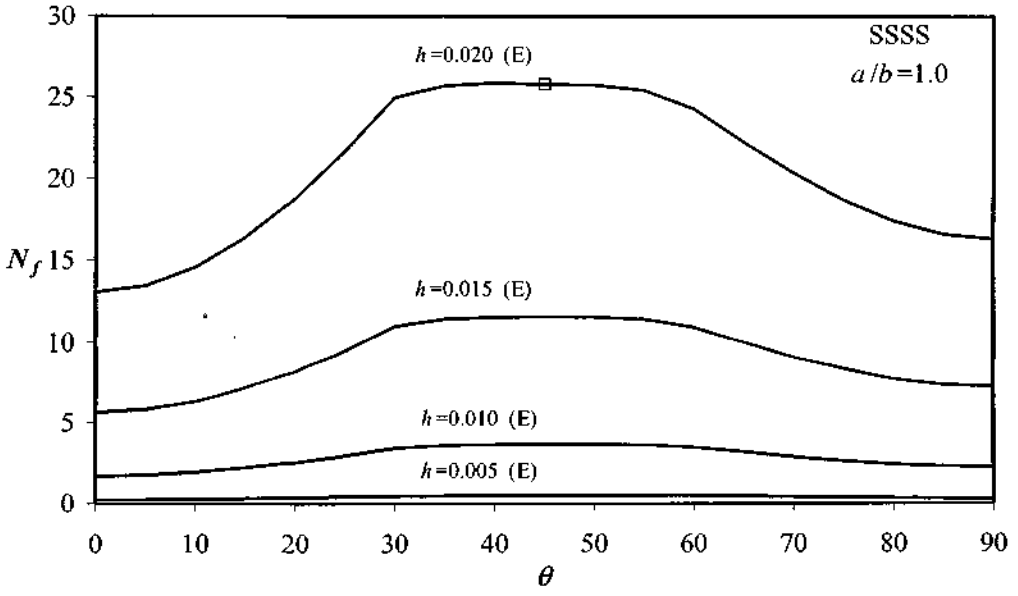

Figure 4-17. Failure load vs. θ for non-cylindrical panel, SSSS, and a/b=1.0

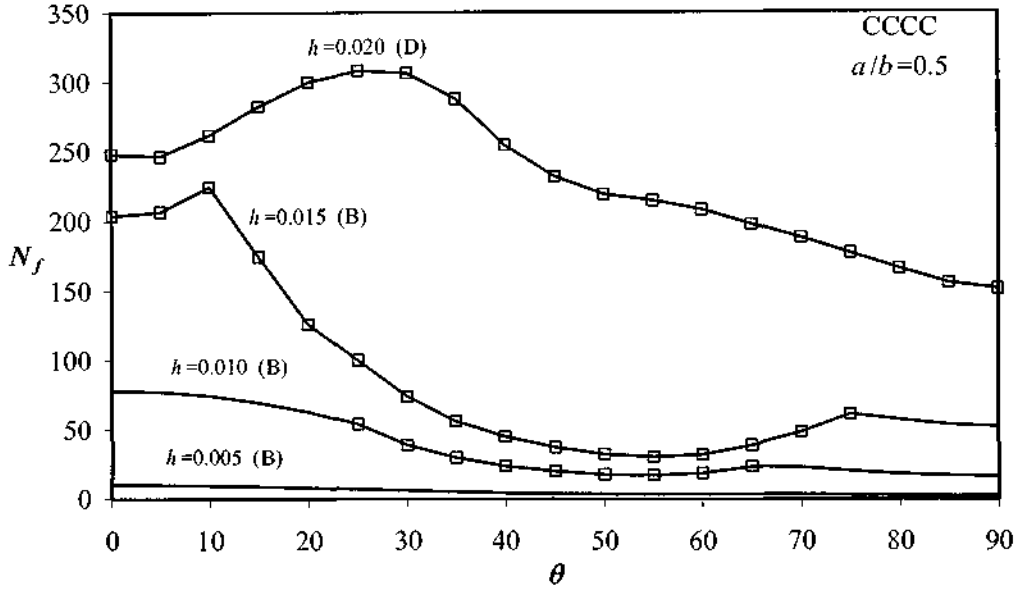

Figure 4-18. Failure load vs. θ for non-cylindrical panel, CCCC, and a/b=0.5

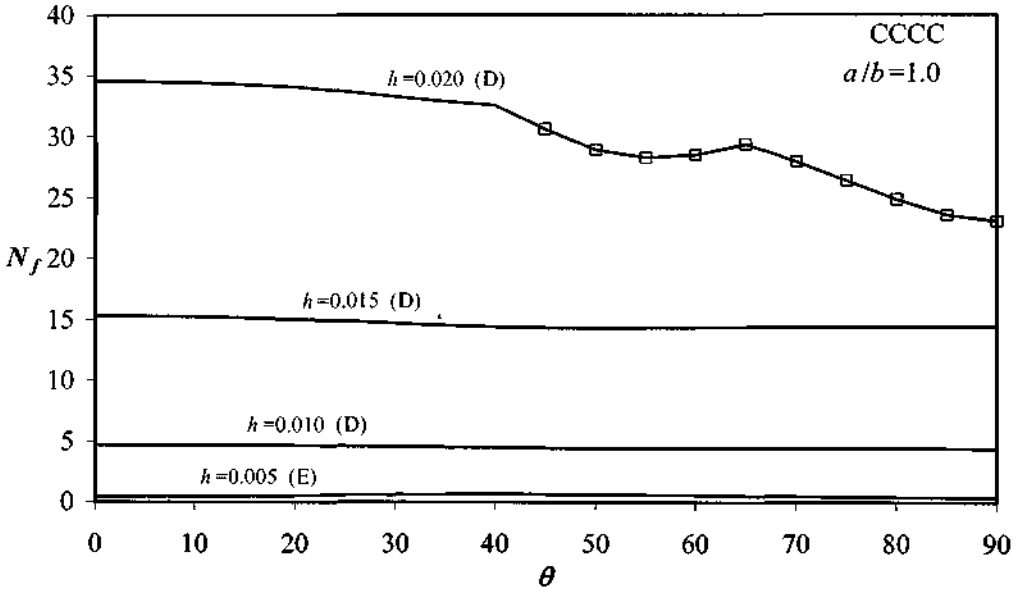

Figure 4-19. Failure load vs. θ for non-cylindrical panel, CCCC, and a/b=1.0

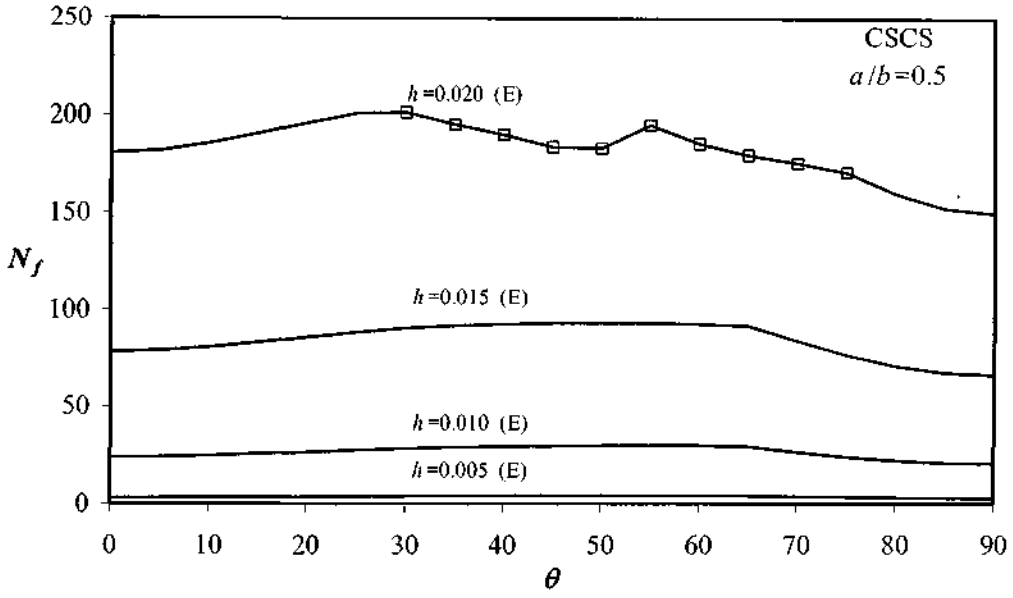

Figure 4-20. Failure load vs. θ for non-cylindrical panel, CSCS, and a/b=0.5

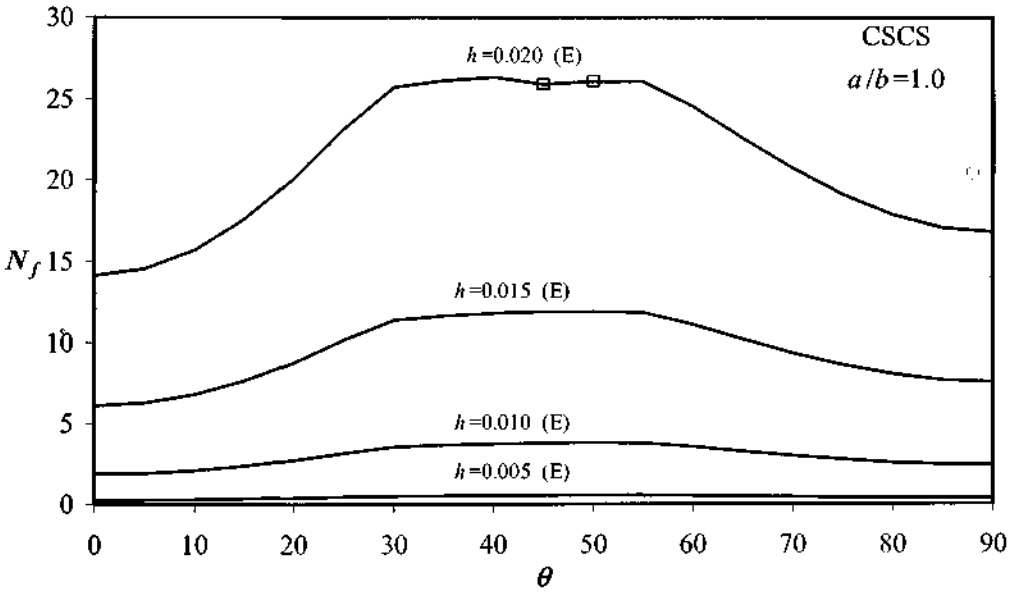

Figure 4-21. Failure load vs. θ for non-cylindrical panel, CSCS, and a/b=1.0

Table 4-9. Optimization results, cylindrical panels, SSSS

		a/b=0.5			a/b=1.0		
h	Stacking sequence	θ_{opt}	$N_{f,opt}$	Failure Mode*	θ_{opt}	$N_{f,opt}$	Failure Mode*
0.020	A	20	67.951	S	20	8.494	S
	B	15	62.521	B	15	7764	S
	C	**25**	**73.848**	S	25	11.208	B
	D	25	73.487	S	**25**	**12.245**	S
	E	25	67.448	S	25	11.028	S
0.015	A	20	51.208	S	**25**	**7.865**	B
	B	15	34.957	B	15	4.354	B
	C	25	50.558	B	30	6.306	B
	D	**25**	**55.142**	B	30	7.185	S
	E	25	50.769	S	25	7.809	B
0.010	A	30	26.521	B	30	3.323	B
	B	15	16.248	B	15	1.939	B
	C	60	23.910	S	60	3.030	B
	D	30	26.132	B	60	3.293	B
	E	**30**	**27.952**	S	**30**	**3.548**	B
0.005	A	35	6.348	B	35	0.793	B
	B	15	3.889	B	75	0.486	B
	C	55	5.927	B	55	0.773	B
	D	55	6.408	B	45	0.817	B
	E	**35**	**7.034**	B	**35**	**0.871**	B

* B and S denote failure due to buckling and first-ply failure, respectively

Table 4-10. Optimization results, non-cylindrical panels, SSSS

		a/b=0.5			a/b=1.0		
h	Stacking sequence	θ_{opt}	$N_{f,opt}$	Failure Mode*	θ_{opt}	$N_{f,opt}$	Failure Mode*
0.020	A	**25**	**194.443**	B	40	25.111	B
	B	10	176.695	B	20	15.080	B
	C	70	176.475	B	75	22.079	B
	D	10	178.848	B	70	22.537	B
	E	20	193.823	B	**40**	**25.885**	B
0.015	A	45	88.687	B	45	11.292	B
	B	15	77.097	B	25	7.282	B
	C	75	78.589	B	70	9.802	B
	D	75	79.018	B	65	9.871	B
	E	**45**	**90.771**	B	**45**	**11.584**	B
0.010	A	50	28.556	B	45	3.624	B
	B	15	23.806	B	35	2.738	B
	C	65	24.876	B	60	3.114	B
	D	70	24.687	B	60	3.094	B
	E	**45**	**29.002**	B	**45**	**3.693**	B
0.005	A	50	4.174	B	45	0.524	B
	B	20	3.143	B	50	0.425	B
	C	60	3.649	B	35	0.455	B
	D	65	3.490	B	60	0.437	B
	E	**55**	**4.182**	B	**50**	**0.530**	B

* B and S denote failure due to buckling and first-ply failure, respectively

Table 4-11. Optimization results, cylindrical panels, CCCC

		a/b=0.5			a/b=1.0		
h	Stacking sequence	θ_{opt}	$N_{f,opt}$	Failure Mode*	θ_{opt}	$N_{f,opt}$	Failure Mode*
0.020	A	30	78.856	S	25	12.148	S
	B	**20**	**94.020**	S	15	10.702	B
	C	30	80.255	S	25	12.189	S
	D	30	80.423	S	**25**	**12.213**	S
	E	30	79.119	S	25	12.153	S
0.015	A	30	59.043	S	30	8.030	B
	B	**15**	**67.408**	S	15	5.504	B
	C	30	60.135	S	35	7.059	B
	D	30	60.225	S	30	8.300	B
	E	30	59.325	S	**30**	**8.954**	B
0.010	A	30	31.858	B	30	3.369	B
	B	15	25.151	B	20	2.322	B
	C	55	28.921	S	60	3.234	B
	D	35	33.732	B	50	3.701	B
	E	**30**	**34.941**	B	**35**	**3.760**	B
0.005	A	30	6.817	B	35	0.810	B
	B	20	5.229	B	20	0.525	B
	C	55	6.435	B	55	0.800	B
	D	50	7.390	B	45	0.858	B
	E	**35**	**7.804**	B	**35**	**0.911**	B

* B and S denote failure due to buckling and first-ply failure, respectively

Table 4-12. Optimization results, non-cylindrical panels, CCCC

		a/b=0.5			a/b=1.0		
h	Stacking sequence	θ_{opt}	$N_{f,opt}$	Failure Mode*	θ_{opt}	$N_{f,opt}$	Failure Mode*
0.020	A	25	288.290	S	30	32.909	B
	B	10	300.071	S	0	24.397	B
	C	25	305.373	S	0	28.530	B
	D	**25**	**307.753**	S	**0**	**34.529**	B
	E	20	286.109	S	40	33.134	B
0.015	A	15	207.795	S	30	14.720	B
	B	**10**	**224.265**	S	5	10.620	B
	C	0	154.362	B	0	12.728	B
	D	15	200.785	B	**0**	**15.309**	B
	E	20	216.333	S	40	14.825	B
0.010	A	0	73.230	B	30	4.622	B
	B	**0**	**78.271**	B	40	3.303	S
	C	0	47.930	B	0	3.982	B
	D	0	63.392	B	**0**	**4.709**	B
	E	0	77.999	B	40	4.671	B
0.005	A	0	9.514	B	30	0.630	B
	B	**0**	**10.146**	B	40	0.487	B
	C	0	6.312	B	15	0.538	B
	D	0	8.258	B	10	0.621	B
	E	0	10.119	B	**40**	**0.639**	B

* B and S denote failure due to buckling and first-ply failure, respectively

Table 4-13. Optimization results, cylindrical panels, CSCS

		a/b=0.5			a/b=1.0		
h	Stacking sequence	θ_{opt}	$N_{f,opt}$	Failure Mode*	θ_{opt}	$N_{f,opt}$	Failure Mode*
0.020	A	30	77.481	S	25	12.403	S
	B	15	63.306	B	15	7.913	B
	C	**30**	**80.075**	S	30	11.515	S
	D	30	79.975	S	**25**	**12.420**	S
	E	25	72.555	S	25	11.385	S
0.015	A	25	58.434	S	25	7.506	B
	B	15	35.095	B	15	4.387	B
	C	30	51.764	B	35	6.467	B
	D	**25**	**59.835**	S	30	7.448	B
	E	25	54.895	S	**25**	**8.057**	B
0.010	A	30	26.849	B	30	3.245	B
	B	15	15.619	B	15	1.952	B
	C	60	25.629	B	60	3.111	B
	D	60	27.068	S	55	3.461	S
	E	**30**	**29.082**	B	**30**	**3.573**	B
0.005	A	35	6.369	B	30	0.793	B
	B	75	3.912	B	75	0.489	B
	C	55	6.015	B	55	0.786	B
	D	50	6.588	B	50	0.834	B
	E	**35**	**7.052**	B	**35**	**0.873**	B

* B and S denote failure due to buckling and first-ply failure, respectively

Table 4-14. Optimization results, non-cylindrical panels, CSCS, CSCS

		a/b=0.5			a/b=1.0		
h	Stacking sequence	θ_{opt}	$N_{f,opt}$	Failure Mode*	θ_{opt}	$N_{f,opt}$	Failure Mode*
0.020	A	35	201.024	B	40	25.598	B
	B	10	177.407	B	20	15.548	B
	C	70	184.551	B	75	23.112	B
	D	70	187.079	B	80	23.544	B
	E	**30**	**201.416**	S	**40**	**26.362**	B
0.015	A	50	91.572	B	45	11.643	B
	B	15	77.425	B	25	7.578	B
	C	90	84.453	B	65	10.349	B
	D	85	83.217	B	80	10.349	B
	E	**50**	**93.32**	B	**50**	**11.914**	B
0.010	A	55	29.526	B	45	3.734	B
	B	15	23.858	B	35	2.812	S
	C	75	26.682	B	55	3.270	B
	D	75	25.734	B	70	3.208	B
	E	**55**	**29.833**	B	**50**	**3.798**	B
0.005	A	50	4.199	B	45	0.527	B
	B	20	3.146	B	50	0.430	B
	C	65	3.722	B	35	0.460	B
	D	70	3.509	B	60	0.439	B
	E	**55**	**4.211**	B	**50**	**0.533**	B

* B and S denote failure due to buckling and first-ply failure, respectively

4.2.4.3 Discussion of optimization results for curved panels

Obviously, as the number of free degrees of freedom increases, the buckling load decreases. Therefore, CCCC panels have the highest and SSSS panels have the lowest buckling loads.

For both cylindrical and non-cylindrical panels, and for both a/b=0.5 and a/b=1, there's small difference between the $N_{f,opt}$ values and the corresponding angles for boundary conditions SSSS and CSCS. The $N_{f,opt}$ values increase drastically for the case where all of the edges are restrained against rotation (CCCC). The optimal lamination angles differ substantially for different stacking sequences even for the same boundary condition, t, and a/b ratio. The influence of (rotational) boundary conditions on optimization results decrease with decreasing h.

The differences between the $N_{f,opt}$ values corresponding to the cases a/b=0.5, and a/b=1 and boundary conditions SSSS and CSCS are minor for all of the h values. However, $N_{f,opt}$ values of CCCC panels are higher than those of SSSS and CSCS panels, especially for higher h values.

Cylindrical panels:

The optimization of cylindrical panels is studied first. The optimization results are tabulated in Tables 4-2, 4-4, and 4-6 for the boundary conditions SSSS, CCCC, and CSCS respectively and the following deductions are reached:

For all h, θ_{opt} values are generally low, due to the direction of the load.

For both h=0.005 and h=0.010, the best stacking sequence is E, and the optimal lamination angles are 35° and 30° for these cases, respectively. This result shows that θ_{opt} value and the best stacking sequence design don't considerably change for h=0.010. As expected, the failure is due to buckling for these cases.

For h=0.015, most of the optimal designs are based on buckling. However, it seems that there's a transition thickness which determines the mode of failure. This transition thickness (or h value) is higher at a/b=1.0, comparing to the one at a/b=0.5. This result shows that panels become more susceptible to buckling with increasing a/b ratio, and to first-ply failure with decreasing a/b ratio. For this special case, stacking sequence never gave the best design.

For h=0.020, all of the optimal designs are based on f.p.f., or in other words, the buckling constraint is never active for the optimal layouts. It is interesting to note that, the influence of boundary conditions increase with increasing a/b ratio as well as increasing h. At a/b=0.5, stacking sequences B and C, and at a/b=1.0, stacking sequences C and D resulted in the best optimization results, where the corresponding θ_{opt} values vary between 20° and 30°.

Non- Cylindrical panels:

Next, the optimization of non-cylindrical panels is studied. The optimization results are tabulated in Tables 4-3, 4-5, and 4-7 for the boundary conditions SSSS, CCCC, and CSCS respectively. The following deductions are reached.

At a/b=1.0 and for all h values and for the boundary conditions considered, optimization is dominated by buckling. This shows that, the transition thickness is higher for non-cylindrical panels comparing to the cylindrical counterparts. This is an important outcome of the study, as

for this case, the extra calculations related to first-ply failure analysis are not necessary for high a/b values.

As observed for the cylindrical panels, the influence of boundary conditions on optimization results increase with increasing h. Moreover, if the design is based on first-ply failure, then this influence is higher. It is also observed that the influence of boundary conditions is higher comparing to the cylindrical panels, which is due to the more complex shape of the curved edge.

Comparison of the results given in Tables 4-3 and 4-7 show that θ_{opt} and $N_{f,opt}$ values are very close at a/b=0.5 and at a/b=1.0 for h values lower than 0.020. However, comparison of these tables with Table 4-5, where results for CCCC panels are tabulated, show that $N_{f,opt}$ values extremely increase (up to more than 100%) when the curved edges are clamped. Considering this result, it may be stated that, the use of stiffeners to decrease a/b ratio is more feasible for thicker panels.

For SSSS and CSCS panels, failure is found out to be due to buckling for all h and a/b values. However, the behavior of CCCC panels is different; at a/b=1.0, failure is due to buckling for all h values but at a/b=0.5, there's a transition thickness as observed in cylindrical panels, and the design is dominated by first-ply failure for h=0.020.

For h=0.005, all of the optimal designs are based on buckling. For SSSS and CSCS panels with h=0.005, the best stacking sequence is E, and the optimal lamination angles at a/b=0.5 and at a/b=1.0 are 55° and 50°, respectively. For CCCC panels with h=0.005, the best stacking sequence is B and the corresponding θ_{opt}=0° and similarly for all of the stacking sequences θ_{opt}=0°.

For h=0.010, again, the first-ply failure constraint is never active. For SSSS panels, the best stacking sequence is E, and θ_{opt}=45° at both a/b=0.5 and 1.0. Stacking sequence E is again the best for the CSCS case, however, the optimal lamination angles at a/b=0.5 and a/b=1.0 are 55° and 50°, respectively. For the CCCC panels, the best stacking sequence is B at a/b=0.5 and D at a/b=1.0 and the corresponding θ_{opt} values are 0° and 40°. There's negligible difference between the $N_{f,opt}$ values of SSSS and CSCS panels as observed for the case h=0.005. However, the $N_{f,opt}$ values of CCCC panels are extremely higher than those of SSSS and CSCS panels especially for low h values and for higher h values this behavior diminishes as for high h values failure is generally due to first-ply failure.

For h=0.015, the strength constraint is never active for boundary conditions SSSS and CSCS θ_{opt}=50° at a/b=0.5, and a/b=1.0 and E is the best stacking sequence. For CCCC panels, strength constraint is active for stacking sequences A, E, and E at a/b=0.5 and not active at a/b=1.0. Stacking sequences B and D are the best, and θ_{opt}=10°, 0° at a/b=0.5 and a/b=1.0 respectively.

For h=0.020, For SSSS panels, A and E are the best stacking sequences and θ_{opt} values are 25° and 40°at a/b=0.5 and a/b=1.0 respectively. For CSCS panels, E is the best stacking sequence with θ_{opt}=30°, 40° at a/b=0.5 and a/b=1.0 respectively. For CCCC panels, D is the best stacking sequence with θ_{opt}=325°, 0° at a/b=0.5 and a/b=1.0 respectively. The strength constraint is active for CCCC and CSCS panels at a/b=0.5.

4.3 Conclusions

4.3.1 Rectangular plates

Optimum thickness and lamination angle designs of rectangular plates were given with the objective of maximizing the buckling load. The results presented were obtained for rectangular plates with three different aspect ratios, six different combinations of boundary conditions implemented at the four edges of the plate, three different α values, and two design problems. Analytical results based on the assumption that the in-plane forces are constant through the length results in erroneous results when the in-plane restraints exist. Thus, FEM was used to calculate the buckling loads as it is not possible to solve these problems analytically due to the complicating factors arising from the influence of boundary conditions. The influence of thickness, i.e. the contribution of shear deformation was not examined here by taking the a/H ratio equal to 100.

Optimization results show that, as would be expected, the buckling loads are higher for clamped plates compared with simply supported plates and the presence of in-plane restraints cause an increase in buckling load and in general, efficiency increases as a/b and α increase. Buckling load decreases drastically with increasing a/b ratio at a/b ratios between 0.5 and 1.0. However, for all of the cases, the difference between the buckling loads calculated at a/b=1.0 and a/b=2.0 were very small. This phenomenal behaviour should be kept in mind while interpreting the optimization results. It was found that, the influence of rotational restraints on optimization is higher than the influence of in-plane restraints. However, especially at high aspect ratios (a/b), in-plane restraints have a strong effect on the results and this effect is more pronounced for simply supported plates. It was observed that, the influence of in-plane restraints was higher for plates with high a/b ratios. Also the behavior of angle-ply and cross-ply laminates considerably differs.

It may be stated that, optimization without considering the in-plane restraints yields a conservative design especially for high a/b ratios.

Composite ply thicknesses in a laminate are fixed and also, manufacturing considerations make it desirable to limit the ply orientations to a set of integer values. Thus, the continuous designs should be rounded-off to the nearest discrete valued designs, which brings an additional difficulty. Gürdal et al (1999) suggest the use of genetic algorithms, which are powerful tools for discrete valued optimization problems, and therefore ideally suited for the design of laminated composite structures.

There is an additional level of complication that is due to the rotational boundary conditions. Here, it was assumed that the edges are either simply supported or clamped; however, in practice these assumptions do not always hold. Thus, the presence of elastic rotational restraints should also be investigated. Implementation of a failure criteria may result in different conclusions, so this issue should also be investigated.

4.3.2 Curved panels

Optimum lamination angle designs of cylindrical and non-cylindrical panels under uni-axial compressive in-plane loads were given with the objective of maximizing the failure load which was defined as the minimum of the buckling and the first-ply failure loads. An eight-node degenerated shell element was employed for the buckling and stress analysis which includes the effect of shear deformation. The parameters affecting the optimal design include the aspect ratio and the boundary conditions.

The use of shear deformable theory is important for the present study due to the effect of laminate thickness on the optimal lamination angles. The influence of shear deformation becomes more important while the thickness increases. If the panel to be optimized is very thick, the use of a higher order theory may be required, as the first-ply failure load will have to be calculated more precisely. However, it should be kept in mind that the formulation of a shell element based on a higher order deformation theory should be accompanied with the formulation of a compatible stiffener element to be able to model stiffened panels.

For thick panels failure was found out to be due to first-ply failure rather than buckling. However, for thin panels, buckling was the dominant failure mode. It was shown that there's a transition thickness between buckling-dominant behavior and first-ply failure-dominant behavior. This means that exclusion of a first-ply failure analysis may lead to wrong results for moderately thick and especially for thick panels.

It was observed that, there is negligible difference between the boundary conditions SSSS and CSCS or between the all edges simply supported case and the straight edges clamped, and curved edges simply supported case. However, the optimal buckling load increases drastically for the case where the curved edges were restrained against rotation (CCCC panels). Note that, for stiffened panels, the rotational restraint at an edge is proportional to the torsional stiffness of the stiffener at the edge. Thus, under uni-axial loads, the torsional stiffness of the stiffeners attached to the curved edges is an extremely important design consideration, comparing to those of longitudinal stiffeners.

The pre-selected stacking sequences with only one unknown angle are most probably not the best designs. However, due to construction difficulties they may be better (or feasible) designs than real optimal designs. Also, when there's one unknown, it is easier to understand the problem and to have a general opinion on the problem as the optimization will be relatively fast.

The greatest obstacle was the computational time required due to the numerical method used. Considering this, it can be stated that, the use of a very fine finite element mesh should be avoided at the initial stages of optimization, and the final design should be checked by using a finer mesh. However, use of a finer mesh may be inevitable due to stress concentrations around the holes inside the panel and/or at the corners of the panel which may cause premature first-ply failure. Considering this, the engineer may initially ignore the ply failure at some of the nodes during optimization and decrease the stress levels at the problematic points by locally increasing the thickness.

It was shown that the geometry of the panel has a profound effect especially if the thickness is high. Considering this, it may be more profitable to optimize the panel geometry, instead of optimizing the stacking sequence (if possible).

5. CONCLUSIONS

The formulations of the Hermite beam, iso-parametric plate, and super-parametric shell elements which are used in modeling the optimization problems considered here were given. Several verification problems were solved which not only verify the computer codes used but also give valuable information on the accuracy of the elements. The related functions are listed in the Appendix section.

The first optimization problem considered here was the strongest column problem. Optimal cross-sectional shapes of elastically restrained columns under distributed and concentrated axial loads were given. Unimodal and bimodal optimality conditions related to the problems defined were derived and an iterative computational solution based on finite element method has been developed. The results obtained using the iterational procedure were compared with the results available in the literature and it was shown that the iterative technique defined here is very accurate. The efficiencies calculated were higher for higher values of n and the spring constants.

The iterative solution starts with the unimodal optimality condition and the bimodal optimality condition is used only when the buckling load corresponding to the second mode is greater than the buckling load corresponding to the first mode. This approach considerably reduces the computational time as it is easier to obtain the area distribution using the unimodal optimality condition. It was found that there exists a certain value for the minimum area constraint which determines whether if the solution is unimodal or bimodal. The resulting columns were bimodal for a_0 values less than, and unimodal for a_0 values greater than this certain value, which depends on the boundary conditions. Also, this a_0 value increases with increasing n, but decreases with decreasing spring constant.

It was stated by Frauenthal (1972) that, for columns under concentrated loads only, the constraint on maximum allowable stress is equivalent to a constraint on the minimum allowable area. However, this is not the case for columns under distributed compressive loads. Considering this, a constraint is placed upon the maximum allowable stress, which leads to different minimum areas along the column length. It was shown that, unlike the minimum area constraint, the stress constraint leads to the correct minimum thickness to carry the maximum load. Also, the maximum stress constraint is of more practical value in a structural optimization problem because the maximum buckling load can only be determined after the optimal shape of the column is obtained.

Next, optimal design of laminated composite plates and curved panels were considered. Optimum thickness and lamination angle designs of rectangular plates were given with the objective of maximizing the buckling load. The a/H ratio was taken equal to 100 in order to minimize the contribution of shear deformation. Also, the first-ply failure loads were not calculated, as the plate was assumed to fail due to buckling only. Before proceeding with optimization the graphs showing the normal force distributions were obtained, which clearly indicate the influence of the in-plane restraints. It was shown that, the normal force distributions were not uniform inside the plate boundaries mainly due to the presence of in-plane restraints. This was the reason of using FEM to calculate the buckling loads. The influence of the in-plane restraints on optimization was investigated and it was found that, optimization without considering the in-plane restraints yields wrong results and a conservative design. The influence of rotational restraints on optimization was higher than the influence of in-plane restraints for low aspect ratios. However, it was observed that, the influence of in-plane restraints increase with increasing aspect ratio. Both thickness and lamination angle optimization were considered and the related problems were defined.

The optimization results revealed the fact that, the two optimization problems defined yield considerably different optimal loads. Different load conditions were also examined by defining

the axial load distribution using a constant α, where $\alpha = 2$, $\alpha < 2$, and $\alpha > 2$ corresponds to pure bending, a combination of bending and compression, and a combination of bending and tension respectively. The cases α=0, α=1, and α=2 were examined seperately, and it was shown that the value of α has a strong effect on optimization.

Optimum lamination angle designs of cylindrical and non-cylindrical panels under uniaxial loads were given with the objective of maximizing the failure load which was defined as the minimum of the buckling and the first-ply failure loads. The results presented were obtained for panels with aspect ratios a/b=0.5 and a/b=1 and thickness to width ratios h=H/b varying from 0.005 to 0.020. FEM was selected as the computational tool due to the difficulties related to the complex geometry of the non-cylindrical panels and the presence of in-plane restraints. The panels were modelled using the eight-noded super-parametric shell elements and the pre-buckling and first-ply failure loads were calculated for pre-selected stacking sequences with one unknown lamination angle. A maximum strain failure criterion was employed to calculate the first-ply failure loads.

It was observed from the N_f vs. θ graphs that, some of the pre-designated stacking sequences were more sensitive to differences in θ. As was expected, for very low h values only the buckling constraint was active, and for moderate h values both buckling and strength constraints were active, and for very high h values only the strength constraint was active. It was concluded that, stability analysis and first-ply failure analysis are more important, for thin and thick panels, respectively.

Three different boundary conditions were considered. The optimization results showed that, the all edges simply supported case and the straight edges clamped, and curved edges simply supported case yield very similar results. However, the optimal failure loads obtained for the all edges clamped case were considerably higher than those for the all edges simply supported case.

6. FUTURE RESEARCH

In this study, the buckling loads were calculated by employing linearized stability analysis. However, the assumptions made in linearized stability analysis are not always valid and as a result, in most of the applications, a geometrically non-linear analysis is sought which may take a long time and also prone to errors. Also, the software used for analysis must be capable of tracking jumping from one buckling mode to another while increasing the load. Considering these issues, it can be stated that a linearized stability analysis is necessary, especially at the early stages of design.

Several researchers have tried to solve the strongest column problem analytically or by employing numerical techniques for different support and loading conditions. However, the influences of shear deformation and axial shortening have never been considered, even for the discrete optimization approaches. The contribution of shear deformation becomes very important especially when the column length is small, as stated by Banarjee and Williams (1994). Also, it was stated by Ziegler (1982) that, the effect of axial shortening on buckling load may be comparable in magnitude to that of the shear deformation. Also, optimal design of frames against buckling is a problem of great significance. These issues should be addressed in the future studies.

Skew fiber reinforced composite plates are extensively used in ship and aircraft industry, and several researchers have investigated the stability of these plates. However, the influence of in-plane restraints on stability of optimal skew plates was not considered in the previous studies. The computer code given here, which was used to calculate the buckling loads of rectangular plates, is capable of calculating the buckling loads of skew plates. Thus, skew plates may be analyzed using the same computer code.

Higher order theories may be used to model laminated composites, however, compatible stiffener elements should also be formulated. Formulation of a compatible stiffener element, which can be used in conjunction with the shell element used in this study was given by Ferguson and Clark (1979). The geometry of the element results from the degeneration of a 3D iso-parametric element. Using the offset property of this element, laminated beams can also be modelled by grouping elements sharing the same degrees of freedom.

It is well known that stiffeners extremely increase the initial buckling loads of plates with a very small increase in total weight. However, problems like pillowing of the plate, stress concentrations next to the stiffeners, etc. should be considered. To solve these problems, functionally graded materials may be used, which, unlike the fiber-reinforced composite materials, lack the advantages of directional strength. However, the granular material can be concentrated at places where the stresses are higher, or where they are needed. Finite element modeling of structures made of FGM is a straight forward application and the computer codes used in this study may be used after minor modifications.

Genetic algorithms (GA), developed by Holland (1975), can be applied to optimal structural design. However, as the stability analysis of structures is time consuming, implementation of GA was not considered in this study, even for the column problems.

The sub-structuring methods are often the best and sometimes the only strategy for the analysis of complex structures. Thus, sub-structuring can be used to decrease the time needed for optimization.

REFERENCES

[1] M. Abouhamze, M. Shakeri, 'Multi-objective stacking sequence optimization of laminated cylindrical panels using a genetic algorithm and neural networks', Compos. Struct., in press, corrected proof, available online, (2006).

[2] S. Adali, 'Optimal shape and non-homogeneity of a non-uniformly compressed column', Int. J. Solids Structures, Vol. 15, pp. 935-949, (1979).

[3] S. Adali, I.U. Cagdas, 'Optimal design of simply supported columns subject to distributed axial load and stress constraint', Engineering Optimization, accepted for publication and to appear in 2007.

[4] S. Adali, V.E. Verijenko, 'Strength optimization of laminates under uncertain loads', ICCM-14, San Diego, California, July 14-18, (2003).

[5] S. Adali, I.U. Cagdas, 'Iterative methods in optimal design of elastically clamped columns', Journal of the Franklin Institute, in press, corrected proof, available online, (2006).

[6] S. Ahmad, B.M. Irons, O.C. Zienkiewicz, 'Analysis of thick and thin shell structures by curved elements', Int. J. Numer. Meth. Engng., Vol. 2, pp. 419-451, (1970).

[7] H. Akbulut, O. Sayman, 'An investigation on buckling of laminated plates with central square hole', J. Reinf. Plas. & Compos., Vol. 20, No. 13, (2001).

[8] H.G. Allen, P.S. Bulson, '*Background to buckling*', New York : McGraw-Hill Book Co., (1980).

[9] H. Altenbach, J. Altenbach, W. Kissing, '*Mechanics of composite structural elements*', Springer-Verlag, Berlin, Germany, (2004).

[10] J. S. Anastasiadis, A. Tabiei, G. J. Simitses, 'Instability of moderately thick, laminated, cylindrical shells under combined axial compression and pressure', Compos. Struct., Vol. 27, pp. 367-378, (1994).

[11] M.S. Anderson, W.J. Stroud, 'General panel sizing computer code and its application to composite structural panels', AIAA J., Vol. 17, No. 8, pp. 892-897, (1979).

[12] F. Arbabi, F. Li, 'Buckling of variable cross-section columns: integral-equation approach', ASCE J. Struct. Engng., Vol. 117, No. 8, pp. 2426–2441, (1991).

[13] F. Auricchio, E. Sacco, 'A mixed-enhanced finite-element for the analysis of laminated composite plates', Int. J. Numer. Meth. Engng., Vol. 44, pp. 1481-1504, (1999).

[14] C.S. Babu, T. Kant, 'Two shear deformable finite element models for buckling analysis of skew fibre-reinforced composite and sandwich panels', Compos. Struct, Vol. 46, pp. 115-124, (1999).

[15] J.R. Banarjee, F.W. Williams, 'The effect of shear deformation on the critical buckling of columns', Journal of Sound and Vibration, Vol. 174:5, pp. 607-616, (1994).

[16] N.V. Banichuk, '*Problems and methods of optimal structural design*', Plenum Press, NY, (1983).

[17] K.J. Bathe, '*Finite Element Procedures*', Prentice-Hall, Englewood Cliffs, (1995).

[18] M.L. Becker, A.N. Palazotto, N.S. Khot, 'Instability of composite panels', AIAA / ASME / ASCE / AHS 21st Structural Dynamics and Materials Conf., paper 80-0687, (1980).

[19] O.K. Bedair, 'Influence of in-plane restraint on the buckling behavior of plates under compression, shear and in-plane bending', Computer Methods in Applied Mechanics and Engineering, Vol. 148, pp. 1-10, (1997).

[20] O.K. Bedair, 'Effects of lateral restraint on the buckling behavior of plates under non-uniform edge compression', Struct. Engng. Mech., Vol. 5, No. 1, pp. 85-104, (1997).

[21] D. Bushnell, 'PANDA2 – program for minimum weight design of stiffened, composite, locally buckled panels', LMSC-DO67175, Lockheed Missiles and Space Company Report, (1986).

[22] I.U. Cagdas, S. Adali, 'Effect of in-plane boundary conditions on the non-uniform buckling loads of rectangular composite plates', Proceedings of Sixth Int. Conf. on Composite Science and Technology, Durban, South Africa, 22-24 January 2007.

[23] I.U. Cagdas, S. Adali, 'Optimal design of clamped columns subject to distributed axial load and stress constraint', Engineering Optimization, accepted for publication and to appear in 2007.

[24] G.B. Chai, P.W. Khong, 'The effect of varying the support conditions on the buckling of laminated composite plates', Compos. Struct., Vol. 24, pp. 99-106, (1993).

[25] C.A. Coello Coello, A.D. Christiansen, F.A. Farrera, Carlos A., 'Genetic Algorithm for the Optimal Design of Axially Loaded Non-prismatic Columns', Civil Engineering Systems, Vol. 14, pp. 111-146 (1996).

[26] R.D. Cook, '*Concepts and applications of finite element analysis*', John Wiley & Sons, Inc., (1973).

[27] M.A. Crisfield, '*Non-linear finite element analysis of solids and structures: Volume 1*', John Wiley & Sons, England, (1991).

[28] M. Cho, J.Y. Yoon, 'First-ply flexural failure analysis of symmetric cross-ply laminates by the postprocess method', Compos. Struct, Vol. 40, No.2, pp. 115-127, (1998).

[29] T.Y. Chang, K. Sawamiphakdi, 'Large deformation analysis of laminated shells by finite element method', Comput. Struct., Vol. 13, pp. 331-340, (1981).

[30] G.A. Cohen, R.T. Haftka, 'Sensitivity of buckling loads of anisotropic shells of revolution to geometric imperfections and design changes', Comput. Struct., Vol. 31, Issue 6, pp. 985-995, (1989).

[31] K.T. Danielson, J.T. Tielking, 'Membrane boundary condition effects on unsymmetric laminates', Journal of Engineering Mechanics, Vol. 114, No. 12, December, (1988).

[32] K.K.V. Devarakonda, C.W. Bert, 'Buckling of rectangular plate with nonlinearly distributed compressive loading on two opposite sides: comparative analysis and results', Mechanics of Advanced Materials and Structures, Vol. 11, pp. 433-444, (2004).

[33] Y.V. Egorov, V.A. Kodratiev, 'On the optimal column shape', Doklady Mathematics, 54(2): 748-750 (1996).

[34] H. A. El-Ghazaly, R. N. Dubey and A. N. Sherbourne, 'Elasto-plastic buckling of stiffener plates in beam-to-column flange connections', Comput. Struct., Vol. 18, Issue. 2, pp. 201-213, (1984).

[35] G.H. Ferguson, R.D. Clark, 'A variable thickness, curved beam and shell stiffening element with shear deformations', Int. J. Num. Meth. Engng., Vol. 14, pp. 581-592, (1979).

[36] J.A. Figueiras, D.R.J. Owen, 'Analysis of elasto-plastic and geometrically non-linear anisotropic plates and shells', In. E. Hinton, D.R.J. Owen, editors, Finite element software for plates and shells, pp. 235, (1984).

[37] A.A. Groenwold, R.T. Haftka, 'Optimization with non-homogeneous failure criteria like Tsai–Wu for composite laminates', Structural and Multidisciplinary Optimization, Vol. 32, No. 3, (2006).

[38] Z. Gürdal, R.T. Haftka, P. Hajela, '*Design and Optimization of Laminated Composite Materials*', J. Wiley & Sons, New York, (1999).

[39] R.T. Haftka, Z. Gurdal, M.P. Kamat, '*Elements of Structural Optimization*', 2nd ed. Dordrecht: Kluwer Academic Publishers, (1990).

[40] H.T. Hahn, J.B. Erikson, S.W. Tsai, 'Characterization of matrix/interface-controlled strength of unidirectional composites', in Fracture of Composite Materials, ed. G. Sih and V.P. Tamuzs, pp. 197-214, The Hague: Martinus Nijhoff, (1982).

[41] Z. Hashin, 'Failure criteria for unidirectional fiber composites', J. Appl. Mech., Vol. 102, pp. 329-334, (1980).

[42] G.Z. Harris, 'The buckling of orthotropic rectangular plates, including the effect of lateral edge restraint', Int. J. Solids Struct., Vol. 11, pp. 877-885, (1975).

[43] E. Hinton, D.R.J. Owen, '*Finite element programming*', Academic Press, (1977).

[44] Y. Hirano, 'Optimum design of laminated plates under shear', J. Comp. Mat., Vol. 13, pp. 329-334, (1973).

[45] Y. Hirano, 'Optimum design of laminated plates under axial compression', AIAA Journal, Vol. 17, pp. 1017-1019, (1979).

[46] Y. Hirano, '*Optimization of laminated composite plates and shells*', In. Z. Hashin, C.T. Herakovich, editors, Mechanics of composite materials – recent advances, New York, Pergamon, (1982).

[47] J.H. Holland, '*Adaptation of natural and artificial systems*', University of Michigan Press, Ann Arbor, (1975).

[48] Hou-Cheng Huang, '*Static and dynamic analyses of plates and shells: theory software and applications*', Springer Verlag, Berlin, (1989).

[49] H.T. Hu, J.S. Yang, 'Buckling optimization of laminated cylindrical panels subjected to axial compressive load', Compos Struct, in press, corrected proof, available online, (2006).

[50] P. Jana, K. Bhaskar, 'Stability analysis of simply-supported rectangular plates under non-uniform uniaxial compression using rigorous and approximate plane stress solutions', Thin-Walled Struct., Vol. 44, pp. 507–516, (2006).

[51] N. Jaunky, N.F. Knight, 'An assessment of shell theories for buckling of circular cylindrical composite panels loaded in axial compression', Int. J. Solids Struct., Vol. 36, pp. 3799-3820, (1999).

[52] R.M. Jones, '*Mechanics of composite materials*', 2nd Ed., Taylor & Francis, (1999).

[53] S.M. Jun, C.S. Hong, 'Buckling behaviour of laminated composite cylindrical panels under axial compression', Comput. Struct., Vol. 29, pp. 479-490, (1988).

[54] J.H. Kang, A.W. Leissa, 'Exact solutions for the buckling of rectangular plates having linearly varying in-plane loading on two opposite simply supported edges', Int. J. Solids and Struct., Vol. 42, pp. 4220-4238, (2005).

[55] W. Kanok-Nukulchai, 'A simple and efficient finite element for general shell analysis', Int. J. Num. Meth. Engng., Vol. 14, pp. 179-200, (1979).

[56] J.B. Keller, 'The shape of the strongest column', Arch. Rat. Mech. Anal., Vol. 5, pp. 275-285, (1960).

[57] A.A. Khdeir, L. Librescu, 'Analysis of symmetric cross-ply laminated elastic plates using higher order theory: part II – buckling and free vibration', Compos. Struct., Vol. 9, pp. 259-277 (1988).

[58] N. Kikuchi, '*Finite element methods in mechanics*', Cambridge University Press, (1986).

[59] K.D. Kim, 'Buckling behaviour of composite panels using the finite element method', Compos. Struct., Vol. 36, pp. 33-43, (1996).

[60] K.D. Kim, T.Y. Park, G.Z. Voyiadjis, 'Postbuckling analysis of composite panels with imperfection damage', Comput. Mech., Vol. 22, No. 5, pp. 375-387, (1998).

[61] K. Kim, G.Z. Voyiadjis, 'Non-linear finite element analysis of composite panels', Composites: Part B, Vol. 30, pp. 365-381, (1999).

[62] K. Kim, G.Z. Voyiadjis, 'Buckling strength prediction of CFRP cylindrical panels using finite element method', Composites: Part A, Vol. 30, pp. 1093-1104, (1999).

[63] S.A. Kulkarni, K.M. Bajoria, 'Finite element modeling of smart plates/shells using higher order shear deformation theory', Compos. Struct. Vol. 62, pp. 41-50, (2003).

[64] C.S. Krishnamoorthy, '*Finite Element Analysis - Theory and Programming*', McGraw-Hill Publ., Tata, New Delhi, (1987).

[65] J.L. Lagrange, 'Sur la figure des colonnes', Miscellanea Taurinensia, vol. 123, pp. 123, (1770-1773).

[66] A.W. Leissa, J.H. Kang, 'Exact solutions for vibration and buckling of an SS-C-SS-C rectangular plate loaded by linearly varying in-plane stresses', International Journal of Mechanical Sciences, Vol. 44, pp. 1925–1945, (2002).

[67] Q.S. Li, 'Buckling of elastically restrained non-uniform columns', Engineering Structures, Vol. 22, Issue 10, pp. 1231-1243, (Oct. 2000).

[68] Q.S. Li, 'Analytical solutions for buckling of multi-step non-uniform columns with arbitrary distribution of flexural stiffness or axial distributed loading', International Journal of Mechanical Sciences, Vol. 43, Issue 2, pp 349-366, (Feb. 2001) (a).

[69] Q.S. Li. 'Exact solutions for buckling of non-uniform columns under axial concentrated and distributed loading', European Journal of Mechanics - A/Solids, Vol. 20, Issue 3, pp. 485-500, (May 2001) (b).

[70] Q.S. Li, 'Buckling analysis of non-uniform bars with rotational and translational springs', Engineering Structures, Vol. 25, Issue 10, pp. 1289-1299, (August 2003).

[71] J. Li, Z.H. Xiang, M.D. Xue, 'Buckling analysis of rotationally periodic laminated composite shells by a new multilayered shell element', Compos. Struct., Vol. 70, pp. 24-32, (2005).

[72] C.C. Liang, H.W. Chen, C. Y. Jen, 'Optimum design of filament-wound multilayer-sandwich submersible pressure hulls', Ocean Engineering, Vol. 30, pp. 1941-1967, (2003).

[73] C.L. Liao, J.N. Reddy, 'Continuum-based stiffened composite shell element for geometrically nonlinear analysis', AIAA J., Vol. 27, No. 1, (Jan. 1989).

[74] C.C. Lin, A.J. Yu, 'Optimum weight design of composite laminated plates', Comput. Struct., Vol. 38, No. 5/6, pp. 581-587, (1991).

[75] J. Loughlan, 'The buckling of composite stiffened box sections subjected to compression and bending', Compos. Struct, Vol. 35, pp. 101-116, (1996).

[76] K.Y. Maalawi, 'Buckling optimization of flexible columns', Int. J. Solids Structures, Vol. 39, pp. 5865-5876 (2002).

[77] Mallikarjuna, T. Kant, 'A general fibre-reinforced composite shell element based on a refined shear deformation theory', Comput. Struct., Vol. 42, No. 3, p. 381-388, (1992).

[78] D. Manickarajah, Y.M. Xie, G.P. Steven, 'Optimization of columns and frames against buckling', Comput. Struct., Vol. 75, pp. 45-54 (2000).

[79] H.C. Mateus, C.M. Mota Soares, C.A. Mota Soares, 'Buckling sensitivity analysis and optimal design of thin laminated structures', Comput. Struct., Vol. 64, No. 1-4, pp. 461-472, (1997).

[80] T. Messager, M. Pyrz, B. Gineste, P. Chauchot, 'Optimal laminations of thin underwater composite cylindrical vessels', Compos. Struct., Vol. 58, pp. 529-537, (2002).

[81] K.T. Min, F.X. de Charenteney, 'Optimum weight design of sandwich cylinders with orthotropic facings and core under combined loads', Comput. Struct., Vol. 24, No. 2, (1986).

[82] J.S. Moita, C.M. Mota Soares, C.A. Mota Soares, 'Buckling behaviour of laminated composite structures using a discrete higher-order displacement model', Compos. Struct., Vol. 35, pp. 75-92, (1996).

[83] C.M. Mota Soares, C.A. Mota Soares, H.C. Mateus, 'A model for the optimum design of thin laminated plate-shell structures for static, dynamic and buckling behaviour', Compos. Struct., Vol. 32, pp. 69-79, (1995).

[84] A. Muc, 'On the buckling of composite shells of revolution under external pressure', Compos. Struct., Vol. 21, pp. 107-119, (1992).

[85] M.P. Nemeth, 'Buckling of long compression-loaded anisotropic plates restrained against inplane lateral and shear deformations', Thin-Walled Struct., Vol. 42, pp. 639-685, (2004).

[86] A.K. Noor, 'Stability of multi-layered composite plates', Fibre Sci. Technol., Vol. 8, pp. 81-89, (1975).

[87] Y.S. Nshanian, M. Pappas, 'Optimal laminated composite shells for buckling and vibration', AIAA J., Vol. 21, No. 3, pp. 430-437, (1983).

[88] I.F. Obraztsov, V.V. Vasil'ev, '*Optimal design of composite structures*', In. C.T. Herakovich, Y.M. Tarnapol'skii, editors. Handbook of composites, Vol. 2 – structure and design, Amsterdam, Elsevier Publishing Co, pp. 3-84, (1989).

[89] N. Olhoff and S.H. Rasmussen, 'On single and bimodal optimum buckling loads of clamped columns', Int. J. Solids Struct., Vol. 13, pp. 605-614 (1977).

[90] N. Olhoff and A.P. Seyranian, 'On the bifurcation and initial post-buckling behaviour of bimodal optimal columns', Proceedings of 15th Nordic Seminar on Computational Mechanics (NSCM 15), 18-19 October, 2002, Aalborg, Denmark, Eds. E Lund, N Olhoff and J Stegmann, pp. 249-252.

[91] Y. Onoda, 'Optimal laminate configurations of cylindrical shells for axial buckling', AIAA J., Vol. 23, No. 7, pp. 1093-1098, (1985).

[92] M. Ostwald, 'Optimum weight design of sandwich cylindrical shells under combined loads', Comput. Struct. Vol. 37, No. 3, pp. 247-257, (1990).

[93] A.N. Palazatto, A.D. Straw, 'Shear buckling of cylindrical composite panels', Comput. Struct., Vol. 27, No. 5, pp. 689-692, (1987).

[94] A.N. Palazotto, S.T. Dennis, '*Nonlinear Analysis of Shell Structures*', AIAA Education Series, Washington, DC.,(1992).

[95] D.E. Panayatounakos, 'Classes of solutions in the problem of stability analysis in bars with varying cross-section and axial distributed loading', Int. J. Solids Struct., Vol. 32, No. 21, pp. 3229–3236, (1994).

[96] S. Panda, R. Natarajan, 'Analysis of laminated composite shell structures by finite element method', Comput. Struct., Vol. 14, No. 3-4, p. 225-230, (1981).

[97] V.J. Papazoglou, N.G. Tsouvalis, G.D. Kyriakopoulos, 'Buckling of unsymmetric laminates under linearly varying biaxial in-plane loads, combined with shear', Compos. Struct., Vol. 20, pp. 155-163, (1992).

[98] K.C. Park, G.M. Stanley, 'A Curved C^0 shell element based on assumed natural-coordinate strains', J. Applied Mechanics, Vol. 53, pp. 278-290, (1986).

[99] J.H. Park, J.H. Hwang, C.S. Lee, W. Hwang, 'Stacking sequence design of composite laminates for maximum strength using genetic algorithms, Compos. Struct., Vol. 52, p. 217-231, (2001).

[100] S.F. Pawsey, '*The analysis of moderately thick and thin shells*', Ph.D. thesis, Department of Civil Engineering, University of California, Berkeley, (1970).

[101] B. Peseux, S. Dubigeon, 'Equivalent homogeneous finite elements for composite materials via Reissner principle. Part II: finite element for shells', Int. J. Num. Meth. Engng., Vol. 31, pp. 1497-1509, (1991).

[102] J.L. Phillips, Z. Gürdal, 'Analysis and optimal design of geodesically stiffened composite panels', Proceedings of the 2nd Int. Conf. on Computer Adided Design in Composite Material Technology, Free University of Brussels/Wessex Institute of Technology, Computational MechanicsPublications, Southampton, (1990).

[103] O.G. Privalova and A.P. Seyranian, 'Post buckling behaviour of bimodal optimal columns', Mech. Solids, Vol. 28, No. 2, pp. 168-177 (1999).

[104] B.G. Prusty, S.K. Satsangi, C. Ray, 'First ply failure analysis of laminated panels under transverse loading', Journal of Reinforced Plastics and Composites, Vol. 20, No. 8, (2001).

[105] B.G. Prusty, C. Ray, S.K. Satsangi, 'First ply failure analysis of stiffened panels – a finite element approach', Compos. Struct, Vol. 51, pp. 73-81, (2001).

[106] P.V. Raghuram, A.V. Krishna-Murty, 'A high precision coupled bending-extension triangular finite element for laminated plates', Comput. Struct., 72:763-777, (1999).

[107] K.S.S. Ram, T.S. Babu, 'Buckling of laminated composite shells under transverse load', Compos. Struct, Vol. 55, pp. 157-168, (2002).

[108] K.P. Rao, B. Tripathy, 'Composite cylindrical panels – optimum lay-up for buckling by ranking', Comput. Struct., Vol. 38, No.2, pp. 217-225, (1991).

[109] J. N. Reddy, W.C. Chao, 'A comparison of closed-form and finite-element solutions of thick laminated anisotropic rectangular plates', Nuclear Engineering and Design, Vol. 64, Issue 2, pp. 153-167, (1981).

[110] J.N. Reddy, '*Energy and Variational Methods in Applied Mechanics*', John Wiley, New York, (1984).

[111] J.N. Reddy, A.K. Pandey, 'A first-ply failure analysis of composite laminates', Comput. Struct., Vol. 25, No.3, pp. 371-393, (1987).

[112] J.N. Reddy, C.F. Liu, 'A higher order theory for geometrically non-linear analysis of composite laminate', NASA Report CR 4056, (1987).

[113] Y.S.N. Reddy and J.N. Reddy, 'Linear and non-linear failure analysis of composite laminates with transverse shear', Composites Science and Technology, Vol. 44, Issue 3, pp. 227-255, (1992).

[114] J.N. Reddy, '*Mechanics of laminated composite plates: theory and analysis*', CRC Press, Inc. USA, (2004).

[115] J.N. Reddy, A. Miravete, 'Practical analysis of composite laminates', CRC Press, Boca Raton, Fla., (2004).

[116] R.E. Rowlands, 'Strength (failure) theories and their experimental correlation: Hand book of composites fracture mechanics of composites', in: Sih GC, Skudra AM, editors, vol. 3. Amsterdam: Elsevier, (1985).

[117] C.T. Sambandam, B.P. Patel, S.S. Gupta, C.S. Munot, M. Ganapathi, 'Buckling characteristics of cross-ply elliptical cylinders under axial compression', Compos. Struct., Vol. 62, pp. 7-17, (2003).

[118] A.P. Seyranian, 'New solutions of Lagrange's problem', Doklady Physics, 342(2): pp. 182-184 (1995).

[119] A.P. Seyranian, O.G. Privalova, 'Supercritical behaviour of optimum columns with two modes of buckling', Doklady Physics, 44(6): pp. 368-372, (1999).

[120] A.P. Seyranian, O.G. Privalova, 'The Lagrange problem on an optimal column: old and new results', Struct Multidisc. Optim., Vol. 25, pp. 393-410 (2003).

[121] A.N. Sherbourne, M.D. Pandey, 'Effects of in-plane restraint on the stability of laminated composite plates', Compos. Struct., Vol. 20, pp. 73-81, (1992).

[122] G. Singh, Y.V.K.S. Rao, 'Stability of thick angle-ply composite plates', Comput. Struct., Vol. 29, No. 2, pp. 317-322, (1988).

[123] B.N. Singh, D. Yadav, N.G.R. Iyengar, 'Stability analysis of laminated cylindrical panels with uncertain material properties', Compos. Struct. Vol. 54, pp. 17-26, (2001).

[124] A. Smerdov, 'A computational study in optimum formulations of optimization problems on laminated cylindrical shells for buckling I. shells under axial compression', Compos. Sci. Tech., Vol. 60, pp. 2057-2066, (2000).

[125] A. Smerdov, 'A computational study in optimum formulations of optimization problems on laminated cylindrical shells for buckling II. shells under external pressure', Compos. Sci. Tech., Vol. 60, pp. 2067-2076, (2000).

[126] L.H. Sobel, T. Weller, B.L. Agarwal, 'Buckling of cylindrical panels under axial compression', Comput. Struct., Vol. 6, pp. 29-35, (1976).

[127] S. R. Soni, 'A new look at commonly used failure theories in composite laminates', 24th AIAA/ASME/ASCE/AHS Structures, Structural Dynamics and Materials Conference Proc., (1983).

[128] S. Sridharan, A. Kasagi, 'On the buckling of moderately thick composite cylinders under hydrostatic pressure', Composites Part B, Vol. 28B, pp. 583-596, (1997).

[129] M. Stein, J.G. Williams, 'Buckling and structural efficiency of sandwich-blade stiffened composite compression panels', Technical paper, NASA-TP-1269, (1978).

[130] W.J. Stroud, M.S. Anderson, 'PASCO: structural panel analysis and sizing code, capability and analytical foundations', NASA-TM-80181, (1981).

[131] G. Sun, 'A practical approach to optimum design of laminated cylindrical shells for buckling', Comp. Sci. Tech., Vol. 36, pp. 243-253, (1989).

[132] Y. Tada, L. Wang, 'Reinvestigation on optimisation of clamped–clamped columns and symmetry of corresponding eigenfunctions', JSME Int. J, Vol. 38, No. 1, pp. 38--43, (1995).

[133] I. Tadjbakhsh, J.B. Keller, 'Strongest columns and isoperimetric inequalities for eigenvalues', J. Appl. Mech., Vol. 29 pp. 159-164, (1962).

[134] M.A. Talha, 'A theoretically improved and easily implemented version of the Ahmad thick shell element', Int. J. Num. Meth. Engng., Vol. 14, pp. 125-142, (1979).

[135] S. Timoshenko, '*Theory of Elastic Stability*', McGraw-Hill,New York, (1936).

[136] T.C. Triantafillou, P. Kim, U. Meier, 'Optimization of hybrid aluminium /c.f.r.p. box beams', Int. J. Mech. Sci., Vol. 33, No. 9, pp. 313-322, (729-739).

[137] S.M. Variyar, N.S. Prasad, 'Estimation of residual stresses in weldments using a nine-noded degenerated shell element', J. Materials Processing Tech., Vol. 91, pp. 150-160, (1999).

[138] H.H. Vaziri and J. Xie, 'Buckling of columns under variably distributed axial loads', Comput. Struct., Vol. 45, No. 3, pp. 505–509, (1992).

[139] M. Walker, T. Reiss, S. Adali, 'Optimal design of symmetrically laminated plates for minimum deflection and weight', Compos. Struct., Vol. 39, No. 3-4, pp. 337-346, (1997).

[140] J.T.S. Wang, 'Best angles against buckling of rectangular laminates', Proceedings of the 4th international conference on composite materials, pp. 575-582, (1982).

[141] C.M. Wang, C.Y. Wang, J.N. Reddy, '*Exact Solutions for buckling of structural members*', CRC Press, Florida, USA, (2005).

[142] X. Wang, L. Gan, Y.Wang, 'A differential quadrature analysis of vibration and buckling of an SS-C-SS-C rectangular plate loaded by linearly varying in-plane stresses', J. Sound & vibration, Vol. 298, pp. 420-431, (2006).

[143] P.M. Weaver, 'Design of laminated composite cylindrical shells under axial compression', Composites Part B, Vol. 31, pp. 669-679, (2000).

[144] J.M. Whitney, 'The effect of boundary condition on the response of laminated composites', J. Compos. Mater., Vol. 4, No. 2, pp. 192-203, (1970).

[145] P.M. Wung, 'Laminated composite structures by continuum-based shell elements with transverse deformation', Comput. Struct., Vol. 62, No. 6, pp. 1073-1090, (1997).

[146] T.Y. Yang, '*Finite element structural analysis*', Prentice-Hall, Englewood Cliffs, N.J., (1986).

[147] W.C. Young, '*Roark's formulas for stress & strain*', 6th Ed., McGraw-Hill, New York, (1989).

[148] Y.X. Zhang, K.S. Kim, 'Two simple and efficient displacement-based quadrilateral elements for the analysis of composite laminated plates', Int. J. Numer. Meth. Engng., Vol. 61, pp.1771-1796, (2004).

[149] H. Zhong, C. Gu, 'Buckling of Simply Supported Rectangular Reissner–Mindlin Plates Subjected to Linearly Varying In-Plane Loading', Journal of Engineering Mechanics, Vol. 132, No. 5, May 1, (2006).

[150] H. Ziegler, 'Arguments for and against Engesser's buckling formulas', Ingenieur-Archiv, Vol. 52, pp. 105-113, (1982).

[151] A. Zureick, B. Shih, 'Local buckling of fiber-reinforced polymeric structural members under linearly varying edge loading – Part 1. Theoretical formulation', Compos. Struct., Vol. 41, pp. 79-86, (1998).

[152] R. Zimmermann, 'Quick optimal buckling design of axially compressed, fiber composite cylindrical shells', AIAA J., Vol. 33, No. 10, pp. 1993-1995, (1995).

APPENDIX

A. Matlab Functions for Finite Element Analysis

The functions listed here are based on the formulations given in Section II of this thesis.

A.1 Function for the finite element analysis of columns

The function used for the computation of the buckling load and corresponding deformed shape of a column is listed here. This function is used to solve the structural part of the plate optimization problem given in Section 3 of this thesis.

```
%_____________________________________________________________________
function [w1,dw1,w2,dw2,K1,K2]=OPT_P_comp_Pwdw(...
P,q0,Atop,E,Length,ne,Itop,beta_a,beta_b,alpha,Vol,yuk,guided,sup_guided)
% Izzet Ufuk Çagdas, 2006
%_____________________________________________________________________
% INPUT VARIABLES (All of the variables are dimensional)
% P: axial load at B
% q0: intensity of distributed load
% E: modulus of elasticity
% Length: length of the column
% ne: number of elements (odd number!)
% Itop: vector of moment of inertia values at the nodes
% beta_a, beta_b: rotational spring constants
% alpha: dimensional constant depending on the cross section
% Vol: volume
% yuk: yuk=1 for uniformly distributed load / yuk=2 for triangularly distributed load, etc.
% guided: if =1, guided else, not guided
% right support is guided if sup_guided=1, left support is guided if sup_guided=2
%_____________________________________________________________________
% OUTPUT VARIABLES
% w1,dw1: deflections and rotations at the nodes corresponding to the 1st mode
% w2,dw2: deflections and rotations at the nodes corresponding to the 2nd mode
% K1, K2: buckling parameters corresponding to the first and the second modes
%_____________________________________________________________________
step=Length/ne; % discretize the column using a total of 'ne' elements
x=0:step:Length; % vector x has M+1 elements
Ltop(1:ne)=Length/ne; % length of an element
% for ne elements there're ne+1 nodes and 3*(ne+1) dof
KGE(3*(ne+1),3*(ne+1))=0;% initialize the global stiffness matrix
KGG(3*(ne+1),3*(ne+1))=0;% initialize the global geometric stiffness matrix
% set up the global stiffness matrix
for i=1:ne
  % add contributions of all of the elements
  L=Ltop(i); % length of an element
  A=(Atop(i)+Atop(i+1))/2;
  Ii=Itop(i);
  Ij=Itop(i+1);
  I=(Ii+Ij)/2;
  % compute element stiffness matrix
  ke=E*I/L^3*[A*L^2/I 0 0 -1*A*L^2/I 0 0;
    0 12 6*L 0 -12 6*L;
    0 6*L 4*L^2 0 -6*L 2*L^2;
```

```
   -1*A*L^2/I 0 0 A*L^2/I 0 0;
   0 -12 -6*L 0 12 -6*L;
   0 6*L 2*L^2 0 -6*L 4*L^2];
% compute element geometric stiffness matrix, kg
if yuk==1 % UDL : uniformly distributed load
   alp=1;      Phi=P+q0*(Length-x(i));
   Phi_p1=P+q0*(Length-x(i+1));
   po=q0;
   r=(1+alp)*((Phi-Phi_p1)/po/L-1);
   %
elseif yuk==2 %TDL: triangularly distributed load
   alp=1;      po=q0*(1-x(i)/Length);
   r=-1*q0*L/(po*Length);
   Phi_p1=P+q0*(1-x(i+1)/Length)*(Length-x(i+1))/2;
elseif yuk==3 % Cubic distribution
   alp=1;      po=4*q0*(1-x(i)/Length)^3;
   r=(1+alp)*(Length/4/L/(1-x(i)/Length)^3*((1-x(i)/Length)^4-(1-x(i+1)/Length)^4)-1);
   Phi_p1=P+q0*Length*(1-x(i)/Length)^4;
elseif yuk==4 % Cubic distribution
   alp=1;      po=4*q0*(x(i)/Length)^3;
   r=(1+alp)*((x(i+1)^4-x(i)^4)/(4*x(i)^3*L+1e-12)-1);
   Phi_p1=P+q0*Length*(1-(x(i)/Length)^4);
elseif yuk==5 % half length loaded by uniform load
   if i<=ne/2 % not loaded part
      alp=1;      po=0;      r=0;
      Phi_p1=P+q0*Length*1/2;
   else % loaded part
      alp=1;      Phi=P+q0*(Length-x(i));
      Phi_p1=P+q0*(Length-x(i+1));
      po=q0;
      r=(1+alp)*((Phi-Phi_p1)/po/L-1);
      %
   end
elseif yuk==6 % half loaded by uniform load at the middle
   if i<1*ne/4 % not loaded part
      alp=1;      po=0;      r=0;
      Phi_p1=P+q0*Length*1/2;
   elseif i>=1*ne/4 & i<=3*ne/4 % loaded part
      alp=1;
      Phi=P+q0*(3/4*Length-x(i));
      Phi_p1=P+q0*(3/4*Length-x(i+1));
      po=q0;
      r=(1+alp)*((Phi-Phi_p1)/po/L-1);
   elseif i>1*3*ne/4 % not loaded part
      alp=1;      po=0;      r=0;      Phi_p1=P;
   end
elseif yuk==7 % half loaded by uniform load at the middle
   if i<(ne+1)/2 % not loaded part
      alp=1;      po=0;      r=0;
      Phi_p1=P+q0*Length/ne;
   elseif i==(ne+1)/2 % loaded part
      alp=1;      Phi=P+q0*(Length/ne);
      Phi_p1=P;
      po=q0;
      r=(1+alp)*((Phi-Phi_p1)/po/L-1);
```

```
    elseif i>(ne+1)/2 % not loaded part
      alp=1;        po=0;        r=0;
      Phi_p1=P;%P?
    end
  elseif yuk==8 % half loaded by uniform load at the middle
    if i<(ne+1)/4 % not loaded part
      alp=1;
      po=0;
      r=0;
      Phi_p1=P+q0*Length/ne;
    elseif i==(ne+1)/4 % loaded part
      alp=1;
      Phi=P+q0*(Length/ne);
      Phi_p1=P;
      po=q0;
      r=(1+alp)*((Phi-Phi_p1)/po/L-1);
    elseif i>(ne+1)/4 % not loaded part
      alp=1;
      po=0;
      r=0;
      Phi_p1=P;%P?
      %
    end
  elseif yuk==9 % half left loaded by uniform load
    if i>ne/2 % not loaded part
      alp=1;
      po=0;
      r=0;
      Phi_p1=P;
    else % loaded part
      alp=1;
      Phi=P+q0*(Length/2-x(i));
      Phi_p1=P+q0*(Length/2-x(i+1));
      po=q0;
      r=(1+alp)*((Phi-Phi_p1)/po/L-1);
      %
    end
  end
  load(i)=Phi_p1;
  P0=Phi_p1;
  % Calculate entries of the geometric stiffness matrix
  n11=6*P0/5/L+po*(3/5+(r/(1+alp))*(6/5-36/(4+alp)+72/(5+alp)-36/(6+alp)));
  n33=n11;
  n31=-1*n11;
  n13=n31;
  n21=P0/10+po*r*L/(1+alp)*(1/10+6/(3+alp)-30/(4+alp)+42/(5+alp)-18/(6+alp));
  n32=-1*n21;
  n23=n32;
  n12=n21;
  n41=P0/10+po*L*(1/10+r/(1+alp)*(1/10-12/(4+alp)+30/(5+alp)-18/(6+alp)));
  n43=-1*n41;
  n14=n41;
  n34=n43;
  n22=2*P0*L/15+po*L^2*(1/10+r/(1+alp)*(2/15-1/(2+alp)+8/(3+alp)-22/(4+alp)+...
24/(5+alp)-9/(6+alp)));
```

```
    n42=-1*P0*L/30-po*L^2*(1/60+r/(1+alp)*(1/30-2/(3+alp)+11/(4+alp)-18/(5+alp)+...
9/(6+alp)));
    n24=n42;
    n44=2*P0*L/15+po*L^2*(1/30+r/(1+alp)*(2/15-4/(4+alp)+12/(5+alp)-9/(6+alp)));
    % generate geometric stiffness matrix of element i
    kg=[0 0   0   0 0   0;
      0 n11  n12  0 n13  n14;
      0 n21  n22  0 n23  n24;
      0 0   0   0 0   0;
      0 n31  n32  0 n33  n34;
      0 n41  n42  0 n43  n44];
    % place the stiffness components into the global stiffness matrix
    % 1st elements dof are 1-2-3-4, 2nd elements are 5-6-7-8... so on
    vec=[3*i-2,3*i-1,3*i,3*(i+1)-2,3*(i+1)-1,3*(i+1)];% numbers of the dofs of the ith element
    % add the contributions of the elastic rotational restraints at the ends
    if i==1
      ke(3,3)=ke(3,3)+beta_a;
    end
    if i==ne
      ke(6,6)=ke(6,6)+beta_b;
    end
    KGE(vec,vec)=KGE(vec,vec)+ke;
    KGG(vec,vec)=KGG(vec,vec)+kg;
end
% apply boundary conditions
free=[];
for i=1:ne-1
    free=[free [3*(i+1)-1 3*(i+1)]];% free dofs of the inner nodes
end
if guided==0
    free=[3 free (ne+1)*3];
elseif guided==1 & sup_guided==2 % left support guided
    free=[2 3 free (ne+1)*3];
elseif guided==1 & sup_guided==1
    free=[3 free (ne+1)*3-1 (ne+1)*3];% right support guided
end
% %
KGE=KGE(free,free);
KGG=KGG(free,free);
% re-write the equation
Klast=inv(KGE)*KGG;
% solve for eigenvalues
[w,K]=eig(Klast);
K=diag(K);
K=1./K; % vector of buckling parameters
%_____________________________________________________________________
if guided==0
    % Seperate deflections and rotations corresponding to 1st mode
    K1=K(1);
    wbir=w(:,1);
    w_cr=wbir(2:length(wbir)-1);
    for i=1:length(w_cr)/2
      w1(i)=w_cr(2*i-1);
      dw1(i)=w_cr(2*i);
    end
```

```
    w1=[0 w1 0];
    dw1=[wbir(1) dw1 wbir(length(wbir))];%
    % Seperate deflections and rotations corresponding to 2nd mode
    K2=K(2);
    wiki=w(:,2);
    w_cr=wiki(2:length(wiki)-1);
    for i=1:length(w_cr)/2
       w2(i)=w_cr(2*i-1);
       dw2(i)=w_cr(2*i);
    end
    w2=[0 w2 0];
    dw2=[wiki(1) dw2 wiki(length(wiki))];%
elseif guided==1 & sup_guided==1
    % Seperate deflections and rotations corresponding to 1st mode
    K1=K(1);
    wbir=w(:,1);
    w_cr=wbir(2:length(wbir)-1);
    for i=1:(length(w_cr)-1)/2
       w1(i)=w_cr(2*i-1);
       dw1(i)=w_cr(2*i);
    end
    w1=[0 w1 wbir(length(wbir)-1)];
    dw1=[wbir(1) dw1 wbir(length(wbir))];%
    % Seperate deflections and rotations corresponding to 2nd mode
    K2=K(2);   wiki=w(:,2);   w_cr=wiki(2:length(wiki)-1);
    for i=1:length(w_cr)/2
       w2(i)=w_cr(2*i-1);
       dw2(i)=w_cr(2*i);
    end
    w2=[0 w2 wiki(length(wiki)-1)];
    dw2=[wiki(1) dw2 wiki(length(wiki))];%
elseif guided==1 & sup_guided==2
    % Seperate deflections and rotations corresponding to 1st mode
    K1=K(1);   wbir=w(:,1);   w_cr=wbir(1:length(wbir));
    for i=1:(length(w_cr)-1)/2
       w1(i)=w_cr(2*i-1);
       dw1(i)=w_cr(2*i);
    end
    w1=[w1 0];
    dw1=[dw1 wbir(length(wbir))];%
    % Seperate deflections and rotations corresponding to 2nd mode
    K2=K(2);   wiki=w(:,2);   w_cr=wiki(1:length(wiki));
    for i=1:(length(w_cr)-1)/2
       w2(i)=w_cr(2*i-1);
       dw2(i)=w_cr(2*i);
    end
    w2=[w2 0];   dw2=[dw2 wiki(length(wiki))];%
end
%_____________________________________________________________________
```

A.2 Functions for the finite element analysis of laminated plates

The function used for the calculation of the buckling load of a rectangular (or skew) plate subject to linearly varying edge loading is listed here. This function is used to solve the structural part of the plate optimization problem given in Section 4 of this thesis.

```
%_____________________________________________________________________
function [Pcr_nondim]=program_01(katsayi,alpha1, aci,a_bolu_b,rb,prob_num)
% Izzet Ufuk Çagdas, 2006
%_____________________________________________________________________
% INPUT VARIABLES
% katsayi: A constant between 0 and 0.5. the case katsayi=0.25 corresponds to equal ply
% thickness situation
% alpha1: loading, equal to 0, 1, or 2.
% aci: skew/transformation angle in degrees
% a_bolu_b: a/b
% rb: rotational restraint coefficient. (if rb=0, then there's no rotational restraint)
% prob_num: number of the problem to be solved (there're 6 different problems solved)
% INPUT DATA
ne=128; % total number of elements
nnode=433; % total number of nodes
n_layer=4; % total number of layers
t=1;% total laminate thickness
hzero=katsayi*t;
teta_vec1=[0 90 90 0]; % lamination angles (in degrees)
E1=25e4;E2=1e4;nu12=0.25;G12=0.5*E2;G23=0.3*E2;G13=0.5*E2; % material properties
% generate input vectors related to materials
E1_vec(1:n_layer)=E1;
E2_vec(1:n_layer)=E2;
nu12_vec(1:n_layer)=nu12;
G12_vec(1:n_layer)=G12;
G23_vec(1:n_layer)=G23;
G13_vec(1:n_layer)=G13;
%_____________________________________________________________________
% OUTPUT VARIABLES
% Pcr_nondim: The non-dimensional buckling load
%_____________________________________________________________________
% Calculation of the transformation matrix (note that each element has 8 nodes)
Trans_vec(128,8)=0;
Trans_vec(1:8,[1 7 8])=-aci*pi/180;Trans_vec(121:128,[3 4 5])=-aci*pi/180;
%_____________________________________________________________________
% calculation of consistent nodal forces for 16x8 mesh
load_vec(nnode*5)=0;% initialize load vector
[F_vec]=calculate_consist_nodal_force(100,alpha1)*t;% multiply by thickness!
if aci==0% transformation angle
   load_vec([417:433]*5-4)=F_vec;
   load_vec([1:17]*5-4)=-1*F_vec;
else% transform the loads for the skew plate problem
   F1_vec=F_vec*cos(aci*pi/180);
   load_vec([1:17]*5-4)=-1*F1_vec*cos(aci*pi/180);
   load_vec([1:17]*5-3)=-1*F1_vec*sin(aci*pi/180);
   load_vec([417:433]*5-4)=1*F1_vec*cos(aci*pi/180);
   load_vec([417:433]*5-3)=1*F1_vec*sin(aci*pi/180);
end
%_____________________________________________________________________
```

```
% Calculate global stiffness matrix
KGE=[]; initialize global stiffness matrix
[KGE,conn,x_vec,y_vec,A,B,free]=yellow_submarine_1(...
n_layer,t,ne,nnode,teta_vec1,E1_vec,E2_vec,nu12_vec,G12_vec,G23_vec,G13_vec,...
a_bolu_b,Trans_vec,hzero,aci,prob_num);
%_____________________________________________________________________
% add contribution of rotational restraints to the global stiffness matrix
if rb~=0
  % Add rigidities of rotational restraints
  D=E1*t^3/12/(1-nu12^2);
  C=(rb/100)*D*(a_bolu_b*100)^2/pi^2;
  C=C/(a_bolu_b*100);
  alt_dugum_vec=...
    [17 18 43 44 69 70 95 96 121 122 147 148 173 174 199 200 225 226 251 252 277 278 303
304 329 330 355 356 381 382 407 408 433]*5;
  for i=1:length(alt_dugum_vec)
    if i==1 | i==length(alt_dugum_vec)
      KGE(alt_dugum_vec(i),alt_dugum_vec(i))=KGE(...
          alt_dugum_vec(i),alt_dugum_vec(i))+C*32/(100)/2;
    else
      KGE(alt_dugum_vec(i),alt_dugum_vec(i))=KGE(...
          alt_dugum_vec(i),alt_dugum_vec(i))+C*32/(100);
    end
  end
end
%_____________________________________________________________________
% solve static problem to calculate membrane forces at the gauss points
% Call Sub Program (yellow_submarine_2) for primer analysis
[deplasman,Pcr]=yellow_submarine_2(KGE,GSM,load_vec,free,nnode,1);
%_____________________________________________________________________
% Plot smoothed membrane forces (if necessary)
[xMat,yMat,NxxMat,NyyMat,NxyMat]=sub_program_calc_nodal_inplane_force(nnode,...
conn,deplasman,x_vec,y_vec,A,B,Trans_vec,1);
%_____________________________________________________________________
% Calculate global geometric stiffness matrix using the results of the primer analysis
GSM=[]; % initialize global geometric stiffness matrix
[GSM]=sub_program_assemble_GSM_plate(ne,nnode,conn,x_vec,y_vec,deplasman,A,B,t,...
Trans_vec);
%_____________________________________________________________________
% CALCULATE THE BUCKLING LOAD
[deplasman2,Pcr]=yellow_submarine_2(KGE,GSM,load_vec,free,nnode,2);
% Display non-dimensional buckling parameter
D=E1*t^3/12/(1-nu12^2);
Pcr_nondim=-1*abs(Pcr/(pi^2*D/100^2/100)/100)
%_____________________________________________________________________
%
function [KGE,conn,x_vec,y_vec,A,B,free]=yellow_submarine_1(...
n_layer,t,ne,nnode,teta_vec,E1_vec,E2_vec,nu12_vec,G12_vec,G23_vec,G13_vec,a_bolu_b,...
Trans_vec,hzero,aci,prob_num)
if prob_num==1
[z,conn,x_vec,y_vec,free]=geometric_prop_program01(n_layer,t,ne,nnode,...
1,a_bolu_b,hzero,aci);
  elseif prob_num==2
[z,conn,x_vec,y_vec,free]=geometric_prop_program02(n_layer,t,ne,nnode,...
1,a_bolu_b,hzero,aci);
```

```
   elseif prob_num==3
[z,conn,x_vec,y_vec,free]=geometric_prop_program03(n_layer,t,ne,nnode,...
1,a_bolu_b,hzero,aci);
   elseif prob_num==4
[z,conn,x_vec,y_vec,free]=geometric_prop_program04(n_layer,t,ne,nnode,...
1,a_bolu_b,hzero,aci);
   elseif prob_num==5
[z,conn,x_vec,y_vec,free]=geometric_prop_program05(n_layer,t,ne,nnode,...
1,a_bolu_b,hzero,aci);
   elseif prob_num==6
[z,conn,x_vec,y_vec,free]=geometric_prop_program06(n_layer,t,ne,nnode,...
1,a_bolu_b,hzero,aci);
end
% Calculate material matrices
[A,B,D,Cs]=sub_program_calculate_material_matrices(teta_vec,E1_vec,E2_vec,...
nu12_vec,G12_vec,G23_vec,G13_vec,n_layer,z);
% Calculate element stiffness matrix
[KGE]=sub_program_assemble_KGE_plate(ne,nnode,conn,x_vec,y_vec,A,B,D,Cs,t,...
Trans_vec);
%_____________________________________________________________________
function [deplasman,Pcr]=yellow_submarine_2(KGE,GSM,load_vec,free,nnode,problem)
Pcr=0;deplasman=0;
KGE2=KGE(free,free);
KGE=KGE2;
if problem==1
   % Solve primer problem
   load_vec=load_vec(free);
   deplas=inv(KGE)*load_vec';
   deplasman(nnode*5)=0;
   deplasman(free)=deplas;
elseif problem==2
   % Linearized buckling analysis
   GSM=GSM(free,free);
   % Calculate buckling load
   % re-write the equation
   Klast=inv(KGE)*GSM;
   % solve for eigenvalues
   Klast=sparse(Klast);
   [aygenvec,P]=eigs(Klast,1);
   P=diag(P);
   P(P==0)=[];
   P=1./P;
   P1=P(1);
   Pcr=P1
   % re-arrange
   aygenvec_duz(nnode*5)=0;
   aygenvec_duz(free)=aygenvec;
   deplasman=aygenvec_duz;
end
%_____________________________
% Calculate consistent nodal forces (valid only for the 16x8 mesh)
function [F_vec]=calculate_consist_nodal_force(b,alpha1)
% yi: y coordinate of the node
% b: width of the plate
sigma0=1;
```

```
F_vec(8,3)=0;
% use 4-point rule / 2 point rule gives the same result
ksi_vec=[sqrt((3+sqrt(4.8))/7) -1*sqrt((3+sqrt(4.8))/7) sqrt((3-sqrt(4.8))/7) -1*...
sqrt((3-sqrt(4.8))/7)];
a_vec=[.5-sqrt(30)/36 .5-sqrt(30)/36 .5+sqrt(30)/36 .5+sqrt(30)/36];
y_vec=(16:-1:0)*b/16;
%
for k=1:8
   % extract y values of the nodes of element k
   y(1)=y_vec(k*2-1);
   y(2)=y_vec(k*2);
   y(3)=y_vec(k*2+1);
   % integrate using GQ
   for i=1:4
      ksi=ksi_vec(i);
      % evaluate the shape function values at the Gauss points
      N(1)=.5*ksi*(ksi-1);
      N(2)=(1-ksi)*(1+ksi);
      N(3)=.5*ksi*(1+ksi);
      top1=0;
      for j=1:3
         top1=top1+N(j)*y(j);% y value at the Gauss point
      end
      for ind=1:3
         F_vec(k,ind)=F_vec(k,ind)+N(ind)*a_vec(i)*(b/16)*sigma0*(1-alpha1*top1/b);
      end
   end
end
% re-arrange force vector
F_vec2=F_vec(1,1);
for i=1:8
   F_vec2=[F_vec2 F_vec(i,2) F_vec(i,3)*2];
end
F_vec2(17)=F_vec2(17)/2;
F_vec=F_vec2;
%_____________________________________________
%
function [z,conn,x_vec,y_vec,free]=geometric_prop_program01(...
n_layer,t,ne,nnode,problem,abolub,hzero,aci)
% h=lamina thickness
%_____________________________________________
% Generate vector z
% z(k,1)=coordinate of the upper surface
% z(k,2)=coordinate of the lower surface

%
if n_layer==2
   h=t/2;
   z=[0 -h;
      h 0];
elseif n_layer==4
   z=[hzero-t/2 -t/2;
      0 hzero-t/2;
      t/2-hzero 0;
      t/2 t/2-hzero];
```

```
end
%
% ne: number of elements 64
% connectivity data
conn1=[1 26 27 28 29 25 3 2;   3 25 29 30 31 24 5 4;   5 24 31 32 33 23 7 6;
   7 23 33 34 35 22 9 8;   9 22 35 36 37 21 11 10;   11 21 37 38 39 20 13 12;
   13 20 39 40 41 19 15 14;   15 19 41 42 43 18 17 16];
conn=[conn1;  conn1+26*1;  conn1+26*2;  conn1+26*3;  conn1+26*4;  conn1+26*5;
   conn1+26*6;  conn1+26*7;  conn1+26*8;  conn1+26*9;  conn1+26*10;
   conn1+26*11;  conn1+26*12;  conn1+26*13;  conn1+26*14;  conn1+26*15;];
vec1=ones(1,17);
vec2=ones(1,9);
x_vec=[vec1*0,     vec2*0.5,     vec1*1,     vec2*1.5,     vec1*2,     vec2*2.5,...
     vec1*3,     vec2*3.5,     vec1*4,     vec2*4.5,     vec1*5,     vec2*5.5,...
     vec1*6,     vec2*6.5,     vec1*7,     vec2*7.5,     vec1*8,     vec2*8.5,...
     vec1*9,     vec2*9.5,     vec1*10,     vec2*10.5,     vec1*11,     vec2*11.5,...
     vec1*12,     vec2*12.5,     vec1*13,     vec2*13.5,     vec1*14,     vec2*14.5,...
     vec1*15,     vec2*15.5,     vec1*16]*100/16*abolub;
vec3=0:16;
vec4=16:-2:0;
y_vec=[vec3,vec4,     vec3,vec4,     vec3,vec4,     vec3,vec4,     vec3,vec4,...
     vec3,vec4,     vec3,vec4,     vec3,vec4,     vec3,vec4,     vec3,vec4,...
     vec3,vec4,     vec3,vec4,     vec3,vec4,     vec3,vec4,     vec3,vec4,...
     vec3,vec4,     vec3]*100/16;
%
aci=abs(aci);
x_vec=x_vec+y_vec*sin(aci*pi/180);
y_vec=y_vec*cos(aci*pi/180);
%
% apply simply supported boundary conditions
% inner nodes
vec5=[19:25,28:42];
vec6=[vec5+26*0,...
     vec5+26*1,     vec5+26*2,     vec5+26*3,     vec5+26*4,     vec5+26*5,...
     vec5+26*6,     vec5+26*7,     vec5+26*8,     vec5+26*9,     vec5+26*10,...
     vec5+26*11,     vec5+26*12,     vec5+26*13,     vec5+26*14,     409:415];
f1=[vec6]*5-4;% u
f2=[vec6]*5-3;% v
f3=[vec6]*5-2;% w
f4=[vec6]*5-1;% teta_x
f5=[vec6]*5;% teta_y
%
% node 1 is excluded from the list (y=b)
f6=[26 27 52 53 78 79 104 105 130 131 156 157 182 183 208 209 234 235 260 261 286 287
312 313 338 339 364 365 390 391 416 417]*5-4;%u~=0
f7=[26 27 52 53 78 79 104 105 130 131 156 157 182 183 208 209 234 235 260 261 286 287
312 313 338 339 364 365 390 391 416 417]*5-3;%v~=0
f8=[26 27 52 53 78 79 104 105 130 131 156 157 182 183 208 209 234 235 260 261 286 287
312 313 338 339 364 365 390 391 416 417]*5;%tetay~=0
% x=0
f9=[];%[2:16]*5-4;%u~=0
f10=[];%[2:16]*5-3;%v~=0
f11=[1:17]*5-1;%tetax~=0
% node 17 is excluded from the list (y=0)
```

```
f12=[18 43 44 69 70 95 96 121 122 147 148 173 174 199 200 225 226 251 252 277 278 303
304 329 330 355 356 381 382 407 408 433]*5-4;%u~=0
f13=[18 43 44 69 70 95 96 121 122 147 148 173 174 199 200 225 226 251 252 277 278 303
304 329 330 355 356 381 382 407 408 433]*5-3;%v~=0
f14=[18 43 44 69 70 95 96 121 122 147 148 173 174 199 200 225 226 251 252 277 278 303
304 329 330 355 356 381 382 407 408 433]*5;%tetay~=0
% x=a
f15=[418:432]*5-4;%u~=0
f16=[418:432]*5-3;%v~=0
f17=[418:432]*5-1;%tetax~=0
%
free=sort([f1 f2 f3 f4 f5 f6 f7 f8 f9 f10 f11 f12 f13 f14 f15 f16 f17]);% free dof
%_____________________________________________________________________
```

A.2.1 Plate element sub-programs

A.2.1.1 Plate element stiffness matrix

```
%_____________________________________________________________________
function [kelem]=sub_program_element_stiffness(...
x_vec,y_vec,A,B,D,Cs,thickness,alpha_vec)
% Izzet Ufuk Çagdas, 2005
%_____________________________________________________________________
% INPUT VARIABLES
% x_vec: vector of x coordinates of the nodes
% y_vec: vector of y coordinates of the nodes
% A,B,D,Cs: Material matrices
% thickness: plate thickness
% alpha_vec: vector of transformation angles of the nodes of an element, which has 8 entries. A
% zero entry in this vector means that the corresponding node will not be transformed.
%_____________________________________________________________________
% OUTPUT VARIABLES
% kelem: element stiffness matrix
%_____________________________________________________________________
% Calculation of the element stiffness matrix
kelem=[]; initialize element stiffness matrix
ngl=2;% number of Gauss points (reduced integration!)
% Determine Gauss points and corresponding weights
nglx=ngl;ngly=ngl;
[point,weight]=sub_program_gauss_point_plate(nglx);
% Calculate element stiffness matrix
kelem(40,40)=0;% Initialize matrices by equating all of the elements to zero
kelem1(40,40)=0;
kelem2(40,40)=0;
kelem3(40,40)=0;
kelem4(40,40)=0;
kelem5(40,40)=0;
% Start numerical integration to compute matrix 'kelem'
for intx=1:nglx
   r=point(intx);
   wtx=weight(intx);
   for inty=1:ngly
      s=point(inty);
      wty=weight(inty);
      % Evaluate values of shape function and its derivative at the gauss point
```

```
      [N,Nt]=sub_program_sfrsh8_plate(r,s);
      % Calculate Jacobian at r,s
      [Jacob]=sub_program_calculate_jacobian_8node(Nt,x_vec,y_vec);
      % Calculate B matrices
      [BM1,BM2,BM3]=sub_program_bmatrix_plate(N,Nt,Jacob);
      kelem1=kelem1+BM1'*A*BM1*wtx*wty*det(Jacob);%thickness*
      kelem2=kelem2+BM2'*B*BM1*wtx*wty*det(Jacob);%thickness*
      kelem3=kelem3+BM2'*D*BM2*wtx*wty*det(Jacob);
      kelem4=kelem4+BM1'*B*BM2*wtx*wty*det(Jacob);
      kelem5=kelem5+BM3'*Cs*BM3*wtx*wty*det(Jacob);
   end
end
kelem=kelem1+kelem2+kelem3+kelem4+kelem5;
%_____________________________________________________________________
% Transformation due to inclined boundaries
% extract element nodal transformation angles from transformation matrix
[TMat]=sub_program_transform_matrix(alpha_vec);
kelem=TMat*kelem*TMat';
%_____________________________________________________________________
```

A.2.1.2 Plate element geometric stiffness matrix

```
%_____________________________________________________________________
function [gelem]=sub_program_element_geometric_stiffness(...
elem_no,conn,deplasman,x_vec,y_vec,A,B,thickness,alpha_vec)
% Izzet Ufuk Çagdas, 2005
%_____________________________________________________________________
% INPUT VARIABLES
% elem_no: element number
% deplasman: nodal displacement vector
% x_vec: vector of x coordinates of the nodes
% y_vec: vector of y coordinates of the nodes
% A,B: Material matrices
% thickness: plate thickness
% alpha_vec: vector of transformation angles of the nodes of an element, which has 8 entries. A
% zero entry in this vector means that the corresponding node will not be transformed.
%_____________________________________________________________________
% OUTPUT VARIABLES
% gelem: element geometric stiffness matrix
%_____________________________________________________________________
% First calculate the membrane stresses at the Gauss points.
[N_mat]=sub_program_calculate_membrane_forces(...
elem_no,conn,deplasman,x_vec,y_vec,A,B,alpha_vec);
%_____________________________________________________________________
% Calculation of the element stiffness matrix
gelem=[]; initialize element geometric stiffness matrix
ngl=2;% number of Gauss points (reduced integration!)
% Determine Gauss points and corresponding weights
nglx=ngl;ngly=ngl;
[point,weight]=sub_program_gauss_point_plate(nglx);
% Calculate element geometric stiffness matrix
gelem(40,40)=0;% Initiate 'gelem' by equating all of the elements to zero
% Start integration to compute matrix kelem
gelem1(8,8)=0;gelem2(8,8)=0;gelem3(8,8)=0;gelem4(8,8)=0;
sayac=0;
```

```
for intx=1:nglx
  r=point(intx);
  wtx=weight(intx);
  for inty=1:ngly
    sayac=sayac+1;
    s=point(inty);
    wty=weight(inty);
    % extract membrane forces from the membrane stress matrix 'N_mat'
    Nxx=N_mat(1,sayac);
    Nyy=N_mat(2,sayac);
    Nxy=N_mat(3,sayac);
    %
    % Evaluate values of shape function and its derivative at the gauss point
    [N,Nt]=sub_program_sfrsh8_plate(r,s);
    % Calculate Jacobian at r,s
    [Jacob]=sub_program_calculate_jacobian_8node(Nt,x_vec,y_vec);
    % Calculate B matrices
    [GM1,GM2]=gmatrix_plate(N,Nt,Jacob);
    gelem1=gelem1+Nxx*thickness*GM1*GM1'*wtx*wty*det(Jacob);
    gelem2=gelem2+Nxy*thickness*GM1*GM2'*wtx*wty*det(Jacob);
    gelem3=gelem3+Nxy*thickness*GM2*GM1'*wtx*wty*det(Jacob);
    gelem4=gelem4+Nyy*thickness*GM2*GM2'*wtx*wty*det(Jacob);
  end
end
gelem_tmp=gelem1+gelem2+gelem3+gelem4;
gelem([3 8 13 18 23 28 33 38],[3 8 13 18 23 28 33 38])=gelem_tmp;
% add the second order terms of u and v.
gelem([1 6 11 16 21 26 31 36],[1 6 11 16 21 26 31 36])=gelem_tmp;
gelem([2 7 12 17 22 27 32 37],[2 7 12 17 22 27 32 37])=gelem_tmp;
%_____________________________________________________________________
% Transformation due to inclined boundaries
% extract element nodal transformation angles from transformation matrix
[TMat]=sub_program_transform_matrix(alpha_vec);
gelem=TMat*gelem*TMat';
%_____________________________________________________________________
function [GM1,GM2]=gmatrix_plate(N,Nt,J)
% N and Nt were calculated for a given Gauss point
% Calculate GM matrices
Js=inv(J);
GM1=[];
GM2=[];
%
for i=1:8
  Nix=Nt(1,i)*Js(1,1)+Nt(2,i)*Js(1,2);
  Niy=Nt(1,i)*Js(2,1)+Nt(2,i)*Js(2,2);
  % 1
  GM1=[GM1;Nix];
  GM2=[GM2;Niy];
end
%_____________________________________________________________________
```

A.2.1.3 Plate element strain-displacement matrices

```
%_____________________________________________________________________
function [Bepsilon,Bkappa,Baf]=sub_program_bmatrix_plate(N,Nt,J);
% Izzet Ufuk Çagdas, 2005
%_____________________________________________________________________
% INPUT VARIABLES
% N, Nt: The vectors of shape functions and their first derivatives at the Gauss point
% J: Jacobian matrix
%_____________________________________________________________________
% OUTPUT VARIABLES
% Bepsilon, Bkappa, Bafi: strain-displacement matrices at the Gauss point
%_____________________________________________________________________
% Calculate B matrix
Js=inv(J);
Bepsilon=[];Bkappa=[];Baf=[]; % initialize output matrices
for i=1:8
   Nix=Nt(1,i)*Js(1,1)+Nt(2,i)*Js(1,2);
   Niy=Nt(1,i)*Js(2,1)+Nt(2,i)*Js(2,2);
   % 1
   Bepsilon_i=[Nix 0 0 0 0;
      0 Niy 0 0 0;
      Niy Nix 0 0 0];
   Bepsilon=[Bepsilon Bepsilon_i];
   % 2
   Bkappa_i=[0 0 0 -1*Nix 0;
      0 0 0 0 -1*Niy;
      0 0 0 -1*Niy -1*Nix];
   Bkappa=[Bkappa Bkappa_i];
   % 3
   Baf_i=[0 0 Nix -1*N(i) 0;
      0 0 Niy 0 -1*N(i)];
   Baf=[Baf Baf_i];
end
%_____________________________________________________________________
```

A.2.1.4 Plate element Jacobian matrix

```
%_____________________________________________________________________
function [Jacob]=sub_program_calculate_jacobian_8node(Nt,x,y)
% Izzet Ufuk Çagdas, 2005
%_____________________________________________________________________
% INPUT VARIABLES
% Nt: The vector of first derivatives of the shape functions at the Gauss point
% x,y: Cartesian coordinates of the Gauss point
%_____________________________________________________________________
% OUTPUT VARIABLES
% Jacob: Jacobian matrix at the Gauss point
%_____________________________________________________________________
% Calculate Jacobian at given Gauss Point - r,s
A=[Nt(1,1) Nt(1,2) Nt(1,3) Nt(1,4) Nt(1,5) Nt(1,6) Nt(1,7) Nt(1,8);
   Nt(2,1) Nt(2,2) Nt(2,3) Nt(2,4) Nt(2,5) Nt(2,6) Nt(2,7) Nt(2,8)];
B=[x(1) y(1); x(2) y(2); x(3) y(3); x(4) y(4); x(5) y(5); x(6) y(6); x(7) y(7); x(8) y(8)];
Jacob=A*B;
%_____________________________________________________________________
```

A.2.1.5 Assembly of the global stiffness matrix

```
%_____________________________________________________________________
function [KGE]=sub_program_assemble_KGE_plate(...
nelem,nnode,conn,x_vec,y_vec,A,B,D,Cs,t,Trans_vec)
% Izzet Ufuk Çagdas, 2005
%_____________________________________________________________________
% INPUT VARIABLES
% nelem: total number of elements
% nnode: total number of nodes
% conn: element connectivity matrix
% x_vec, y_vec: cartesian coordinate vectors
% A,B,D,Cs: material matrices
% Trans_vec: Transformation matrix
%_____________________________________________________________________
% OUTPUT VARIABLES
% KGE: global stiffness matrix
% Note: All of the elements are made of same material with same thicknesses
%_____________________________________________________________________
% set Trans_vec equal to zero if the transformation vector is not entered
if nargin==10;
   Trans_vec(nelem,8)=0;
end
KGE(nnode*5,nnode*5)=0;% initialize the global stiffness matrix
KGE=sparse(KGE);
% set up the global stiffness matrix
for i=1:nelem%number of elements
   % add contributions of all of the elements
   % calculate stiffness matrix of element i
[ke]=sub_program_element_stiffness(x_vec(conn(i,:)),y_vec(conn(i,:)),A,B,D,Cs,t,...
Trans_vec(i,:));
   % place the stiffness components in the global stiffness matrix
   vec=[];
   for j=1:8
      % numbers of the dofs of the ith element
      vec=[vec conn(i,j)*5-4 conn(i,j)*5-3 conn(i,j)*5-2 conn(i,j)*5-1 conn(i,j)*5];
   end
   KGE(vec,vec)=KGE(vec,vec)+ke;
end
%_____________________________________________________________________
```

A.2.1.6 Assembly of the global geometric stiffness matrix

```
%_____________________________________________________________________
function [GSM]=sub_program_assemble_GSM_plate(...
nelem,nnode,conn,x_vec,y_vec,deplasman,A,B,t,Trans_vec)
% Izzet Ufuk Çagdas, 2005
%_____________________________________________________________________
% INPUT VARIABLES
% nelem: total number of elements
% nnode: total number of nodes
% conn: element connectivity matrix
% x_vec, y_vec: cartesian coordinate vectors
% A,B: material matrices
% t: thickness
```

```
% Trans_vec: Transformation matrix
%_____________________________________________________________________
% OUTPUT VARIABLES
% GSM: global geometric stiffness matrix
% Note: All of the elements are made of same material with same thicknesses
%_____________________________________________________________________
% set Trans_vec equal to zero if the transformation vector is not defined.
if nargin==9;
   Trans_vec(nelem,8)=0;
end
GSM(nnode*5,nnode*5)=0; % set up the global geometric stiffness matrix
GSM=sparse(GSM);
for i=1:nelem%number of elements
   % add contributions of all of the elements
[gelem]=sub_program_element_geometric_stiffness(i,conn,deplasman,x_vec(conn(i,:)),...
y_vec(conn(i,:)),A,B,t,Trans_vec(i,:));
   % place the stiffness components in GSM
   vec=[];
   for j=1:8
      % numbers of the dofs of the ith element
      vec=[vec conn(i,j)*5-4 conn(i,j)*5-3 conn(i,j)*5-2 conn(i,j)*5-1 conn(i,j)*5];
   end
   GSM(vec,vec)=GSM(vec,vec)+gelem;
end
%_____________________________________________________________________
```

A.2.1.7 Calculation of material matrices

```
%_____________________________________________________________________
function [A,B,D,Cs]=sub_program_calculate_material_matrices(...
teta_vec,E1,E2,nu12,G12,G23,G13,N,z)
% Izzet Ufuk Çagdas, 2005
%_____________________________________________________________________
% INPUT VARIABLES
% teta_vec: lamination angles of the layers (starting from the top layer)
% E1,E2,nu12,G12,G23,G13: material properties. It is assumed that all of the layers are made
% up of the same material
% N: number of layers
% z(k,1)=coordinate of the upper surface
% z(k,2)=coordinate of the lower surface
%_____________________________________________________________________
% OUTPUT VARIABLES
% A,B,D,Cs: material matrices
%
% initialize matrices
A(3,3)=0;B(3,3)=0;Cs(2,2)=0;D(3,3)=0;
for k=1:N
   % calculate stiffness coefficients
[Qh,Qh2]=sub_program_calculate_reduced_stiff(teta_vec(k),E1(k),E2(k),nu12(k),G12(k),...
G23(k),G13(k));
   for i=1:3
      for j=1:3
         A(i,j)=A(i,j)+Qh(i,j)*(z(k,1)-z(k,2));
         B(i,j)=B(i,j)+Qh(i,j)*(z(k,1)^2-z(k,2)^2);
         D(i,j)=D(i,j)+Qh(i,j)*(z(k,1)^3-z(k,2)^3);
```

```
      end
   end
end
B=(1/2)*B;
D=(1/3)*D;
for k=1:N
   % calculate stiffness coefficients
[Qh,Qh2]=sub_program_calculate_reduced_stiff(teta_vec(k),E1(k),E2(k),nu12(k),G12(k),...
G23(k),G13(k));
   for i=1:2
      for j=1:2
         Cs(i,j)=Cs(i,j)+Qh2(i,j)*(z(k,1)-z(k,2));
      end
   end
end
% correction for shear
Cs=5/6*Cs; % shear correction factor is taken as equal to 5/6
%_____________________________________________________________________
```

A.2.1.8 Calculation of reduced stiffnesses

```
%_____________________________________________________________________
function [Qh,Qh2]=sub_program_calculate_reduced_stiff(...
angle_1,E1,E2,nu12,G12,G23,G13)
% Izzet Ufuk Çagdas, 2005
%_____________________________________________________________________
% INPUT VARIABLES
% angle_1: the angle from the x-axis to the 1-axis (in degrees)
% E1,E2: Young's moduli in the 1,2 directions
% G12: Shear modulus in the 1-2 plane
% nu12: Poisson's ratio (extension-extension coupling coefficient)
% the negative of the transverse strain in the 2-direction over the strain in the 1 direction when
% stress is applied in the 1-direction.
%_____________________________________________________________________
% OUTPUT VARIABLES
% Qh1, Qh2: reduced stiffnesses
%_____________________________________________________________________
%
nu21=(E2/E1)*nu12;
Q11=E1/(1-nu12*nu21);
Q12=nu12*E2/(1-nu12*nu21);
Q22=E2/(1-nu12*nu21);
Q66=G12;
Q44=G23;
Q55=G13;
c=cos(angle_1*pi/180); % convert into radians
s=sin(angle_1*pi/180); % convert into radians
%
Qh11=Q11*c^4+2*(Q12+2*Q66)*s^2*c^2+Q22*s^4;
Qh12=(Q11+Q22-4*Q66)*s^2*c^2+Q12*(s^4+c^4);
Qh22=Q11*s^4+2*(Q12+2*Q66)*s^2*c^2+Q22*c^4;
Qh16=(Q11-Q12-2*Q66)*s*c^3+(Q12-Q22+2*Q66)*s^3*c;
Qh26=(Q11-Q12-2*Q66)*s^3*c+(Q12-Q22+2*Q66)*s*c^3;
Qh66=(Q11+Q22-2*Q12-2*Q66)*s^2*c^2+Q66*(s^4+c^4);
Qh=[Qh11 Qh12 Qh16;
```

```
   Qh12 Qh22 Qh26;
   Qh16 Qh26 Qh66];
%
Qh44=Q44*c^2+Q55*s^2;
Qh45=(Q55-Q44)*c*s;
Qh55=Q44*s^2+Q55*c^2;
Qh2=[Qh55 Qh45;
   Qh45 Qh44];
%_____________________________________________________________________
```

A.2.1.9 Gauss integration

```
%_____________________________________________________________________
function [point1,weight1]=sub_program_gauss_point_plate(ngl)
% Izzet Ufuk Çagdas, 2005
%_____________________________________________________________________
% INPUT VARIABLES
% ngl: number of Gauss points
%_____________________________________________________________________
% OUTPUT VARIABLES
% point1, weight1: Gauss point coordinates in the local C.S., and corresponding weights
%_____________________________________________________________________
point1=zeros(ngl,1);weight1=zeros(ngl,1);
if ngl==1
   point1(1)=0;
   weight1(1)=2;
elseif ngl==2
   point1=[-1/sqrt(3);1/sqrt(3)];
   weight1=[1;1];
elseif ngl==3
   point1=[-1*sqrt(0.6);0;sqrt(0.6)];
   weight1=[5/9;8/9;5/9];
elseif ngl==4
   point1=[-0.861136311594053;...
-0.339981043584856;0.339981043584856;0.861136311594053];
weight1=[0.347854845137454;0.652145154862546;0.652145154862546;0.347854845137454];
end
%_____________________________________________________________________
```

A.2.1.10 Calculation of element transformation matrix

```
%_____________________________________________________________________
function [TMat]=sub_program_transform_matrix(alpha_vec)
% Izzet Ufuk Çagdas, 2005
%_____________________________________________________________________
% INPUT VARIABLES
% alpha_vec: vector of transformation angles of the nodes of an element, which has 8 entries. A
% zero entry in this vector means that the corresponding node will not be transformed.
%_____________________________________________________________________
% OUTPUT VARIABLES
% TMAt: Element transformation matrix
%_____________________________________________________________________
%
```

```
for i=1:8
   c=cos(alpha_vec(i));
   s=sin(alpha_vec(i));%*pi/180
   Ti(5,5)=0;  Ti(1,1)=c;  Ti(1,2)=s;  Ti(2,1)=-1*s;  Ti(2,2)=c;  Ti(3,3)=1;  Ti(4,4)=c;
   Ti(4,5)=s;  Ti(5,4)=-1*s;  Ti(5,5)=c;
   %
   TMat(i+4*(i-1):i+4*(i-1)+4,i+4*(i-1):i+4*(i-1)+4)=Ti;
end
% Assembly of the global matrices is performed in the usual way. However, the displacements
% and reactions are transformed back to the global reference frame before evaluating the
% stresses.
%_____________________________________________________________________
```

A.2.1.11 Calculation of membrane forces at the Gauss points

```
%_____________________________________________________________________
function [N_mat]=sub_program_calculate_membrane_forces(...
elem_no,conn,deplasman,x_vec,y_vec,A,B,alpha_vec)
% Izzet Ufuk Çagdas, 2005
%_____________________________________________________________________
% INPUT VARIABLES
% elem_no: number of the element
% nnode: total number of nodes
% conn: element connectivity matrix
% x_vec, y_vec: cartesian coordinate vectors
% A,B: material matrices
% t: thickness
% alpha_vec: vector of transformation angles of the nodes of an element, which has 8 entries. A
% zero entry in this vector means that the corresponding node will not be transformed.
%_____________________________________________________________________
% OUTPUT VARIABLES
% In-plane (membrane) forces of element elem_no are calculated. First calculate strains at the
% Gauss point. Then multiply strain vectors with B and A matrices to calculate the membrane
% forces at the GP. The membrane forces are stored in output matrix. (3x4 matrix), i.e. 1 force
% component at 4 Gauss points (N_mat => 3x4)
%_____________________________________________________________________
% i: element number
% GP: Gauss Point
%
% Calculation of element displacement vector
i=elem_no;
% extract nodes of the element from the connectivity vector
element_nodes=conn(i,:);
% generate displacement vector for element i
disp_i=[];
for j=1:8
   node_j=element_nodes(j);% jth node of ith element
   vec_ij=[node_j*5-4,node_j*5-3,node_j*5-2,node_j*5-1,node_j*5];
   disp_i=[disp_i deplasman(vec_ij)];
end
% Transform displacements into the global c.s.
[TMat]=sub_program_transform_matrix(alpha_vec);
disp_i=TMat'*disp_i';
disp_i=disp_i';
```

```
%_____________________________________________________________________
% Calculation of strains and stresses at the gauss point
% Calculate strains at the Gauss points using B matrices
[point,weight]=sub_program_gauss_point_plate(2);% 2x2
sayac=0;
for intx=1:2
   r=point(intx);
   for inty=1:2
      sayac=sayac+1;
      s=point(inty);
      [N,Nt]=sub_program_sfrsh8_plate(r,s);
      [Jacob]=sub_program_calculate_jacobian_8node(Nt,x_vec,y_vec);
      [Bepsilon,Bkappa,Baf]=sub_program_bmatrix_plate(N,Nt,Jacob);
      % Calculate strain vectors at the Gauss point
      epsilon0_i=Bepsilon*disp_i';
      kappa_i=Bkappa*disp_i';
      %fi_i=Baf*disp_i';
      N_mat(:,sayac)=A*epsilon0_i+B*kappa_i;% constitutive eqn.
   end
end
%_____________________________________________________________________
```

A.2.1.12 Calculation of smoothed in-plane forces at the corner nodes

```
%_____________________________________________________________________
function [xMat,yMat,NxxMat,NyyMat,NxyMat]=sub_program_calc_nodal_inplane_force(...
   nnode,conn,deplasman,x_vec,y_vec,A,B,alpha_vec,graph_iste)
% Izzet Ufuk Çagdas, 2005
%_____________________________________________________________________
% INPUT VARIABLES
% nnode: total number of nodes
% conn: element connectivity matrix
% deplasman: nodal displacement matrix
% x_vec, y_vec: cartesian coordinate vectors
% A,B: material matrices
% alpha_vec: vector of transformation angles of the nodes of an element, which has 8 entries. A
% zero entry in this vector means that the corresponding node will not be transformed.
% graph_iste: plot in-plane force distributions if =1
%_____________________________________________________________________
% OUTPUT VARIABLES
% xMat, yMat: nodal cartesian coordinate matrices
% NxxMat,NyyMat,NxyMat : nodal in-plane force matrices
%_____________________________________________________________________
% Note: smoothed stresses can be calculated as well, but the function has to be modified to deal
% with layers.
x_vecydk=x_vec;
y_vecydk=y_vec;
%
track_vec=1:nnode; % keep track of corner nodes
% smoothing-bilinear extrapolation matrix
smooth_mat=[1+sqrt(3)/2 -1/2 1-sqrt(3)/2 -1/2;
   -1/2 1+sqrt(3)/2 -1/2 1-sqrt(3)/2;
   1-sqrt(3)/2 -1/2 1+sqrt(3)/2 -1/2;
   -1/2 1-sqrt(3)/2 -1/2 1+sqrt(3)/2];
```

```
%
% the stresses at the nodes will be stored in matrix N_node_mat
N_node_mat(nnode,4)=0;% explained below!
for ielem=1:length(conn)
   % First calculate the membrane stresses at the Gauss points.
   [N_mat]=sub_program_calculate_membrane_forces(...
ielem,conn,deplasman,x_vec(conn(ielem,:)),y_vec(conn(ielem,:)),A,B,alpha_vec(ielem,:));
   % N_mat is a 3x4 matrix
   % Note: The positions of the Gauss points are different in Hinton andOwen (1979)
   % Thus, N_mat will be modified as follows. Columns 1 2 3 4 becomes 1 4 3 2.
   N_mat_ydk=N_mat;
   N_mat(:,2)=N_mat_ydk(:,3);
   N_mat(:,3)=N_mat_ydk(:,4);
   N_mat(:,4)=N_mat_ydk(:,2);
   % now the formulation can be used.
   %
   % extract node 1 of element i
   node1=conn(ielem,1);% number of the 1st corner node of element i
   % extract node 3
   node3=conn(ielem,3);% number of the 1st corner node of element i
   % extract node 5
   node5=conn(ielem,5);% number of the 1st corner node of element i
   % extract node 7
   node7=conn(ielem,7);% number of the 1st corner node of element i
   %
   track_vec(node1)=0;track_vec(node3)=0;track_vec(node5)=0;track_vec(node7)=0;
   % only the node numbers of the midside nodes will not be equal to zero
   % extract the stresses at the Gauss points of element i
   Nxx_Gauss=N_mat(1,:);
   Nyy_Gauss=N_mat(2,:);
   Nxy_Gauss=N_mat(3,:);
   %
   % Calculate the membrane forces at the corner nodes
   tmp_vec1=smooth_mat*[Nxx_Gauss(1);Nxx_Gauss(2);Nxx_Gauss(3);Nxx_Gauss(4)];
Nxx_node1=tmp_vec1(1);Nxx_node3=tmp_vec1(2);Nxx_node5=tmp_vec1(3);Nxx_node7=tmp
_vec1(4);
   tmp_vec1=smooth_mat*[Nxy_Gauss(1);Nxy_Gauss(2);Nxy_Gauss(3);Nxy_Gauss(4)];
Nxy_node1=tmp_vec1(1);Nxy_node3=tmp_vec1(2);Nxy_node5=tmp_vec1(3);Nxy_node7=tmp
_vec1(4);
   tmp_vec1=smooth_mat*[Nyy_Gauss(1);Nyy_Gauss(2);Nyy_Gauss(3);Nyy_Gauss(4)];
Nyy_node1=tmp_vec1(1);Nyy_node3=tmp_vec1(2);Nyy_node5=tmp_vec1(3);Nyy_node7=tmp
_vec1(4);
   %
% smoothed values should subsequently be averaged to obtain unique values at nodes. This
% averaging can be done as follows;
% there are 3 force components at each node. Nxx,Nxy,Nyy will be stored (added) in the 1st,
% 2nd and 3rd columns. The 4th column will be used to count the number of elements which
% contribute to the node. The average can easily be found by dividing the first 3 columns by the
% 4th column.
   N_node_mat(node1,1)=N_node_mat(node1,1)+Nxx_node1;
   N_node_mat(node1,2)=N_node_mat(node1,2)+Nxy_node1;
   N_node_mat(node1,3)=N_node_mat(node1,3)+Nyy_node1;
   N_node_mat(node1,4)=N_node_mat(node1,4)+1;
% keep track of contributions from elements
   %
```

```
   N_node_mat(node3,1)=N_node_mat(node3,1)+Nxx_node3;
   N_node_mat(node3,2)=N_node_mat(node3,2)+Nxy_node3;
   N_node_mat(node3,3)=N_node_mat(node3,3)+Nyy_node3;
   N_node_mat(node3,4)=N_node_mat(node3,4)+1;
% keep track of contributions from elements
   %
   N_node_mat(node5,1)=N_node_mat(node5,1)+Nxx_node5;
   N_node_mat(node5,2)=N_node_mat(node5,2)+Nxy_node5;
   N_node_mat(node5,3)=N_node_mat(node5,3)+Nyy_node5;
   N_node_mat(node5,4)=N_node_mat(node5,4)+1;
% keep track of contributions from elements
   %
   N_node_mat(node7,1)=N_node_mat(node7,1)+Nxx_node7;
   N_node_mat(node7,2)=N_node_mat(node7,2)+Nxy_node7;
   N_node_mat(node7,3)=N_node_mat(node7,3)+Nyy_node7;
   N_node_mat(node7,4)=N_node_mat(node7,4)+1;
% keep track of contributions from elements
end
%
% Calculate average values
for inode=1:nnode
   if N_node_mat(inode,4)~=0 % if not a mid-side node, i.e. corner node
      N_node_mat(inode,[1 2 3])=N_node_mat(inode,[1 2 3])/N_node_mat(inode,4);
   end
end
%
track_vec2=1:nnode;
track_vec2=track_vec2-track_vec;
track_vec2(track_vec2==0)=[];% corner node numbers are in this vector
% Nxx
Nxx_mat=N_node_mat(:,1);
Nxx_mat=Nxx_mat(track_vec2,:);
Nxx_mat(abs(Nxx_mat)<1e-5)=0;
% Nxy
Nxy_mat=N_node_mat(:,2);
Nxy_mat=Nxy_mat(track_vec2,:);
Nxy_mat(abs(Nxy_mat)<1e-20)=0;
% Nyy
Nyy_mat=N_node_mat(:,3);
Nyy_mat=Nyy_mat(track_vec2,:);
Nyy_mat(abs(Nyy_mat)<1e-20)=0;
%
x_vec=x_vec';
y_vec=y_vec';
x_vec=x_vec(track_vec2,:);
y_vec=y_vec(track_vec2,:);
% This part is valid only for the specific example problem solved _____
for i=1:17
   NxxMat(i,:)=Nxx_mat(i*9-8:i*9)';
   NxyMat(i,:)=Nxy_mat(i*9-8:i*9)';
   NyyMat(i,:)=Nyy_mat(i*9-8:i*9)';
   xMat(i,:)=x_vec(i*9-8:i*9)';
   yMat(i,:)=y_vec(i*9-8:i*9)';
end_____________________________________________________________
%
```

```
figure(4)
if graph_iste==1
   % note: CONTOUR(X,Y,Z,N) X and Y specify the (x,y) coordinates of the surface
   % draw N contour lines, overriding the automatic value.
   [c,h]=contour(xMat,yMat,NxxMat,10);%Nxx_mat
   clabel(c,h);
   title('N_x_x','FontSize',12)
end
hold on
aa1=line([x_vecydk(1),x_vecydk(17)],[y_vecydk(1),y_vecydk(17)]);
aa2=line([x_vecydk(417),x_vecydk(433)],[y_vecydk(417),y_vecydk(433)]);
set(aa1,'linewidth',1,'color',[0 0 0]);
set(aa2,'linewidth',1,'color',[0 0 0]);
hold off
%print -djpeg program01_figureNxx
%
figure(5)
if graph_iste==1
   % note: CONTOUR(X,Y,Z,N) X and Y specify the (x,y) coordinates of the surface
   % draw N contour lines, overriding the automatic value.
   [c,h]=contour(xMat,yMat,NyyMat,10);%Nxx_mat
   clabel(c,h);
   title('N_y_y','FontSize',12)
end
%print -djpeg program01_figureNyy
%
figure(6)
if graph_iste==1
   % note: CONTOUR(X,Y,Z,N) X and Y specify the (x,y) coordinates of the surface
   % draw N contour lines, overriding the automatic value.
   [c,h]=contour(xMat,yMat,NxyMat,10);%Nxx_mat
   clabel(c,h);
   title('N_x_y','FontSize',12)
end
%print -djpeg program01_figureNxy
%_____________________________________________________________________
```

A.3 Functions for the finite element analysis of laminated shells

The function used for the calculation of the buckling load of a cylindrical panel subject to uni-axial edge loading is listed here. This function is used to solve the structural part of the panel optimization problem given in Section 4 of this thesis. Functions related to assembly of global matrices are not listed here as they're very similar to the ones given for plates.

```
%_____________________________________________________________________
function [Pcr,MS_failure_load_coeff]=program_panel_buckling_01(lam_ang,t,a,SS,BC,prob)
% Izzet Ufuk Çagdas, 2005 (Check the equations first!)
% Note: manually change V1=V3 x e2 in sub program 'sub_program_calc_normals_tangents'
%_____________________________________________________________________
% INPUT VARIABLES
% lam_ang: vector of lamination angles
% t: panel thickness
% a: panel length
% SS: stacking sequence number
```

```
% BC: boundary set number. BC=1,2,3 for SSSS, CCCC, CSCS cases, respectively
% prob: prob=2 axial compression / prob=1 uniform pressure
%_____
% OUTPUT VARIABLES
% Pcr: buckling load
% MS_failure_load_coeff: failure coefficient calculated according to maximum strain theory
%_____
nelem=128; % total number of elements
nnode=433;% total number of nodes
katsayi=1;
%_____
if SS==1
   teta_vec=90-[lam_ang -lam_ang 90 0 0 90 -lam_ang lam_ang];
elseif SS==2
   teta_vec=90-[lam_ang -lam_ang lam_ang -lam_ang -lam_ang lam_ang -lam_ang lam_ang];
elseif SS==3
   teta_vec=90-[90 0 lam_ang -lam_ang -lam_ang lam_ang 0 90];
elseif SS==4
   teta_vec=90-[0 90 lam_ang -lam_ang -lam_ang lam_ang 90 0];
elseif SS==5
   teta_vec=90-[lam_ang -lam_ang 0 90 90 0 lam_ang -lam_ang];
end
%_____
% INPUT DATA
aci=45*pi/180;kenar_aci=pi/2-aci/2;ara_aci=aci/16;
n_layer=8;
b=200;%
R=b/aci;%mm % aci*R=a
q=0;%N/mm^2
%_____material properties_____
E1=181e3;E2=10.3e3; %MPa
nu12=0.28;
G12=7.17e3;G23=G12;G13=G12;
% generate input vectors related to material
E1_vec(1:8)=E1;
E2_vec(1:8)=E2;
nu12_vec(1:8)=nu12;
G12_vec(1:8)=G12;
G23_vec(1:8)=G23;
G13_vec(1:8)=G13;
%_____
%
% Generate vector z
% z(k,1)=coordinate of the upper surface
% z(k,2)=coordinate of the lower surface
zet=t/8*[-3 -4;  -2 -3;  -1 -2;  0 -1;  1 0;  2 1;  3 2;  4 3];% mm.
%
%_____connectivity data_____
conn1=[1 26 27 28 29 25 3 2;
   3 25 29 30 31 24 5 4;
   5 24 31 32 33 23 7 6;
   7 23 33 34 35 22 9 8;
   9 22 35 36 37 21 11 10;
   11 21 37 38 39 20 13 12;
   13 20 39 40 41 19 15 14;
```

```
   15 19 41 42 43 18 17 16];
conn=[conn1;  conn1+26*1;  conn1+26*2;  conn1+26*3;  conn1+26*4;  conn1+26*5;
   conn1+26*6;  conn1+26*7;  conn1+26*8;  conn1+26*9;  conn1+26*10;
   conn1+26*11;  conn1+26*12;  conn1+26*13;  conn1+26*14;  conn1+26*15];
%_____________________________________________
% Generate the cartesian coordinate vectors of the mid. nodes
alp=aci/32;% 32 divisions
y_divis=a/16;
for i=1:16
   % MIDDLE NODES
   vec1=[1+(i-1)*26:17+(i-1)*26];
   vec2=[26+(i-1)*26:-1:18+(i-1)*26];
   %
   z_vec(vec1)=R*sin(pi/2-aci/2+alp*(i-1)*2)-R*cos(aci/2);
   z_vec(vec2)=R*sin(pi/2-aci/2+alp*(i-1)*2+alp)-R*cos(aci/2);
   y_vec(vec1)=y_divis*[0:16];
   y_vec(vec2)=y_divis*[0:2:16];
   x_vec(vec1)=R*cos(pi-(pi/2-aci/2+alp*2*(i-1)));
   x_vec(vec2)=R*cos(pi-(pi/2-aci/2+alp*2*(i-1)+alp));
   % UPPER NODES
   zu_vec(vec1)=(R+10*t/2)*(sin((pi/2-aci/2+alp*(i-1)*2)))-R*cos(aci/2);
   zu_vec(vec2)=(R+10*t/2)*(sin((pi/2-aci/2+alp*(i-1)*2+alp)))-R*cos(aci/2);
   yu_vec(vec1)=y_divis*[0:16];
   yu_vec(vec2)=y_divis*[0:2:16];
   xu_vec(vec1)=(R+10*t/2)*cos(pi-(pi/2-aci/2+alp*2*(i-1)));
   xu_vec(vec2)=(R+10*t/2)*cos(pi-(pi/2-aci/2+alp*2*(i-1)+alp));
   % LOWER NODES
   zl_vec(vec1)=(R-10*t/2)*(sin((pi/2-aci/2+alp*(i-1)*2)))-R*cos(aci/2);
   zl_vec(vec2)=(R-10*t/2)*(sin((pi/2-aci/2+alp*(i-1)*2+alp)))-R*cos(aci/2);
   yl_vec(vec1)=y_divis*[0:16];
   yl_vec(vec2)=y_divis*[0:2:16];
   xl_vec(vec1)=(R-10*t/2)*cos(pi-(pi/2-aci/2+alp*2*(i-1)));
   xl_vec(vec2)=(R-10*t/2)*cos(pi-(pi/2-aci/2+alp*2*(i-1)+alp));
end
% right hand side additional nodes
vec1=[417:433];
z_vec(vec1)=R*(sin((pi/2-aci/2+alp*32))-cos(aci/2));
y_vec(vec1)=y_divis*[0:16];
x_vec(vec1)=R*cos(pi-(pi/2-aci/2+alp*32));
%
zu_vec(vec1)=(R+10*t/2)*(sin((pi/2-aci/2+alp*32)))-R*cos(aci/2);
yu_vec(vec1)=y_divis*[0:16];
xu_vec(vec1)=(R+10*t/2)*cos(pi-(pi/2-aci/2+alp*32));
%
zl_vec(vec1)=(R-10*t/2)*(sin((pi/2-aci/2+alp*32)))-R*cos(aci/2);
yl_vec(vec1)=y_divis*[0:16];
xl_vec(vec1)=(R-10*t/2)*cos(pi-(pi/2-aci/2+alp*32));
%
% check mesh_____________________________
grafik_ciz=1;
grafik_ciz==1
figure(1)
hold on
for i=1:nelem
   cizgi=line(x_vec(conn(i,:)),y_vec(conn(i,:)),z_vec(conn(i,:)));
```

```
    set(cizgi,'color',[0 0 0],'linewidth',1);
    cizgi=line(xu_vec(conn(i,:)),yu_vec(conn(i,:)),zu_vec(conn(i,:)));
    set(cizgi,'color',[0 0 0],'linewidth',1)
    cizgi=line(xl_vec(conn(i,:)),yl_vec(conn(i,:)),zl_vec(conn(i,:)));
    set(cizgi,'color',[0 0 0],'linewidth',1)
end
xlabel('x-axis')
ylabel('y-axis')
zlabel('z-axis')
view(20,20)
hold off
pause
end
%___ SOLUTION _____________________________________________________________
%
% Calculate material matrices_____________________
[A,B,D,Cs]=sub_program_calculate_material_matrices(...
   teta_vec,E1_vec,E2_vec,nu12_vec,G12_vec,G23_vec,G13_vec,n_layer,zet);
%
% Assemble global stiffness matrix_____________________
[KGE]=assemble_KGE(nelem,nnode,conn,x_vec,y_vec,z_vec,xu_vec,yu_vec,zu_vec,xl_vec,y
l_vec,zl_vec,A,B,D,Cs,t);
%
% Assemble global load vector_____________________
load_vec(nnode*5)=0;% initialize load vector
if prob==1 % uniform pressure
   % set up the global stiffness matrix
   for i=1:nelem%number of elements
      % add contributions of all of the elements
      [fe]=sub_program_element_load_vector_shell_pr1(...
         x_vec(conn(i,:)),y_vec(conn(i,:)),z_vec(conn(i,:)),...
         xu_vec(conn(i,:)),yu_vec(conn(i,:)),zu_vec(conn(i,:)),...
         xl_vec(conn(i,:)),yl_vec(conn(i,:)),zl_vec(conn(i,:)),q);
      % place the load vector components into the global load vector
      vec=[];
      for j=1:8
         % numbers of the dofs of the ith element
         vec=[vec conn(i,j)*5-4 conn(i,j)*5-3 conn(i,j)*5-2 conn(i,j)*5-1 conn(i,j)*5];
      end
      load_vec(vec)=load_vec(vec)+fe;
   end
elseif prob==2 % uniaxial load
   load_vec([1 26 27 52 53 78 79 104 105 130 131 156 157 182 183 208 209 234 235 260...
 261 286 287 312 313 338 339 364 365 390 391 416 417]*5-3)=...
[2 4 2 4 2 4 2 4 2 4 2 4 2 4 2 4 2 4 2 4 2 4 2 4 2 4 2 4 2]/98*R*aci*katsayi;
   load_vec([17 18 43 44 69 70 95 96 121 122 147 148 173 174 199 200 225 226 251 252...
 277 278 303 304 329 330 355 356 381 382 407 408 433]*5-3)=...
[2 4 2 4 2 4 2 4 2 4 2 4 2 4 2 4 2 4 2 4 2 4 2 4 2 4 2 4 2]/98*R*aci*katsayi;
end
% Apply boundary conditions _____________________
if BC==1
   % inner nodes
   vec5=[19:25,28:42];
   vec6=[vec5+26*0,vec5+26*1,vec5+26*2,vec5+26*3,vec5+26*4,vec5+26*5,...
         vec5+26*6,vec5+26*7,vec5+26*8,vec5+26*9,vec5+26*10,vec5+26*11,...
```

```
        vec5+26*12,vec5+26*13,vec5+26*14,409:415];
   f1=[vec6]*5-4;% u
   f2=[vec6]*5-3;% v
   f3=[vec6]*5-2;% w
   f4=[vec6]*5-1;% teta_x
   f5=[vec6]*5;% teta_y
   % top nodes: vec_top
vec_top=[18 43 44 69 70 95 96 121 122 147 148 173 174 199 200 225 226 251 252 277 278
303 304 329 330 355 356 381 382 407 408];%17 and 433 are discarded
   % bottom nodes: vec_bot
vec_bot=[1 26 27 52 53 78 79 104 105 130 131 156 157 182 183 208 209 234 235 260 261 286
287 312 313 338 339 364 365 390 391 416 417];
   % straight edges: vec_str
   vec_str=[2:16 418:432];
   % Add rotations beta at the curved edges
   f6=[vec_top vec_bot]*5;% beta
   % Add rotations alpha at the straight edges
   f7=[vec_str]*5-1;% alpha
   % Add v of bottom nodes where the load is applied and the straight edges
   f8=[vec_bot vec_str]*5-3;% v
   free=sort([f1 f2 f3 f4 f5 f6 f7 f8]);
elseif BC==2% CCCC
...
% rest of the code is note listed as the calculations for the other boundary conditions are similar
...
end
%_____________________________________________________________________
% Solve static problem, calculate displacements and rotations
KGE=KGE(free,free);
load_vec2=load_vec(free);
inv_KGE=inv(KGE);
deplas=inv_KGE*load_vec2';
deplasman(nnode*5)=0;
deplasman(free)=deplas;% displacements of all of the nodes
%_____________________________________________________________________
% Plot normal force distributions (pre-buckling force distribution)
plot_membrane_forces=1;
if plot_membrane_forces==1
   % The forces at the nodes are extrapolated from the Gauss points
   Trans_vec(128,8)=0;
   [xMat,yMat,NxxMat,NyyMat,NxyMat]=sub_program_calc_stress_corner_node(nnode,...
   conn,deplasman,x_vec,y_vec,A,B,Trans_vec,1);
end
%_____________________________________________________________________
%
% Linearized buckling analysis
[GSM]=assemble_FGE(nelem,nnode,conn,deplasman,x_vec,y_vec,z_vec,xu_vec,yu_vec,...
   zu_vec,xl_vec,yl_vec,zl_vec,A,B,D,Cs,t);
Pcr=0;deplasman2=0;
GSM=GSM(free,free);
Klast=inv(KGE)*GSM;%
[aygenvec,P]=eigs(Klast,1);
P=diag(P);
P(P==0)=[];
P=1./P;P1=P(1);Pcr=P1;
```

```
% re-arrange
aygenvec_duz(nnode*5)=0;aygenvec_duz(free)=aygenvec;
deplasman3=aygenvec_duz;% use to plot the buckled geometry
disp('buckling parameter');
load=Pcr
%
%_____
% CHECK FAILURE USING MS FAILURE THEORY
% first-ply failure loads are calculated only if the buckling load causes failure
deplasman2=abs(Pcr)*deplasman;
%____calculate first-ply failure load using Maximum Strain failure criterion
if max(max(max(result_MS)))>1
[MS_failure_load_coeff]=fminbnd('sub_program_panel_buckling_03',0,1,[],Pcr,nelem,conn,...
   deplasman,x_vec,y_vec,z_vec,xu_vec,yu_vec,zu_vec,xl_vec,yl_vec,zl_vec,A,B,...
   n_layer,teta_vec,E1_vec,E2_vec,nu12_vec,G12_vec,G23_vec,G13_vec,zet,material)
else
   MS_failure_load_coeff=1000+max(max(max(result_MS)))
end
%_____
```

A.3.1 Shell element sub-programs

A.3.1.1 Shell element stiffness matrix

```
%_____
function [kelem]=stiffness_shell(x_mid,y_mid,z_mid,x_upper,y_upper,z_upper,...
   x_lower,y_lower,z_lower,A,B,D,Cs,thickness)
% Izzet Ufuk Çagdas, 2005
%_____
% INPUT VARIABLES
% x_mid,y_mid,z_mid: cartesian coordinate vectors of the mid-surfafe nodes
% x_upper,y_upper,z_upper: cartesian coordinate vectors of the upper-surfafe nodes
% x_lower,y_lower,z_lower: cartesian coordinate vectors of the lower-surfafe nodes
% A,B,D,Cs: material matrices
% thickness: element thickness (same for all of the nodes. May be modified if necessary)
%_____
% OUTPUT VARIABLES
% kelem: element stiffness matrix
%_____
%
% calculate normals and tangents to the midsurface at the nodes
[V1,V1_hat,V2,V2_hat,V3,V3_hat]=sub_program_calc_normals_tangents(...
   x_upper,x_lower,y_upper,y_lower,z_upper,z_lower);
%
% Determine Gauss points and corresponding weights
ngl=2; % reduced integration (solves shear locking problem)
nglx=ngl;ngly=ngl;
[point,weight]=sub_program_gauss_point_plate(nglx);
% Start integration to compute matrix kelem
kelem(40,40)=0;
kelem1(40,40)=0;
kelem2(40,40)=0;
kelem3(40,40)=0;
kelem4(40,40)=0;
```

```
kelem5(40,40)=0;
for intx=1:nglx
   r=point(intx);
   wtx=weight(intx);
   for inty=1:ngly
      s=point(inty);
      wty=weight(inty);
      [N,Nt]=sub_program_sfrsh8_plate(r,s);
% the normals and tangents at the Gauss point will be calculated using shape function
% interpolation from the nodal values. Thus an orthogonal  set of local coordinate axes
% (xpr,ypr,zpr) are constructed at any point (r,s) on the midsurface.
      xpr_vec=N*V1;
      xpr_hat=xpr_vec/sqrt(xpr_vec(1)^2+xpr_vec(2)^2+xpr_vec(3)^2);
      % xpr_hat: unit normal vector in xpr direction
      ypr_vec=N*V2;
      ypr_hat=ypr_vec/sqrt(ypr_vec(1)^2+ypr_vec(2)^2+ypr_vec(3)^2);
      zpr_vec=N*V3;
      zpr_hat=zpr_vec/sqrt(zpr_vec(1)^2+zpr_vec(2)^2+zpr_vec(3)^2);
      % define the transformation matrix btw local and global coord. sys.
      mupr=[xpr_hat;ypr_hat;zpr_hat];
      % call shell_jacob to calculate Jacobian
      [Jacob_rs]=shell_jacob(Nt,x_mid,y_mid,z_mid,xpr_hat,ypr_hat);
      % Calculate B matrices
      [BM1,BM2,BM3]=sub_program_bmatrix_shell(...
      N,Nt,Jacob_rs,mupr,V1_hat,V2_hat,V3_hat);
      % Numerical integration
      kelem1=kelem1+BM1'*A*BM1*wtx*wty*det(Jacob_rs);
      kelem2=kelem2+BM2'*B*BM1*wtx*wty*det(Jacob_rs);
      kelem3=kelem3+BM2'*D*BM2*wtx*wty*det(Jacob_rs);
      kelem4=kelem4+BM1'*B*BM2*wtx*wty*det(Jacob_rs);
      kelem5=kelem5+BM3'*Cs*BM3*wtx*wty*det(Jacob_rs);
   end
end
kelem=kelem1+kelem2+kelem3+kelem4+kelem5;
%_____________________________________________________________________
```

A.3.1.2 Shell element geometric stiffness matrix

```
function [gelem]=geometric_stiffness_shell3(elem_no,conn,deplasman,x_mid,y_mid,z_mid,...
   x_upper,y_upper,z_upper,x_lower,y_lower,z_lower,A,B,D,Cs)
% Izzet Ufuk Çagdas, 2005
%_____________________________________________________________________
% INPUT VARIABLES
% x_mid,y_mid,z_mid: cartesian coordinate vectors of the mid-surfafe nodes
% x_upper,y_upper,z_upper: cartesian coordinate vectors of the upper-surfafe nodes
% x_lower,y_lower,z_lower: cartesian coordinate vectors of the lower-surfafe nodes
% A,B,D,Cs: material matrices
%_____________________________________________________________________
% OUTPUT VARIABLES
% gelem:element geometric stiffness matrix
%_____________________________________________________________________
%
% First calculate the membrane forces, bending moments, and shear forces at the Gauss points
% of the shell element (in local coordinate system).
```

```
[N_mat,M_mat,SF_mat]=sub_program_calculate_NFBMSF_shell(...
   elem_no,conn,deplasman,x_mid,y_mid,z_mid,...
   x_upper,y_upper,z_upper,x_lower,y_lower,z_lower,A,B,D,Cs);
%_____________________________________________
% calculate normals and tangents to the midsurface at the nodes
[V1,V1_hat,V2,V2_hat,V3,V3_hat]=sub_program_calc_normals_tangents(...
   x_upper,x_lower,y_upper,y_lower,z_upper,z_lower);
%_____________________________________________
% Start numerical integration to compute matrix gelem
ngl=2;% reduced integration
nglx=ngl;ngly=ngl;
[point,weight]=sub_program_gauss_point_plate(nglx);
gelem(40,40)=0;% initialize gelem
sayac=0;%
for intx=1:nglx
   r=point(intx);
   wtx=weight(intx);
   for inty=1:ngly
      sayac=sayac+1;
      s=point(inty);
      wty=weight(inty);
      [N,Nt]=sub_program_sfrsh8_plate(r,s);
      % extract forces, moments, and shear forces.
      N11=N_mat(1,sayac);
      N22=N_mat(2,sayac);
      N12=N_mat(3,sayac);
      %
      Mx=M_mat(1,sayac);
      My=M_mat(2,sayac);
      Mxy=M_mat(3,sayac);
      %
      Qx=SF_mat(1,sayac);
      Qy=SF_mat(2,sayac);
      % the normals and tangents at the Gauss point will be calculated using shape function
      % interpolation from the nodal values. Thus an orthogonal set of local coordinate axes
      % (xpr,ypr,zpr) are constructed at any point (r,s) on the midsurface.
      xpr_vec=N*V1;
      xpr_hat=xpr_vec/sqrt(xpr_vec(1)^2+xpr_vec(2)^2+xpr_vec(3)^2);
      ypr_vec=N*V2;
      ypr_hat=ypr_vec/sqrt(ypr_vec(1)^2+ypr_vec(2)^2+ypr_vec(3)^2);
      zpr_vec=N*V3;
      zpr_hat=zpr_vec/sqrt(zpr_vec(1)^2+zpr_vec(2)^2+zpr_vec(3)^2);
      % call shell_jacob to calculate Jacobian
      [Jacob_rs]=shell_jacob(Nt,x_mid,y_mid,z_mid,xpr_hat,ypr_hat);
      % define the transformation matrix btw local and nodal coord. sys. for u,v,w
      mupr=[xpr_hat;ypr_hat;zpr_hat];
      %_____________
      [GM1,GM2]=sub_program_gmatrix_shell(N,Nt,Jacob_rs,mupr,V1_hat,V2_hat,V3_hat);
      % Normal forces
      Spr1=[N11 0 0 N12 0 0;
         0 N11 0 0 N12 0;
         0 0 N11 0 0 N12;
         N12 0 0 N22 0 0;
         0 N12 0 0 N22 0;
         0 0 N12 0 0 N22];
```

```
    % Moments and Shear Forces
    Spr2=[0 0 Mx 0 0 0 Mxy 0 Qx 0;
      0 0 0 Mx 0 0 0 Mxy 0 Qx;
      Mx 0 0 0 Mxy 0 0 0 0 0;
      0 Mx 0 0 0 Mxy 0 0 0 0;
      0 0 Mxy 0 0 0 Mx 0 Qy 0;
      0 0 0 Mxy 0 0 0 Mx 0 Qy;
      Mxy 0 0 0 Mx 0 0 0 0 0;
      0 Mxy 0 0 0 Mx 0 0 0 0;
      Qx 0 0 0 Qy 0 0 0 0 0;
      0 Qx 0 0 0 Qy 0 0 0 0];
    %
    gelem=gelem+GM1'*Spr1*GM1*wtx*wty*det(Jacob_rs)+...
      GM2'*Spr2*GM2*wtx*wty*det(Jacob_rs);
  end
end
%_____ Sub function used for the calculation of G matrices
function [GM1,GM2]=sub_program_gmatrix_shell(N,Nt,J,mupr,V1,V2,V3)
% N and Nt were calculated at a given Gauss point
% Calculate GM matrices
Js=inv(J);
GM1=[];
GM1_i=[];
GM2=[];
GM2_i=[];
%
for i=1:8
  Nix=Nt(1,i)*Js(1,1)+Nt(2,i)*Js(1,2);
  Niy=Nt(1,i)*Js(2,1)+Nt(2,i)*Js(2,2);
  % calculate matrix E
  E=mupr*[V1(i,:)' V2(i,:)' V3(i,:)'];
  %
  GM1_i=[Nix*mupr(1,1) Nix*mupr(1,2) Nix*mupr(1,3) 0 0;
    Nix*mupr(2,1) Nix*mupr(2,2) Nix*mupr(2,3) 0 0;
    Nix*mupr(3,1) Nix*mupr(3,2) Nix*mupr(3,3) 0 0;
    Niy*mupr(1,1) Niy*mupr(1,2) Niy*mupr(1,3) 0 0;
    Niy*mupr(2,1) Niy*mupr(2,2) Niy*mupr(2,3) 0 0;
    Niy*mupr(3,1) Niy*mupr(3,2) Niy*mupr(3,3) 0 0];
  %
  GM1=[GM1 GM1_i];
  %_____
  GM2_i=[Nix*mupr(1,1) Nix*mupr(1,2) Nix*mupr(1,3) 0 0;%u_x ok
    Nix*mupr(2,1) Nix*mupr(2,2) Nix*mupr(2,3) 0 0;%v_x ok
    0 0 0 Nix*E(2,2) Nix*E(2,1);%Tx_x ok
    0 0 0 -1*Nix*E(1,2) -1*Nix*E(1,1);%Ty_x ok
    Niy*mupr(1,1) Niy*mupr(1,2) Niy*mupr(1,3) 0 0;%u_y ok
    Niy*mupr(2,1) Niy*mupr(2,2) Niy*mupr(2,3) 0 0;%v_y ok
    0 0 0 Niy*E(2,2) Niy*E(2,1);%Tx_y ok
    0 0 0 -1*Niy*E(1,2) -1*Niy*E(1,1);%Ty_y ok
    0 0 0 E(2,2) E(2,1);%Tx ok
    0 0 0 -1*E(1,2) -1*E(1,1)];%Ty
  %
  GM2=[GM2 GM2_i];
end
%_____
```

A.3.1.3 Shell element strain-displacement matrices

```
%_____________________________________________________________________
function [Bepsilon,Bkappa,Baf]=sub_program_bmatrix_shell(N,Nt,J,mupr,V1,V2,V3);
% Izzet Ufuk Çagdas, 2005
%_____________________________________________________________________
% INPUT VARIABLES
% N, Nt: The value of shape functions and its first derivatives at the Gauss point
% J: Jacobian matrix
% mupr: μ'
% V1,V2,V3: surface normal and tangent vectors at the Gauss point
%_____________________________________________________________________
% OUTPUT VARIABLES
%Bepsilon, Bkappa, Baf: Strain-displacement matrices
%_____________________________________________________________________
%
Js=inv(J);
% B matrix is divided into three parts
Bepsilon=[];
Bkappa=[];
Baf=[];
E=[];%
for i=1:8
  % calculate matrix E
  E=mupr*[V1(i,:)' V2(i,:)' V3(i,:)']';% transformation matrix
  %
  Nix=Nt(1,i)*Js(1,1)+Nt(2,i)*Js(1,2);
  Niy=Nt(1,i)*Js(2,1)+Nt(2,i)*Js(2,2);
  % 1
  Bepsilon_i=[Nix*mupr(1,1) Nix*mupr(1,2) Nix*mupr(1,3) 0 0;
    Niy*mupr(2,1) Niy*mupr(2,2) Niy*mupr(2,3) 0 0;
    Nix*mupr(2,1)+Niy*mupr(1,1) Nix*mupr(2,2)+...
    Niy*mupr(1,2) Nix*mupr(2,3)+Niy*mupr(1,3) 0 0];
%
  Bepsilon=[Bepsilon Bepsilon_i];
%
  Bkappa_i=-1*[0 0 0 Nix*E(2,2) Nix*E(2,1);%(check -1) ok
    0 0 0 -1*Niy*E(1,2) -1*Niy*E(1,1);
    0 0 0 Niy*E(2,2)-Nix*E(1,2) Niy*E(2,1)-Nix*E(1,1)];
  %
  Bkappa=[Bkappa Bkappa_i];
  %
  Baf_i=[Nix*mupr(3,1) Nix*mupr(3,2) Nix*mupr(3,3) N(i)*E(2,2) N(i)*E(2,1);
    Niy*mupr(3,1) Niy*mupr(3,2) Niy*mupr(3,3) -1*N(i)*E(1,2) -1*N(i)*E(1,1)];
  Baf=[Baf Baf_i];% ;)
end
%_____________________________________________________________________
```

A.3.1.4 Shell element Jacobian matrix

```
%
function [Jacob]=shell_jacob(Nt,x_mid,y_mid,z_mid,xpr_hat,ypr_hat)
% Izzet Ufuk Çagdas, 2005
%_____________________________________________________________________
% INPUT VARIABLES
% Nt: first derivatives of the shape functions at the Gauss point
% x_mid,y_mid,z_mid: Cartesian coordinate vectors of the Gauss point
% xpr_hat,ypr_hat: unit vectors
%_____________________________________________________________________
% OUTPUT VARIABLES
% Jacob: Jacobian matrix
%_____________________________________________________________________
%
% Calculate Jacobian matrix relating the area integral in the xpr,ypr coordinates to the one in
% the r,s coordinates
% _____________first calculate x,r y,r z,r and x,s y,s z,s
delxdelr=Nt(1,:)*x_mid';
delydelr=Nt(1,:)*y_mid';
delzdelr=Nt(1,:)*z_mid';
%
delxdels=Nt(2,:)*x_mid';
delydels=Nt(2,:)*y_mid';
delzdels=Nt(2,:)*z_mid';
%_____________
%
Vr_vec=[delxdelr delydelr delzdelr];
Vs_vec=[delxdels delydels delzdels];
%
Jacob(1,1)=dot(Vr_vec,xpr_hat);
Jacob(1,2)=dot(Vr_vec,ypr_hat);
Jacob(2,1)=dot(Vs_vec,xpr_hat);
Jacob(2,2)=dot(Vs_vec,ypr_hat);
%_____________________________________________________________________
```

A.3.1.5 Calculation of surface normals and tangents

```
%_____________________________________________________________________
function [V1,V1_hat,V2,V2_hat,V3,V3_hat]=sub_program_calc_normals_tangents(...
x_upper,x_lower,y_upper,y_lower,z_upper,z_lower)
% Izzet Ufuk Çagdas, 2005
%_____________________________________________________________________
% INPUT VARIABLES
% x_upper,x_lower,y_upper,y_lower,z_upper,z_lower : Cartesian coordinate vectors
%_____________________________________________________________________
% OUTPUT VARIABLES
% V1,V1_hat,V2,V2_hat,V3,V3_hat: Surface normal and tangent vectors
%_____________________________________________________________________
%
% calculate normals and tangents to the midsurface at the nodes
for i=1:8
   V3x(i)=x_upper(i)-x_lower(i);
   V3y(i)=y_upper(i)-y_lower(i);
```

```
    V3z(i)=z_upper(i)-z_lower(i);
    V3(i,[1,2,3])=[V3x(i) V3y(i) V3z(i)];
    V3_hat(i,[1,2,3])=V3(i,[1,2,3])/...
       sqrt(V3(i,1)^2+V3(i,2)^2+V3(i,3)^2);
    % V1i=V3ixi % Manually change!
    V1(i,[1,2,3])=cross(V3(i,[1,2,3]),[0 -1 0]);
    V1_hat(i,[1,2,3])=V1(i,[1,2,3])/sqrt(V1(i,1)^2+V1(i,2)^2+V1(i,3)^2);
    % V2i=V3i x V1i
    V2(i,[1,2,3])=cross(V3_hat(i,[1,2,3]),V1_hat(i,[1,2,3]));
    V2_hat(i,[1,2,3])=V2(i,[1,2,3])/sqrt(V2(i,1)^2+V2(i,2)^2+V2(i,3)^2);
end
%
%_____________________________________________________________________
```

A.3.1.6 Functions used for the first-ply failure load calculations

```
%_____________________________________________________________________
function [failure_index_minus_one]=sub_program_panel_buckling_03(...
   coeff,Pcr,nelem,conn,deplasman,x_vec,y_vec,z_vec,xu_vec,yu_vec,zu_vec,...
   xl_vec,yl_vec,zl_vec,A,B,n_layer,teta_vec,E1_vec,E2_vec,nu12_vec,...
   G12_vec,G23_vec,G13_vec,zet,material)
% Izzet Ufuk Çagdas, 2005
%_____________________________________________________________________
% INPUT VARIABLES
% defined earlier
%_____________________________________________________________________
% OUTPUT VARIABLES
% failure_index_minus_one : failure index
%_____________________________________________________________________
%
deplasman2=coeff*abs(Pcr)*deplasman;
%
[result_wu,result_hill,result_MS]=sub_program_check_stresses_shell(nelem,conn,...
   deplasman2,x_vec,y_vec,z_vec,xu_vec,yu_vec,zu_vec,xl_vec,yl_vec,zl_vec,A,B,...
   n_layer,teta_vec,E1_vec,E2_vec,nu12_vec,G12_vec,G23_vec,G13_vec,zet,material,1);
max_failure_index=max(max(max(result_MS)));
failure_index_minus_one=abs(max_failure_index-1);
%_____________________________________________________________________

%_____________________________________________________________________
function [result_wu,result_hill,result_MS]=sub_program_check_stresses_shell(...
   nelem,conn,deplasman,x_mid,y_mid,z_mid,x_upper,y_upper,z_upper,x_lower,y_lower,...
   z_lower,A,B,nlayer,teta_vec,E1_vec,E2_vec,nu12_vec,G12_vec,G23_vec,G13_vec,...
   z,material,check_stress)
% Izzet Ufuk Çagdas, 2005
%_____________________________________________________________________
% INPUT VARIABLES
% if check_stress=1,2,3 then check failure using Tsai-Wu, Tsai-Hill, Max. Strain failure criteria
% other variables were defined earlier
%_____________________________________________________________________
% OUTPUT VARIABLES
% result_wu,result_hill,result_MS: failure indices
%_____________________________________________________________________
% Note: Check stresses at the Gauss points of element elem_no according to Tsi-Wu, Tsai
```

```
% Hill or maximum strain failure criteria. First calculate strains at the Gauss point using the
% nodal deformations. Then multiply strain vectors with B and A matrices to calculate the
% membrane forces at the GP (in local C.S.). the membrane forces are stored in output matrix.
% (3x4 matrix)i.e. 1 force component at 4 Gauss points then calculate the Gauss Point stresses
% at the upper and lower faces of the layers. (GP: Gauss Point)
% material: Graphite-Epoxy:1, Boron-Epoxy:2, Glass-Epoxy:3
%_____________________________________________________________________
% Strengths of unidirectional composites
% sigma1T: longitudinal tensile strength
% sigma1C: longitudinal compressive strength
% sigma2T: transverse tensile strength
% sigma2C: transverse tensile strength
% sigma12F: shear strength
if material==1% Graphite-Epoxy
   sigma1T=1500;%MPa  XT
   sigma1C=1500;%MPa  XC
   sigma2T=40;%MPa    YT
   sigma2C=246;%MPa   YC
   sigma12F=68;%MPa   T
   %
   sigma3C=0;%
   sigma3T=0;%
   sigma13F=0;%
   sigma23F=0;%psi
elseif material==2% Boron-Epoxy
   sigma1T=1260;%MPa
   sigma1C=2500;%MPa
   sigma2T=61;%MPa
   sigma2C=202;%MPa
   sigma12F=67;%MPa
elseif material==3% Glass-Epoxy
   sigma1T=1062;%MPa
   sigma1C=610;%MPa
   sigma2T=31;%MPa
   sigma2C=118;%MPa
   sigma12F=72;%MPa
elseif material==7% graphite-epoxy, Reddy
   sigma1T=219.5e3;%psi
   sigma1C=246.0e3;%psi
   sigma2T=6.35e3;%psi
   sigma2C=6.35e3;%psi
   sigma3C=0;%sigma2C;%psi
   sigma3T=0;%sigma2T;%psi
   sigma12F=12.60e3;%psi =sigma13F
   sigma13F=0;%sigma12F;
   sigma23F=0;%9.8e3;%psi
else %
   disp('unknown material')
end
%_____________________________________________________________________
% Extraction of element displacement vector
for i=1:nelem
   % extract nodes of the element from the connectivity vector
   element_nodes=conn(i,:);
   % generate displacement vector for element i
```

```
    disp_i=[];
    for j=1:8
      node_j=element_nodes(j);% jth node of ith element
      vec_ij=[node_j*5-4,node_j*5-3,node_j*5-2,node_j*5-1,node_j*5];
      disp_i=[disp_i deplasman(vec_ij)];
    end
%_____________________________________________________________________
    % Calculation of strains and stresses at the gauss point
    % calculate normals and tangents to the midsurface at the nodes
    [V1,V1_hat,V2,V2_hat,V3,V3_hat]=sub_program_calc_normals_tangents(...
    x_upper(conn(i,:)),x_lower(conn(i,:)),y_upper(conn(i,:)),y_lower(conn(i,:)),...
    z_upper(conn(i,:)),z_lower(conn(i,:)));
    % calculate strains at the Gauss points (using B matrices)
    [point,weight]=sub_program_gauss_point_plate(2);% reduced integration!
    sayac=0;fenasi=0;
    for intx=1:2
      r=point(intx);
      for inty=1:2
        sayac=sayac+1;
        s=point(inty);
        [N,Nt]=sub_program_sfrsh8_plate(r,s);
        xpr_vec=N*V1;
        xpr_hat=xpr_vec/sqrt(xpr_vec(1)^2+xpr_vec(2)^2+xpr_vec(3)^2);
        ypr_vec=N*V2;
        ypr_hat=ypr_vec/sqrt(ypr_vec(1)^2+ypr_vec(2)^2+ypr_vec(3)^2);
        zpr_vec=N*V3;
        zpr_hat=zpr_vec/sqrt(zpr_vec(1)^2+zpr_vec(2)^2+zpr_vec(3)^2);
        % define the transformation matrix btw local and global coord. sys.
        mupr=[xpr_hat' ypr_hat' zpr_hat'];
        % call shell_jacob to calculate Jacobian
[Jacob_rs]=shell_jacob(Nt,x_mid(conn(i,:)),y_mid(conn(i,:)),z_mid(conn(i,:)),xpr_hat,ypr_hat)
        % Calculate strain-displacement matrices
[Bepsilon,Bkappa,Baf]=sub_program_bmatrix_shell(N,Nt,Jacob_rs,mupr,...
  V1_hat,V2_hat,V3_hat);
        % Calculate strain vectors at the Gauss point
        epsilon0_i=Bepsilon*disp_i';
        kappa_i=Bkappa*disp_i';
        fi_i=Baf*disp_i';% not needed for calculating membrane forces.
        % The membrane forces are in local coordinate system.
        N_mat(:,sayac)=A*epsilon0_i+B*kappa_i;% constitutive eqn.
        % STRESS IS CALCULATED AT Z=H/2
        for i2=1:nlayer% layers
          [Qh,Qh2]=sub_program_calculate_reduced_stiff...
  (teta_vec(i2),E1_vec(i2),E2_vec(i2),nu12_vec(i2),G12_vec(i2),G23_vec(i2),G13_vec(i2));
          % Calculate stresses at the upper and lower surfaces of the layer in concern
          % there are 4 Gauss points. Stresses are calculated at each Gauss point seperately.
          % UPPER SURFACE
          moment_arm=z(i2,1);
          epsilon_i=epsilon0_i+(moment_arm)*kappa_i;
          sigmaxx_u(i,i2,sayac)=Qh(1,:)*epsilon_i;
          sigmayy_u(i,i2,sayac)=Qh(2,:)*epsilon_i;
          sigmaxy_u(i,i2,sayac)=Qh(3,:)*epsilon_i;
          %
          % LOWER SURFACE
          moment_arm=z(i2,2);
```

```
            epsilon_i=epsilon0_i+(moment_arm)*kappa_i;
            sigmaxx_l(i,i2,sayac)=Qh(1,:)*epsilon_i;
            sigmayy_l(i,i2,sayac)=Qh(2,:)*epsilon_i;
            sigmaxy_l(i,i2,sayac)=Qh(3,:)*epsilon_i;
            %
            % MID SURFACE
            moment_arm=(z(i2,1)+z(i2,2))/2;
            epsilon_i=epsilon0_i+(moment_arm)*kappa_i;
            sigmaxx_mid(i,i2,sayac)=Qh(1,:)*epsilon_i;
            sigmayy_mid(i,i2,sayac)=Qh(2,:)*epsilon_i;
            sigmaxy_mid(i,i2,sayac)=Qh(3,:)*epsilon_i;
            %
            % sigmaxz and sigmayz are constant through the thickness
            sigmaxz(i,i2,sayac)=Qh2(1,:)*fi_i;
            sigmayz(i,i2,sayac)=Qh2(2,:)*fi_i;
            %_____________________________________________________
            if check_stress==1
              %fprintf('element:%g - Gauss Point :%g - layer: %g\n',i,i2,sayac);
% TRANSFORM THE STRESSES Sxx,Sxy,Syy INTO PRINCIPAL MATERIAL C.S.
              c=cos(teta_vec(i2)*pi/180);
              s=sin(teta_vec(i2)*pi/180);
sigma1_lo(i,i2,sayac)=c^2*sigmaxx_l(i,i2,sayac)+s^2*sigmayy_l(i,i2,sayac)+...
              2*c*s*sigmaxy_l(i,i2,sayac);
sigma2_lo(i,i2,sayac)=s^2*sigmaxx_l(i,i2,sayac)+c^2*sigmayy_l(i,i2,sayac)-...
               2*c*s*sigmaxy_l(i,i2,sayac);
sigma12_lo(i,i2,sayac)=-c*s*(sigmaxx_l(i,i2,sayac)-sigmayy_l(i,i2,sayac))+...
               (c^2-s^2)*sigmaxy_l(i,i2,sayac);
sigma1_up(i,i2,sayac)=c^2*sigmaxx_u(i,i2,sayac)+s^2*sigmayy_u(i,i2,sayac)+...
               2*c*s*sigmaxy_u(i,i2,sayac);
sigma2_up(i,i2,sayac)=s^2*sigmaxx_u(i,i2,sayac)+c^2*sigmayy_u(i,i2,sayac)-...
               2*c*s*sigmaxy_u(i,i2,sayac);
sigma12_up(i,i2,sayac)=-c*s*(sigmaxx_u(i,i2,sayac)-sigmayy_u(i,i2,sayac))+...
               (c^2-s^2)*sigmaxy_u(i,i2,sayac);
sigma1_mid(i,i2,sayac)=c^2*sigmaxx_mid(i,i2,sayac)+s^2*sigmayy_mid(i,i2,sayac)+...
               2*c*s*sigmaxy_mid(i,i2,sayac);
sigma2_mid(i,i2,sayac)=s^2*sigmaxx_mid(i,i2,sayac)+c^2*sigmayy_mid(i,i2,sayac)-...
               2*c*s*sigmaxy_mid(i,i2,sayac);
sigma12_mid(i,i2,sayac)=-c*s*(sigmaxx_mid(i,i2,sayac)-sigmayy_mid(i,i2,sayac))+...
               (c^2-s^2)*sigmaxy_mid(i,i2,sayac);
%
              sigma23=c*sigmayz(i,i2,sayac)-s*sigmaxz(i,i2,sayac);
              sigma23_up(i,i2,sayac)=sigma23;
              sigma23_lo(i,i2,sayac)=sigma23;
              sigma23_mid(i,i2,sayac)=sigma23;
              %
              sigma13=s*sigmayz(i,i2,sayac)-c*sigmaxz(i,i2,sayac);
              sigma13_up(i,i2,sayac)=sigma13;
              sigma13_lo(i,i2,sayac)=sigma13;
              sigma13_mid(i,i2,sayac)=sigma13;
%_____________________________________________________________________
              % CHECK PLY FAILURE USING TSAI-WU FAILURE CRITERIA
              F1=1/sigma1T-1/sigma1C;
              F2=1/sigma2T-1/sigma2C;
              F3=0;%1/sigma3T-1/sigma3C;
              % F1,F2,F3 are also used in the calculation of max. strain criterion
```

```
F11=1/(sigma1T*sigma1C);
F22=1/(sigma2T*sigma2C);
F66=1/sigma12F^2;
F12=-1/2*sqrt(F11*F22);% Tsai-Hahn approximate formula (maybe taken as 0)
F33=0;%1/(sigma3C*sigma3T);
F44=0;%1/sigma23F^2;
F55=0;%1/sigma13F^2;
F13=0;%-1/2*sqrt(F11*F33);
F23=0;%-1/2*sqrt(F22*F33);
% check upper and lower layers seperately
Tsai_Wu_up=F11*sigma1_up(i,i2,sayac)^2+...
   F22*sigma2_up(i,i2,sayac)^2+...
   F66*sigma12_up(i,i2,sayac)^2+...
   F1*sigma1_up(i,i2,sayac)+...
   F2*sigma2_up(i,i2,sayac)+...
   2*F12*sigma1_up(i,i2,sayac)*sigma2_up(i,i2,sayac)+...
   F44*sigma23_up(i,i2,sayac)^2+F55*sigma13_up(i,i2,sayac)^2;
%
Tsai_Wu_lo=F11*sigma1_lo(i,i2,sayac)^2+...
   F22*sigma2_lo(i,i2,sayac)^2+...
   F66*sigma12_lo(i,i2,sayac)^2+...
   F1*sigma1_lo(i,i2,sayac)+...
   F2*sigma2_lo(i,i2,sayac)+...
   2*F12*sigma1_lo(i,i2,sayac)*sigma2_lo(i,i2,sayac)+...
   F44*sigma23_lo(i,i2,sayac)^2+...
   F55*sigma13_lo(i,i2,sayac)^2;
%
Tsai_Wu_mid=F11*sigma1_mid(i,i2,sayac)^2+...
   F22*sigma2_mid(i,i2,sayac)^2+...
   F66*sigma12_mid(i,i2,sayac)^2+...
   F1*sigma1_mid(i,i2,sayac)+...
   F2*sigma2_mid(i,i2,sayac)+...
   2*F12*sigma1_mid(i,i2,sayac)*sigma2_lo(i,i2,sayac)+...
   F44*sigma23_mid(i,i2,sayac)^2+...
   F55*sigma13_mid(i,i2,sayac)^2;
%_____________________________________________________________________
% CHECK PLY FAILURE USING TSAI-HILL FAILURE CRITERIA
if sigma1_lo(i,i2,sayac)<0
   sigma1F=sigma1C;
else
   sigma1F=sigma1T;
end
if sigma2_lo(i,i2,sayac)<0
   sigma2F=sigma2C;
else
   sigma2F=sigma2T;
end
%
Tsai_Hill_lo=sigma1_lo(i,i2,sayac)^2/sigma1F^2-...
   sigma1_lo(i,i2,sayac)*sigma2_lo(i,i2,sayac)/sigma1F^2+...
   sigma2_lo(i,i2,sayac)^2/sigma2F^2+...
   sigma12_lo(i,i2,sayac)^2/sigma12F^2;
%_____________
if sigma1_up(i,i2,sayac)<0
   sigma1F=sigma1C;
```

```
            else
              sigma1F=sigma1T;
            end
            if sigma2_up(i,i2,sayac)<0
              sigma2F=sigma2C;
            else
              sigma2F=sigma2T;
            end
            %
            Tsai_Hill_up=sigma1_up(i,i2,sayac)^2/sigma1F^2-...
              sigma1_up(i,i2,sayac)*sigma2_up(i,i2,sayac)/sigma1F^2+...
              sigma2_up(i,i2,sayac)^2/sigma2F^2+...
              sigma12_up(i,i2,sayac)^2/sigma12F^2;
            %_____________
            if sigma1_mid(i,i2,sayac)<0
              sigma1F=sigma1C;
            else
              sigma1F=sigma1T;
            end
            if sigma2_mid(i,i2,sayac)<0
              sigma2F=sigma2C;
            else
              sigma2F=sigma2T;
            end
            %
            Tsai_Hill_mid=sigma1_up(i,i2,sayac)^2/sigma1F^2-...
              sigma1_mid(i,i2,sayac)*sigma2_mid(i,i2,sayac)/sigma1F^2+...
              sigma2_mid(i,i2,sayac)^2/sigma2F^2+...
              sigma12_mid(i,i2,sayac)^2/sigma12F^2;
%_____________________________________________________________________
        % CHECK PLY FAILURE USING MAXIMUM STRAIN FAILURE CRITERIA
        % Calculate stiffness coefficients
        nu21=(E2_vec(i2)/E1_vec(i2))*nu12_vec(i2);
        Q11=E1_vec(i2)/(1-nu12_vec(i2)*nu21);
        Q12=nu12_vec(i2)*E2_vec(i2)/(1-nu12_vec(i2)*nu21);
        Q22=E2_vec(i2)/(1-nu12_vec(i2)*nu21);
        Q66=G12_vec(i2);
        %
        Q=[Q11 Q12 0;
           Q12 Q22 0;
           0 0 Q66];
        Qh2=inv(Q);
S11=Qh2(1,1);S12=Qh2(1,2);S13=Qh2(1,3);S22=Qh2(2,2);S23=Qh2(2,3);S33=Qh2(3,3);
            xt=sigma1T;xc=sigma1C;
            yt=sigma2T;yc=sigma2C;
            zt=sigma3T;zc=sigma3C;
            F1MS=F1+S12/S22*F2+S13/S33*F3;
            F2MS=S12/S11*F1+F2+S23/S33*F3;
            F11MS=1/(xt*xc)+(S12/S22)^2/(yt*yc)-S13/S33*F1*F3-...
              S12/S22*F1*F2;%-S12*S13/(S22*S23)*F2*F3+(S13/S33)^2/(zt*zc);
            F22MS=1/(yt*yc)+(S12/S11)^2/(xt*xc)-S12/S11*F1*F2-...
              S23/S33*F2*F3-S12*S23/(S11*S33)*F1*F3;%+(S23/S33)^2/(zt*zc)
            F12MS=S12/S11/(xt*xc)+S12/S22/(yt*yc)-...%+S13*S23/S33^2/(zt*zc)
              .5*(S12^2/(S11*S22)+1)*F1*F2-...
              .5*(S13*S12/(S11*S33)+S23/S33)*F1*F3-...
```

```
        .5*(S12*S23/(S22*S33)+S13/S33)*F2*F3;
      F44MS=0;%1/sigma23F^2;
      F55MS=0;%1/sigma13F^2;
      F66MS=1/sigma12F^2;
      F33MS=0;
      F13MS=0;
      F23MS=0;
      % check upper and lower layers seperately
      MS_up=F11MS*sigma1_up(i,i2,sayac)^2+...
        F22MS*sigma2_up(i,i2,sayac)^2+...
        F66MS*sigma12_up(i,i2,sayac)^2+...
        F1MS*sigma1_up(i,i2,sayac)+...
        F2MS*sigma2_up(i,i2,sayac)+...
        2*F12MS*sigma1_up(i,i2,sayac)*sigma2_up(i,i2,sayac)+...
        F44MS*sigma23_up(i,i2,sayac)^2+...
        F55MS*sigma13_up(i,i2,sayac)^2;
      %
      MS_lo=F11MS*sigma1_lo(i,i2,sayac)^2+...
        F22MS*sigma2_lo(i,i2,sayac)^2+...
        F66MS*sigma12_lo(i,i2,sayac)^2+...
        F1MS*sigma1_lo(i,i2,sayac)+...
        F2MS*sigma2_lo(i,i2,sayac)+...
        2*F12MS*sigma1_lo(i,i2,sayac)*sigma2_lo(i,i2,sayac)+...
        F44MS*sigma23_lo(i,i2,sayac)^2+...
        F55MS*sigma13_lo(i,i2,sayac)^2;
      %
      MS_mid=F11MS*sigma1_mid(i,i2,sayac)^2+...
        F22MS*sigma2_mid(i,i2,sayac)^2+...
        F66MS*sigma12_mid(i,i2,sayac)^2+...
        F1MS*sigma1_mid(i,i2,sayac)+...
        F2MS*sigma2_mid(i,i2,sayac)+...
        2*F12MS*sigma1_mid(i,i2,sayac)*sigma2_lo(i,i2,sayac)+...
        F44MS*sigma23_mid(i,i2,sayac)^2+...
        F55MS*sigma13_mid(i,i2,sayac)^2;
    %_____________________________________________________
      result_wu(i,i2,sayac)=max([Tsai_Wu_up,Tsai_Wu_lo,Tsai_Wu_mid]);
      result_hill(i,i2,sayac)=max([Tsai_Hill_up,Tsai_Hill_lo,Tsai_Hill_mid]);
      result_MS(i,i2,sayac)=max([MS_up,MS_lo,MS_mid]);
    end
    %_____________________________________________________
  end
 end
end
%_____________________________________________________
```

A.3.1.7 Calculation of in-plane and shear forces and bending moments

```
%_____________________________________________________________________
function [N_mat,M_mat,SF_mat]=sub_program_calculate_NFBMSF_shell(...
  elem_no,conn,deplasman,x_mid,y_mid,z_mid,x_upper,y_upper,z_upper,...
  x_lower,y_lower,z_lower,A,B,D,Cs)
% Izzet Ufuk Çagdas, 2005
%_____________________________________________________________________
% INPUT VARIABLES
% defined earlier
%_____________________________________________________________________
% OUTPUT VARIABLES
% N_mat: in-plane force vector
% M_mat: bending moment vector
% SF_mat: shear force vector
%_____________________________________________________________________
%
% CALCULATION OF ELEMENT DISPLACEMENT VECTOR
i=elem_no; % i: element number
% extract nodes of the element from the connectivity vector
element_nodes=conn(i,:);
% generate displacement vector for element i
disp_i=[];
for j=1:8
   node_j=element_nodes(j);% jth node of ith element
   vec_ij=[node_j*5-4,node_j*5-3,node_j*5-2,node_j*5-1,node_j*5];
   disp_i=[disp_i deplasman(vec_ij)];
end
%
%_____________________________________________________________________
% CALCULATION OF STRAINS AND STRESSES AT THE GAUSS POINT
% First calculate normals and tangents to the midsurface at the nodes
[V1,V1_hat,V2,V2_hat,V3,V3_hat]=sub_program_calc_normals_tangents(...
x_upper,x_lower,y_upper,y_lower,z_upper,z_lower);
% Calculate B matrices
% calculate strains at the Gauss points
[point,weight]=sub_program_gauss_point_plate(2);% 2x2
sayac=0;
for intx=1:2
   r=point(intx);
   for inty=1:2
      sayac=sayac+1;
      s=point(inty);
      [N,Nt]=sub_program_sfrsh8_plate(r,s);
      xpr_vec=N*V1;
      xpr_hat=xpr_vec/sqrt(xpr_vec(1)^2+xpr_vec(2)^2+xpr_vec(3)^2);
      ypr_vec=N*V2;
      ypr_hat=ypr_vec/sqrt(ypr_vec(1)^2+ypr_vec(2)^2+ypr_vec(3)^2);
      zpr_vec=N*V3;
      zpr_hat=zpr_vec/sqrt(zpr_vec(1)^2+zpr_vec(2)^2+zpr_vec(3)^2);
      % define the transformation matrix btw local and global coord. sys.
      mupr=[xpr_hat;ypr_hat;zpr_hat];
      % call shell_jacob to calculate Jacobian
      [Jacob_rs]=shell_jacob(Nt,x_mid,y_mid,z_mid,xpr_hat,ypr_hat);
      % Calculate strain-displacement matrices
```

```
[Bepsilon,Bkappa,Baf]=sub_program_bmatrix_shell(...
    N,Nt,Jacob_rs,mupr,V1_hat,V2_hat,V3_hat);
      % Calculate strain vectors at the Gauss point
      epsilon0_i=Bepsilon*disp_i';
      kappa_i=Bkappa*disp_i';
      fi_i=Baf*disp_i';
      % The membrane forces are in local coordinate system.
      N_mat(:,sayac)=A*epsilon0_i;%+B*kappa_i;% constitutive eqn.
      M_mat(:,sayac)=B*epsilon0_i+D*kappa_i;% constitutive eqn.
      SF_mat(:,sayac)=Cs*fi_i;% constitutive eqn.
   end
end
%_____________________________________________________________________
```

B. Matlab Functions Used for Optimization Purposes

B.1 Optimization of columns

The functions listed here are used in Section III of this thesis.

B.1.1 Main function

```
%_____________________________________________________________________
function [A,K1_vec,K2_vec,stress_atX]=OPT_P_MAIN(...
ne,alpha_1,ZET,p,n,beta_a,beta_b,problem,solved,yuk,guided,sup_guided)
% Izzet Ufuk Çagdas, 2006 - % Optimization of elastically restrained columns
%_____________________________________________________________________
% INPUT VARIABLES
% ne= number of elements
% alpha_1: the non-dimensional minimum area constraint
% ZET: material constant
% p: non-dimensional axial load at right end
% n: cross-sectional constant
% beta_a, beta_b: rotational spring constants
% Problem I: a>a0;
% Problem II: stress < yield stress
% problem III: stress+minimum area constraints.
% solved: =1 if unimodal, =2 if bimodal
% yuk: yuk=1 for uniformly distributed load / yuk=2 for triangularly distributed load
% guided: if =1, guided else, not guided
% right support is guided if sup_guided=1, left support is guided if sup_guided=2
%_____________________________________________________________________
% OUTPUT VARIABLES
% A: optimal area vector
% K1_vec,K2_vec: γ values corresponding to the first and the second modes
% stress_atX: vector of stress values at the nodes
%_____________________________________________________________________
% display the type of problem being solved
if solved==1
   disp('PROBLEM IS UNIMODAL')
else
   disp('PROBLEM IS BIMODAL OR UNIMODAL')
end
%_____________________________________________________________________
```

```
% Default values for L,b,h,q0,E
L=100;b=1;h=1;% cm
Vol=b*h*L;V=Vol;
q0=1;E=2e6; sigma_ys=E/ZET; %kg/cm2
% ____________________________________________________________
% P and Q are both dimensional
if yuk==1
   P=p*q0*L;%  (UDL)
elseif yuk==2
   P=p*q0*L/2;%  (triangular)
elseif yuk==3
   P=p*q0*L;%  (cubic) S=q0*L
elseif yuk==4
   P=p*q0*L;%  S=q0*L q(x)=4x^3
elseif yuk==5
   P=p*q0*L*1/2;%  S=q0*L/2 q(x)=0 if x<L/2 =1 if x>L/2
elseif yuk==6
   P=p*q0*L*1/2;%  S=q0*L/2 q(x)=q0 if L/4<x<3L/4
elseif yuk==7
   P=p*q0*L/ne;%  S=q0*L/ne q(x)=q0 if L/2-delta/2<x<L/2+delta/2
   % where delta=L/ne
elseif yuk==8
   P=p*q0*L/ne;%  S=q0*L/ne q(x)=q0 if L/4-delta/2<x<L/4+delta/2
   % where delta=L/ne
elseif yuk==9
   P=p*q0*L*1/2;%  S=q0*L/2 q(x)=q0 if x<L/2 else, 0
end
%  calculate alpha value
if n==1
   alpha=h^2/12;%for n=1
elseif n==2
   alpha=h/12/b;%for n=2
else
   alpha=1/12/b^2;%for n=3
end
% Convert non-dimensional beta into dimensional
beta_a_dim=beta_a/(L^(n+1)/(V^n*alpha*E));beta_b_dim=beta_b/(L^(n+1)/(V^n*alpha*E));
s=sigma_ys*L^(n+1)/(E*alpha*V^(n-1))
% ____________________________________________________________
% define vectors x,A,I
step=L/ne; x=0:step:L;% vector x has M+1 elements
% starting value for I(x)=1, ie. uniform column
for i=1:ne+1
   A(i)=b*h;
end
M=ne;
%
if n==1
   I=alpha*A;
elseif n==2
   I=alpha*A.^2;
else
   I=alpha*A.^3;
end
% ____________________________________________________________
```

```
% Initialize variables which will be used during the iterations
ind=1;
gamma1=0;
A1ydk=A;% A values will be stored in this vector
K1_vec(1)=0; K2_vec(1)=0; % gamma values will be stored in these vectors
% ____________________________________________________________________
% ENTER MAIN ITERATION LOOP
while ind<=100 % number of iterations is limited with 100 iterations
  % CALCULATE DISPLACEMENTS, THEIR DERIVATIVES AND BUCKLING LOADS
[w1,dw1,w2,dw2,K1,K2]=OPT_P_comp_Pwdw(P,q0,A,E,L,M,I,beta_a_dim,beta_b_dim,alph
a,Vol,yuk,guided,sup_guided);
  % CALCULATE THE NON-DIMENSIONAL BUCKLING LOAD
  %____________________________________________________________________
  % K1_nd is the minimum non-dimensional buckling load parameter
  if yuk==1
    K1_nd=K1*(L^(n+2))/E/alpha/(Vol^n)*(q0*L);
    K2_nd=K2*(L^(n+2))/E/alpha/(Vol^n)*(q0*L);
  elseif yuk==2
    K1_nd=K1*(L^(n+2))/E/alpha/(Vol^n)*(q0*L/2);
    K2_nd=K2*(L^(n+2))/E/alpha/(Vol^n)*(q0*L/2);
  elseif yuk==3
    K1_nd=K1*(L^(n+2))/E/alpha/(Vol^n)*(q0*L);%
    K2_nd=K2*(L^(n+2))/E/alpha/(Vol^n)*(q0*L);%
  elseif yuk==4
    K1_nd=K1*(L^(n+2))/E/alpha/(Vol^n)*(q0*L);%
    K2_nd=K2*(L^(n+2))/E/alpha/(Vol^n)*(q0*L);%
  elseif yuk==5
    K1_nd=K1*(L^(n+2))/E/alpha/(Vol^n)*(q0*L*1/2);
    K2_nd=K2*(L^(n+2))/E/alpha/(Vol^n)*(q0*L*1/2);
  elseif yuk==6
    K1_nd=K1*(L^(n+2))/E/alpha/(Vol^n)*(q0*L*1/2);
    K2_nd=K2*(L^(n+2))/E/alpha/(Vol^n)*(q0*L*1/2);
  elseif yuk==7
    K1_nd=K1*(L^(n+2))/E/alpha/(Vol^n)*(q0*L/ne);
    K2_nd=K2*(L^(n+2))/E/alpha/(Vol^n)*(q0*L/ne);
  elseif yuk==8
    K1_nd=K1*(L^(n+2))/E/alpha/(Vol^n)*(q0*L/ne);
    K2_nd=K2*(L^(n+2))/E/alpha/(Vol^n)*(q0*L/ne);
  elseif yuk==9
    K1_nd=K1*(L^(n+2))/E/alpha/(Vol^n)*(q0*L*1/2);
    K2_nd=K2*(L^(n+2))/E/alpha/(Vol^n)*(q0*L*1/2);
  end
  % ____________________________________________________________________
  % CHECK STRESS / PROBLEM II
  %if problem==2
    % loop over all of the points to check whether if the stress is exceeded or not.
    % attention: q0=1
    for i=1:M+1
      if yuk==1
        stress_atX(i)=(K1*(P+L-x(i)))/A(i);
      elseif yuk==2
        stress_atX(i)=(K1*(P+L/2-x(i)+(x(i))^2/2/L))/A(i);
      elseif yuk==3
        stress_atX(i)=(K1*(P+q0*L*(1-x(i)/L)^4))/A(i);
      elseif yuk==4
```

```
            stress_atX(i)=(K1*(P+L*(1-x(i)^4/L^4)))/A(i);
        elseif yuk==5
            if i<=ne/2
                stress_atX(i)=K1*(P+q0*L/2)/A(i);
            else
                stress_atX(i)=K1*(P+q0*(L-x(i)))/A(i);
            end
        elseif yuk==6
            if i<ne/4
                stress_atX(i)=K1*(P+q0*L/2)/A(i); %
            elseif i>=1*ne/4 & i<=3*ne/4
                stress_atX(i)=K1*(P+2*(1-x(i)))/A(i); %
            else
                stress_atX(i)=K1*(P)/A(i); %
            end
        elseif yuk==7
            if i<(ne+1)/2
                stress_atX(i)=(K1*(P+1))/A(i);%
            else
                stress_atX(i)=(K1*(P))/A(i);%
            end
        elseif yuk==8
            if i<(ne+1)/4
                stress_atX(i)=(K1*(P+1))/A(i);%
            else
                stress_atX(i)=(K1*(P))/A(i);%
            end
        elseif yuk==9
            if i<=ne/2
                stress_atX(i)=K1*(P+q0*(L/2-x(i)))/A(i);
            else
                stress_atX(i)=K1*(P)/A(i);
            end
        end
    end
    if problem==2
        if max(stress_atX)>1.001*sigma_ys
            ind=200000;% stop iterations
            break
        end
    end
%_____________________________________________________________________
%
% CALCULATION OF MOMENTS CORRESPONDING TO 1ST & 2ND MODES
[M1,M2,sonuc]=OPT_P_calc_M1M2(...
P,q0,K1,K2,w1,w2,dw1,dw2,beta_a_dim,beta_b_dim,L,ne,yuk,guided,sup_guided)
convert_nondim=L^(n+1)/E/alpha/V^n;
M1=M1*convert_nondim;
M2=M2*convert_nondim;
% If the problem is bimodal, then swap the variables.
if solved==2 & sonuc==2
    % store variables first
    w1_ydk=w1;dw1_ydk=dw1;K2_ydk=K2;M2_ydk=M2;
    w2_ydk=w2;dw2_ydk=dw2;K1_ydk=K1;M1_ydk=M1;
    %
```

```
      % if the smallest buckling load corresponds to anti-symmetrical mode
      % ONLY FOR BIMODAL PROBLEMS!!!
      w1=w2_ydk;
      dw1=dw2_ydk;
      K1=K2_ydk;
      M1=M2_ydk;
      w2=w1_ydk;
      dw2=dw1_ydk;
      K2=K1_ydk;
      M2=M1_ydk;
      % BUCKLING LOADS
      K1_vec(ind)=K2_nd;
      K2_vec(ind)=K1_nd;
   else
      K1_vec(ind)=K1_nd;
      K2_vec(ind)=K2_nd;
   end
   %
   Kcr=K1_nd;
   % Display result for the ith iteration step
   fprintf('step:%g   K1=%g K2=%g result=%g\n',ind,K1_nd,K2_nd,sonuc);
%_____________________________________________________________________
   % CHECK CONVERGENCE
   PP1(ind)=K1_nd;    PP2(ind)=K2_nd;
   if ind>2
      if abs(PP1(ind)-PP1(ind-1))<1e-5 | abs(K1_nd-K2_nd)<1e-5
         ind=100001
         break
      end
      if abs(PP2(ind)-PP2(ind-1))<1e-12 | abs(K1_nd-K2_nd)<1e-5
         ind=100002
         break
      end
      if K1_vec(ind)>K2_vec(ind) & sonuc~=2
         disp(Error!')
         ind=100003
         break
      end
   end
%_____________________________________________________________________
% CALCULATE AREA USING OPTIMALITY CONDITION
[A1]=OPT_P_calc_area(...
sonuc,yuk,dw1,dw2,P,q0,x,L,M,M1,M2,n,E,I,beta_a,beta_b,alpha,...
      Vol,problem,b,h,alpha_1,Kcr,sigma_ys,ind,A1ydk);
   % calculate area and moment of inertia vectors satisfying the constraints
[A,I,error_code]=OPT_P_area_inertia(...
problem,A1,b,h,alpha_1,L,M,Kcr,sigma_ys,P,x,n,alpha,Vol,yuk);
   if error_code==1
      ind=10003;
   end
   ind=ind+1;
end
%_____________________________________________________________________
% DISPLAY RESULTS
disp('iteration step:'); ind-1
```

```
disp('iteration step which gives the highest buckling load:')
stepp=find(K1_vec==max(K1_vec))
fprintf('z=%g s=%g step:%g K1=%g K2=%g ...
K_uni=%g\n',ZET,s,stepp,K1_vec(stepp),K2_vec(stepp),K1_vec(1))
%_____________________________________________________________
```

B.1.2 Related sub-functions

```
%_____________________________________________________________
function [M1,M2,sonuc]=OPT_P_calc_M1M2(...
P,q0,K1,K2,w1,w2,dw1,dw2,beta_a,beta_b,L,ne,yayiliyuk,guided,sup_guided)
% CALCULATION OF MOMENTS CORRESPONDING TO 1ST & 2ND MODES
% Call function calculate_M1de to calculate moment for the two modes
% at the moment it is not known which one is the symmetrical mode of buckling
[M1,M2]=OPT_P_calc_M1de(...
P,q0,K1,K2,w1,w2,dw1,dw2,beta_a,beta_b,L,ne,yayiliyuk,guided,sup_guided);
% seperate the 1st and the 2nd buckling modes after calculating moment
% this is done by calculating the zeros of the moment diagram for the 1st one.
[sonuc]=OPT_P_find_mode(M1,ne);
[sonuc2]=OPT_P_find_mode(M2,ne);
% sonuc==2, if the smallest buckling load corresponds to anti-symmetrical buckling mode
%_____________________________________________________________
%


%_____________________________________________________________
function [sonuc]=OPT_P_find_mode(M1,M)
% find the symmetric mode
isaret=0;% means that w1 is symmetric
tot_zero=0;
% calculate the total number of points where M1=0
for i=1:M
   isaret=M1(i)*M1(i+1);
   if isaret<=0% if the signs are not the same,
      tot_zero=tot_zero+1;% W1 is symmetric
   end
end
%_____________________________________________________________


%_____________________________________________________________
function [M1,M2]=OPT_P_calc_M1de(...
P,q0,Kcr,Kcr2,w1,w2,dw1,dw2,beta_a,beta_b,L,M,yayiliyuk,guided,sup_guided)
% Calculate Moment by integrating the d.e.
% Moment distribution For non-continuously loaded columns will be calculated by numerical
% integration% Note: All of the variables are dimensional
%_____________________________
% CALCULATE MOMENT FOR THE 1ST MODE
ne=M;step=L/ne;
x=0:step:L;% vector x has M+1 elements
%_____________________________
if yayiliyuk==1% valid for only udl
   %_____________________________
   if guided==0
```

```
    c1=Kcr*OPT_P_integrate(w1*q0,L,M)-beta_a*dw1(1)-beta_b*dw1(M+1);
    c2=beta_a*dw1(1);
  elseif guided==1 & sup_guided==1 % right support is guided
    c1=-beta_a*dw1(1)-beta_b*dw1(M+1)+...
      Kcr*(P*w1(M+1)+OPT_P_integrate(w1*q0,L,M));
    c2=beta_a*dw1(1);
  elseif guided==1 & sup_guided==2 % left support is guided
    c1=-beta_a*dw1(1)-beta_b*dw1(M+1)+...
      Kcr*(-1*P*w1(1)-w1(1)*q0*L+OPT_P_integrate(w1*q0,L,M));
    c2=beta_a*dw1(1);
  end
  %_____________________________________
  for i=1:M+1
    entegral=0;
    for j=1:i-1
      entegral=entegral+q0*(w1(j)+w1(j+1))/2*step;%use trapezoid rule to calculate integral
    end
    second=Kcr*(P*w1(i)+w1(i)*q0*(L-x(i))+entegral-w1(1)*q0*L);
    M1(i)=c1*x(i)/L+c2-second+Kcr*P*w1(1);
    % only for guided columns      % Calculate Shear Force for the 1st mode
    Shear(i)=c1/L-Kcr*(P*dw1(i)+dw1(i)*q0*(L-x(i)));
  end
  %
  %CALCULATE MOMENT FOR THE 2ND MODE
  if guided==0
    c1=Kcr2*OPT_P_integrate(w2*q0,L,M)-beta_a*dw2(1)-beta_b*dw2(M+1);
    c2=beta_a*dw2(1);
  elseif guided==1 & sup_guided==1 % right support is guided
    c1=-beta_a*dw2(1)-beta_b*dw2(M+1)+...
      Kcr2*(P*w2(M+1)+OPT_P_integrate(w2*q0,L,M));
    c2=beta_a*dw2(1);
  elseif guided==1 & sup_guided==2 % left support is guided
    c1=-beta_a*dw2(1)-beta_b*dw2(M+1)+...
      Kcr2*(-1*P*w2(1)-w2(1)*q0*L+OPT_P_integrate(w2*q0,L,M));
    c2=beta_a*dw2(1);
  end
  %_____________________________________
  for i=1:M+1
    entegral=0;
    for j=1:i-1
      entegral=entegral+q0*(w2(j)+w2(j+1))/2*step;%use trapezoid rule to calculate integral
    end
    second=Kcr2*(P*w2(i)+w2(i)*q0*(L-x(i))+entegral-w2(1)*q0*L);
    M2(i)=c1*x(i)/L+c2-second+Kcr2*P*w2(1);
    % only for guided columns      % Calculate Shear Force for the 1st mode
    Shear2(i)=c1/L-Kcr2*(P*dw2(i)+dw2(i)*q0*(L-x(i)));
  end
  %
%_____________________________
elseif yayiliyuk==2% valid for only tdl
  % Note: Rest of the code is not listed here, as the calculations are similar for the other loads.
  ....
end
%_____________________________________________________________
```

```
%_____________________________________________________________________
function [volume]=OPT_P_integrate(I,L,M)
% use Simpson's Method to calculate the integrals to obtain volume
step=L/M;volume=0;
WW=[1 4 1];% 7 32 12 32 7 %4 point newton-cotes
for i=1:2:M-1
   % sum of I values for odd values of i
   w(1)=i;w(2)=i+1;w(3)=i+2;%w(4)=i+3;w(5)=i+4;%0 1 2 3 4
   for j=1:3
      volume=volume+(step/3)*(I(w(j))*WW(j));
   end
end
%_____________________________________________________________________


%_____________________________________________________________________
function [A1]=OPT_P_calc_area(...
sonuc,yayiliyuk,dw1,dw2,P,q0,x,L,M,M1,M2,n,E,I,beta_a,beta_b,alpha,...
   Vol,problem,b,h,alpha_1,Kcr,sigma_ys,ind,A1ydk)
%_____________________________________________
% CALCULATE AREA USING OPTIMALITY CONDITION
if sonuc==2
   % evaluate gamma1 without changing area distribution
   if yayiliyuk==1
      % evaluate gamma1 without changing area distribution
      Kat2=OPT_P_integrate(dw1.^2.*(P+q0*(1-x)),L,M);
      Kat1=OPT_P_integrate(dw2.^2.*(P+q0*(1-x)),L,M);
   elseif yayiliyuk==2
      % evaluate gamma1 without changing area distribution
      Kat2=OPT_P_integrate(dw1.^2.*(P+q0*(L/2-x+x.^2/2)),L,M);
      Kat1=OPT_P_integrate(dw2.^2.*(P+q0*(L/2-x+x.^2/2)),L,M);
   elseif yayiliyuk==3
      % Note: Rest of the code is not listed here, as the calculations are similar
      ....
   end
   [gamma1]=OPT_P_calc_gamma1(...
M1,M2,n,Kat1,Kat2,P,q0,E,L,M,I,beta_a,beta_b,alpha,Vol,yayiliyuk,problem,b,h,alpha_1,...
Kcr,sigma_ys,x);
   for i=1:M+1
      A1(i)=abs(((1-gamma1)*((M1(i))^2)*Kat1+gamma1*((M2(i))^2)*Kat2))^(1/(n+1));
   end
   [V]=OPT_P_integrate(A1,L,M);
   A1=A1*Vol/V;
   % solve numerical stability problem
   A1=(90*A1ydk+10*A1)/100;
   [V]=OPT_P_integrate(A1,L,M);
   A1=A1*Vol/V;   A1ydk=A1;
   %
elseif sonuc==1
   if yayiliyuk==1 | yayiliyuk==2 | yayiliyuk==3 | yayiliyuk==4 | yayiliyuk==5 ...
| yayiliyuk==6 | yayiliyuk==7 | yayiliyuk==8 | yayiliyuk==9
      for i=1:M+1
         sabit=1; A1(i)=abs((M1(i))^2/sabit)^(1/(n+1));
      end
```

```
    end
    [V]=OPT_P_integrate(A1,L,M);
    A1=A1*Vol/V;
    % solve numerical stability problem
    if ind==1
      A1=(99.9*A1ydk+2*A1)/100;
    end
    if ind>1
      A1=(99*A1ydk+1*A1)/100;
    end
    [V]=OPT_P_integrate(A1,L,M);   A1=A1*Vol/V;
end
%_____________________________________________________________________

%_____________________________________________________________________
function [gamma1]=OPT_P_calc_gamma1(...
M1,M2,n,Kat1,Kat2,P,q0,E,L,M,I,beta_a,beta_b,alpha,Vol,yayiliyuk,problem,b,h,alpha_1,...
Kcr,sigma_ys,x)
% if solution is multimodal for a given area distribution,
% then calculate the gamma1 value which is making P1=P2 (or closest),using golden section
method. % M1 and M2 are already calculated
% Apply Golden Section Method
b=1;a=0;c=a+0.618*(b-a);d=b-0.618*(b-a);% initalization
counter=0; fark=1;
while abs(c-d)>1e-8 & counter<20
[Ta,K1d,K2d,res]=FARK_hesap(M1,M2,n,Kat1,Kat2,P,q0,E,L,M,I,beta_a,beta_b,alpha,Vol,...
yayiliyuk,problem,b,h,alpha_1,Kcr,sigma_ys,x,a);
[Tb,K1d,K2d,res]=FARK_hesap(M1,M2,n,Kat1,Kat2,P,q0,E,L,M,I,beta_a,beta_b,alpha,Vol,...
yayiliyuk,problem,b,h,alpha_1,Kcr,sigma_ys,x,b);
[Tc,K1,K2,res]=FARK_hesap(M1,M2,n,Kat1,Kat2,P,q0,E,L,M,I,beta_a,beta_b,alpha,Vol,...
yayiliyuk,problem,b,h,alpha_1,Kcr,sigma_ys,x,c);
[Td,K1d,K2d,res]=FARK_hesap(M1,M2,n,Kat1,Kat2,P,q0,E,L,M,I,beta_a,beta_b,alpha,Vol,...
yayiliyuk,problem,b,h,alpha_1,Kcr,sigma_ys,x,d);
  if Td<Tc
    a=a;     b=c;
  elseif Td>Tc
    a=d;     b=b;
  else
    counter=1e6;
  end
  if Td<Tc
    c=d;     d=b-0.618*(b-a);
  elseif Td>Tc
    d=c;     c=a+0.618*(b-a);
  end
  counter=counter+1;
  if counter>1 & abs(Tc-farkydk)<1e-5
    counter=1e6;
  end
  farkydk=Tc;
end
gamma1=(c+d)/2;
%_____________________________________________________________________
```

```
%_____________________________________________________________________
function [fark,K1_nd,K2_nd,sonuc]=FARK_hesap(...
M1,M2,n,Kat1,Kat2,P,q0,E,L,M,I,beta_a,beta_b,alpha,Vol,yayiliyuk,problem,b,h,alpha_1,...
Kcr,sigma_ys,x,gamma1)
%
ne=M;
% Calculate area for the given M1,M2,Kat1,Kat2
for i=1:M+1
   A22(i)=abs(((1-gamma1)*((M1(i))^2)*Kat1+gamma1*((M2(i))^2)*Kat2))^(1/(n+1));
end
[V]=OPT_P_integrate(A22,L,M);
A22=A22*Vol/V;
% correct area according to the constraints and calculate I
[A,I,hata_kodu]=OPT_P_area_inertia(problem,A22,b,h,alpha_1,L,M,Kcr,sigma_ys,P,x,n,...
alpha,Vol,yayiliyuk);
%
[w1,dw1,w2,dw2,K1,K2]=OPT_P_comp_Pwdw(P,q0,A,E,L,M,I,beta_a,beta_b,alpha,Vol,...
yayiliyuk);
% K1_nd is the minimum non-dimensional buckling load parameter
if yayiliyuk==1
   K1_nd=K1*(L^(n+2))/E/alpha/(Vol^n)*(q0*L);% only valid for udl
   K2_nd=K2*(L^(n+2))/E/alpha/(Vol^n)*(q0*L);% only valid for udl
elseif yayiliyuk==2
   K1_nd=K1*(L^(n+2))/E/alpha/(Vol^n)*(q0*L/2);% only valid for triangular
   K2_nd=K2*(L^(n+2))/E/alpha/(Vol^n)*(q0*L/2);% only valid for triangular
elseif yayiliyuk==3
   % Note : rest of the code is not given as calculations are similar
end
fark=abs(K1_nd-K2_nd);
% calculate moment for the 1st and 2nd modes
[M1,M2]=OPT_P_calc_M1de(P,q0,K1,K2,w1,w2,dw1,dw2,beta_a,beta_b,L,M,yayiliyuk);
[sonuc]=OPT_P_find_mode(M1,M);
%_____________________________________________________________________


%_____________________________________________________________________
function [A,I,hata_kodu]=OPT_P_area_inertia(...
problem,A1,b,h,alpha_1,L,M,Kcr,sigma_ys,P,x,n,alpha,Vol,yayiliyuk)
E=2e6;q0=1; % default values
hata_kodu=0;% if stress constraint is violated by yielding of material
donotwriteagain=0;% report only once
if problem==1
   % convert non-dimensional alpha_1 into dimensional alpha_0
   alpha_0=alpha_1*b*h;% min area required
   for jj=1:10
      [V]=OPT_P_integrate(A1,L,M);
      % modify area.
      for i=1:M+1
         if A1(i)<alpha_0
            A1(i)=alpha_0;%A1(A1<=alpha_0)=alpha_0;
         end
      end
      % Volume is increased. Calculate volume again
      [V]=OPT_P_integrate(A1,L,M);
```

```
      % decrease volume by dividing by increased volume
      A1=A1*Vol/V;
    end
end
% Solve problem II / valid for udl and tdl
if problem==2
  % convert nondimensional buckling parameter into dimendisonal
  K_dim=Kcr/(L^(n+2))*E*alpha*(Vol^n)/(q0*L);% valid for udl and tdl
  % min area required at x (dimensional)
  for i=1:M+1
    if yayiliyuk==1
      a_0(i)=(K_dim/sigma_ys)*(P+L-x(i));% 07 October 2004
    elseif yayiliyuk==2
      a_0(i)=(K_dim/sigma_ys)*(P+L/2-x(i)+(x(i))^2/2/L);% 28 October 2004
    elseif yayiliyuk==5
      if i<=M/2
        a_0(i)=(K_dim/sigma_ys)*(P+q0*L/2);
      else
        a_0(i)=(K_dim/sigma_ys)*(P+q0*(L-x(i)));
      end
    end
  end
  % a_0 varies along length
  for jj=1:10
    % modify area.
    [V]=OPT_P_integrate(A1,L,M);
    % modify area.
    for i=1:M+1
      if A1(i)<a_0(i)
        A1(i)=a_0(i);
        %pause
      end
    end
    % Volume is increased. Calculate volume again
    [V]=OPT_P_integrate(A1,L,M);
    % decrease volume by dividing by increased volume
    A1=A1*Vol/V;
  end
end
%_____________________
% vector A1 contains areas at the nodes. Calculate A values at the center of each element
A=A1;
if n==1
  I=alpha*A;
elseif n==2
  I=alpha*A.^2;
else
  I=alpha*A.^3;
end
%_____________________________________________________________
```

B.2 Optimization of plates

Matlab built-in function **fminbnd** is used as given below.

```
%_____________________________________________________________________
[hzero_optimal(1),lambda_crit(1)]=fminbnd('program_01',0,0.5,[],1)% h0

[teta_optimal(1),lambda_crit(1)]=fminbnd('program_02',0,90,[],1)% lamination angle
%_____________________________________________________________________
```

B.3 Optimization of shells

```
%_____________________________________________________________________
clear
clc
format long
lam_ang_vec=[0:5:90]; % lamination angle vector
a=100; t=1;
BC=3; % CSCS
SS=1;% stacking sequence A
for i=1:length(lam_ang_vec)
    [Pcr(i),MS_failure_load_coeff(i)]=program_panel_buckling_01(lam_ang_vec(i),t,a,SS,BC);
end
save results_aoverb05__t1_BC3_SSA % save data
%_____________________________________________________________________
```